Concealed Explosives Detection using Swept Millimetre Waves

A thesis submitted in partial fulfilment

of the requirements of the

Manchester Metropolitan University

for the degree of

Doctor of Philosophy

Department of Engineering and Technology

Sarah Elizabeth Smith

June 2012

Contents

List of Figures

List of Tables

Nomenclature

$3D$	three dimensions
δ	skin depth of electromagnetic wave
ϵ	emissivity
ϵ_0	permittivity of free space
ϵ_r	relative permittivity
λ	wavelength
μ_0	permeability of free space
μ_r	relative permeability
ν	frequency
ω	angular frequency $= 2\pi\nu$
σ	radar cross section
τ	pulse width
τ_ω	maximum pulse width
τ_s	time between pulses
θ	resolution
D	lens diameter

f_c cut-off frequency

G_t antenna gain

nd optical depth

P_r received signal power for a radar

$tan\delta$ loss tangent

$TE_{1,0}$ transverse electric mode

AM Amplitude Modulated

c Speed of light in vacuum

CW continuous wave

FM Frequency Modulation

FMCW Frequency Modulated Continuous Wave

IF intermediate frequency

IFFT Inverse Fast Fourier Transform

L target distance

MMIC monolithic microwave integrated circuit

n refractive index

PRF Pulse Repetition Frequency

RADAR Radio Detection and Ranging

RF radio frequency

t round trip time

t time

VSWR voltage standing wave ratio

Abstract

The aim of this project is to develop a system for the stand-off detection (typically ten metres) of concealed body-worn explosives. The system must be capable of detecting a layer of explosive material hidden under clothing and distinguishing explosives from everyday objects. Millimetre wave radar is suitable for this application. Millimetre Waves are suitable because they are not significantly attenuated by atmospheric conditions and clothing textiles are practically transparent to this radiation. Detection of explosive layers from a few mm in thickness to a few cm thickness is required. A quasi optical focussing element is required to provide sufficient antenna directivity to form a narrow, highly directional beam of millimetre waves, which can be directed and scanned over the person being observed.

A system of antennae and focussing optics has been modelled and built using designs from finite element analysis (FEA) software. Using the developed system, representative data sets have been acquired using a Vector Network Analyser (VNA) to act as transmitter and receiver, with the data saved for processing at a later time. A novel data analysis algorithm using Matlab has been developed to carry out Fourier Transforms of the data and then perform pattern matching techniques using artificial neural networks (ANN's). New ways of aligning and sorting data have been found using cross-correlation to order the data by similar data slices and then sorting the data by amplitude to take the strongest 50% of data sets.

The significant contribution to knowledge of this project will be a system which can be field tested and which will detect a layer of dielectric at a standoff distance, typically of ten metres, and signal processing algorithms which can recognise the difference

between the response of threat and non-threat objects. This has partially been achieved by the development of focussing optics to acquire data sets which have then been aligned by cross-correlation, sorted and then used to train a pattern matching technique using neural networks. This technique has shown good results in differentiating between a person wearing simulated explosives and a person not carrying simulated explosives.

Further work for this project includes acquiring more data sets of everyday objects and training the neural network to distinguish between threat objects and non-threat objects. The operational range also needs increasing using either a larger aperture optical element or a similarly sized Cassegrain antenna. The system needs adapting for real time use with the data processing techniques developed in Matlab.

The VNA is operated over a band of 14 to 40 GHz, future work includes moving to a stand-alone transmitter and receiver operating at w-band (75 to 110 GHz).

Aims and Objectives

Academic Aim

To demonstrate the feasibility of a portable and deployable millimetre wave radar system for the detection of on body concealed explosives consisting of layers of dielectric media containing no fragmentation at standoff distances of up to 10 metres. Fragmentation is shrapnel contained within the explosive device, such as ball bearings or nails.

Objectives

- To model and have manufactured beam forming optics such as lenses and high gain antenna, for operation at millimetre wavelengths that will focus and move a beam at a stand-off distance, so that the detector can spatially discriminate a target against the background, e.g. a human. High gain antenna can be made using standard gain waveguide horns and Gaussian Optics Lens Antenna (GOLA).

- To develop techniques to detect the presence or otherwise of a person borne improvised explosive device (PBIED), under practical conditions, at standoff distances. The PBIED is typically a dielectric layer that may or may not contain metallic fragments.

- To develop signal processing software that will autonomously identify the presence of a threat object by analysis of the return signature.

- To construct and test a millimetre wave radar system that will scan an object at a stand-off distance.
- To develop appropriate wideband receivers working at an appropriate frequency range.

Chapter 1

Introduction

1.1 Introduction

This thesis is part of a larger project, partly funded by EPSRC, to produce a concealed weapons detector that will detect explosive devices and handguns concealed on the body of a subject typically at a distance of a few metres and up to ten metres away. Changes in global security requirements mean that conventional metal detectors cannot provide sufficiently broad screening to ensure public safety. A screening device which can detect explosives and / or handguns concealed on the body and discriminate these objects from benign / non-threat objects is needed for security applications such as airports and sports venues. The system developed here uses an active, non-imaging technique to detect explosives concealed under clothing. Other widely employed techniques rely on active and passive imagery taken at MMW bands.

The detector operates using a radar ranging technique which transmits Continuous Wave millimetre waves and receives the radiation scattered from the target. The centre frequency for the detector is based around a well known low attenuation, atmospheric window centred on 94 GHz.

The reflected signal is received by the Vector Network Analyser (VNA), saved and presented to software which performs a Inverse Fast Fourier Transform into the time domain. Peaks are produced in the time domain resulting from reflections from the

surfaces of objects and discontinuities in dielectric properties.

In the time domain multiple peaks are often produced but this pattern is usually dominated by two principle returns: that from the front of the concealed material and that from the body behind.

An automatic way of detecting these dominant peaks was needed to allow autonomous operation of the detector. The data were simplified and presented to a pattern recognition algorithm known as an Artificial Neural Network (ANN) to be classified as either a threat or a non-threat item.

To enable the ANN to be trained on the data from the VNA, an algorithm to align the data sets was developed that would remove the temporal shifting effect of a moving person on the data set and align the peaks from the body and any explosives present. This can then be used to train the ANN.

To increase the standoff distance, and as an extension to the work, a cassegrain reflecting antenna was chosen as large diameter dishes can be made which are lightweight and steerable compared with a refractive lens of the same size. The cassegrain system uses a MMIC receiver operating at w-band (75-110 GHz) and a swept 12.5 to 18 GHz microwave frequency source into a six times multiplier giving an output of 75 to 110 GHz.

The frequency band 75 to 110 GHz was chosen because of the availability of commercial transmitters and receivers and at higher frequencies the absolute bandwidth available is larger than is achievable at lower frequencies of operation. The bandwidth available is important because the bandwidth determines the range resolution of the radar system.

Most clothing is transparent to EM radiation at millimetre wavelengths whereas terahertz wavelengths approach the size of the weave of the fabric so do not penetrate the fabric as well as MMW radiation.

Different methods of detection will be required depending on the environment the detector is to be used in.

Particular challenges occur with lossy materials of high dielectric constant, this

means a lot of incident energy is reflected and that which is transmitted is quickly attenuated. Polar liquids such as water are difficult because of their high reflectivity.

The development of a robust and efficient detection algorithm is important because the usefulness of a system will depend on its ability to distinguish between threat and non-threat items.

Explosives containing fragmentation can be detected in the same way as metallic objects and detection algorithms can be trained to recognise the signatures from metallic objects and explosives containing fragmentation. Algorithms that are trained to detect dielectrics may not be optimised for detecting metals and vice versa. The signature from a dielectric contains an optical depth, relating to the separation between the front and back surfaces of the object, whereas the signature from a metallic target generally contains a single bright reflection. In this work, the dielectric detection algorithm is trained to recognise a depth; indicating a thickness of explosive in front of the body. The metallic detection algorithm is trained on the amplitude of the signal reflected from the metal. Therefore a scattered radar signal from a target can be put through two different detection algorithms or intelligence of the suspected target can be used to select one of the algorithms best suited for each case.

1.1.1 Advantages of Working in the Millimetre Wave Band

Millimetre wavelengths are appropriate to standoff concealed threat radar because there is an atmospheric window centred on 94 GHz which allows these waves to propagate through the atmosphere without significant attenuation, atmospheric attenuation against frequency is shown by figure 1.1.

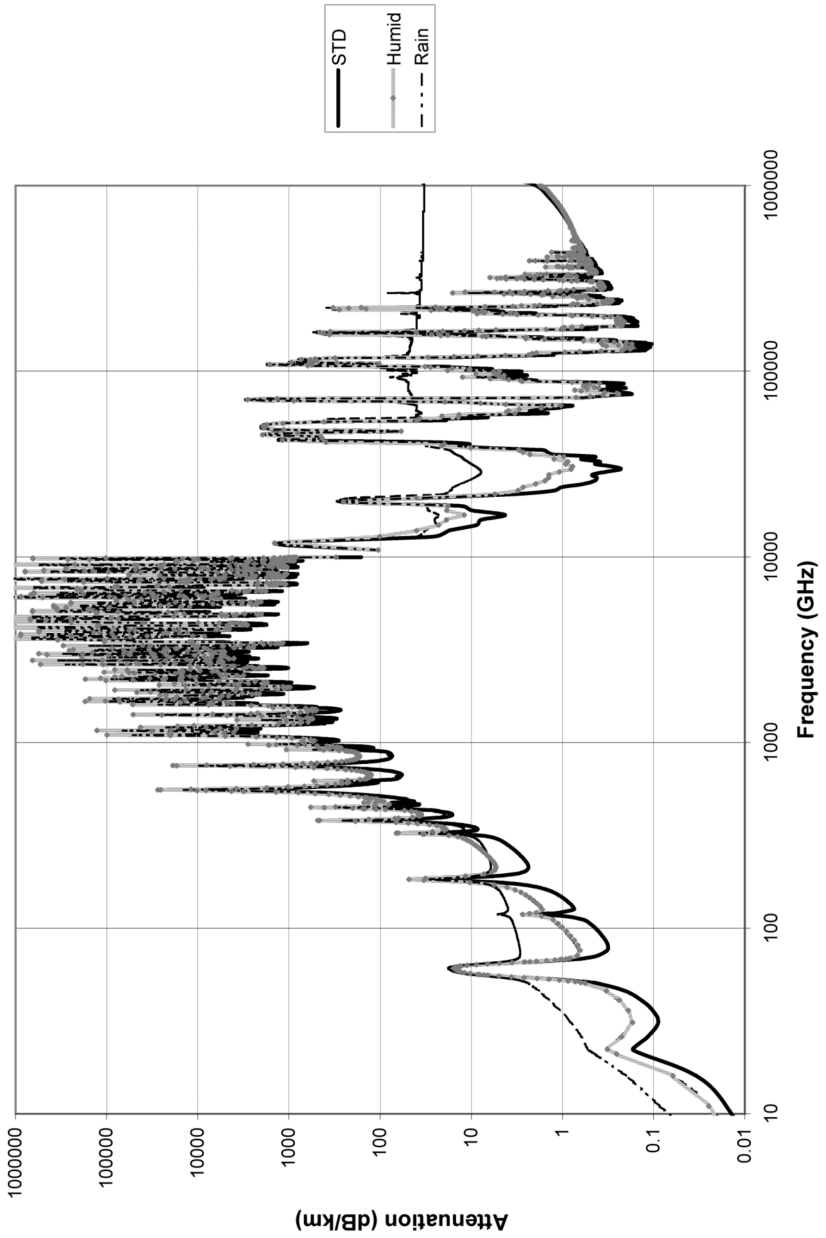

Figure 1.1: Attenuation across the electromagnetic spectrum, at sea level, based on currently accepted models. Rain = 4mm/h, fog=100m visibility, STD (standard atmosphere) = $7.5gm/m^3$ water vapour and 2 x STD (humid conditions) = 15 gm/m^3 water vapour. Figure and caption taken from (Appleby & Wallace, 2007).

Clothing also appears transparent at millimetre wavelengths whereas THz waves are more strongly attenuated than MMW and the weave periodicity enhances scattering (like a diffraction grating).

1.1.2 Electromagnetic Spectrum

Millimetre waves occupy a region of the electromagnetic spectrum between the microwave and the far infrared region, their wavelengths are in the range of 1 to 10 mm (300 GHz and 30 GHz respectively) making them suitable for radar and imaging because they give acceptable resolution. Techniques developed first at microwave frequencies (such as mixing, up/down conversion, amplification etc) can also be used at MMW frequencies. At MMW frequencies refractive and reflective elements are often used to focus the radiation in a quasi-optical way. Examples of applications where MMW are used include automobile collision radar, security screening and spectroscopy. MMW waveguide and receivers are physically smaller than their microwave equivalents, since the wavelength of MMW radiation is shorter than that of microwave radiation. The radar cross section (RCS) of objects is generally strongly dependent on wavelength and smaller targets can be detected with MMW than can be detected with microwaves. The waveguide bandwidth available increases with decreasing wavelength, allowing improved radar range resolution at MMW frequencies than is obtainable at microwave frequencies. Three types of scattering or scattering regions can be defined for the radar-target interaction: the Rayleigh region, the Mie region, and the optical region. In the Rayleigh region, the dimensions of the targets are small compared to the wavelength, the radar cross section varies as λ^{-4}. In the Mie region, the dimensions of the target are comparable to the wavelength, and the RCS varies in an oscillatory manner as a function of wavelength. In the optical region, the dimensions of the target are much greater than the wavelength (Currie & Brown, 1987).

Millimetre waves are better for penetrating through dust and fog in imaging applications where optical wavelengths fail, because longer wavelengths penetrate mist and fog better than shorter ones due to Rayleigh scattering. Figure 1.2 shows the range of

the electromagnetic spectrum from radio waves to gamma rays (Wikimedia-Commons, 2010).

Figure 1.3 shows the position of millimetre waves in the electromagnetic spectrum between microwaves and terahertz.

1.1.3 Cost and availability of hardware

The frequency band 75 to 110 GHz was chosen because of the availability of commercial transmitters and receivers and that at higher frequencies there is a greater absolute bandwidth in metallic waveguides carrying the $TE_{1,0}$ mode. The bandwidth available is important because the bandwidth determines the range resolution of the radar system. 220 GHz was not chosen because of the higher cost of transmitters and receivers in this band and also absorption due to water vapour and oxygen generally increase with frequency (Appleby & Anderton, 2007).

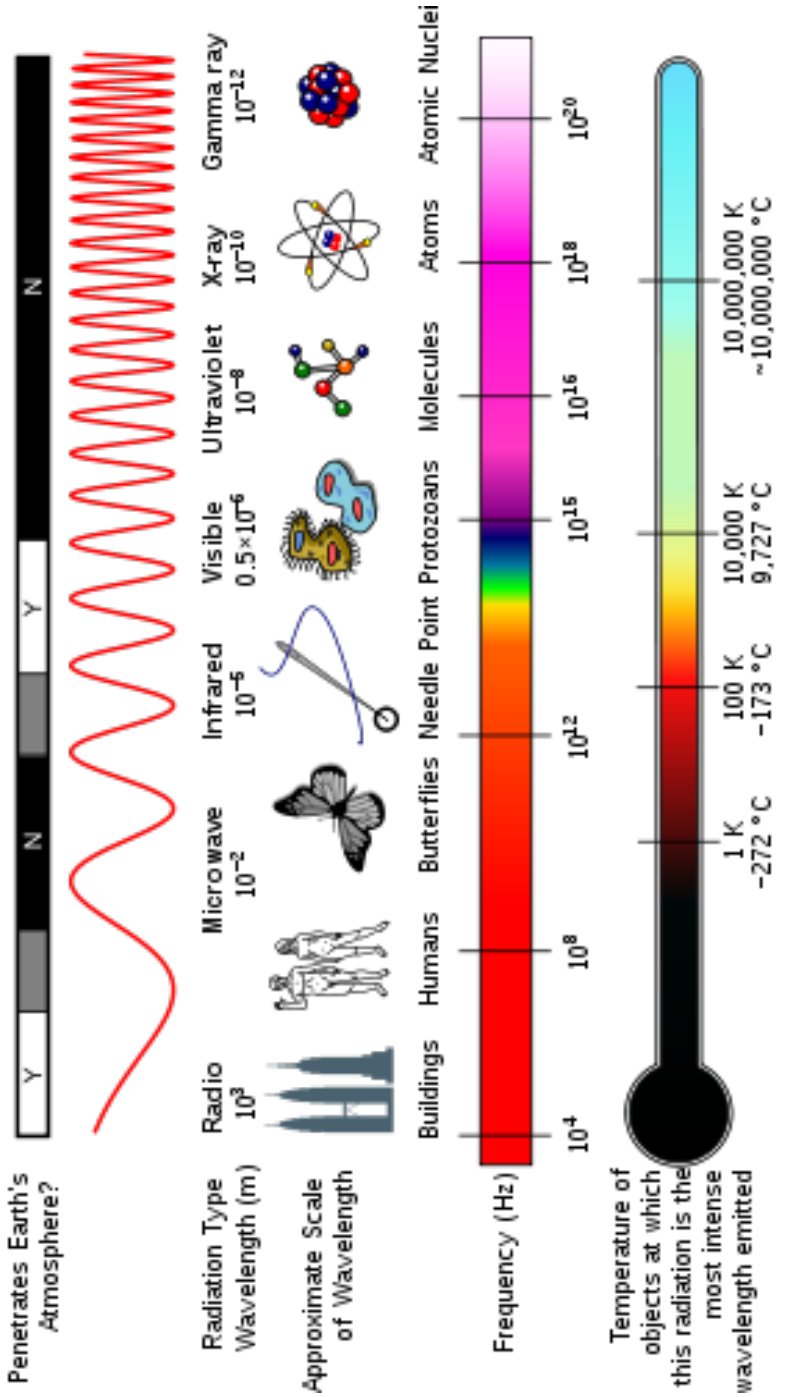

Figure 1.2: This figure shows the range of the electromagnetic spectrum from radio waves to gamma rays (Wikimedia-Commons, 2010).

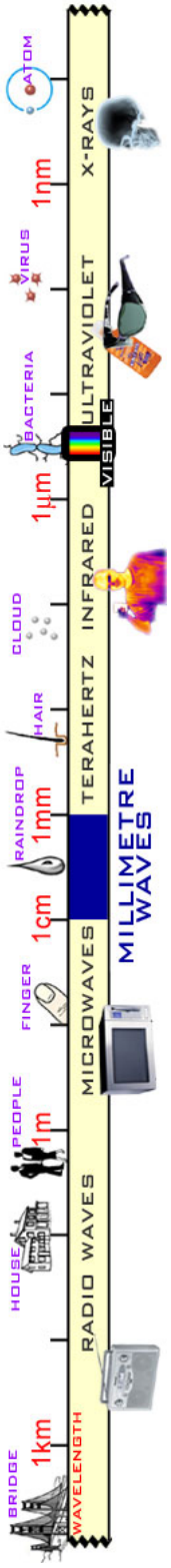

Figure 1.3: This figure shows the location of millimetre waves in the electromagnetic spectrum between microwaves and terahertz (of St-Andrews, 2011).

Chapter 2

Technical Introduction

2.1 Radar

The word Radar (derived from "RAdio Detection And Ranging") summarises the two main tasks of radar: remotely detecting the presence of an object and determining the range to that object. The bearing and target velocity can also be measured using radar techniques. Radar techniques are applied in many areas of technology from automobile radar and chemical tank fill sensors to more traditional fields of aircraft detection and tracking and meteorological measurements. The application of simple Radar techniques to the field of security screening is a more recent development but one that is becoming increasingly relevant. The simplest example of a radar system is an Amplitude Modulated (AM) radar; this forms a pulse in the time domain and the pulse can have any shape. Important figures of merit of radar systems are: range resolution, unambiguous range and the cross correlation of transmitted pulse and received pulse to determine range.

The Fourier transform allows decomposition of a function defined in time domain to a continuous function of frequency which represents the original function's frequency spectrum. The reverse operation is also defined, where a frequency spectrum is transformed into the time signal possessing that frequency spectrum. When discussing the frequency and time domain we mean that, in the term frequency domain we have a

function with an explicit frequency dependance and in the time domain a function with an explicit time dependance. Generally, the frequency spectrum is a complex quantity, containing the magnitude and phase of the signal.

The Fourier Transform is defined as

$$f(t) = \int_{-\infty}^{\infty} F(\omega) e^{i\omega t} d\omega \tag{2.1}$$

where $\omega = 2\pi\nu$ where ν is frequency.

$$F(\omega) = \frac{1}{2\pi} \int_{-\infty}^{\infty} f(t) e^{-i\omega t} dt \tag{2.2}$$

Or, written more succinctly,

$$f(t) = \mathscr{F}^{-1}\{F\} \tag{2.3}$$

$$F(\omega) = \mathscr{F}\{f\} \tag{2.4}$$

Equations 2.3 and 2.4 are equivalent to equations 2.1 and 2.2 respectively.

For example, a delta function in the frequency domain becomes a sinusoidal wave in the time domain. Mathematically, $F(\omega) = \delta(\omega - \omega_0)$ then $f(t) = e^{i\omega_0 t}$ therefore a single valued frequency spectrum gives a continuous, sinusoidal function in time.

Conversely, $f(t) = \delta(t - t_0)$,

$$F(\omega) = \frac{1}{2\pi} \int \delta(t - t_0) e^{i\omega t}, dt = \frac{e^{i\omega t_0}}{2\pi} \tag{2.5}$$

$$F = \mathscr{F}\{\delta(t - t_0)\} = \frac{e^{i\omega t_0}}{2\pi} \tag{2.6}$$

$$|F(\omega)|^2 = \frac{1}{(2\pi)^2} \tag{2.7}$$

For a delta function in the time domain the power spectrum is flat (constant) for

all frequencies i.e. contains equal power in all frequency bands.

A key figure of merit in Radar is the range resolution that can be achieved. If a target is a distance L from the radar and a second target is a distance $L + \Delta L$ further from the target, then the range resolution is the smallest distance between the targets at which they are resolved into separate targets. Different applications will typically have wide range resolution requirements. For example a liquid fill measuring radar in a chemical engineering process might require an accuracy of 1 cm while a radar for aircraft detection might only need an accuracy of 10 metres.

Consider a pulse width, τ, that is transmitted and reflects from two targets that are separated by a distance ΔL. The time taken for the transmitted pulse to travel the round trip between the targets is $t = \frac{2\Delta L}{c}$ where t is the round trip time and c is the speed of light. If the pulse width, τ, is greater than this value then the two targets will not be properly resolved i.e. the reflected pulses will overlap in time. If $\tau < \frac{2\Delta L}{c}$ then the targets will be temporally distinct.

Practical radar systems send out a train of pulses which often have a fixed duty cycle. The Pulse Repetition Frequency (PRF) is the inverse of the time between pulses, where the time between pulses is τ_s, PRF is given by

$$PRF = \frac{1}{\tau_s} \tag{2.8}$$

Where two successive pulses are transmitted, the earlier pulse travels a round trip distance of $2R = c\tau_s$ where R is the distance to the target. Therefore objects that are further than $c\tau_s/2$ will have ambiguous range because one cannot be certain which pulse in the train was reflected.

A detection scheme whereby the transmitted pulse is correlated with the received pulse allows the determination of the temporal reflections. Such a correlation is, in fact, equivalent to a convolution of the time reversed complex conjugate of the transmitted pulse with the received pulse.

After correlation in the time domain the reflections can be isolated, provided that they are not too close together. There is a minimum temporal spacing, below which two

reflected pulses cannot be resolved from one another. This corresponds to a minimum spatial separation of reflectors. The minimum resolvable temporal spacing is related to the spatial resolution by

$$t = \frac{2\Delta L}{c} \tag{2.9}$$

where c is the speed of light.

The required maximum pulse width, τ_ω of the transmitted pulse is related to the distance between the objects detected by equation 2.10, where c is the speed of light.

$$\tau_\omega \leq \frac{2\Delta L}{c} \tag{2.10}$$

$$\Delta L \geq \frac{c\tau_\omega}{2} \tag{2.11}$$

Therefore, to achieve better range resolution, the pulse width, τ_ω, needs to be reduced. However, the pulse width cannot be reduced indefinitely, since an antenna cannot pass an infinite spectrum of frequencies. In fact there exists an uncertainty between time and frequency that limits the precision to which both can be measured or known simultaneously.

$$\Delta t \Delta \nu \geq \frac{1}{2} \tag{2.12}$$

where Δt is the root mean square duration (pulse width) in the time domain and $\Delta \nu$ the root mean square bandwidth (bandwidth) in the frequency domain. Clearly a more precise measure of one necessitates less precise knowledge of the other.

To improve time resolution, the bandwidth must increase. The available bandwidth is however limited by amplification, up conversion and antenna feed bandwidth (carried down a waveguide). This imposes a spatial limit on range resolution.

$$\Delta L \geq \frac{c}{2 * bandwidth} \tag{2.13}$$

CW (Continuous Wave) radar emits a continuous signal; transmission and reception occur simultaneously. Ranging to target in the case of CW radar is achieved by frequency modulation of the signal; this provides ability to determine round trip times by measuring a quantity associated with the modulation. For example: Homodyne radars use frequency modulation to measure range. These radars involve mixing the received signal with the transmitted signal.

The optical depth of a material is the refractive index of the material multiplied by its physical thickness. This is important in explosives detection because the minimum thickness of explosive which can be detected by a system is determined by its resolution. In an optically dense medium, such as polyethylene, the refractive index is a complex number, n'; while the real part describes refraction, the imaginary part accounts for absorption:

$$n' = n + j\kappa \tag{2.14}$$

where the real part of the refractive index, n indicates the phase speed, while the imaginary part κ indicates the amount of absorption loss when the electromagnetic wave propagates through the material (Hecht, 2002). The resolution is related to the frequency sweep of the transmitter and receiver. The optical depth depends on the frequency sweep Δf, and is related to the speed of light in free space, c by

$$\Delta L = \frac{c\tau_\omega}{2} = \frac{c}{2BW} \tag{2.15}$$

so wideband sources and detection systems are required with a typical sweep of 20 GHz to detect dielectrics with a thickness of less than a cm. The frequency band does not affect the resolution, so the bands 20-40 GHz and 80-100 GHz have the same resolution, the 80-100 GHz band is preferred though because it can be better focussed (Andrews et al., 2009).

The dielectric loss tangent is defined by the angle between the impedance vector and the negative reactive axis, as shown by figure 2.1. It determines the lossyness of the medium, as given by $\epsilon = \epsilon_{Re} + j\epsilon_{Im}$ (RFcafe, 2012).

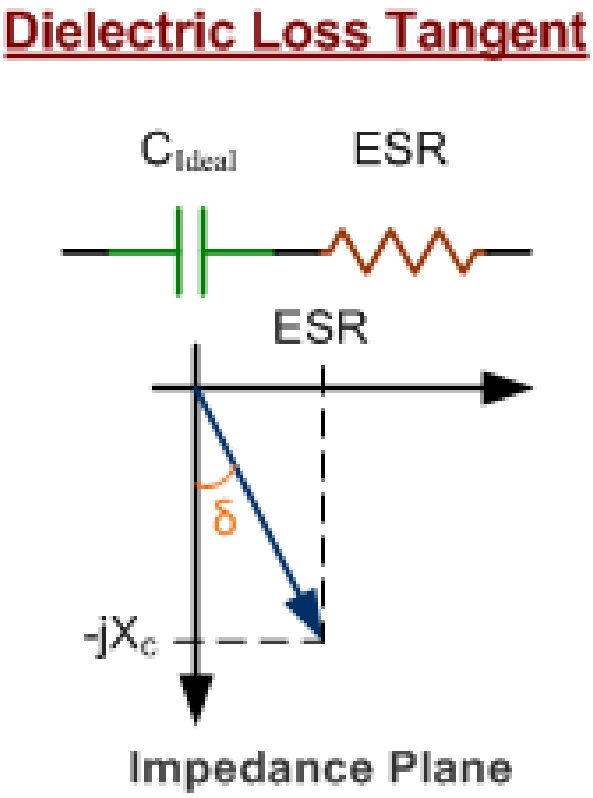

Figure 2.1: This figure shows how loss tangent is related to the impedance vector (RFcafe, 2012)

.

The absorption coefficient, α, is related to the transmitted intensity I_x, the incident intensity, I_0, of the incident wave onto a material of thickness, x, by

$I_x = I_0 e^{-\alpha x}$

where α has units of cm^{-1}; this is known as the exponential law of absorption (Jenkins & White, 1982).

It was found that paraffin wax has a similar dielectric constant to plastic explosives (Lamb, 1996), (Kemp et al., 2006) and (Hu et al., 2006), so wax was a suitable replacement for using real explosives. Kemp et al (Kemp et al., 2006) give values around 1.5 to 1.6 for the refractive index of explosives at a few terahertz. Hu et al. (2006) gives the average refractive index of RDX as 1.7 for 0.2 to 2.6 THz and an absorption coefficient for RDX of between 30 to 60 cm^{-1} for the 0.2 to 2.6 THz band. Yamamoto et al. (2004) gives a refractive index of 1.9 for C4 and an absorption coefficient of $40/cm^{-1}$ in the terahertz range. Paraffin wax has a refractive index of 1.48 at 120 GHz and a loss tangent of 27×10^4 given by Lamb (1996).

Another variety of frequency modulated radar makes use of a technique known as pulse compression. Pulse compression involves transmitting a wide band frequency waveform without resorting to a narrow time duration pulse. This is often done using a chirped pulse, where the frequency of the pulse changes with time. Figure 2.2 shows a chirped pulse, which is essentially the same as pulse compression. If one can transmit in the frequency domain with constant amplitude, then in the time domain this will be a delta function. The technique is often called pulse synthesis - the narrow time domain pulse is synthesised in the frequency domain.

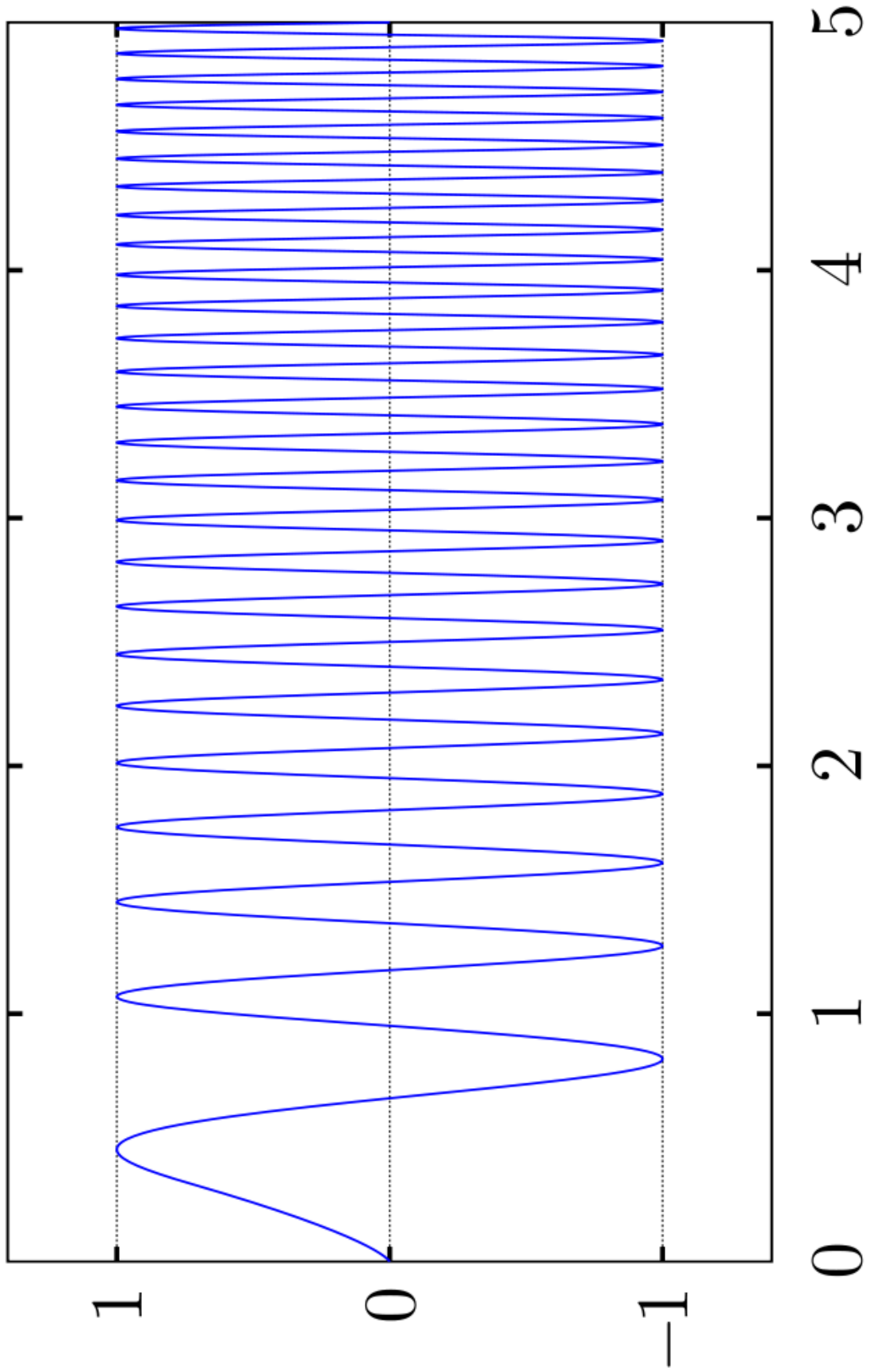

Figure 2.2: A linear chirped pulse, the frequency increases with time (WikiCommons, 2011).

Mixing of multiple radio frequency signals is a key concept of radar, although the technique is used in many other areas of electronics, optics and other processes where nonlinear effects are present. Mathematically, mixing is the multiplication of signals in the time domain. When two real signals are multiplied the resultant signal is the inverse Fourier transform of the convolution of the Fourier transforms of the two signals. In the simple case where the multiplied signals are sinusoidal (i.e. they have only one non-zero frequency component in their spectra), then the resultant, multiplied, signal is composed of sinusoids with frequency components equal to the sum and the difference of the original signals' frequency components.

A good example of the mixing of signals in radar is found in homodyne FMCW (Frequency Modulated Continuous Wave) radar, where the modulation of frequency in a linear manner with time allows ranging according to the following argument:

A pulse is transmitted which ramps linearly with frequency, it scatters off a target and is then received. The received frequency is related to time because the pulse is ramped and a frequency shift is caused by the time it takes the pulse to travel to the target and back.

The transmitted and received signals are mixed together and FFT'd; this produces the sum and difference frequencies and these are low pass filtered to give only the difference frequency and that difference frequency is a function of the range to the target. This arises because a time reference is coded in to the frequency ramping (Brooker, 2005).

A similar FM technique is known as stepped frequency; in this case the transmitted frequency is changed with time in a series of discrete steps. A stepped frequency pulse is transmitted and then the return received; this is repeated for several hundred frequencies to create a discrete frequency domain response which can then be transformed into the time domain (Hausner & West, 2007).

Using FM techniques it is possible to synthesise a sharp pulse in the time domain. This synthesis is possible because a wide frequency band is equivalent to a narrow duration pulse (see equation 2.12). The word synthesis is used as the pulse physically

transmitted is not of short temporal duration but contains the wide frequency spectrum of a narrow duration pulse. This was first demonstrated using the stepped frequency method at Stanford University in 1972 (Robinson et al., 1972).

The effect of range on the received signal strength of a radar signal is related to the transmitted power of the signal, the area of the antenna and the antenna gain. The gain of the antenna is determined by the size and shape of the antenna, the frequency of operation and the antenna losses. The gain of some simple shaped antenna are given in (Levanon, 2004).

One form of the radar equation gives the received signal power, P_r, as

$$P_r = \frac{P_t G_t}{4\pi R^2} \frac{\sigma}{4\pi R^2} A_e \tag{2.16}$$

where P_t is the power radiated by a radar in watts from an antenna of gain G_t at a distance R (Skolnik, 1990). A_e is the effective area of the receiving antenna in square metres and a target has a radar cross section σ, located at a range of R. The radar equation is often given using dB-power, for example in dB watts.

The gain of an antenna is defined as

$$G_0 = k_0 D \tag{2.17}$$

where G_0 is gain with respect to an isotropic source, k_0 is ohmic loss factor where $0 \geq k_0 \leq 1$ and D is the directivity. The factor $k_0 = 1$ if the antenna is lossless. It is assumed that the antenna is matched to a specified impedance (Kraus, 1988).

The directivity, D, of an antenna is the ratio of the power radiated in a specific direction to the power radiated by an isotropic antenna.

It is possible to increase antenna directivity and therefore gain by using a suitably positioned reflective or refractive focussing element such as a mirror or lens. Such an addition will increase the size and weight of the antenna.

An antenna with high gain is efficient and projects the majority of the transmitted power into a narrow, directional beam. Conversely, a low gain antenna may be

inefficient and will radiate power in a more isotropic distribution.

A waveguide is a type of microwave transmission line which is used to connect a transmitter or receiver to an antenna. They are almost lossless at microwave frequencies and are capable of transmitting high power. They have a cut-off frequency which determines the lowest useable frequency for a given waveguide. A waveguide uses a single conductor so cannot transmit the transverse magnetic mode. The first allowed mode a waveguide can transmit is the transverse electric or $TE_{1,0}$ mode. Generally the cut-off frequency is given by

$$f_{m,n} = \frac{c}{2\pi\sqrt{\epsilon_r \mu_r}} \sqrt{(\frac{m\pi}{a})^2 + (\frac{n\pi}{b})^2} \tag{2.18}$$

Waveguides used in microwave engineering are metallic transmission lines typically used to connect a transmitter or receiver with an antenna, they are used because they can handle high transmitter powers, are very low loss and are well shielded from adjacent channel interference.

Waveguides act as a high pass filter, frequencies below the cut-off frequency do not propagate along the waveguide. The electric and magnetic fields will not propagate but instead die out quickly within the waveguide. Such EM fields, that decay without dissipative loss are referred to as evanescent waves. The cut-off frequency, f_c, for the $TE_{1,0}$ mode for a rectangular waveguide of dimensions a by b where a is $> b$, is given by

$$f_c = \frac{1}{2a\sqrt{\mu_r \mu_0 \epsilon_r \epsilon_0}} = \frac{c}{2a\sqrt{\epsilon_r \mu_r}} \tag{2.19}$$

where c is the speed of light, μ_r is the relative permeability and ϵ_r is the relative permittivity of the material filling the waveguide, μ_0 and ϵ_0 are the permeability and permittivity of free space respectively. Note that the cut-off frequency of the $TE_{1,0}$ mode is independent of the short length b of the waveguide (Kraus, 1999).

The bandwidth carrying capability of a waveguide operating in the $TE_{1,0}$ mode is inversely proportional to the waveguide dimensions. Therefore a small, high frequency,

waveguide will be able to carry signals with a larger absolute bandwidth. The $TE_{1,0}$ mode has the E-field polarised such that it only has a component across the shorter dimension.

In general, any electromagnetic disturbance in the waveguide can be written as a superposition of the $TE_{m,n}$ and $TM_{m,n}$ modes. Furthermore, in both TE and TM cases the electric and magnetic fields have a non-zero component in both x and y directions, but for the fundamental $TE_{1,0}$ mode the electric field component along the longer dimension of the waveguide is zero. When this radiates into free space the EM waves are linearly polarised (Kraus, 1999).

2.2 Receiver types

A microwave receiver is a device used to amplify the weak signal that is collected by the antenna in a radar, radio or other communications system (P-N Designs, 2011).

A comparison of direct detection, homodyne and heterodyne receivers is given below.

Direct detection is where there is no processing of the received pulse with the transmitted pulse. In this configuration there is simply transmission of a radar waveform and reception of the power in that waveform after it has been scattered. No phase information of the received signal is obtained.

Doppler radar is an example of a homodyne receiver, where the received waveform is mixed with a fraction of the transmitted signal to measure the phase, they are low cost and their uses include police radar guns to measure speed (P-N Designs, 2011).

A heterodyne system uses a mixer, which mixes together two input signal frequencies to produce sum and difference frequencies at the output (Lesurf, 1990). A superheterodyne receiver features a radio frequency (RF) section which selects the desired signal frequency, this is then mixed with a local carrier frequency to produce an intermediate frequency (IF) in a frequency changer. The IF is then amplified and detected by mixing the transmitted waveform. The advantages of the heterodyne re-

ceiver are better selectivity, simple tuning and the RF circuit bandwidth is not critical because the receiver selectivity is mainly determined by the IF amplifiers. The main disadvantage is image channel interference, the image frequency occurs because two RF frequencies can be down converted to the same IF with a single local oscillator (Silva, 2001).

A Vector Network Analyser is a common piece of laboratory equipment used to measure complex (magnitude and phase) transmission and reflection. It can be used to measure impedance, VSWR (voltage standing wave ratio), loss, gain, isolation, and group delay of any two ports of a multi-port network (P-N Designs, 2011). It is used as transmitter and receiver to collect the data in this thesis.

S-parameters can be defined for any collection of linear electronic components and they are algebraically related to the impedance parameters (Z-parameters). A network has n inputs and n outputs which are the complex amplitudes of the waves; the received waves are given by the vector R and the transmitted waves are given by vector T. The transmitted waves are related to the received waves by the matrix equation $R = ST$ where S is an n by n square matrix of complex numbers called the "scattering matrix"(Jefferies, 2012).

$$\begin{pmatrix} R_1 \\ R_2 \end{pmatrix} = \begin{pmatrix} s_{11} & s_{12} \\ s_{21} & s_{22} \end{pmatrix} \begin{pmatrix} T_1 \\ T_2 \end{pmatrix}$$

2.3 Lenses

The diffraction limit is a function of the size and shape of the antenna and the wavelength or frequency of operation. Diffraction limited systems are those where the ultimate resolution of the system is limited by diffraction. The diffraction limited resolution θ of the cassegrain antenna being used is 0.3 degrees for a dish diameter of 64 cm as given by the Rayleigh Criterion

$$\theta = 1.22\lambda/D \tag{2.20}$$

Lenses are generally placed with their focal point near the aperture of the microwave horn and can be treated as a phase shifting device which produces a plane wavefront from the rays emerging from the effective point source at the phase centre of the horn. By using the lens as a phase shifter, the flare-angle of the horn can be made much larger than would be required if its radiation pattern were to be limited by diffraction from the non-phase corrected electric field distribution in the aperture. A lens corrected horn can be much more compact than a simple feed-horn having equal directivity or gain (Goldsmith & Moore, 1984).

In a practical lens system the beam will be truncated by the finite lens diameter. The truncation level of the beam is given by the edge taper, T_E, as the power density at the centre of the lens relative to that at the edge, given by

$$T_E(dB) = 2.17(\frac{D}{\omega(f)})^2 \tag{2.21}$$

where D is the lens diameter and $\omega(f)$ is the beam radius a distance f from the beam waist. For a Gaussian Optics Lens Antenna (GOLA) with a T_E value of approximately 11 dB, the on axis gain , G, is given by

$$G(dB) = 20log(\frac{\pi D}{\lambda}) - \delta G \tag{2.22}$$

from Goldsmith & Moore (1984) where D is the lens diameter, λ is the wavelength and δG is the reduction in gain below an ideal lens.

For a 0.3 metre diameter lens at 3 mm wavelength, taking the value of δG as -1.0 from Goldsmith & Moore (1984) gives an on axis gain of $50dB$, this is a linear intensity concentrating factor of 100,000.

Gaussian Optics Lens Antenna (GOLA) are designed using the principles of Gaussian optics rather than Geometric optics, where the image spot is replaced by a beam waist. The lens is separate from the microwave horn rather than at its aperture. Quasi-optical techniques allow flexibility in designing for highest gain or lowest sidelobes (Goldsmith & Moore, 1984).

The standoff distance requirement is typically ten metres. This comes from the requirement to scan a target without their knowledge and to protect the operator of the detection system.

To avoid interference from different parts of the body, quasi-optical techniques are used to focus a beam onto the torso of the target so that reflections from the arms for example do not interfere with the desired return from the torso. The signal from the detector is a sum from all the targets within the field of view of the receiver, so if the spot size is kept smaller than the body, it can be steered across the target to discriminate the location of a concealed weapon (Andrews et al., 2008).

The most common lens design problem is to convert the spherical phase front from a point source at the focus of the lens into a plane phase front across the aperture. By diffraction theory, a plane phase front results in the most directive pattern for an aperture of a given size with a given amplitude distribution across it (Silver, 1949).

For a cassegrain antenna as shown in figure 8.2, Hannan (2002) says that the antenna is intentionally defocused by moving the sub-dish a small distance toward the main dish. This technique can be used to provide variable beamwidth. By moving the sub-dish away from the main dish the antenna can be focussed toward a point nearer than the far field (Hannan, 2002).

If the secondary mirror of a cassegrain antenna is placed within the focal length of the primary, then the rays will be reflected by the primary mirror.

For a cassegrain antenna, geometry gives the radius of curvature, R, as

$$R = \frac{D^2}{8h} \tag{2.23}$$

where D is the diameter of the dish and h is the height of the bowl, assuming the cassegrain surfaces are spherical. In reality, the cassegrain primary reflector is parabolic and the secondary reflector is hyperbolic. For the dish used here, D was measured as 64cm, and h was measured as $11cm$ so $R = 47$cm.

Assuming paraxial rays

$$f = -\frac{1}{2}R \tag{2.24}$$

where R is radius of curvature and f is focal length of the primary dish. So the focal length of the dish is $f = 24$cm.

Mathematically, the reflecting surfaces are equivalent to lenses (ray optics), then the lens makers equation gives

$$\frac{1}{f} = \frac{1}{u} + \frac{1}{v} \tag{2.25}$$

where f is focal length, u is object distance and v is image distance.

The cassegrain system needed to be able to focus to any distance, so a nearest object point of one metre was chosen and a far point of infinity, for the dish to be focussed to any distance. For a focal length of $24cm$ and an image at infinity, $u = 24$cm. For an image at $100cm$ and a focal length of $24cm$, the object distance is $30cm$. So to vary the focal point of the cassegrain from $100cm$ to infinity, the secondary reflector must be able to move from $24cm$ to $30cm$,neglecting diffraction effects. To allow for the uncertainty in focussing the system, the mechanical movement was designed to be from $18cm$ to $35cm$.

2.4 Refractive Index and Dielectric Constant

Biological tissues behave as lossy dielectrics. They are made of polar molecules, such as water, but they also have charges that can move in a restricted way. The charge carriers are ions, so the biological tissues behave like an electrolytic conductor in which ions are able to migrate in response to an external applied field. They also exhibit characteristics of a dielectric, such as polarisation and orientation of permanent dipoles with the applied field (Peratta et al., 2010). Table 2.1 shows conductivities of various material types. Conductivity is related to the skin depth of an electromagnetic wave in a conductor.

The complex permittivity of human skin at 37 ℃ and 90-100 GHz was measured by Alabaster (2004) as $8.8(+2.6/-2.3) - j5.5(+1.6/-1.4)$.

Type of material	Typical conductivities $\sigma[S/m]$
Perfect Conductor	∞
Metals	10^4
Electrolytes	$1 - 10^2$
Bio-tissues	$10^{-4} - 10^{-2}$
Semiconductors	$10^{-4} - 1$
Dielectrics	10^{-10}
Perfect dielectric	0

Table 2.1: A table of conductivities of different types of materials (Peratta et al., 2010).

The skin depth, δ, of an EM wave in a lossy dielectric is given by

$$\delta = \frac{1}{Im\{\frac{2\pi\nu}{c}\sqrt{\epsilon_r}\}} \tag{2.26}$$

where complex relative permittivity, ϵ_r is given by

$$\epsilon = \epsilon' + j\epsilon'' \tag{2.27}$$

and ϵ' is the dielectric constant, and ϵ'' is given by

$$\epsilon'' = \epsilon_0 \epsilon_r'' \tag{2.28}$$

where $\epsilon_0 = 8.854191 \times 10^{-12} Fm^{-1}$, ϵ_r'' is the relative dielectric loss factor of the dielectric and ν is the frequency and c is the speed of light in free space (Alabaster, 2004).

Therefore, the skin depth of an EM wave at 90GHz in human skin is 500 microns.

Material	f (GHz)	T (K)	n	ϵ'	$tan\delta * 10^4$
PE	100	300	1.5185	2.3058	3.7
Paraffin wax	2-300	300	1.52	2.3	10

Table 2.2: Table of useful refractive indices (Lamb, 1996)

Table 2.2 shows useful refractive indices for materials relating to concealed explosives detection. The loss tangent, $tan\delta$, in table 2.2 is a property of a dielectric material which quantifies its dissipation of electromagnetic energy. The term refers to the tangent of the angle in a complex plane between the resistive (lossy) component of an

electromagnetic field and its reactive (lossless) component (Ramo & Whinnery, 1994). Maxwell's equations are solved for the electric and magnetic field components of the propagating waves that satisfy the boundary conditions for a specific geometry. In such electromagnetic analysis, the parameters permittivity ϵ, permeability μ, and conductivity σ represent the properties of the media through which the waves propagate(Ramo & Whinnery, 1994). The permittivity can have real and imaginary components such that

$$\epsilon_r = \epsilon'_r + j\epsilon''_r \tag{2.29}$$

The real and imaginary parts of the complex permittivity are given by

$$\epsilon' = \epsilon'_r \epsilon_0 \tag{2.30}$$

$$\epsilon'' = \epsilon''_r \epsilon_0 \tag{2.31}$$

respectively, where ϵ' is the real part of the dielectric constant and ϵ'' is the imaginary part of the dielectric constant.

ϵ'' is the imaginary amplitude of permittivity attributed to bound charge and dipole relaxation phenomena, which gives rise to energy loss that is indistinguishable from the loss due to free charge conduction that is quantified by σ. The loss tangent is defined as the ratio (or angle in complex plane) of the lossy reactance to the electric field E in the curl equation of the lossless reactance (Ramo & Whinnery, 1994):

$$tan\delta = \frac{\epsilon''}{\epsilon'} \tag{2.32}$$

The wavelength in the dielectric is given by

$$\lambda = \frac{2\pi}{k} = \frac{\lambda_0}{n} \tag{2.33}$$

where k is the wavenumber, λ_0 is the wavelength in free space and n is the real part of

the refractive index of the material (Read, 1980).

Using active scanned millimeter wave radar gives a detection technique which can provide the depth of the material rather than an intensity contrast image of the target. A plane wave, of amplitude E_T, has electric field, E, incident on the dielectric slab as shown in figure 2.3

$$E = E_T e^{(-2\pi f j(t-z/c))} \tag{2.34}$$

where f is the frequency of the incident wave in the z-direction on a parallel slab of dielectric material of thickness d, refractive index n and distance from the transmitter L (Andrews et al., 2008).

The wave reflects from the front and back faces of the slab R and R' respectively, as shown in figure 2.3. The return wave is given by E_R, if the backing material can be approximated as a semi-infinite layer of refractive index n' and multiple reflections are neglected then

$$E_R = E_T\{R + R'e^{(4\pi f jnd/c)}\}e^{(4\pi f jL/c)} \tag{2.35}$$

where

$$R = \frac{(n-1)}{(n+1)}, \tag{2.36}$$

$$R' = \frac{(n'-n)}{(n'+n)} \tag{2.37}$$

and c is the velocity of light. The relative phase shift between the reflections from the front and back faces gives rise to frequency-dependent interference between two signals. A square law detector is a diode detector used to convert amplitude modulated microwave signals to a voltage. For a certain range of power levels, a detector's output voltage is proportional to its incident power measured in watts. If the return signal is measured by a diode which is a square law detector, then the signal is proportional to

$$|E_R|^2 = |E_T|^2\{|R|^2 + |R'|^2 + 2|R||R'|cos(4\pi fnd/c)\} \tag{2.38}$$

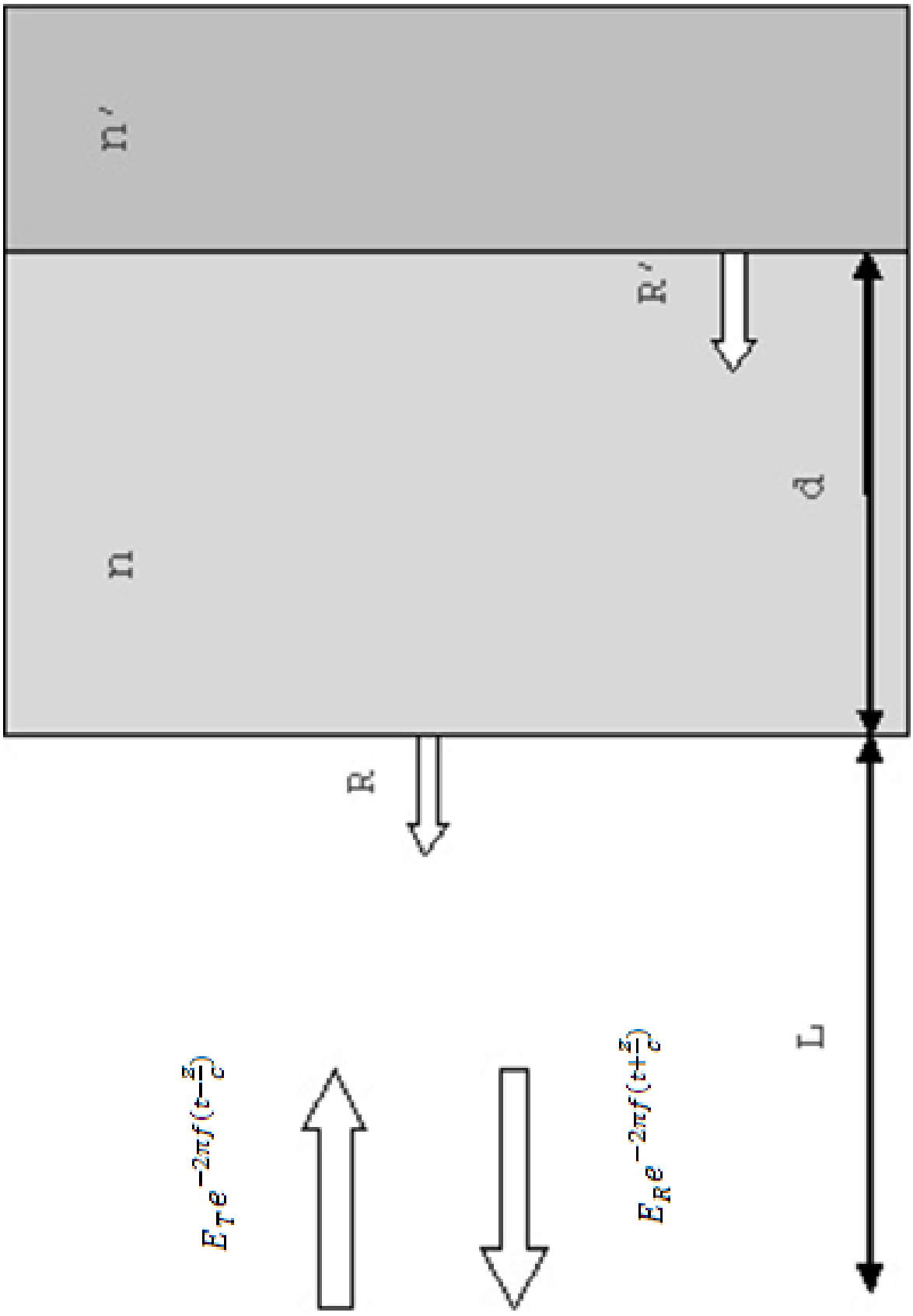

Figure 2.3: This figure shows the incident wave on a paraffin wax block of refractive index n, with a backing of refractive index n'. (Andrews et al., 2008)

This shows the sinusoidal dependence on frequency, and the optical depth of the material, nd is proportional to the period of oscillation (Andrews et al., 2008).

2.5 Black Body Radiation

All objects with a non-zero temperature radiate energy. The relationship between radiated power and frequency of radiation is described by the well known Planck's Law. The human body at 310 kelvin, radiates mostly in the infrared, with a 9350 nm peak wavelength from Wien's Displacement Law, but the blackbody curve still has a significant magnitude at millimetre wavelengths, so this radiation can be detected by using a sensitive millimetre wave receiver such as a MMIC receiver. Tamyis (2005) states that the emissivity of the human hand at 20 GHz is 55% of that of a black body and at 38 GHz it is 68%; these values were calculated from measuring the dielectric constant of the palm of the hand over the frequency range 20 to 38 GHz. Skin emissivity in the infrared region of the electromagnetic spectrum is fairly constant between 3 and 15 μm at a value of 0.975 $\pm$0.05 according to Jones (1998).

The blackbody curve for an object at 300 K is shown in figure 2.4. The human body has contrast against the background because they are at different temperatures and have different emissivities. This phenomenon can be used for concealed weapons detection if there is sufficient contrast between the weapon and the body as a result of temperature and emissivity differences between the objects.

An image is formed by scanning across a scene and measuring the power received at each point. This is then plotted to form an image of the body against the background (Macfarlane et al., 2002) (Dill et al., 2007).

However, the human body is only approximately a blackbody at infrared wavelengths. A blackbody absorbs all incident radiation and obeys the Stefan-Bolztmann Law. The energy emitted from a blackbody is given by the Stefan-Bolzmann Law $M = \sigma T^4$ where M is the energy emitted, T is the temperature in Kelvin and σ is the Stefan-Bolzmann constant ($5.6697 \times 10^{-8} W m^{-2} K{-}4$) (Gibson, 2000). Most objects do not obey this law and a constant, termed emissivity (ϵ), has to be introduced into the Stefan-Bolzmann Law:

$$M = \sigma \epsilon T^4 \tag{2.39}$$

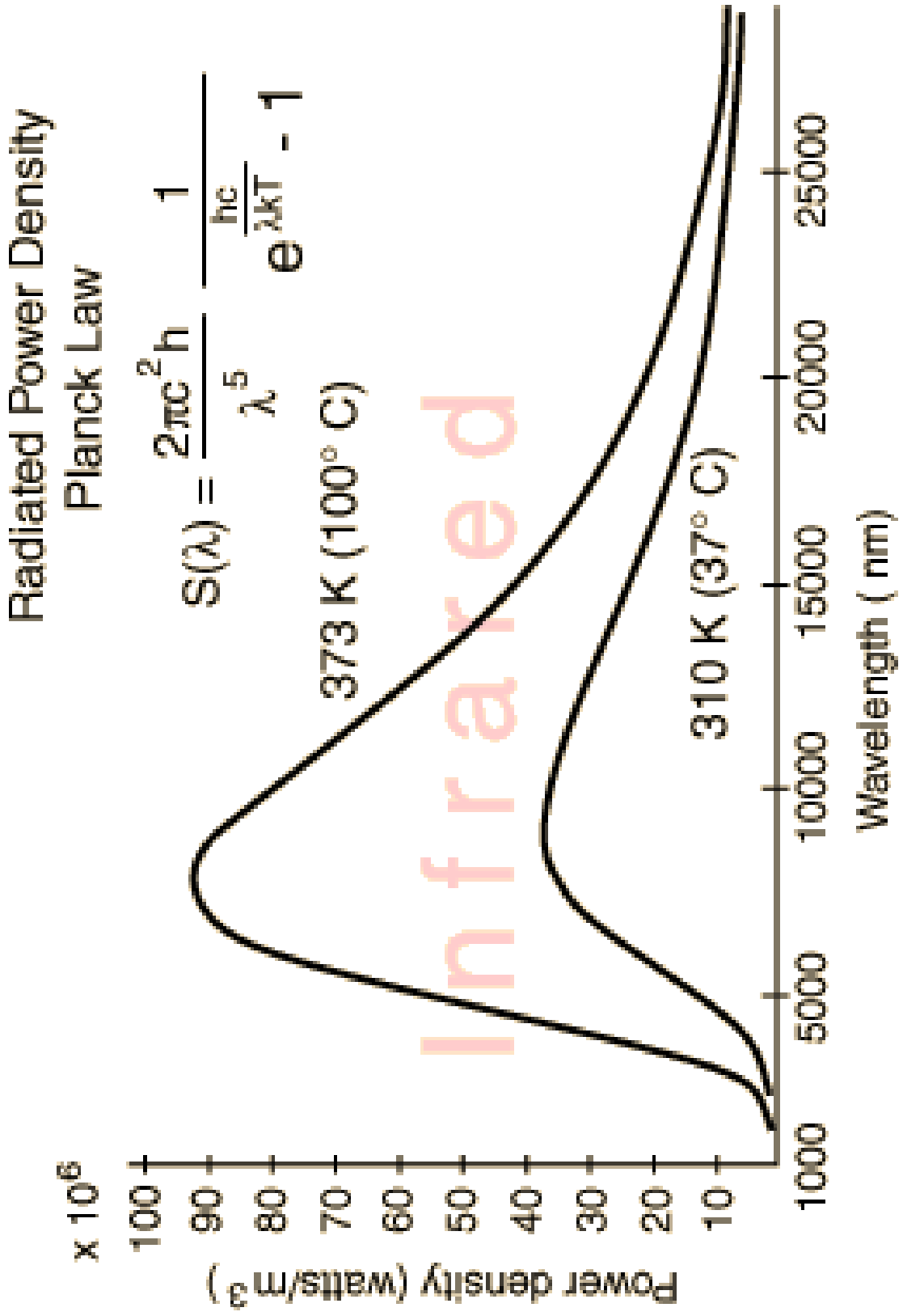

Figure 2.4: Blackbody curve at 310K and 373K (GeorgiaStateUniversity, 2011)

where M is the energy emitted (emittance or exitance), T is the temperature measured in Kelvin, ϵ is the emissivity and σ is the Stefan-Bolzmann constant (Gibson, 2000).

The emissivity is defined as:

$$\frac{\textit{Energy actually emitted by unit area of a surface in unit time at a given temperature}}{\textit{Energy emitted by unit area of a blackbody in unit time at the same temperature}}$$

The emissivity of a blackbody is equal to 1 and all other materials have a value less than 1; most objects have a emissivity which is dependent on wavelength (and therefore frequency) as well. Emissivity is wavelength dependant, a substance may have a particular ϵ value at one wavelength and a different value at another, so the human body will have a different emissivity at millimetre wavelengths than at infrared wavelengths. The emissivity of the human body at millimeter wavelengths is given as approximately 1 by McMillan et al. (1998) and the emissivity of a metallic weapon is given as 0.2. At infrared wavelengths, Herman (2007) gives the emissivity of human skin as 0.95 whereas the emissivity of iron is given as 0.28.

It is often assumed that the variations in grey scale (or colour) on a thermal image show variations in temperature. $M = \sigma\epsilon T^4$ shows that the emittance is also dependant on the emissivity ϵ. The tonal variations will be indicative only of temperature variations if the emissivities of different parts of the scene are similar (Gibson, 2000).

2.6 Neural Networks

Neural networks are made up of inputs and outputs with interconnections which can be tuned or 'trained' to produce a desired output, they are similar to those in a biological nervous system. The connections between inputs and outputs determine the function of the network. By adjusting the values of the connections (weights) between elements the network can be trained. They are usually trained to match an input to a particular output (target) within a specified tolerance. A network usually consists of many input-target pairs (Math-Works, 2009).

Matlab's Signal Processing Toolbox contains a function called 'xcorr', this function performs cross-correlation. Xcorr estimates the cross-correlation sequence of a random

process (Math-Works, 2009). This function was used in processing data to re-order data which was similar to its neighbour in an array of data, by aligning data sets containing more than one peak in the time domain.

Finite Element Analysis is a numerical technique which gives approximate solutions to differential equations. The problem geometry is drawn and then divided into a finite number of smaller regions, triangles can be used in 2-D or tetrahedrons in 3-D. The equations are then solved for each finite element and summed for the whole problem (Pepper, 1992). COMSOL (2009) was used to model and solve lens and horn designs.

Chapter 3

Literature Review

3.1 Introduction

Concealed weapons detection is an active research topic. In 2002 the US Transport Security Administration estimated its funding requirements would be $6.8 billion, mostly for aviation security (Mead, 2002). Passive emission in the millimetre wave band can be used to form images of people which can be used for security screening. Differences in emitted brightness between the human body and a concealed object provides the contrast in the image. The body and the object must have different emissivities, surface temperature or reflectance for the required contrast to be present. The contrast image can then be viewed by an operator or processed autonomously by a computer and a decision as to the potential threat made as shown in figure 3.1.

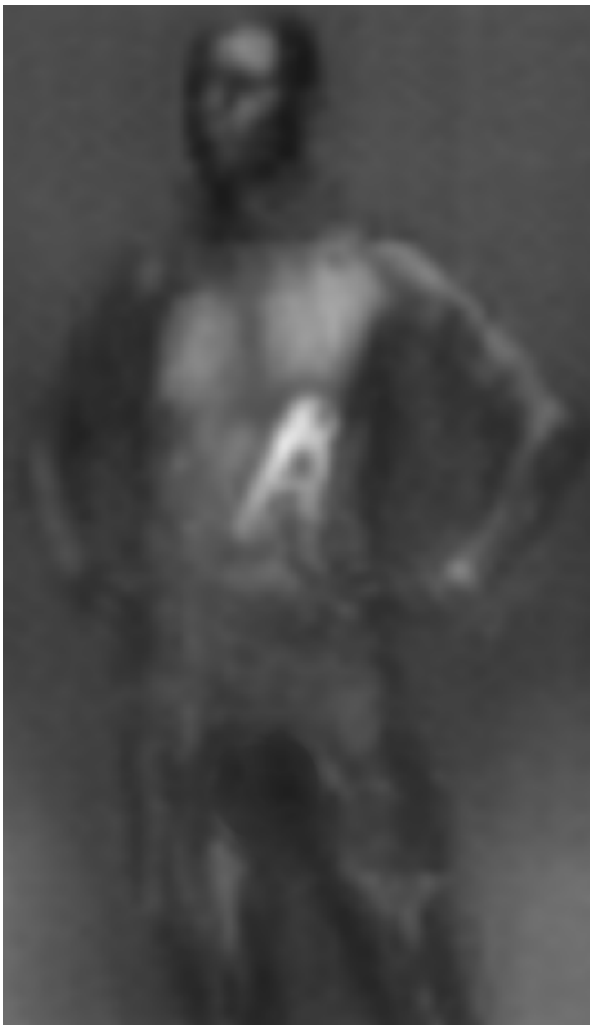

Figure 3.1: This figure shows a concealed metal object on the person when outdoor (cold sky) contrast is used to illuminate the subject (Doyle et al., 2004).

Active imaging uses radiation transmitted from a millimetre wave source and the subsequent reflections to form an image of a target. The difference in reflectivity of the body and any concealed weapon are used to form an image from which the presence of the weapon can be seen. The black body radiation emitted by people and objects can be used, but passive techniques tend to suffer from poor contrast unless used outdoors where the sky provides a cold source which improves contrast; the sky can be used as a reference temperature (Appleby, 2004).

Creating images of people causes privacy issues (Agurto et al., 2007), because of this non-imaging techniques have been investigated. These include active and passive techniques; active techniques produce a stronger signal from the target but passive techniques may be preferred if radiating microwaves would prevent covert use of a detection system. In the work described here, active techniques are used to measure the radar return from a target and the reflections from the concealed weapons.

In 1995 imaging systems that can operate through clothing were reviewed by Currie et al. (1995). As part of this work, a passive millimetre wave radiometer detection system was reviewed. The system looks for small variations in temperature between a concealed weapon and the background. The body and the weapon will be at different temperatures unless the weapon is very close to the body or artificially heated; the system operates in the 94GHz band. The radiometer was scanned across a scene and produced an image showing metallic and ceramic handguns through clothing.

Dallinger et al. (2005) present an active system which uses a wide-band lens and scans a bandwidth of 10GHz. This gives a spatial resolution of 1.5cm at a range of 1.5m. The sweep time is 15 seconds. The image produced covers an area which is 35 by 40 cm. The image contains a lot of clutter, these are bright reflections from the body which are not from the concealed object, they could be from the movement of the arms for example. The concealed object was detected but it is difficult to distinguish it from the background. Imaging systems can be broadly divided into two types. Systems using a lens have a low computer processing requirement, but the physical aperture needs to be large. Synthetic aperture systems require greater processing time, but can

have small apertures which can be scanned. Synthetic aperature systems can have the disadvantage of higher cost due to the multiple receivers needed. The skin effect of electromagnetic waves means that millimetre wavelengths do not penetrate human skin to more than a millimetre, supported by measurements of the permittivity of skin. The human body is a fairly good reflector. In this paper, they are using a PVC dummy to replace the human target. Illuminating the target from different angles would reduce specular reflections which result in bright spots or clutter in the image.

Terrorist threats and gun crime have become an increasing problem for governments and law enforcement agencies over recent years. Agurto et al. (2007) present an overview of different techniques which can be applied to concealed weapons detection.

Power levels used in active systems are typically less than that emitted by a mobile phone, so operating at these low power levels should not cause concern to regulatory bodies for EM power emissions or the public.

At infrared wavelengths (which are defined as $10^{-5}m$ or about 3000 GHz) it is difficult to detect weapons on the body because the temperature of the weapon is close to the body temperature and the infrared radiation is significantly attenuated in the clothing. The sensor simply sees the surface temperature of the clothing and not what lies underneath. Infrared sensors have much, much better noise-equivalent temperature than millimetre wavelength sensors and therefore better sensitivity and they also have far superior spatial resolution, so operate well as night vision cameras (Agurto et al., 2007). Millimetre wavelengths are defined as 1cm to 1mm or 30 GHz to 300 GHz.

Appleby & Wallace (2007) notes that explosives carried close to the body are partially transparent and partially reflective at an operating frequency of 100 GHz which produces a characteristic radar return which can be used to detect concealed explosives, also the reflectivity of the skin closely matches that of water. In their paper Appleby & Wallace (2007) conclude that a passive system required to penetrate all types of clothing will probably need to operate below 500 GHz.

3.2 Passive Imaging

Appleby et al. (2003) present a mechanically scanned real time passive millimetre wave imaging system at 94 GHz. The optics of the mechanical scanner are based on a Schmidt camera and conical scanner. It can be used to image through fog and cloud and could be used in surveillance and reconnaissance. The optics in this system are large and limit the scan rate of a reciprocating scanner. Deploying this scanner would be limited to installation in a fixed position as it would be difficult to follow a suspect along a street for example, with such a large system.

Appleby (2004) describe passive millimetre wave imaging and how it differs from terahertz imaging. Millimetre waves can image through bad weather conditions and can penetrate cloth and polymers, whereas terahertz is attenuated more than MMW by the atmosphere. For wavelengths above 1cm, conventional imaging becomes impractical due to the aperture size, so radar techniques are used such as synthetic apertures. Many materials are partially transparent to millimetre waves and the surface is smooth compared to the wavelength, reflections from the layers can be a useful technique for detecting the material. Atmospheric windows are regions of low attenuation by the atmosphere and are found at 35, 94, 140 and 220 GHz, which restricts the frequencies at which these systems can operate. Clothing is partially transparent to millimetre waves, so threat objects under clothing can be detected (Lamb, 1996). Terahertz frequencies are needed to spectrally identify materials according to Appleby (2004); THz spectra can be used to identify explosives to distinguish them from harmless substances.

Also Grossman et al. (2004) present a 94 GHz scanned millimetre wave imaging system, using polyethylene lenses which are used in a scanned focal plane array, using a microbolometer detector. The system operates at distances greater than one meter with greater than one meter diameter field of view. The system which operates at 94 GHz is being scaled up to 650 GHz (Grossman et al., 2004). Power detection gives greater sensitivity using MMIC amplifiers, the draw backs are high cost and not being able to scale MMICs to frequencies above 200 GHz. Higher frequencies give improved spatial resolution but not improved sensitivity.

Chen et al. (2005) describe passive imaging techniques and the potential problems with active systems, which are; radiating microwaves at members of the public, displaying warning signs and covert operation.

Costianes (2005) describe weapons detection in public places for public safety, the ability to detect these weapons at a standoff distance of 10 metres is desirable. Lockheed Martin, in 2005 were developing a passive system operating from 80 to 100 GHz using Cassegrain optics to focus onto a scanner which produces an image (Costianes, 2005).

Grafulla-Gonzalez et al. (2005) use ray-tracing software, Zeemax and Matlab to model millimetre waves in their 2005 paper. They use a QinetiQ millimetre wave video imaging system at 9mm wavelength and the focal distance is 0.8m, the diffraction limit is 2cm in the focal plane.

Appleby & Anderton (2007) discuss the pros and cons of using millimetre wave and sub-millimetre wave imaging techniques for security applications and for imaging through poor weather conditions. Their conclusion is that millimetre waves are better suited to security applications for standoff distances because they are not as attenuated by the atmosphere as sub-millimetre waves (Appleby & Anderton, 2007).

Howald et al. (2007) shows that to engineer a millimeter wave camera requires the optical properties and RF properties of the system to be modelled. An important figure of merit for describing the performance of a sensor is channel sensitivity, which is also known as Noise Equivalent Difference Temperature. For this system NEDT is typically 0.5K for an integration time of 10 msec, this is the RMS noise which corresponds to an uncertainty in the temperature of the source to 0.5K (Howald et al., 2007).

Dill et al. (2007) present a line scanning imaging system at 30 and 94 GHz used to produce an image of a person behind a radome material in (Dill et al., 2007). The system is a passive radiometer, receiving the emission reflected from the body and sky. The difference in temperature between the material and the sky is used to calculate the dielectric properties of a concealed object.

Mechanical scanning provides a 2-D image from the linear imager. Martin et al.

(2007) present a real-time passive millimeter wave imaging system, for security scanning where a stand-off range is not wanted, using a single millimeter wave amplifier package. It uses frequency multiplexing to produce a large number of pixels. It takes about 20 seconds to scan a human body. The close-up operation allows for a 1.5 cm spot size; the system uses a convolution algorithm to blend adjacent pixels to reduce noise and smooth the image. The focal length is 30 cm and the system is designed to be used indoors, images are formed from the contrast of the body with the surroundings. Clothes are invisible on millimeter wave images, threat objects either reflect or absorb the millimeter waves and look like a dark area against the light body. Passive millimeter wave sensors cannot see through the body, so need to image from different angles. Images collected outdoors have more details due to increased contrast between the body and the cold sky, but low contrast objects can disappear in the clutter.

Reflective spectra have been found to be a way of identifying explosives by Rosker et al. (2007). Standoff distances are assumed to be over ten metres. Water vapour absorbs at terahertz frequencies as the water particles scatter and absorb. For passive imaging outdoors, the sky temperature at millimetre wavelengths is important to the performance of the imaging system. The sky temperature is the noise added to the receiver system dependant on the elevation angle and operating frequency, the temperature is typically less than ten Kelvin at the zenith (directly overhead) for microwave frequencies (Burke & Graham-Smith, 2010). It is an important consideration for detecting objects of different reflectivity. The sky temperature can affect the performance of the detection system by enhancing the reflectivity of objects to be detected such as a metal weapons (Rosker et al., 2007).

For a passive millimetre wave system, as frequency increases the contrast available decreases. The atmosphere has most effect on the signal to noise ratio due to its water vapour content (Rosker et al., 2007).

Timms et al. (2007) present a 190 GHz millimetre wave imager using MMIC-based heterodyne receivers. Higher frequency operation is an advantage because of increased spatial resolution. Different approaches have been tried; an array of millimetre wave

receivers or a mechanically scanned antenna with one receiver. Scanning the receiver produces high frame-rates, which are necessary in high volume applications such as airports. Passive imagers require 20 or more receivers to obtain the required sensitivity for real-time imaging. The transmitter is a 94 GHz source and a frequency doubler (Timms et al., 2007).

Yeom et al. (2011) present a technique which uses a lens and a 1-D receiver array composed of 30 receiver channels, and a mechanical scanner, which rotates the receiver array. They cite the problems of passive imaging as weak signals and system noise. Spatial resolution is limited by aperture size and will limit the quality of the images obtained. They aim to resolve some of these issues by using a segmentation technique to detect objects concealed on the body with an operating frequency of 94 GHz. The segmentation technique separates the body area from the background and then processes only the body area to detect the presence of concealed weapons. Bright patches can be seen in the images after processing, but the technique is computer processor intensive. Identifying multiple objects and classifying them was left as future work. Figure 3.2 shows an example image from this detection system. The gun can be seen on the image as a bright spot.

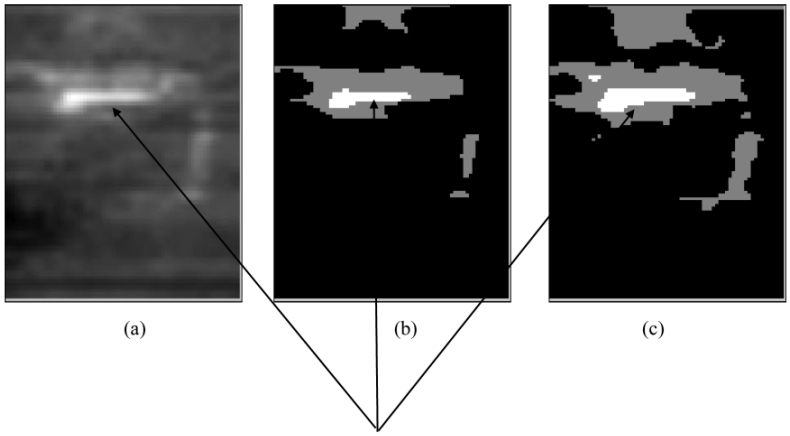

Figure 3.2: This figure shows a MMW image produced by Yeom et al. (2011) passive MMW detector. (a) shows the millimetre wave image, (b) shows the fully processed image and (c) shows the image processed by a shortened method.

3.3 Active Imaging

Goldsmith et al. (1993) aim to develop a focal plane array to operate at 3mm wavelength. Phased arrays have been suggested but developments have been limited by cost and complexity. Focal plane arrays have multiple feeds, a single focussing element, and multiple beams. A mechanically scanned single element produces a single beam, the scanner is moveable in all directions. It requires good illumination of the focussing element by the feed for a focal plane array. A combination of Gaussian beam optics and ray optics is used to simulate the array properties. Development of millimetre wavelength transistor amplifiers can be applied to imaging arrays. The advantages of frequencies between 30 and 300 GHz are low absorption by most dry dielectric materials, moderately high spatial resolution and compact optics. A scanned beam of millimetre wavelengths can suffer from 'glints' from edges of clothing etc. Glints are spurious bright reflections, usually from metallic objects.

Watabe et al. (2003) uses a feed forward neural network in pattern recognition for a real-time imaging system. The network is trained to recognise metallic letters. The operating frequency was 60 GHz using an Yagi-Uda array. To reduce the size of the images to input into the neural network, adjacent pixels were averaged with a 2 by 2 averaging mask. This reduced the number of pixels to a quarter of the original number.

Federici et al. (2005) present a review of terahertz imaging systems used to detect explosives and drugs. In the THz band, explosives and drugs have characteristic transmission or reflection spectra which can be used to detect these substances when concealed on a person. THz spectroscopy can be used to detect explosives and drugs through concealing materials such as clothing, plastics and cardboard because these materials are transparent to THz. By comparing measured spectra with known calibration spectra it is possible to detect and distinguish explosives and drugs from other benign objects, but such a system would have to store a large number of reference spectra to be practical. Federici et al. (2005) state that, in general, non-polar, non-metallic solids such as plastics and ceramics are at least partially transparent and reflective in the 0.2-5 THz range. Non-polar liquids are transparent as well, whereas polar liquids,

such as water, are highly absorbing. This is because absorption in the THz range of the electromagnetic spectrum is generally due to rotational motions of dipoles within a material. This is also true for the millimetre wave range of the electromagnetic spectrum.

One disadvantage of the spectral analysis technique is that features of the THz spectra can be sensitive to the way a sample is prepared, e.g. pellitized form. However, there are many spectral features of explosives which are reproducible and not sensitive to sample preparation so could be used as a method of detecting explosives.

A comparison of focal plane arrays and an interferometric technique was presented by Federici et al. (2005) and it was found that the focal plane array would take 30 times longer than the interferometric approach to acquire an image. Although the interferometric technique required more imaging processing (correlating) therefore it would be difficult to produce an image in real-time.

Federici et al. (2005) conclude that for close range scanning CW or pulsed modes of operation should be competitive, whereas real-time imaging needs development. THz spectra detection has some limitations on the type of materials it can detect, for example some explosives do not have a THz spectra below 3 THz. Stand-off detection is a big challenge because as the distance increases the attenuation by the atmosphere, dust and smoke increases; to overcome this, higher power sources need to be developed.

Doyle & McNaboe (2006) describe a mechanically scanned millimetre wave imaging camera capable of concealed object detection at stand-off distances up to 50m. Range information can be obtained by using FMCW (frequency modulated continuous wave) radar. The system only uses reflective optics, to minimise losses in the optical path. This system can be used in either portal or standoff mode. For use in portal mode it includes a thermally generated illumination scheme to improve image contrast. Metal objects were detected on people at distances up to 20m, with a scan time of 2 to 4 seconds. Combining the range function of FMCW radar and a video image of a scene in real-time would be the ideal user interface for a stand-off weapons detector.

The terahertz imaging technique used by Dickinson et al. (2006) uses full beam

scanned imaging of a target in azimuth and elevation using two-axis Fourier Transforms. A prototype system fast scans a small spot across a target. High resolution images were obtained using a technique similar to synthetic aperture radar.

HEMT (high electron mobility transistor) amplifiers have been developed for the 220 GHz band by Essen et al. (2007). The radar range resolution is determined by the bandwidth of the radar, large bandwidth is easier to achieve at higher frequencies. The radar developed by Essen et al. (2007) has a bandwidth of 8GHz. Imaging of a person with and without a gun was carried out, with a range resolution of 2cm.

Derham et al. (2007) present a prototype imaging system operating in the 60 GHz band using the frequency encoding technique. A single channel coherent receiver is used, the signal contains angular information about the scene encoded in frequency. Processing with a FFT constructs a one-dimensional image, each FFT point represents one of the beams of the antenna. The system was tested with a background of microwave absorber as shown in figure 3.3.

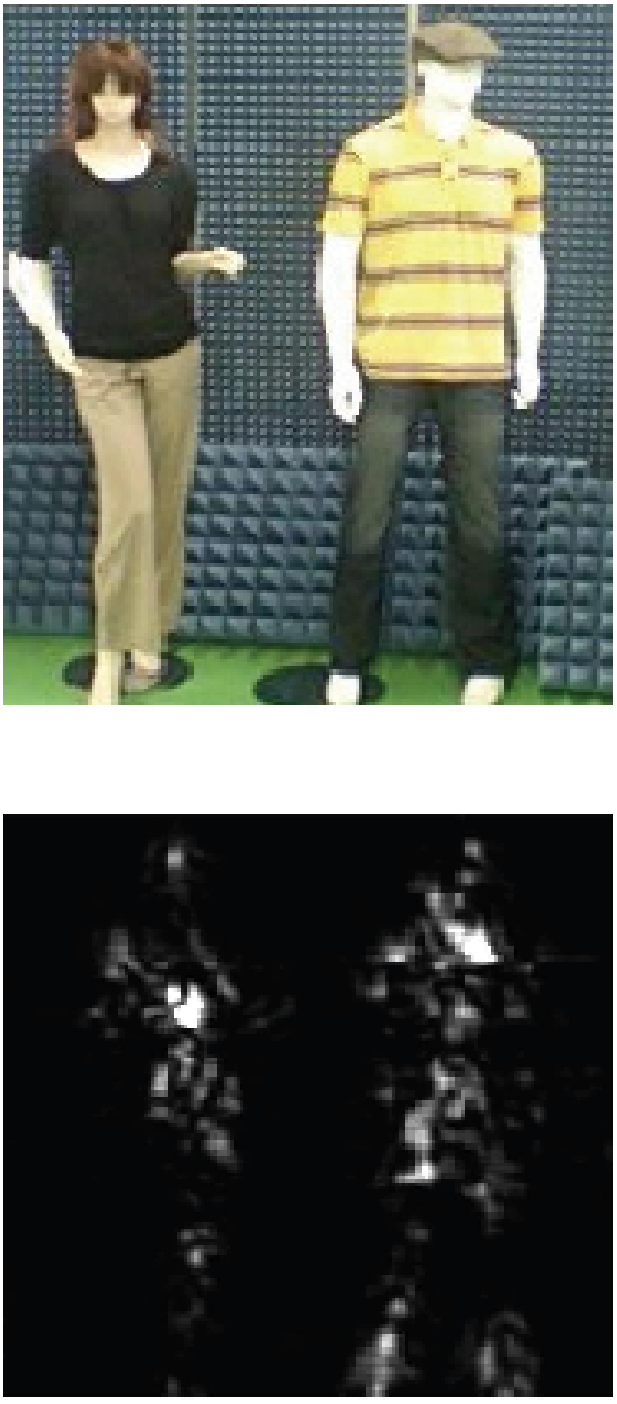

Figure 3.3: The top figure shows the optical image of two mannequins, the bottom figure shows the MMW image of the two mannequins to demonstrate the imaging performance of the system designed by Derham et al. (2007).

The outline of the mannequin is indistinct for both direct observation and through a thin plywood panel as shown in figure 3.4. Specular reflections from the flat panel caused signification image distortion.

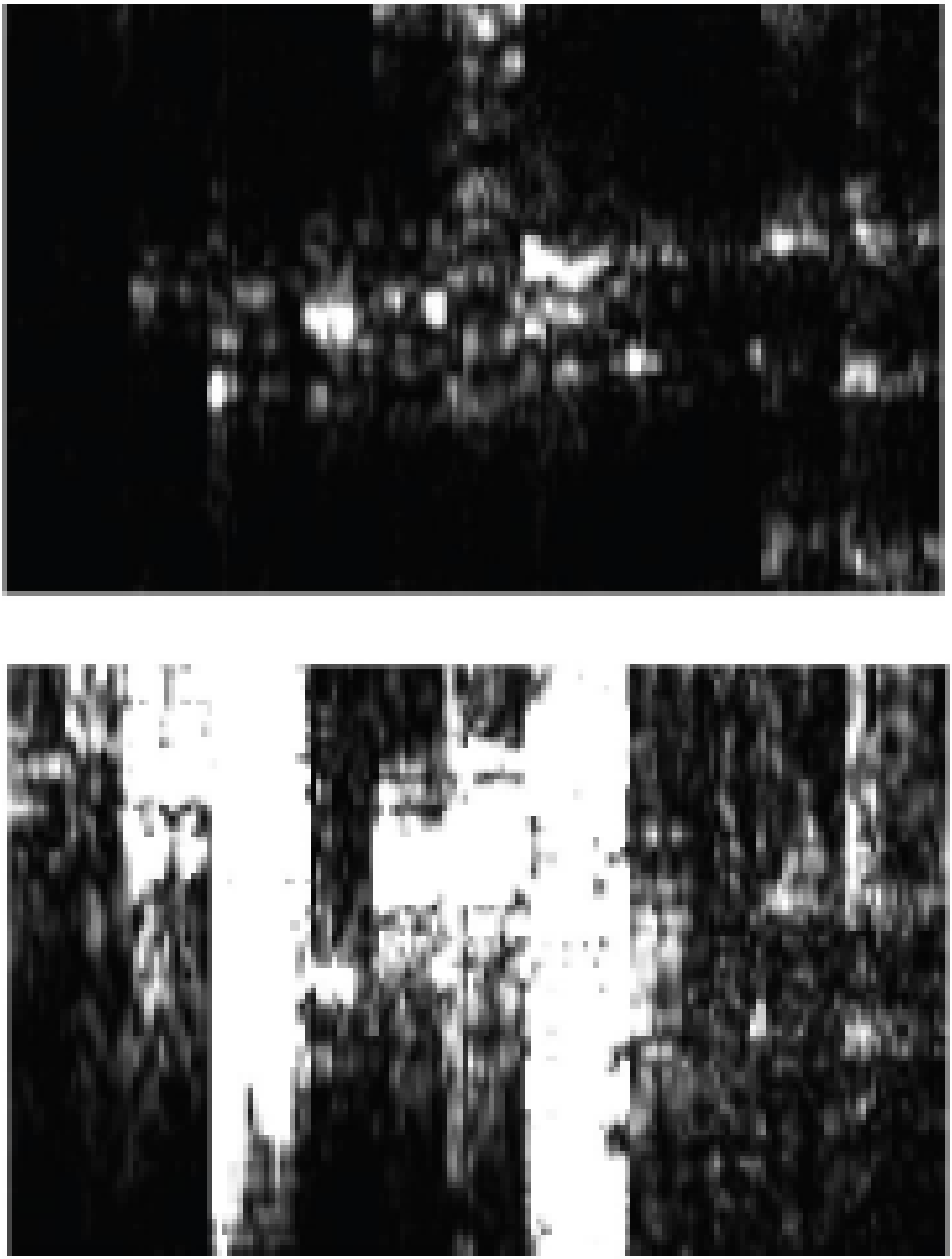

Figure 3.4: The figure shows the MMW image of a mannequin through a 3 mm plywood panel, with the detector on axis and then 30 degrees off axis (Derham et al., 2007).

Volkov et al. (2008) show that in indoor use the image contrast in a passive system is not enough for optimum imager operation (Volkov et al., 2008), artificial illumination mimics the sky illumination. An edge detection system is presented, which separates the return from concealed objects from the background such as the body. The system is fixed at a frequency of 94 GHz and uses a cassegrain mirror. The system provides a spatial resolution of 7 mm at a distance of 1.2 metres.

Two technologies are being tested in US and UK airports, x-ray back scatter imaging; using very low energy x-rays and millimeter-wave imaging (as just described). There are concerns over privacy due to constructing images of people. The manufacturers claim that these scanners pose no risk to human health according to Brown (2008).

Cooper et al. (2008) present a technique for active imaging using a 600 GHz radar. They use an image processing algorithm which will determine if the pixel belongs to the front or back surfaces of the target and use this to determine if there is a potential threat present. The ranges to the nearest and furthest object in the radar beam produce front and back peak pairs. Some peaks require manual re-selection after the image is constructed by the image processing algorithm as they are missed in the automatic process (Cooper et al., 2008). The image collection time was around 6 minutes.

3.4 Image Processing of Millimetre Wave Data

Artificial neural networks (ANN) were used to analyse terahertz images and classify the pixels of the image to their component material. An ANN is a computational mapping which can be optimised or 'trained' to detect patterns. The algorithm inputs are the reflected or transmitted THz power for a finite number of THz frequencies. The ANN is trained to recognise the intensity pattern of THz frequencies corresponding to explosives and other concealing materials. Then a previously unseen intensity pattern is presented as an input to the ANN it attempts to classify it as one of the known materials based on the library of THz spectra, this is done on a pixel by pixel basis.

To train the ANN a set of input / output data is presented to it and a set of internal parameters (weights) is optimised so that the outputs predicted by the ANN match the desired outputs with an acceptable tolerance. Network architectures typically contain a layer of input nodes accepting the input values, one or more hidden layers of nodes and an output layer of nodes. The multilayer perceptron (MLP) and radial basis function (RBF) are two NN architectures that have proved especially useful for THz image analysis. The input values for NN training correspond to spectral intensities at each frequency. The single output for each material of interest is an arbitrarily chosen integer value within a user-defined tolerance (Federici et al., 2005). This technique of training a ANN has proven especially useful in identifying the presence of explosives in millimetre wave data processing.

Haworth et al. (2005) discusses image processing techniques, they trial a sensor which could be used for passenger screening at airports.

3.5 Non-image Based Standoff Concealed Weapons Detection

Non-imaging approaches provide fast and portable solutions to concealed weapons detection which do not generate images and so remove the privacy concerns associated with image-forming systems, as well as significantly lowering the cost.

Millimetre waves are non-ionising radiation so are a safer alternative to using x-ray backscatter and similar techniques (Agurto et al., 2007).

Bowring et al. (2007) show that coherent frequency scanned millimetre waves centred on 60 GHz can be used to detect the presence of and measure the thickness of a block of dielectric material. This technique has applications in drugs and explosives detection. This is a Fabrey-Perot type technique. Fourier transforms of the data are used to detect the optical thickness of the material. The resolution of the system is given by the width of the frequency scan. The resolution obtained in this paper is 10mm. The Fourier transform assumes that the data are periodic, whereas the Berg

transform does not. The technique can be used at gigahertz and terahertz frequencies, as long as the frequency sweep is sufficiently large.

Active millimetre wave detection is suitable for layers of dielectric materials. In a further paper (Bowring et al., 2007) uses a scanned FMCW source. A dielectric slab produces a pattern of peaks and troughs in frequency space, Fourier transforming into optical depth space gives a peak at the optical thickness of the slab. Their method measures the thickness of the dielectric block and can be used to identify the presence of explosives or drugs by identifying a dielectric layer in front of the body. Their operating frequencies were 50-75 GHz and 75-110 GHz. They can get Fast Fourier Transform peaks for samples up to 160mm thickness. A low loss dielectric backed with a lossy dielectric is thought to approximate to layers of drugs or explosives worn close to the human body. The Burg transform gives better results than the Fourier transform, and it also removes the zero frequency spike.

Andrews et al. (2009) has presented a technique which uses active swept millimetre waves to detect concealed guns and explosives hidden on a person; this technique uses a lens to focus a millimetre wave beam onto a target. It allows detection at random points on a target. The only difference between a imaging and non-imaging approach is that in a imaging system multiple pixels are formed corresponding to multiple positions in space; a non imaging system only samples a single pixel.

Hausner & West (2007) show that a gun can be detected using its radar signature. A signal is transmitted in one polarisation and then received in the same polarisation and the orthogonal one, simultaneously. Receiving both polarisations provides more information on which to base a threat decision. The antennas used are patch array sections and the receiver is heterodyne.

Andrews et al. (2008) say explosives consist of a dielectric material and that different detection techniques are needed for dielectrics compared to metallic objects. The technique used is active swept millimetre wave radar in which the reflected signal is Fourier transformed to give the optical depth of the material. Quasi-optical techniques produce a small spot size so that the target area can be selected. Different parts of

the body can be distinguished from range data taken with a VNA (Vector Network Analyser) which provides both the transmitter and receiver. The typical output power of 2mW is several orders of magnitude below the recommended safe exposure limits for human targets. Artificial neural networks are used to analyse the Fourier Transformed data from co and cross polarised receivers and classify the result.

Whether or not the explosives contain fragmentation will change the way that they can be detected. Pure dielectric layers (explosives) are detected by reflections from the layer of dielectric and the boundary with air or the body (Andrews et al., 2008). Explosives containing fragmentation are detected as metallic objects by reflections from the metallic fragmentation as this blocks the transmission of millimetre waves through the material, so the depth of dielectric can not easily be detected (Rezgui et al., 2008).

3.6 Beam Forming for Stand-off Detection

In order to screen a person effectively one must sample small areas of the person's body with the screening system; to achieve this a focussed microwave beam is needed. A microwave lens is a wide band focussing element which can be manufactured simply from a suitably low loss material. A focussed microwave beam can then be used to sample a small area of the body at a time to determine if there is a threat present or benign objects.

To accurately model the behaviour of microwave optics Goldsmith & Moore (1984) conclude that Gaussian optics are required to design lenses which are required to operate at millimetre wavelengths because the radiation pattern of the horns for these frequencies can be accurately modelled. Gaussian optics treat the microwave beam as a Gaussian curve which can be focussed to a beam waist.

Figure 3.5: This shows a Gaussian Optics Lens Antenna from a manufacturer of millimetre wave components (Millitech, 2009). This antenna is designed to operate over the 75 to 110 GHz band, so the waveguide shown is about 3mm across.

Figure 3.5 shows a Gaussian Optic Lens Antenna from a manufacturer of millimetre wave components.

Materials suitable for producing microwave lenses include PTFE, PE (polyethylene) and Nylon. The material needs to have a refractive index greater than 1 and a low loss at the frequency of operation. Manufacturing considerations also need to be taken into account. Lamb (1996) provides tables of dielectric constants and loss tangents of materials that could form lenses at millimetre wavelengths. PE was chosen as a lens material as it has a suitable refractive index at 94 GHz and low loss. It is also cheaper and lighter than PTFE.

Fernandes (1999) shows that dielectric lenses efficiently shape beams from broad band antennas, the feeds for the system presented in this paper are embedded into the lenses themselves for maximum power transfer. Lenses are cheap to produce and can be moulded, the disadvantages of dielectric lenses can be their size and weight, the objective of designing a lens is to alter the radiation pattern of a feed horn into the required radiation pattern in free space.

Geometric optics is only accurate for refractive lenses with the condition that the radius of curvature of the lens surface is greater than the diameter of the lens (Wang & Dou, 2006). If the lens is axially symmetric, then only half of the lens needs to be modelled. The boundary condition of the plane of symmetry is set to perfect magnetic conductor. The thickness of a shaped Teflon lens can be reduced by using the lens zoning technique as presented by Wang & Dou (2006), this uses a lens design with one plane surface and one curved surface, the curved surface is then split into four zones, the wave path is then shortened for each zone independently. The result being a Fresnel-type lens. This has the disadvantage of being frequency dependant but the advantage of being thinner, lighter and also lower loss.

3.7 Late Time Response

Late time response is a technique most suited to detecting metallic objects, The electromagnetic field interacts with the object and when the wavelength is in the Mie regime (wavelength - object - size) the EM fields can constructively / destructively interfere around the object. The result is incident radiation travels around the object and can be seen as a signal after the initial reflection of the EM wave. The early time response is from the direct reflection from the surface of the object. The late time response is a weaker signal than the initial reflection and therefore requires careful processing to extract it from the noise of the detected response. The MUSIC algorithm is one way that has been tried to extract the late time response. Ibrahim et al. (2007) shows that the MUSIC algorithm splits the data into the signal subspace and the noise subspace. It is used to identify natural resonances and extract the resonant frequency. The MUSIC algorithm incorporates an averaging algorithm called the forward-backward averaging method. The frequency domain data is converted into the time domain using the inverse Fourier transform. The data is modelled and not measured in this paper. They extract the resonant frequency of each object, which is unique to individual objects and also independent from the distance to the detector.

Zhang et al. (2007) show that natural resonant frequencies of an object are incidence angle and object orientation independent. The complex resonant frequencies are unique for a given object and material as shown from simulations in CST Microwave Studio. Techniques for extracting the resonances include Prony's, the pencil of functions method and E-pulse method (Zhang et al., 2007). A forced response occurs when the incident signal reflects, this is called the early time response. The incident wave induces current to flow in the surface of the material, it radiates an EM wave at a naturally resonant frequency, this is the late time response. This technique is more applicable to gun and knife detection than to explosives.

3.8 Other techniques

Qiang & Conners (2006) use image processing methods to improve the explosive detection accuracy. The newest X-ray scanners are 3-D multi-sensing technology, but they are expensive and slow. This paper presents a method for improving the explosives detection rate for one-view scanners. It processes X-ray images, it is difficult to find boundaries in an X-ray image. A region growing algorithm is used for image segmentation because this type of algorithm ignores the small variations in textile images. The algorithm developed has been tested with 400 objects in 100 different bags, computation errors were less than 5%. The paper presents a technology that will improve X-ray one-view imaging for detecting explosives in passenger luggage. It models over-lapping effects and determines true grey levels.

Rezgui et al. (2008) show that Vector Network Analysers can be used in time domain reflectometry mode to study smaller objects. The aspect independent response is used to classify the object, called early time responses. Continuous wave signals swept over a wide frequency range are used to detect the aspect independent response from the gun in different orientations against the body. The response from a concealed handgun is non-polarisation conserving and this provides a way to detect it.

Grafulla-Gonzalez et al. (2005) found that flesh is well approximated by saline with a dielectric constant of $\epsilon = 28 + \text{j}34$, therefore it is very lossy.

$$\epsilon = \epsilon' + j\epsilon'' \tag{3.1}$$

where ϵ' is dielectric constant of the material and ϵ'' is the dielectric loss factor. The imaginary part of dielectric constant can be written in terms of conductivity σ.

$$\epsilon'' = \frac{\sigma}{\omega\epsilon_0'} \tag{3.2}$$

and is high for a lossy dielectric (Alabaster, 2004).

Terahertz methods including spectroscopic techniques have been investigated by others (Sinyukov et al., 2008), but require close proximity to the target because of

atmospheric losses and the wavelengths involved do not penetrate clothing well because of the size of the wavelength relative to the size of the weave of fabrics (Federici et al., 2005).

3.9 IEEE standard for human RF exposure

The International Commission on Non-Ionizing Radiation Protection ICNIRP (1998) has published guidelines that state for frequencies between 10 and 300 GHz that the occupational exposure should be less than 50 Wm^{-2} power density. The General public should not be exposed to more than 10 Wm^{-2} power density. The output power used in the system developed is 1.6 mW.

The intensity at a target at one metre is given by $I = P_{emitted}Gain_{linear}/4\pi r^2$ so for a linear gain of 100,000 the intensity at the target is 12 Wm^{-2}; so is less than the recommended maximum occupational exposure levels of 50 Wm^{-2}. The distance of one metre is also the closest possible distance, so the actual power at the target will reduce by $1/r^2$ where r is the distance to the target from the transmitter. Wireless computer networks typically operate with a output power of 23 dBm or 200 mW.

Chapter 4

Methods

4.1 Focussing Optics

For a given frequency, the size a microwave beam can be focussed to depends on the lens diameter and the distance at which it focusses. So a larger lens will produce a smaller spot size for a given frequency and distance, but the lens size is a trade-off between smallest possible spot size and the portability of the system. Ideally, a system detecting explosives gives maximum protection for the operator by keeping them as far away as possible, so a larger lens would be required to increase this stand-off distance. Another limit to the operating distance is the power transmitted, the power that reaches the target falls off as the inverse square of range. In a monostatic radar system the power detected falls off as $1/R^4$. Moving to higher frequency means that the optics can be smaller for a given distance, but transmitters in the terahertz band don't yet have sufficient output power to operate at standoff distances.

A system has been designed for concealed explosives detection that focusses a millimeter wave beam onto a target at a standoff distance and receives the reflected signal, as shown in figure 4.1. This signal includes information about the thickness of the paraffin wax. Paraffin wax is used as a substitute for explosives because its dielectric properties are similar as shown by (Lamb, 1996) and (Hu et al., 2006).

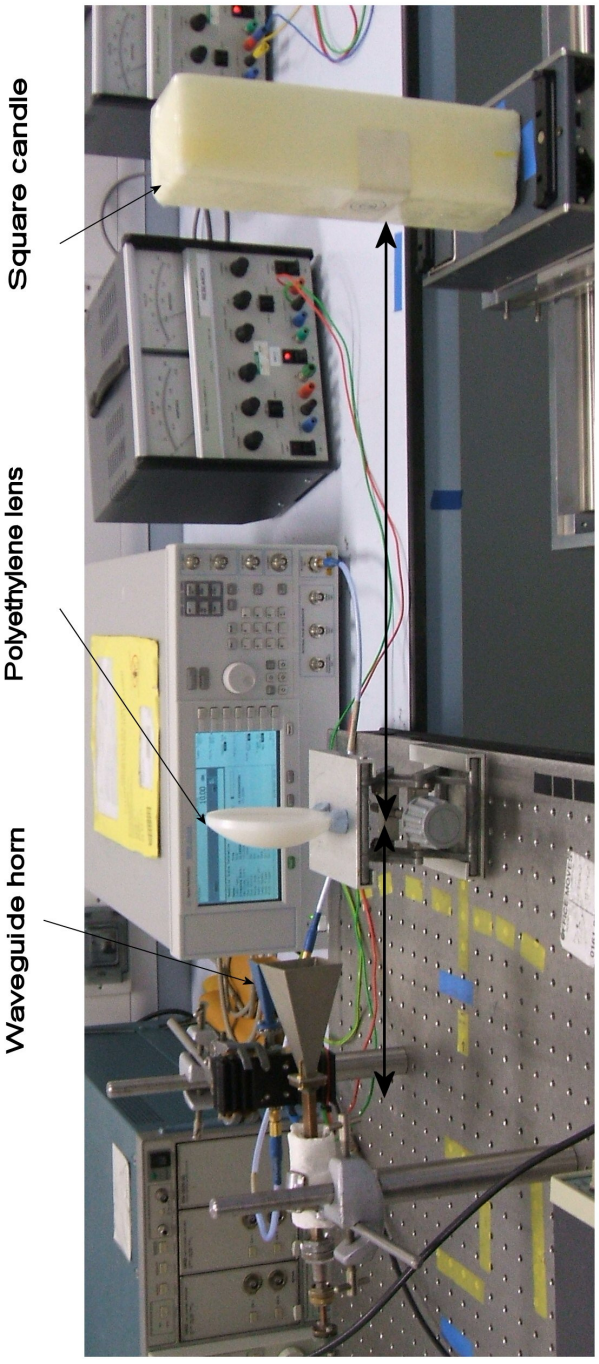

Figure 4.1: Measuring the dielectric properties of simulated explosive block (paraffin wax).

The system needs to be portable and be able to operate at a safe distance from the target without the target persons knowledge, this distance is ideally as far away as possible, but is a tradeoff between transmitter power, size of focussing optics, portability and safety of operator. A lens is needed to focus the microwave beam onto the target, to ensure that the beam samples the target and not the surroundings. The receiving horn also has a lens to focus the reflected signals onto the detector.

There will be a field distribution on the lens from the antenna. The lens will alter the wavefront of the fields, these will then propagate to the target.

The lens size is constrained by the standoff distance which is 10 metres, the operating wavelength, which is typically centred around 3 mm (94 GHz) and the diffraction limit which determines the minimum spot size for a given diameter lens. The beam needs to be focused onto the person with a beam size commensurate with the size of the object being detected, so the spot size needs to be less than 20 cm at 10 metres to cover the torso of the target person or the signal may give spurious results when it originates from the body and the background.

The diffraction limit, d, gives the smallest spot achievable at a particular wavelength with a specified lens size and is given by:

$$d = 1.22\frac{L\lambda}{D} \tag{4.1}$$

where L is the object distance, λ is the wavelength and D is the lens diameter, the diffraction limit constrains the size of the lens and gives a minimum lens diameter of 18cm for a spot size of 20 cm at 10 metres for a wavelength of 3mm. For the smallest possible spot size at 10 metres, the lens size needs to be larger; table 4.1 shows possible values, but in this case a smaller spot size is not necessary. A larger lens would also make the complete system less portable.

The lens had to be designed to operate across a wide frequency band from 75 to 110 GHz (W band), so a narrow bandwidth e.g. Fresnel, lens design could not be used.

Table 4.1: A table of possible values of lens diameter and diffraction limited spot size for a given focal length and operating frequency, given by equation 4.1.

target distance (m)	frequency (GHz)	lens diameter (cm)	spot size (cm)
10	94	10	38.9
10	94	20	19.5
10	94	30	13.0
10	94	40	9.7

A horn antenna is used as a transition from wave-guide to free space and forms the beam pattern of the antenna. The system uses the wave-guide band from 75 to 110 GHz (W band) because the depth resolution of the system and hence the thickness of the explosive layer that can be detected is dependent on the width of the frequency sweep used.

Two identical lenses were designed and manufactured from polyethylene (PE) given that PTFE (Teflon™) has a lower refractive index than PE but is heavier for a given lens diameter. The lens was modelled by ray-tracing software (Lambda-Research, 2005) and then using COMSOL (2009) finite element analysis software. These lenses were mounted in aluminium holders so that they can be focused and fixed on a target.

A lens was also needed to operate at a centre frequency of 94 GHz and a focal length of 7 metres (limited by the length of the lab) for a prototype detection system to produce a small enough spot to focus only on the target person and not the surroundings. The spot size is 18 cm from a 15 cm lens at 7 metres. The lens was modelled with ray-tracing software and in COMSOL (2009) as shown in figure 4.2 and has been incorporated into a prototype detector system.

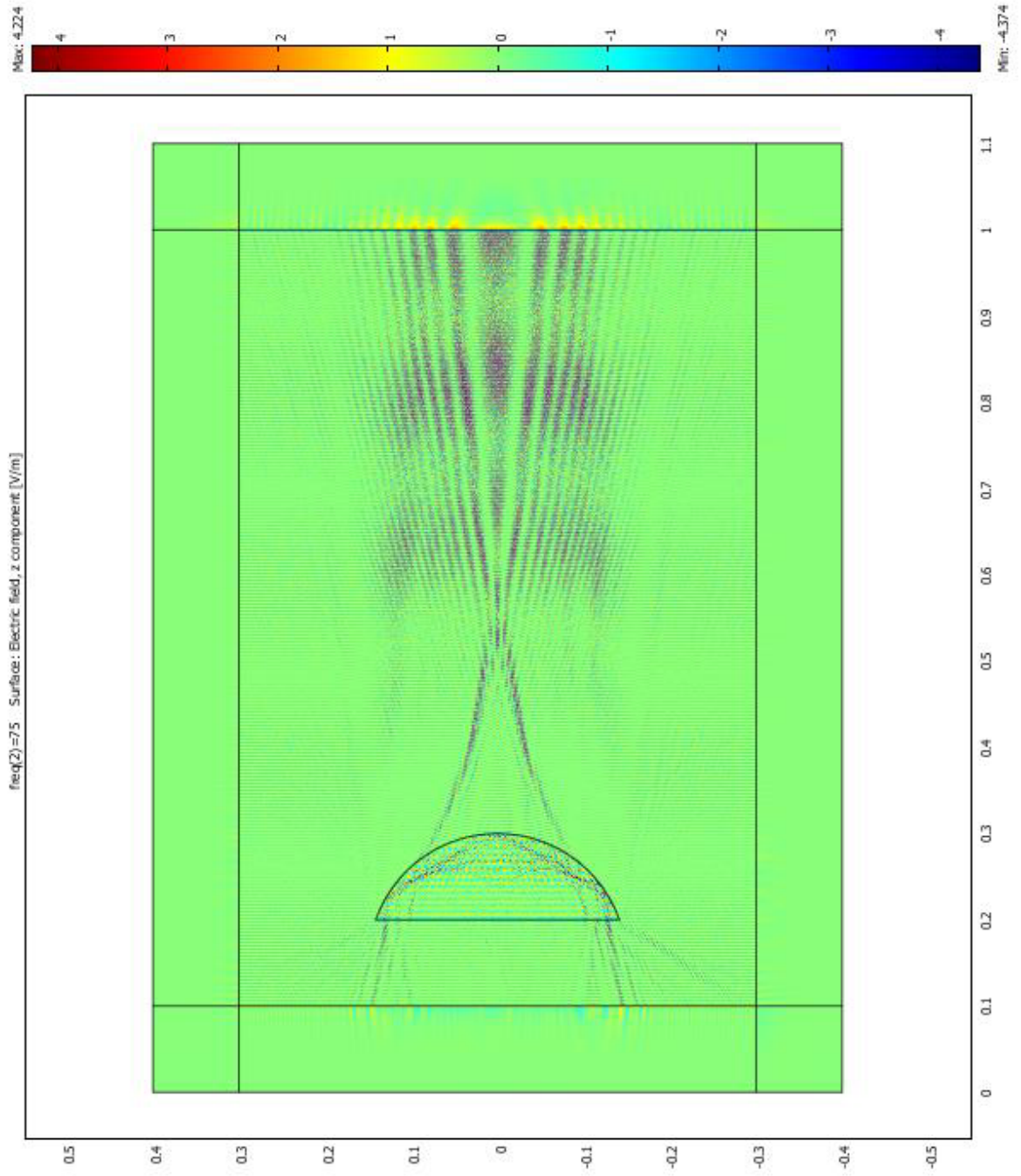

Figure 4.2: This figure shows a COMSOL (2009) model of a lens of 15cm radius of curvature and refractive index n = 1.52 which corresponds to the properties of polyethylene. The parallel waves on the left of the figure are focussed by the PE lens and form a Gaussian beam waist.

The lens surface is given by the hyperbolic lens equation:

$$r = \frac{f(n-1)}{n.cos\theta - 1} \tag{4.2}$$

where r is the radius of curvature of the lens surface, and n is the refractive index of the lens material, f is the focal length and θ is the incident angle of the rays to the lens axis. In the thin lens approximation this becomes:

$$R = (n-1)f \tag{4.3}$$

where R is the radius of curvature of the lens surface.

Equation 4.1 gives the spot size for a given focal length, this produces a lens with a radius of curvature of 15 cm for a 15 cm diameter lens and a focal spot of 18cm at a focal length of 7 metres (Cornbleet, 1976).

A lens of 18 cm diameter was incorporated into a prototype detection system and has been used to detect the presence or absence of guns and explosives simulants at a distance of a few meters by other members of the research group (Rezgui et al., 2008).

4.2 Explosives Detection

4.2.1 Introduction

The aim of this work is to detect explosives concealed under clothing. The method used is transmitting a microwave beam at a target and receiving reflections from the front surface of a partially reflecting layer of dielectric material worn on the body of the target subject, i.e. a 'suicide vest' as shown in figure 4.3.

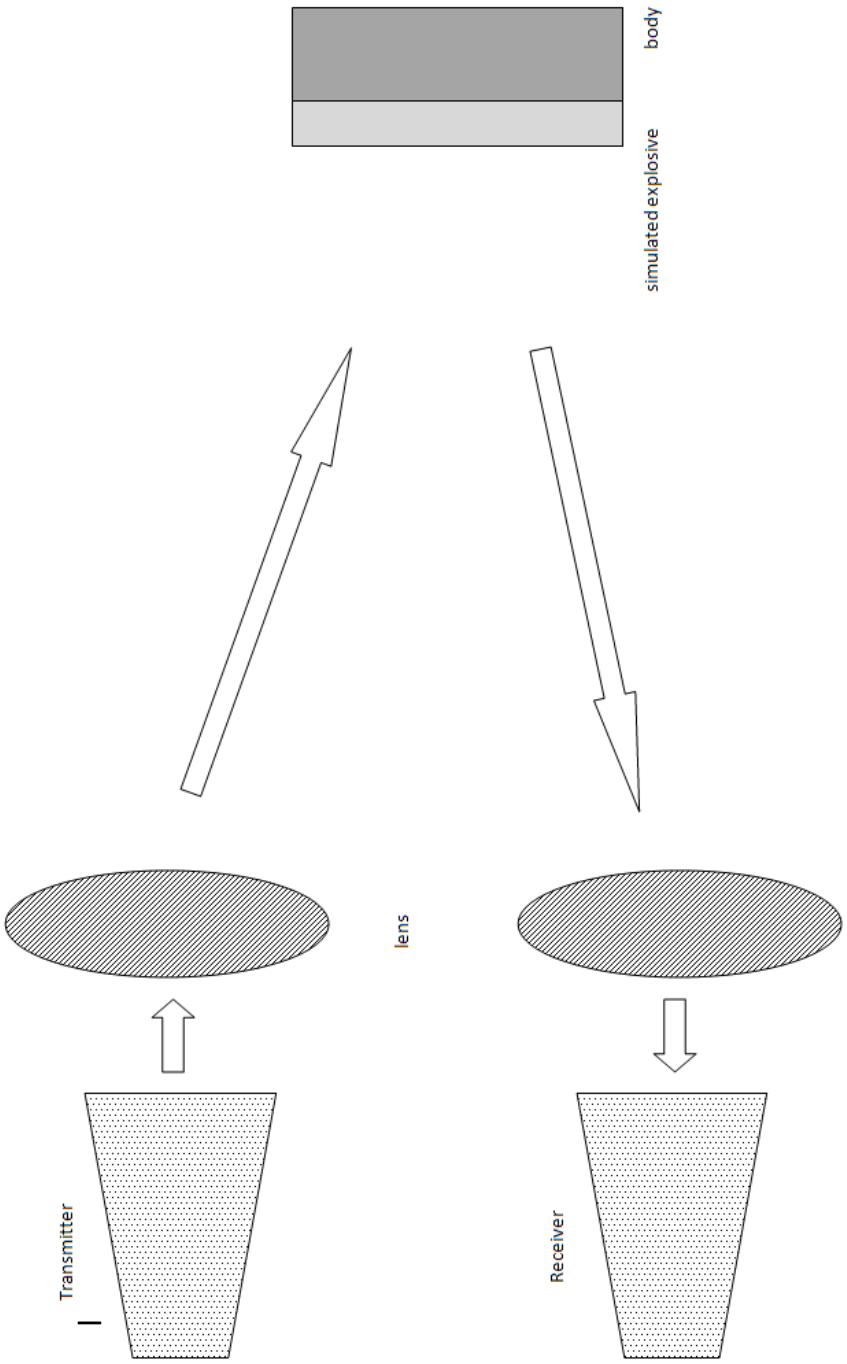

Figure 4.3: This figure shows how the microwave horns are used with lenses to focus a beam onto the target, with the VNA acting as the transmitter and receiver system. Reflections are detected from the front surface of the dielectric and from the body. The simulated explosives are shown in front of a subject under test.

A Vector Network Analyser operating in the band 14 - 40 GHz is used as the transmitter and receiver for this system using lenses to focus the beam onto the target. Microwave horns are used to form a beam in free space which is then focussed onto the target. The beam is transmitted towards the target and the reflections are detected.

The reflected power received has a oscillatory shape as a function of frequency, see Equation 2.35 caused by the reflections from the front surface of the dielectric and the reflections from the body interfering. These responses are then Inverse Fast Fourier transformed (IFFT) into the time domain as shown in figure 4.4 and passed through a signal processing algorithm which has been developed. The Fourier transform produces two peaks when using VNA data which contains phase information, one from the front surface of the explosive simulant and one from the body. The output from the IFFT data can vary in optical depth due to the movement of the person and the data can have gaps in where the target has moved out of the beam at that instant, to remove these effects a signal processing algorithm is needed which sorts the data in some way.

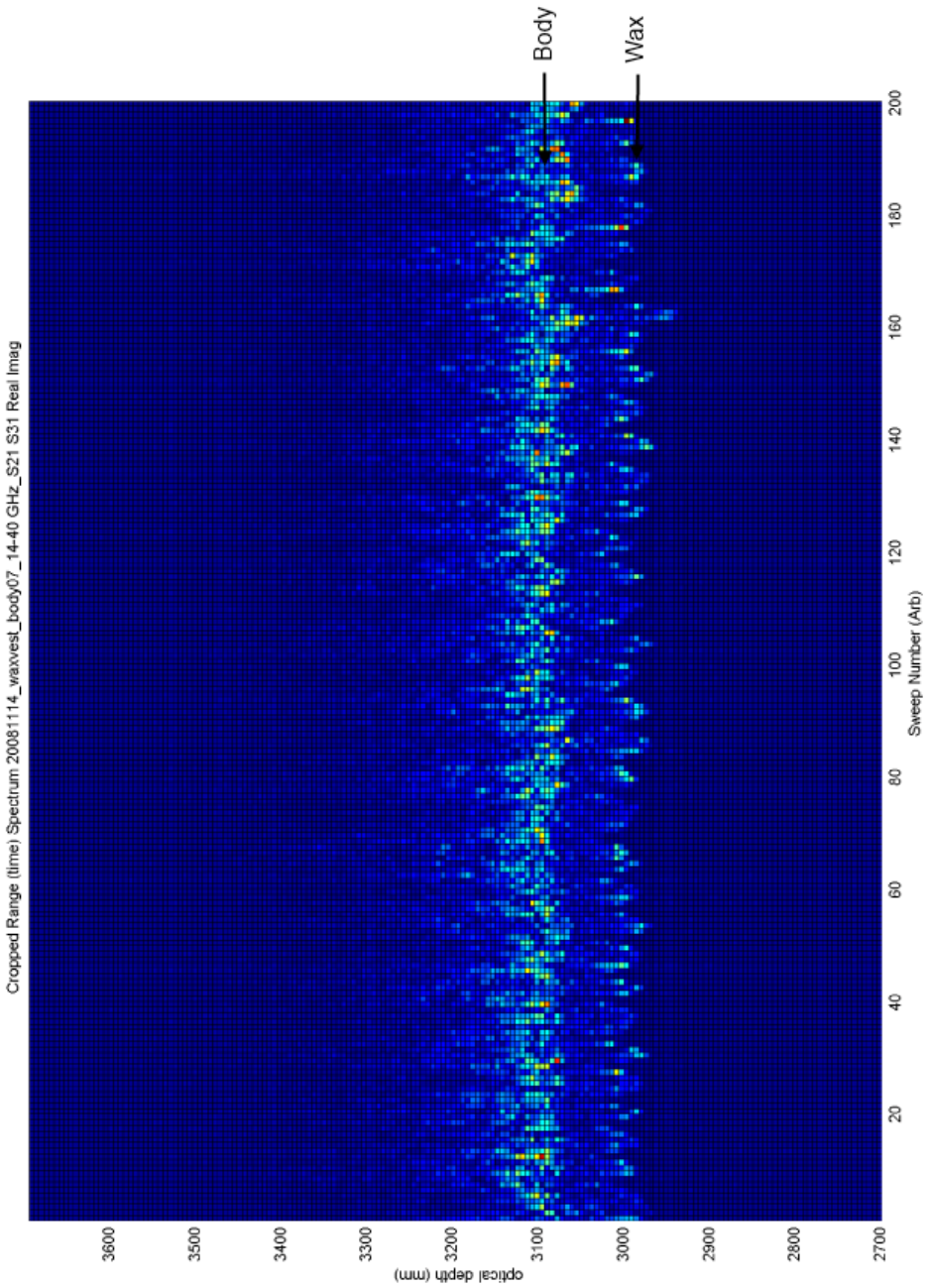

Figure 4.4: This figure shows the data from the 'suicide vest' in front of the body after it has been Fourier transformed into the time domain. The two horizontal lines show the distance to the dielectric and the distance to the body, the difference being the optical depth of the dielectric.

This allows the detection of the optical thickness of the dielectric layer in front of the body and to distinguish it from clothing and other common objects worn in front of the body, such as mobile phones, cameras, keys etc. It is possible to detect explosives concealed on the body by processing the reflected signal from the body after first Inverse Fourier Transforming the signal, a peak is shown in front of the body. A neural network is trained on the patterns produced by different objects and thicknesses of paraffin wax and it then classifies the objects as a threat or not a threat. The steps of the signal processing algorithm are shown in figure 4.5 and these are discussed in detail in Section 4.2.3.

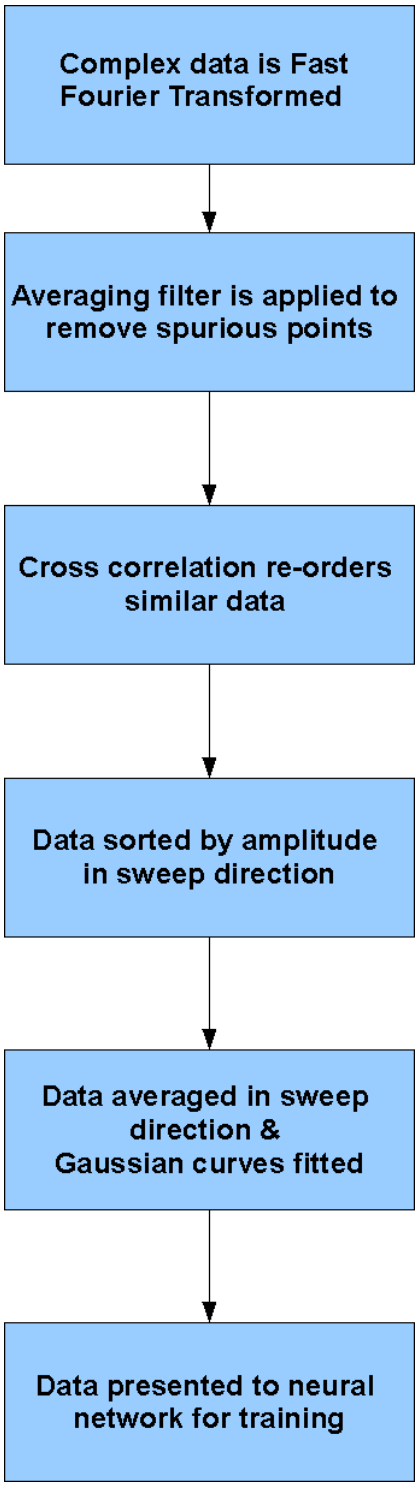

Figure 4.5: This figure shows the steps in the signal processing algorithm applied to the complex data from the VNA. Fourier transforming the data is a standard processing step, but the following steps are the authors own contribution. A neural network is a computational mapping which can be trained to recognise patterns.

4.2.2 Experimental Method of Dielectric Detection

The VNA (Vector Network Analyser) was used in this short range, proof of principle experiment, to sweep the frequency of the source from 14 to 40 GHz (the waveguide band of the horns, up to the maximum frequency the VNA is capable of) to radiate onto a target 1 to 2 metres away using 20 dB gain horns for this band. Small lenses were used to do a short range proof of principle experiment. The range of this system is limited by the size of the optics and the maximum operating frequency of the VNA. Operating at a higher frequency would give improved resolution from the same lens and therefore increase the maximum range of the system, 10 metres range is easily achievable operating in the 94 GHz band. The reflections from the target are measured using S21, which is the forward transmission in a 2-port network on the VNA, using two receivers, so that co-polarisation and cross-polarisation can be received. Typically 801 frequency data points are collected; chosen to prevent the target being beyond ambiguous radar range, which is about 5 metres and repeated for 200 sweeps while the target moves around. The horns are placed side by side facing forwards or with a small vertical offset to reduce cross-talk between the antennas. The target stands in front of the VNA facing the horns, with and without the wax against the body, as shown in figure 4.3. A 100 mm diameter lens made from polyethylene was used on the transmitting horn to focus the beam onto the target. Matlab software was used to take data of 200 sweeps using the amplitude and phase written in complex phasor form and then, using Euler's theorem, decomposed into real and imaginary parts of the data from the VNA. The data were saved to a file for offline processing.

4.2.3 Signal Processing Steps

A script in Matlab was written to read in the complex frequency data from the radar system, perform the inverse Fourier transform of the data and to produce a 3-D plot of sweeps against optical depth as shown in figure 4.6. The Matlab script then prompts the user for the range of optical depth over which to gate the data; this means it will select optical depth data over a certain range of optical depths.

The received signal is Inverse Fourier transformed into the time domain to reveal the reflections from the front and back surfaces of the dielectric material located in front of the body; as phase information can be measured using a heterodyne receiver such as a vector network analyser, the IFFT data are equivalent to the time of flight data from a radar system.

The relationship between phase and range can be explained as follows; an electromagnetic plane wave is given by

$$E(t) = A(\omega)e^{i(kz-\omega t+\phi_0)} \tag{4.4}$$

The transmitter is at z=0 and the receiver is at z=0 with the target at Z=R.

The electric field at the transmitter is given by

$$E_T(t) = Ae^{-i(\omega t+\phi_0)} \tag{4.5}$$

and the electric field at the receiver is given by

$$E_R(t) = Be^{i((2kR-\omega t)+\phi_0)} \tag{4.6}$$

the change in phase between transmit and receive is given by

$$\Delta\phi = \phi_R - \phi_T = 2kR \tag{4.7}$$

Reflections from the front surface of the material produces one peak and the reflections from the back surface produce another peak. The spacing of the optical depths

of the two peaks gives the optical depth of the dielectric present. In a system which uses a direct detection receiver, two peaks are produced but the absolute range to the surface is lost.

The region of interest is 'gated' out by range to reject the background and any unwanted returns such as the length of the cables, these always appear in the same place so they can be cropped from the data.

The subject is moving around whilst the data are being collected so the dielectric may not be present in every sweep of the frequency band, there may also be a return from arms or clothing that are not present or different in every sweep, these are known as 'glints'. Glints are brief, bright reflections from objects such as arms or metal on clothing. The dielectric layer, if present, is expected to be present in most of the sweeps, therefore averaging along the sweep axis will remove these 'glint' effects and make the presence of the dielectric more clearly defined. The function 'imfilter' is used to apply a 3 by 3 averaging filter by treating the data as an image in Matlab.

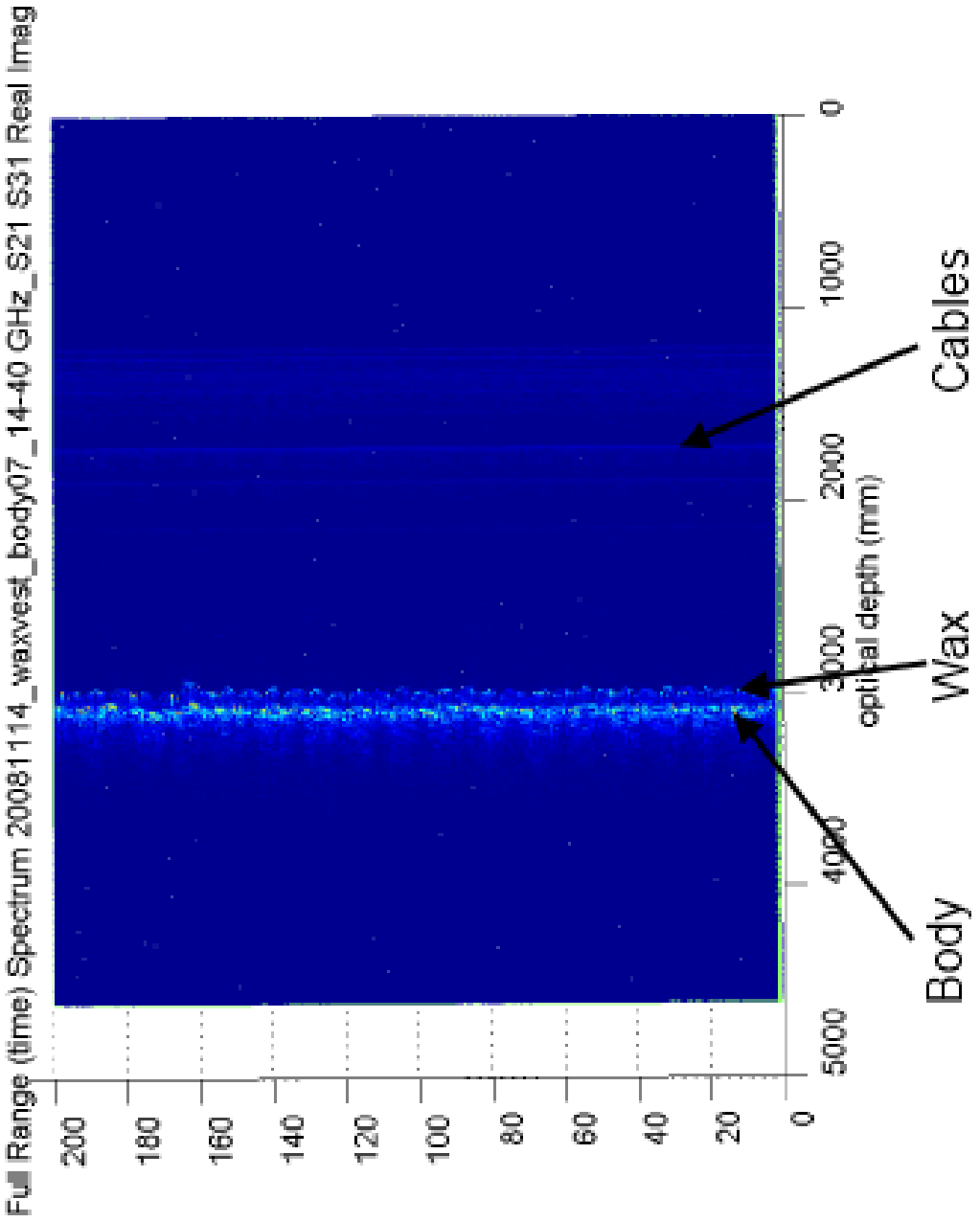

Figure 4.6: This figure shows the data after the inverse Fourier transform, sweep number vs. optical depth. The vertical lines at an optical depth of about 3000 mm contains the simulated explosives response and body response. The fainter lines at optical depths around 1000 mm are from the antennas and cables.

As the target moves around, the range to the target will not always be the same, but the difference between the front and back faces of the dielectric will remain largely constant, by recognising this, the data can be aligned by using these peaks which will be a pattern repeated across many sweeps. The cross-correlation coefficient is a measure of how similar one data set is to another one and has proved to be a useful way of aligning the data by range. The data are then aligned to maximise 'cross-correlation coefficient', to align the data in the optical depth space, as shown in figure 4.7, this cancels out the effects of the target moving around during the data collection.

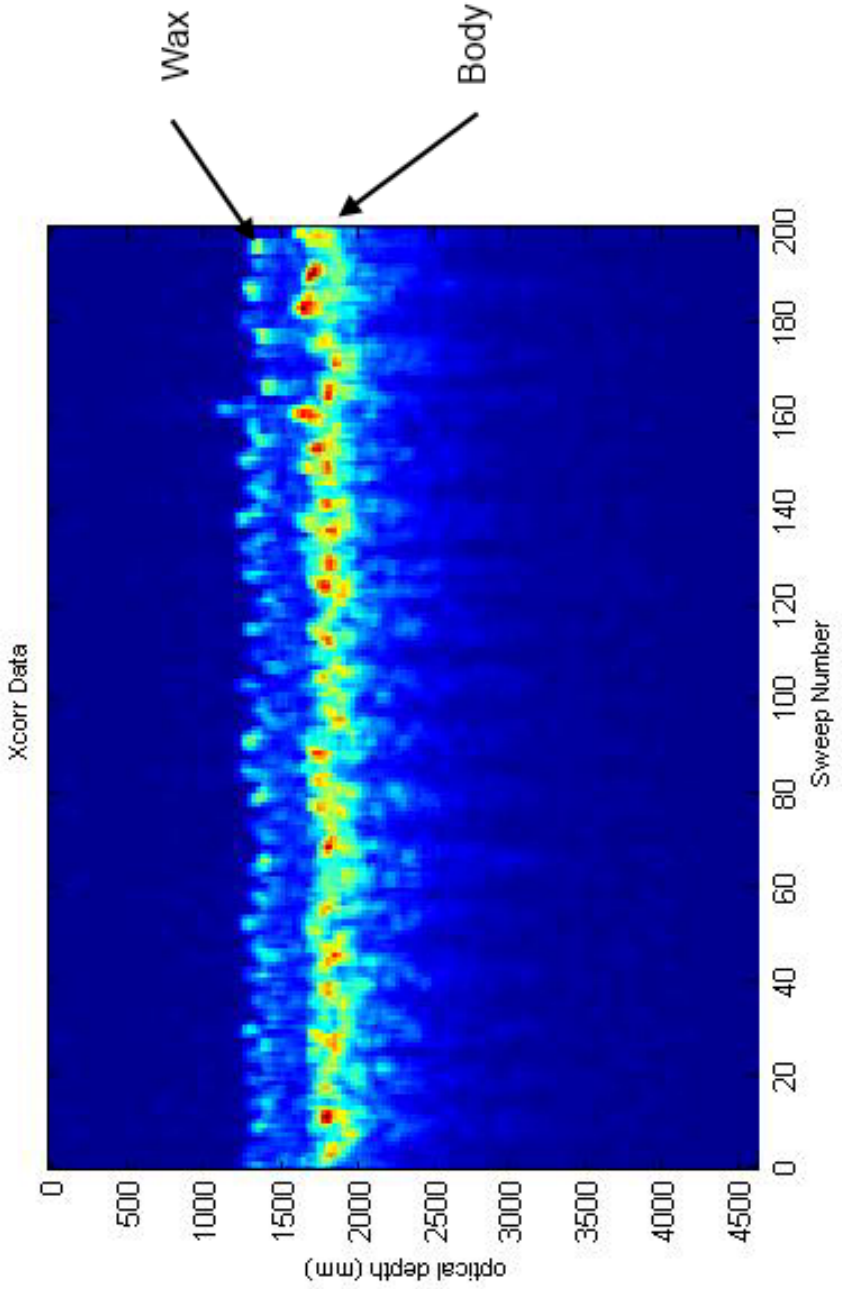

Figure 4.7: This figure shows the data after alignment using cross-correlation coefficients. The simulated explosives can be seen as a line 'in front' of the body response.

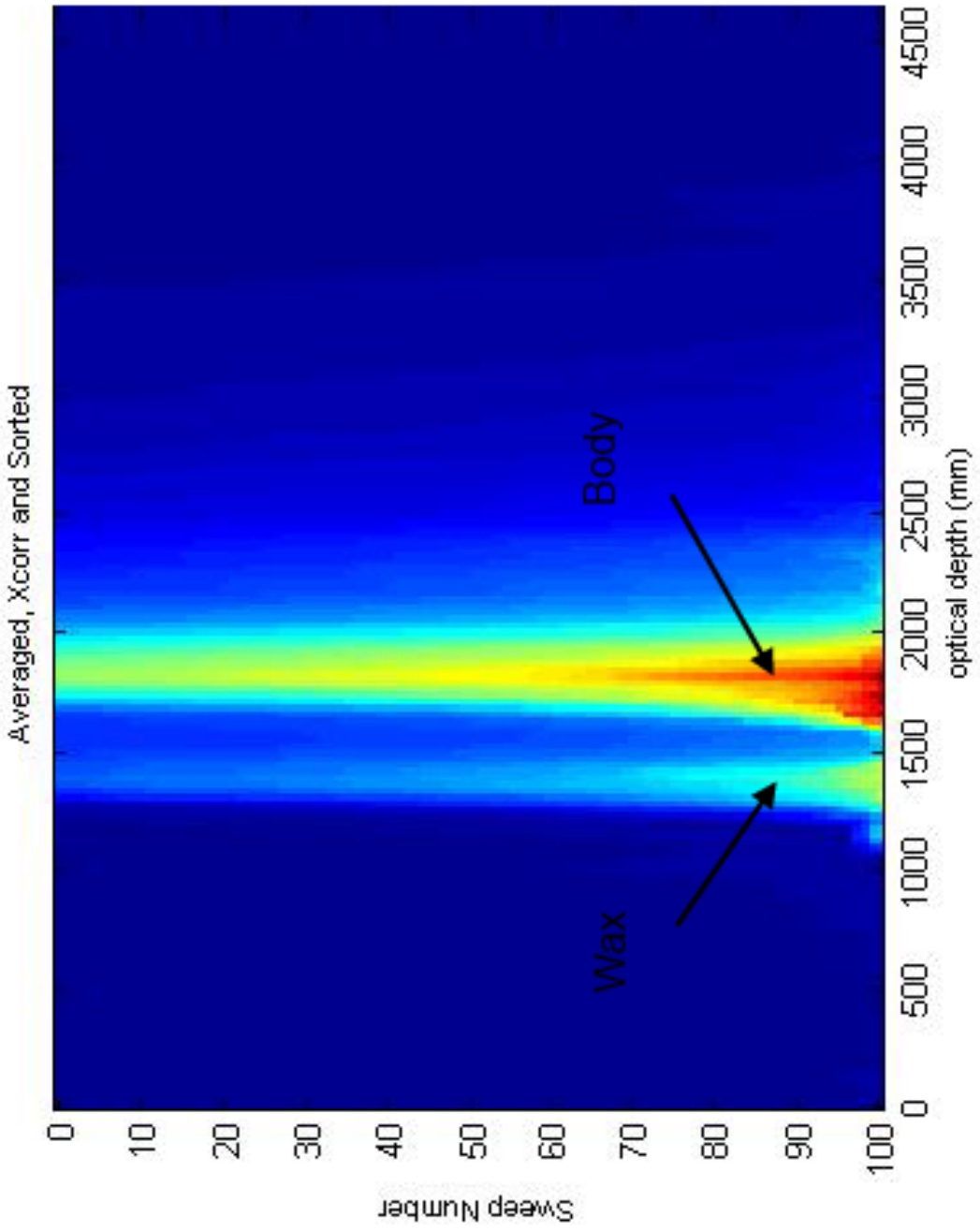

Figure 4.8: This figure shows the data after sorting by amplitude to remove sweeps when the body is out of the beam. The simulated explosives can be seen as a peak 'in front' of the body response. The zero position is in the bottom left-hand corner of the plot.

There are gaps in the data when dielectric is not present in a particular sweep; for example when the subject has turned out of the beam or the layer has been partially obscured by a limb. To reject these sweeps the data are sorted by amplitude in the optical depth space as shown in figure 4.8. This produces a plot where the dielectric shows up as a peak in front of the body response; the body alone shows up as a single pronounced peak. This information can be used to train a pattern matching algorithm such as an artificial neural network (ANN) to automatically classify data as dielectric present or absent. Dielectric present is classified as a threat. Dielectric absent is classified as a non-threat. This is repeated for four data sets, alternating threat and non-threat.

4.2.4 Training of the Neural Network using Gaussian curve fitting output

It is easy to see by eye the difference in this threat or non-threat data as shown in figures 4.8 and 9.4, but the data set is too large to feed the whole image to the ANN so the mean is calculated across the sweeps and then the sum of four Gaussian curves are fitted to the data, using Matlab's ('cftool') curve fitting tool, this can then be used to generate a Matlab script which will fit curves to new data. The parameters of the Gaussian curves are taken from the fitting function in Matlab as Amplitude, Position and Width, so a 3 column by 4 row array is produced. This array is then sorted by increasing position, so that the parameters are in order. This simplifies the data and reduces the number of points presented to the ANN for training.

Once the network is trained, it can be tested by presenting one set of data at a time to it, formatted in the way described above and the ANN classifies it as 'threat' or 'not a threat' on a scale of 0 to 1.

4.2.5 Improved Data Collection

The original Matlab script has been improved by making the gating of the data automatic by looking for the maximum value and then taking 174 points centred on the maximum value because it is time consuming to manually enter each range for a large training set. The script has been modified to be able to take data directly from the VNA and then train the neural network on that data, so that it is ready to be tested without offline processing. The Matlab script clears the VNA display, then sets up the required frequency sweep of 14 to 40 GHz; the power is set to 2 dBm and the number of data points to 801. Once the network is trained it can be saved and recalled so that it doesn't require re-training for each use. The data are then formatted as before and the neural network can be tested by presenting new data to it.

The threat data are acquired by using four blocks of paraffin wax as simulated explosives, held together by a cotton bag, which is held in front of the body to simulate

a ‘suicide vest’. The non-threat data are the body without the ‘suicide vest’.

The results for this are shown in Chapter 9.

Chapter 5

Detection of Dielectric Layers

5.1 Introduction

The aim of the project was to detect weapons and explosives concealed under clothing on the human body and this thesis focusses on detecting explosives, rather than guns or knives. The explosives can be thought of as a layer of dielectric material with a fairly narrow range of refractive indices at MMW frequencies, but much more variable is the thickness of the layer, giving rise to a large possible variation in the optical depth. If the dielectric constant is not equal to that of air, n=1, then refraction and reflection takes place at the boundary with air and this can be used to detect the presence of a layer in front of the body using millimetre wave radiation.

5.2 Initial Investigations

Initial investigations centred around finding a suitable substitute for the human body and for the explosives under test, to satisfy health and safety requirements. The obvious substitute for the body would be a mannequin, but these contain metallic supports and joints, which reflect microwaves. The refractive index of the material needs to be similar to that of the body. An expanded polystyrene mannequin was found, but because this is transparent to microwaves, some way of making it reflect like the human body was needed. The body can be approximated by saline, so a large

water bottle was a possible substitute (Grafulla-Gonzalez et al., 2005). Covering the mannequin in something that could be kept damp was another possibility.

To test the feasibility of using a human shaped mannequin, a cast of the polystyrene mannequin was made with plaster-of-paris and bandages as used medically. This cast could then be used for either moulding ballistic gelatine (Fackler ML, 1988) or a fibre glass mould that could be filled with water. Both of these solutions have disadvantages, the gelatine may not be rigid enough to support its own weight and a mould made of fibre glass would be difficult to seal to hold this mass of water.

After investigating the use of fibre glass and the health and safety considerations of using glass fibre, this idea wasn't used. The large water bottle idea was used, a large bottle from a water dispenser was used as a human substitute. The curvature of the bottle might not be an ideal model for the human body, but this was the simplest solution to implement. This idea wasn't used immediately because it wasn't known if it would be a close enough substitute for the human body.

5.3 Methods

Using a Vector Network Analyser (VNA) as a swept frequency source over a frequency range of 14 to 40 GHz, with horns for this waveguide band radiating in the direction of a block of paraffin wax, the VNA can be used as transmitter and receiver. It also provides a convenient way of acquiring and saving the data. This method involves radiating towards a block of wax a few metres from the transmitter and then receiving the reflected signal as a function of frequency. The amplitude versus frequency response contains information about the depth of the wax block because some of the signal reflects from the front surface and some of it travels through the block and reflects from the back surface of the block. These two reflections interfere with each other and produce an oscillating response in frequency space. The time domain signal is one way to obtain the optical depth of the material, it can also be obtained directly from the frequency domain signal. This produces a peak in the Fourier transformed

data at a particular 'optical depth'. The optical depth of the wax is the physical depth of the block multiplied by the refractive index of the wax. This technique will only work for materials that are sufficiently transparent to microwave frequencies so that the electromagnetic wave can reflect off the back surface of the material without serious attenuation. The 'optical depth resolution' of this technique is dependent on the bandwidth of the sweep, for 14 to 40GHz the bandwidth is 26GHz. The 'optical depth resolution' is discussed in chapter 2.

Therefore, for the frequency sweep 14 to 40 GHz, the minimum optical depth resolution obtainable would be 6mm and for the frequency sweep 75 to 110 GHz the minimum optical depth resolution would be 4mm; they are minimum values of the product of refractive index and range resolution. This means that the minimum detectable thickness of explosive for this system is 4mm under ideal conditions.

The alignment of the transmitting and receiving horns and the wax block are critical so that the maximum available signal is detected and can be processed. Short range, proof of principle experiments used a 100mm polyethylene lens to produce a focused beam onto the paraffin wax (candle) which was used as a target in some of these tests. To extend the range, a 300mm diameter lens was tried on the transmitting horn and the receiving horn was moved to the side of the lens to reduce cross-talk between the lenses.

5.4 Results

5.4.1 Investigations of refractive index of paraffin wax.

It was found that the refractive index of a block of paraffin wax could be measured if the thickness of the block was known, by using a swept frequency source and inverse FFT to obtain the optical depth of the block (see equation 2.5).

To simplify the data and to check the measurement technique, a simple 'square candle' was used. The candle was 80mm square and about 300mm tall. The transmitter and receiver were placed side by side and the frequency was swept from 14 to 40

GHz in 256 steps. The reflected frequency response was measured. Inverse Fourier transforming this response and converting the x-axis to optical depth, gives a peak in the data at 123mm. Dividing 123 by 1.5, the refractive index of the wax given by (Lamb, 1996), gives an accurate estimate for the thickness of the candle thickness for the candle of 80mm.

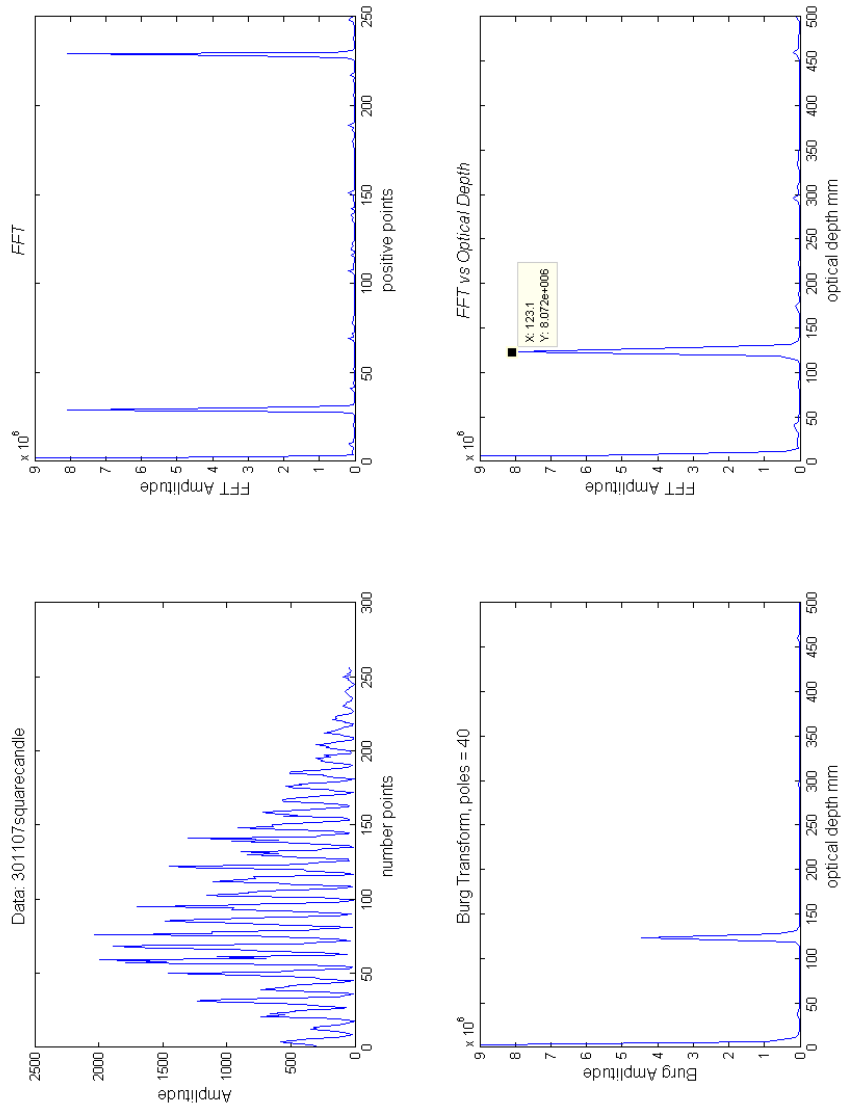

Figure 5.1: This figure shows the reflected frequency response of the square candle, then the Fourier transform of that data against number of data points, then the Burg transform against the number of points converted to optical depth. Matlab implements the Burg algorithm, a parametric spectral estimation method, and returns an estimate of the power spectral density (PSD) of the input vector (Math-Works, 2009). The last plot shows the FFT against optical depth and the peak shows the depth of the square candle as 123mm.

Figure 5.1 shows the reflected frequency response of the wax block, then the Inverse Fast Fourier transform (IFFT) of that data against number of data points, then the Burg transform against the number of points converted to optical depth. The last plot shows the IFFT against optical depth and the peak shows the depth of the wax block as 123mm.

5.4.2 Detecting plastic explosives in containers

There was a requirement to detect plastic explosives in containers, and to develop this technique into detecting explosives contained in a bag.

The aim was to measure the difference between a wax block and a sandwich box (of the same shape). The frequency sweep was 14 to 40 GHz. The data contained 256 points.

Figure 5.2 shows the IFFT amplitude for a sandwich box which is 70mm deep, including the lid. The red line is the empty box, the blue dotted line is the wax block moulded into the box and the green (diamonds) line is the wax block in the box with the lid on. The base of the box was facing the transmit and receive horns and was placed 1.5 metres away. A wax filled container is expected to give an optical depth measurement approximately 1.5 times greater than the same container when empty.

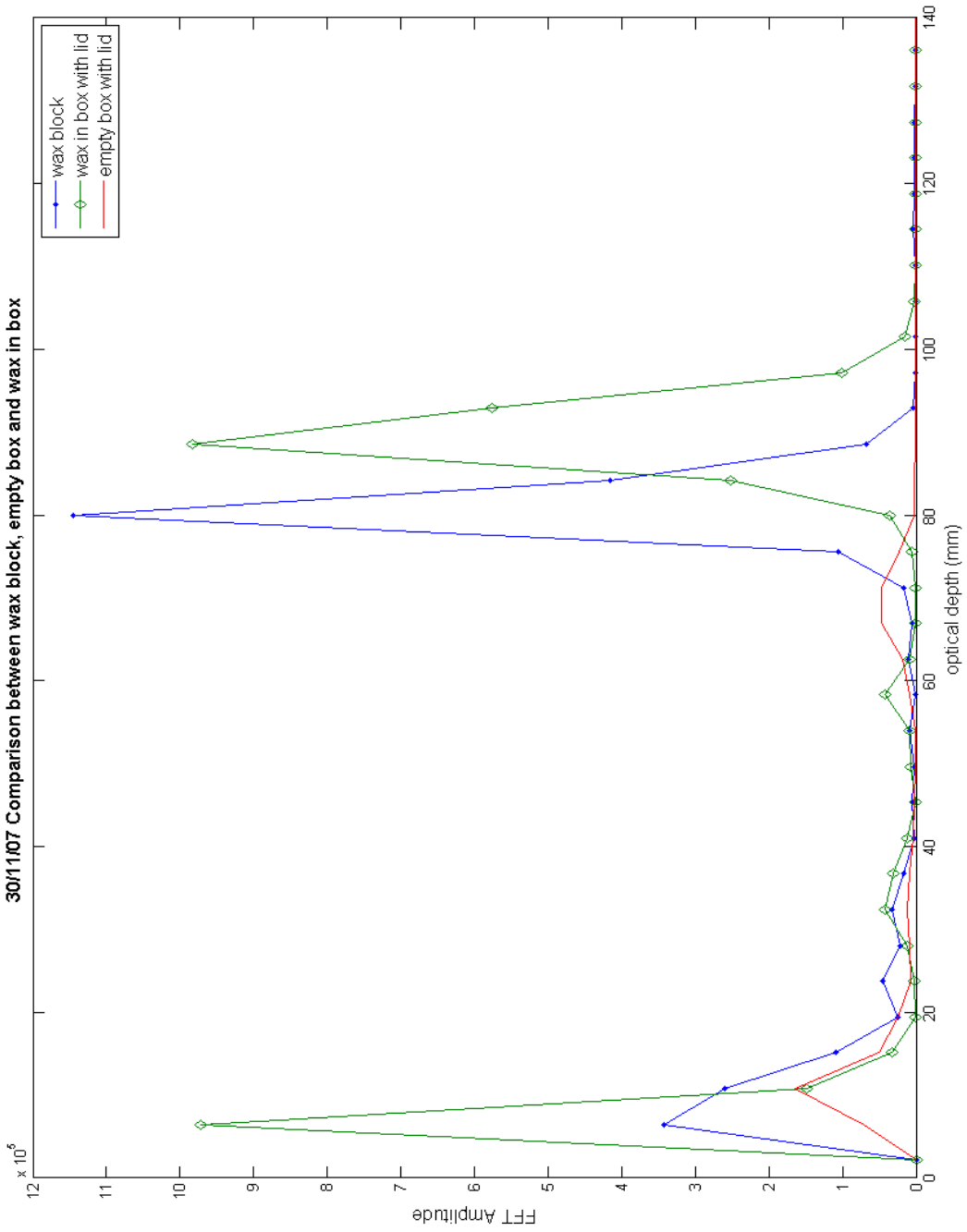

Figure 5.2: This figure shows the FFT data for a sandwich box containing wax which is 70mm deep.

The wax in the box shows a increase in the depth measured, 89mm, compared to the box containing only air, 71mm. The presence of the box affects the estimation of the refractive index of the wax it contains, as the block on its own gives 80mm optical depth, The depth of the empty box was measured as 70mm.

To try to distinguish between the wax and the box the measurements were repeated by scanning from 14 to 40 GHz. The box with either the lid or the base facing the detector gives the same optical depth of 67mm, close to the depth of the box for n=1 for air. The wax only with either the base or the top facing gives an optical depth of 84mm, giving an approximate refractive index of 1.25 for the wax, which is a little low compared with the figure n=1.5 for paraffin wax by Lamb (1996). This could be due to the wax shrinking on cooling and so not being exactly the same shape as the box it was moulded in, or possibly containing air bubbles thus reducing the effective refractive index for microwaves.

A VNA was used as a swept frequency source from 14 to 40 GHz with 1401 data points to increase the unambiguous range to 8 metres, the targets were a wax block and a wax block in the box it was moulded in, with and without a water barrel backing. The aim of this test was to try to show if a box containing air could be distinguished from a box containing a dielectric material or explosive. It was difficult to distinguish the box containing wax from the empty box.

5.4.3 COMSOL modelling of wax block and container

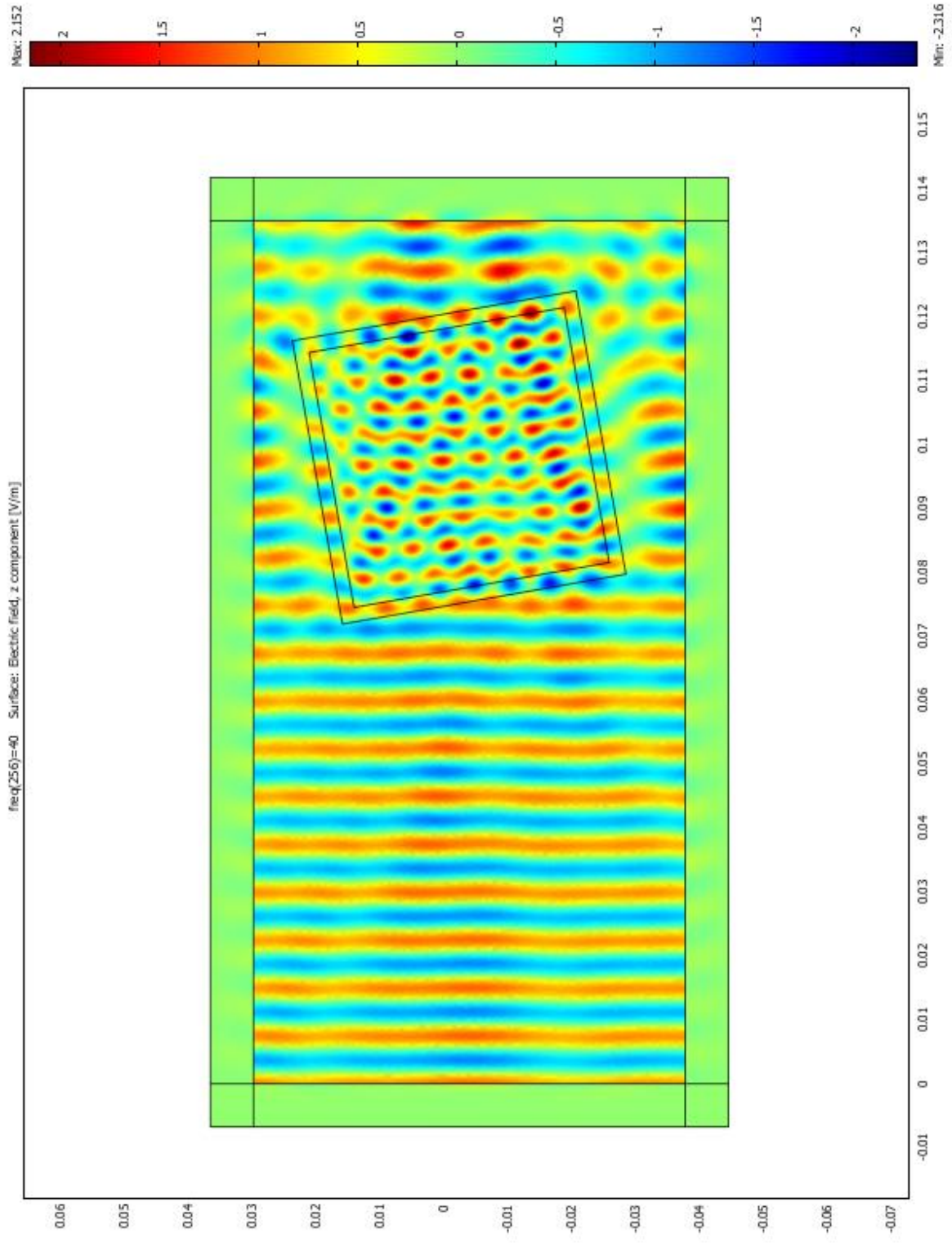

Figure 5.3: This figure shows a COMSOL simulation of a wax block in a PTFE box to simulate explosives contained in a sandwich container. The box was rotated to see if the angle of the box to the millimetre wave beam had an effect on the result.

A model was developed in COMSOL (2009) for the wax block explosives simulant. It consisted of a dielectric cube of refractive index n=1.5 surrounded by air with n=1. The boundary conditions were set to perfectly matched layer, therefore no reflections from the boundary; mimicking the cube being located in infinite space. The source frequency was set to spot frequencies of 14 and 40 GHz. The simulation showed that there was a focusing effect from the wax block on the plane wave source. This was probably due to the change in refractive index at the air to wax boundary. The simulation was repeated with the wax surrounded by a layer of PTFE, to simulate a typical container, it could be seen to focus the beam as it passed through the wax box and container as shown in figure 5.3, again this was probably due to the change in refractive index at the boundary and it was difficult to distinguish between the wax block and the wax in the box, so the box seemed to have little effect on the result. The angle of the wax block to the incident wave was varied in the simulations to see if this changed the focussing effect, it was difficult to see any difference.

A second model was specified in COMSOL; an empty sandwich container, a cube with a thin wall of dielectric constant n=1.3 filled with air, n=1; this simulation was run and then modified to be a container filled with wax, n=1.5. The box with wax showed a focusing effect, whereas the empty box did not. This was done to find a way to detect explosives in containers, possibly in bags; but when this was tried with millimeter waves it was difficult to see any difference between the empty sandwich box and the sandwich box filled with the simulated explosive (wax).

These large, two dimensional models are modelled by finite element analysis. COMSOL splits the geometry into a mesh, the higher the frequencies modelled, the finer the mesh needs to be. This requires a large amount of computer processing, so the frequency sweep was limited to spot frequencies of 20 and 40 GHz.

Measurements of a wax block with a sweep oscillator were carried out; three cases were tried, an empty box looking through the base, the moulded wax looking through the base and the box and the wax combined. The empty box gave a optical depth of 78mm, the wax a depth of 95mm and the wax and the box combined gave a depth of

107mm. A sweep oscillator was used as the source and was swept from 14 to 40GHz. The actual depth of the empty box was 80mm.

Measurements of a wax block with swept frequency source 75 to 110GHz were carried out; the case of the wax block looking through the base was tried for a frequency sweep of 75 to 110GHz, and was repeated for the empty box and the wax and the box combined. Using a value of refractive index n=1.5 (Lamb, 1996) for wax and the wax block gave a depth of 60mm, the empty box 80mm and the wax and the box combined were 100mm.

5.4.4 Dielectrics Detection

Sweeping 14 to 40 GHz was used to measure the optical depth of the 80mm square candle, the depth was measured as 119mm. This was to calibrate the system by using the candle as a check of the system alignment and of the data processing set up each time measurements were taken shows that everything is working correctly.

For a stationary object if multiple sweeps are collected then each frame will be identical; one sweep of the frequency range is sufficient, but if moving objects are to be measured then multiple sweeps will be needed. Taking multiple frames, moving the object between each frame, was a step towards measuring a moving target, such as a person walking. Moving the target between each sweep shows the result of changing the angle on the depth measurement. Plotting multiple frame data can increase the confidence of a detection, if the same optical depth is detected across multiple frames. This shows that a depth measurement is a function of angle but not a very strong one.

Plotting the Fourier transformed data against optical depth and sweep number gives a 3-D type plot where the depth of interest can be tracked across several or all of the sweeps. If there is no optical depth present in a particular sweep then this data can be thrown away and only the data containing an optical depth is kept for analysis.

It became clear that an automatic way of detecting if there was a threat present in a data set or not or if a peak repeated in a number of sweeps was needed to identify a potential threat item from the data.

5.4.5 Training neural network with Co and Cross Polarisation data

Co-polarisation is the case where the receiver and transmitter horns are aligned. Crossed polarisation is the case where receiver and transmitter waveguide horns are at 90 degrees to each other. Two data sets were obtained by sweeping the frequency from 14 to 40 GHz, with 20dB gain horns, one for each polarisation and a target distance of 1.2 metres. The data were then IFFT'd for both co and cross polarisations to form two sets of training data for the neural network. Co-polarisation and crossed-polarisation data were input to the neural network as 2 separate data sets and used to train the network.

Reading in four sets of data to the neural network, using co-polarisation only and using alternate threat and non-threat data sets, to mix training data were tried. The data were normalised to 256 points. The targets were 0 or 1. The neural network was trained on 2 sets of data and tested on 1. This failed to train and produce the required outputs of 0 or 1.

Using the Burg transform rather than the Fourier transform and varying the number of poles used in the Burg transform was tried. The number of poles applied to the Burg transform were varied from 20 to 100. Training the neural network on this data were tried but it failed to show clear results.This could possibly be because the shape of the data doesn't change when the number of poles in the Burg transform are varied and the neural network is training on the shape of the data rather than individual data points.

5.4.6 VNA time domain data

Vector Network Analyser time domain data can be thought of as time of flight data as in a conventional radar system. The wax block is encountered first with the body behind it. To simplify the data presented to the neural network, the data was arranged by amplitude with threat present data to one side and threat absent data to the other

side of the plot, the data without any threat present could then be discarded if needed. The Matlab (Math-Works, 2009) function sort does this for array data.

The data was aligned by cross-correlation and then sorted by maximum amplitude in the scan direction. This data was used to train the neural network, initially the network did not train well. The Matlab function xcorr was used to align the data. This works well for simple data, such as the candle, but did not perform well for the more complicated on body data. The Matlab function sort performs a sort by amplitude on the data, this works well for both sets of data. Training the neural network on this data works well, but testing on similar data gave inconclusive results. Adding thresholding to the data processing was tried, but didn't work well. Removing xcorr function and thresholding and sorting the data produces data that the neural network fails to train on.

Thresholding, correlating (xcorr) and then sorting does not seem to produce results that a neural network can be trained on.

Therefore, to simplify the data, before it is correlated, the Matlab function imfilter was used with the Matlab function fspecial using a 3 by 3 averaging filter; fspecial allows user specified masks to be created, in this case a 3 by 3 averaging filter. A range of optical thickness is selected and values outside of this range are ignored (time gated data); this is then filtered with the averaging filter, before being passed to correlation (xcorr) and then sorted.

Training the neural network on this data works well, training on 1 data set and testing on 2. Time data are gated using a predefined optical depth which is the same as choosing the points to apply the gate. Initial tests as shown in table 5.1 worked well, so two sets of training data were tried and one set of test data.

As can be seen from table 5.2 this method of pre-processing the data works well and the network trains well and gives promising results.

Action	target	threat=1, threat absent=0	hits
training	wax vest body1	0.9364	166
	body1	0.01719	63
testing	wax vest body2	0.9665	87
	body2	0.1834	87
	wax vest body3	0.8513	86
	body3	0.1331	134

Table 5.1: Training and testing data for simulated explosives in front of the body.

Action	target	threat=1, threat absent=0	hits
training	wax vest body1	0.9998	58
	body1	0.03525	51
	wax vest body2	0.9973	193
	body2	0.1279	56
testing	wax vest body3	0.9482	179
	body3	0.08164	102

Table 5.2: Training and testing data for simulated explosives in front of the body with a pre-processing step added.

5.4.7 Co and crossed polarisation

Using heterodyne receivers (Andrews et al., 2009) dielectrics produce a strong response in the co-polarised channel, but a weaker response in the cross-polarised channel when using the VNA in 3-port mode, i.e. one transmitter and two receivers. Dielectrics are strong in the co-polarised channel because dielectrics tend to be large compared to the beam size, the wave is planar and there is no asymmetry to change the polarisation, similar to a metal sphere which reflects in the same polarisation as was transmitted because it is symmetrical. The reflectivity of a dielectric is much less than metallic objects.

Dielectrics with fragmentation produce a strong response in the cross-polarised channel and a weaker response in the co-polarised channel. Crossed polarisation is useful for detecting guns and metallic objects as the crossed polarisation is stronger for these objects than for dielectrics or other non-metallic objects, because fragmentation is not symmetric and the reflections are randomly distributed, there is scattering between fragmentation components. Having Co and crossed polarisations recording data at the same time enables a system to detect metals and dielectrics in one pass.

Chapter 6

Signal Processing

6.1 Introduction

The first step in data processing is to Inverse Fast Fourier Transform (IFFT) the raw data; this produces a series of peaks which correspond to a reflection from a surface or discontinuity in refractive index. The x-axis scale needs to be converted to optical depth, the depth of a simulated explosive can then be read off the scale. The problem is to write an algorithm or set of algorithms to automatically find the peaks in the data and to identify the data set as 'threat present' or 'threat absent'.

The author's contribution was to develop a method of aligning the peaks in the data with similar peaks in each sweep so that the peaks could be used to train a neural network.

The novel method was to average the data and then to cross-correlate in both sweep and optical depth axes which re-orders the data into groups of similar data to remove the effects of the person moving between sweeps. The data are then sorted by amplitude to arrange the strongest reflections together. The weakest reflections can then be discarded. The data can then be plotted as an image as shown in figure 9.3. The region of interest is then selected and presented to a neural network as inputs.

6.2 Methods

6.2.1 Finding peaks in data using Matlab

Finding peaks in data automatically can be a challenge and various techniques were tried including averaging over scans and then finding the maximum IFFT amplitude, then converting that point to an optical depth. This would then give the optical depth of the brightest reflection, although this might not always be from a potential threat object, as it could come from the body or from 'glints' from metal buttons or zips.

Splitting the data into blocks and then finding the maximum value for the block was tried; again this had the problem of finding the brightest response. Fitting Gaussian curves to the data was tried, but even with multiple Gaussian curves, it was found that the curves did not fit well to the data, often with fitted curves missing a peak that could be seen by eye, but the fitting tool in Matlab would miss. Applying the Gaussian filter function from Matlab was tried; this was unsuccessful because it smoothed out the data and then the peaks could no longer be found by curve fitting or by eye. The Gaussian filter function in Matlab was used as an image filter and a mask was created, the mask was tried at 3 by 3 (the smallest possible mask) which didn't produce any useable results; so it was tried with a larger 5 by 5 mask. The larger mask gave poor results because it smoothed out the peaks until the data was useless. The average filter function was tried, but both techniques made finding the peaks harder by smoothing out the peaks rather than emphasising them.

Averaging across sweeps, where Inverse Fourier Transformed data vs optical depth vs sweep number is plotted and then using Matlab's 'findpeaks' function is used to search for peaks in the data, the aim of this technique was to reduce the effect of the range to the target changing (as the person moves) between sweeps and to make the peaks from the dielectric stand out; some of the peaks in the data were found, as this technique was successful it was left in as a processing step and further steps were added to further enhance the peak finding algorithm.

As the person moves, some sweeps are not correctly aligned with the transmitter

and receiver and the reflection might be weak or there could be a bright reflection or 'glint' from a object such as a zip, with the aim of removing the sweeps with this unwanted data, cross-correlation or Matlab's function xcorr was tried. This has the effect of arranging similar data sets (sweeps) together; when there is a dielectric (or threat) present then these sweeps are collected together by this method.

With the aim of only training the neural network on data where the target was present, Matlab's sort function was tried, this rearranges the data with the maximum value of IFFT amplitude at one end and the minimum value at the other. Then the sweeps with no peaks in (caused by the side to side movement of the person and alignment of the target) are at the minimum end and a portion of this data can then be discarded. By eye, about half of the sweeps had no peaks in, so 50 % of the data was ignored and then the 50 % with peaks in was passed to the neural network for training data.

6.2.2 Neural Networks

A set of data (multiple sweeps of the frequency range), at the same distance to the target, with the same antenna gain, output power, distance from transmitter, was taken with the wax on the person and then the person without the wax, the wax is the explosives simulant. This was repeated to build up a training set of data; at least two training sets of data are needed and one test set for training the neural network. The data are processed with the algorithm written previously.

A neural network once created needs to be configured and then tuned, this tuning is called training. Configuring the network means arranging it so that it is suitable for the problem to be solved. Training is achieved by presenting the network with example data, known as training data. The adjustable network parameters (called weights and biases) are tuned to optimise the network performance (Math-Works, 2009). To classify the data as threat present or threat absent, a neural network was presented with the following training data; the person with the wax was given a target of 1, i.e. a threat is present and the person without the wax is given a target of 0, i.e. threat absent.

The neural network is set up in Matlab with an input for each data point and a target for each data set, the type of network was a feed-forward back propagation network which is a type of network particularly suited to pattern matching problems. After training the network it was found that the targets were not being met, therefore the data needed to be simplified in some way as the Neural Network toolbox in Matlab will not accept and process thousands of inputs. An algorithm to plot Fourier transformed data vs optical depth vs sweep number was written in Matlab as shown in section 12.6, then the data was averaged over sweeps, so the amplitude of the Fourier transform is the average over all the sweeps at each point as shown in section 12.7, then a script to format this data into a format suitable for input into a neural network was written.

The neural network required training on data that had been reduced from the original data set to minimise the computer CPU time needed to train the neural network. The raw data was first Inverse Fast Fourier Transformed, then an optical depth range known to contain the target was selected; the data was then normalised to produce a standard range of inputs to train the neural network. This process was repeated for a person carrying simulated explosives and the person alone, these two data sets were presented to the neural network for training as shown in the code in section 12.8. The neural network was tested with data formatted in the same way by the code in section 12.9.

A neural network receives inputs which are summed and passed to the output, the output is usually weighted by the transfer function which is a non-linear function usually with a sigmoid shape.

Training the neural network with various different transfer functions was tried to match the input data with a specified output; the logsig transfer function gives outputs in the range 0 to 1 as the neurons input goes from $-\infty$ to $+\infty$, for multilayer networks; the tansig transfer function gives outputs in the range -1 to +1. Sigmoid neurons are limited to a small output range, whereas purlin can take on any value.

6.2.3 Gaussian Curve Fitting

Fitting Gaussian curves to the optical depth data was tried; the Matlab curve fitting tool, 'cftool' was used. It was used to fit 3 Gaussian curves to the data, this data was then used to train the neural network. Training the neural network with this data under trained the network so that some of the targets were met. As this had partially trained the network it was thought that adding more Gaussian's to the fit would improve the fit and so produce better results from training the neural network with this newly processed data. Fitting 4 Gaussian curves to the data and training a neural network on the three parameters of peak amplitude, peak position and peak width was tried, but didn't train the network well, this was because the Gaussian parameters were not fitting to the data and so the training data was poor. The results are discussed in chapter 9.

Time domain data from the VNA was collected for 200 sweeps of 14 to 40GHz. This data was then gated over the range of optical depths to leave the region containing the body and simulated explosives data. The data forms a 3-D array in Matlab. Using the Matlab image processing toolbox, a 3 by 3 averaging filter is then applied to make any spurious points less significant after averaging. The data are then aligned by correlation coefficient, so that similar sweeps are aligned on more than one peak. The data are then sorted by amplitude and plotted as an image. The data still consists of a 3-D array.

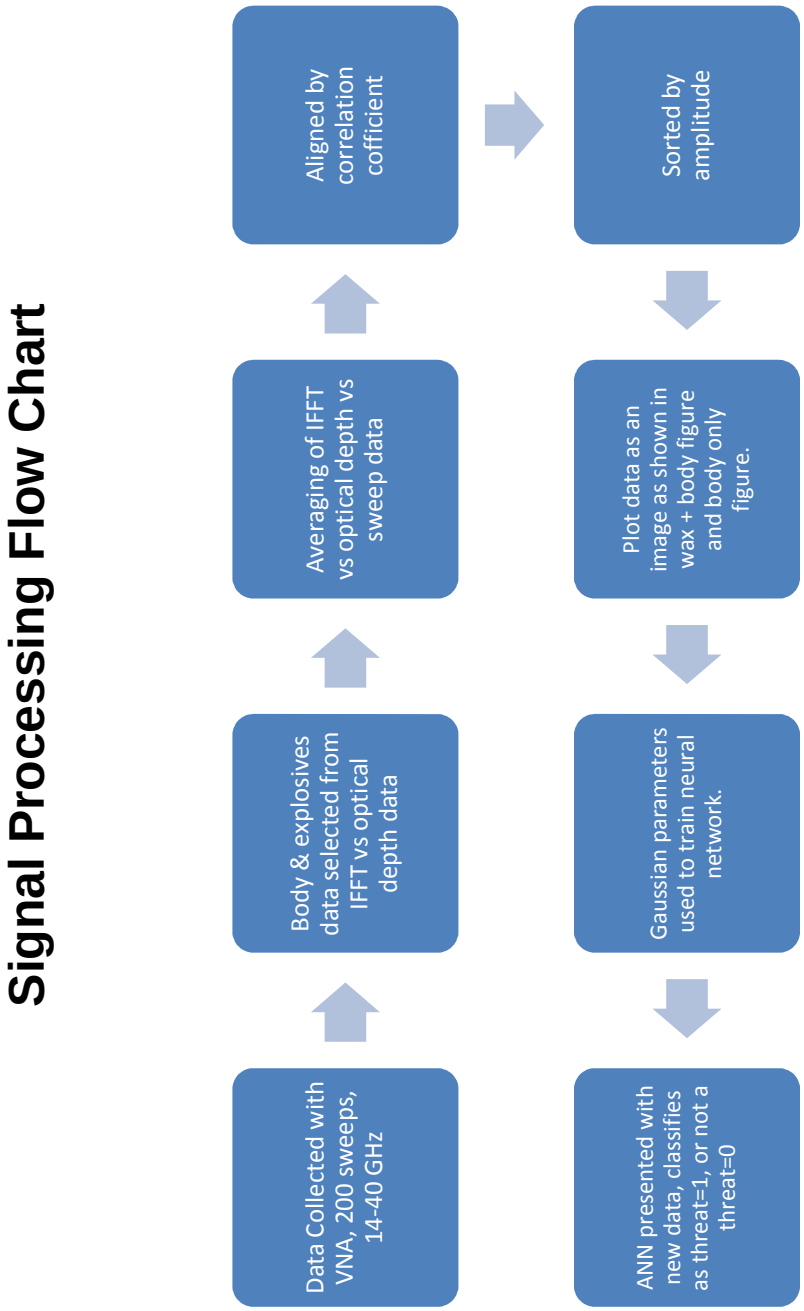

Figure 6.1: This flowchart shows the steps in the signal processing of the VNA data.

This 3-D array is then averaged (the mean was calculated in the sweep number dimension of the data) to obtain one curve. The sum of four Gaussian functions is then fitted to this data for curves containing explosives in front of the body and for curves where no explosive was present. The Gaussian curves are expressed in terms of 3 parameters: Peak amplitude, peak position and peak width. There are 4 sets of this data for each curve, which produces a 4 by 3 array in Matlab. This array is then sorted by position of the curve. The data are then used to train an artificial neural network, with 2 sets of 'threat' and 'non-threat' data. The targets for the network are 1 1 1 and 0 0 0.

Each new set of data are processed in the same way and then presented to the network, the network produces an output in the range 0 to 1, for each of the targets, e.g. 0.7 0.8 0.9. A Matlab GUI was used to provide an indicator either red or green, threat or non-threat, based on the average of the three outputs. So greater than 0.5 gives red and less than 0.5 gives green. This could be improved by giving a sliding scale of threat out of ten, i.e. 0 to 1 in 0.1 increments.

The filter 'imfilter' from the Matlab image processing toolbox was used as a pre-processing step to the neural network because using correlation alone was failing to train the network. Thresholding was tried, but this lost too much data to train the network on. Averaging, sorting by correlation coefficient and then sorting by amplitude produced good results by training on one set of data and testing on a further two data sets of 200 sweeps. This was then increased to 4 training sets and 16 test sets.

Removing the averaging step from the pre-processing of the data results in the neural network incorrectly identifying non-threat data sets as threats. The data are more spread out and spurious points could be causing the mis-classification. Figure 6.1 shows the steps of the signal processing algorithm for the VNA data and Gaussian fitting.

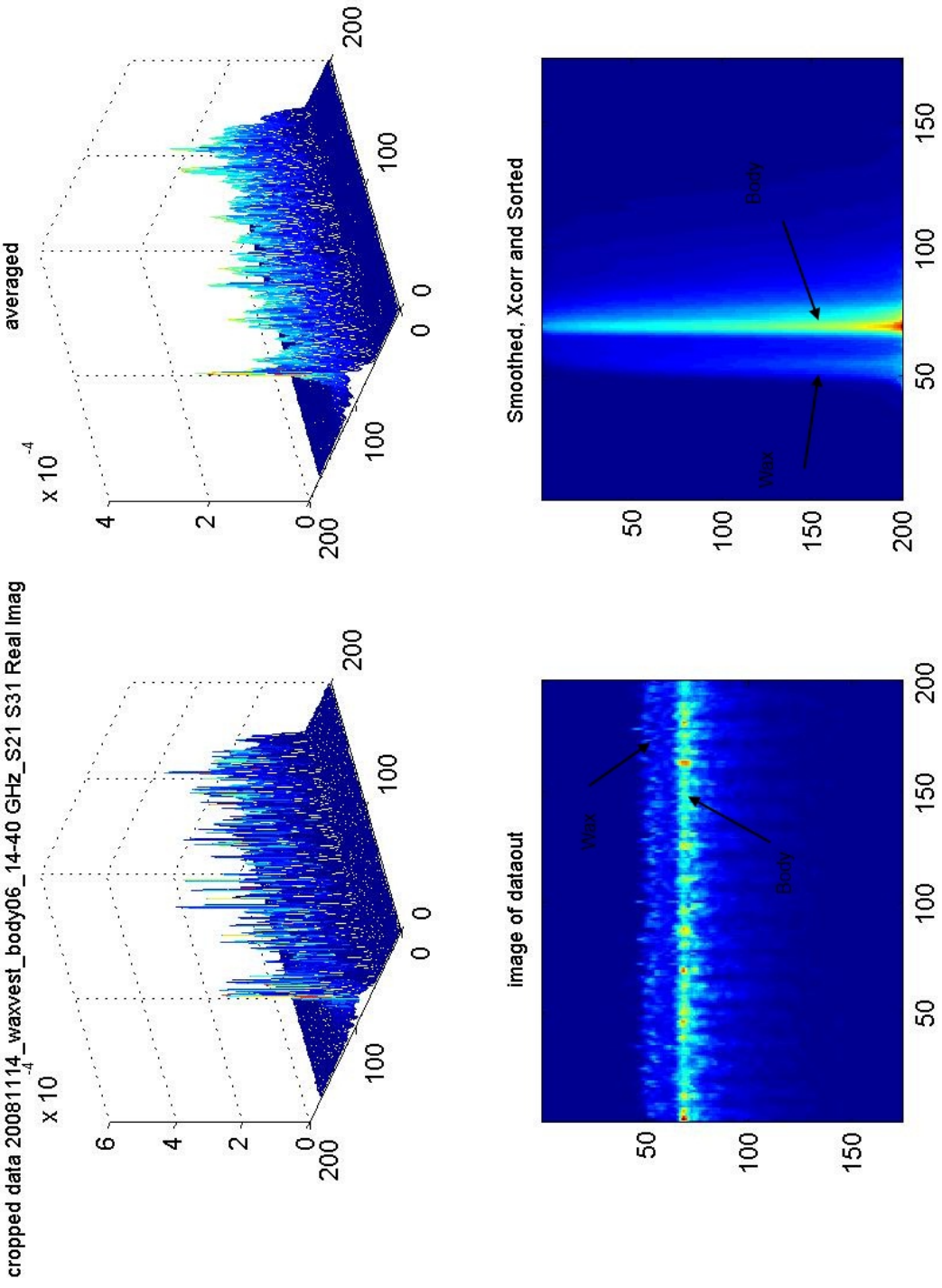

Figure 6.2: Wax in front of body, data set 6

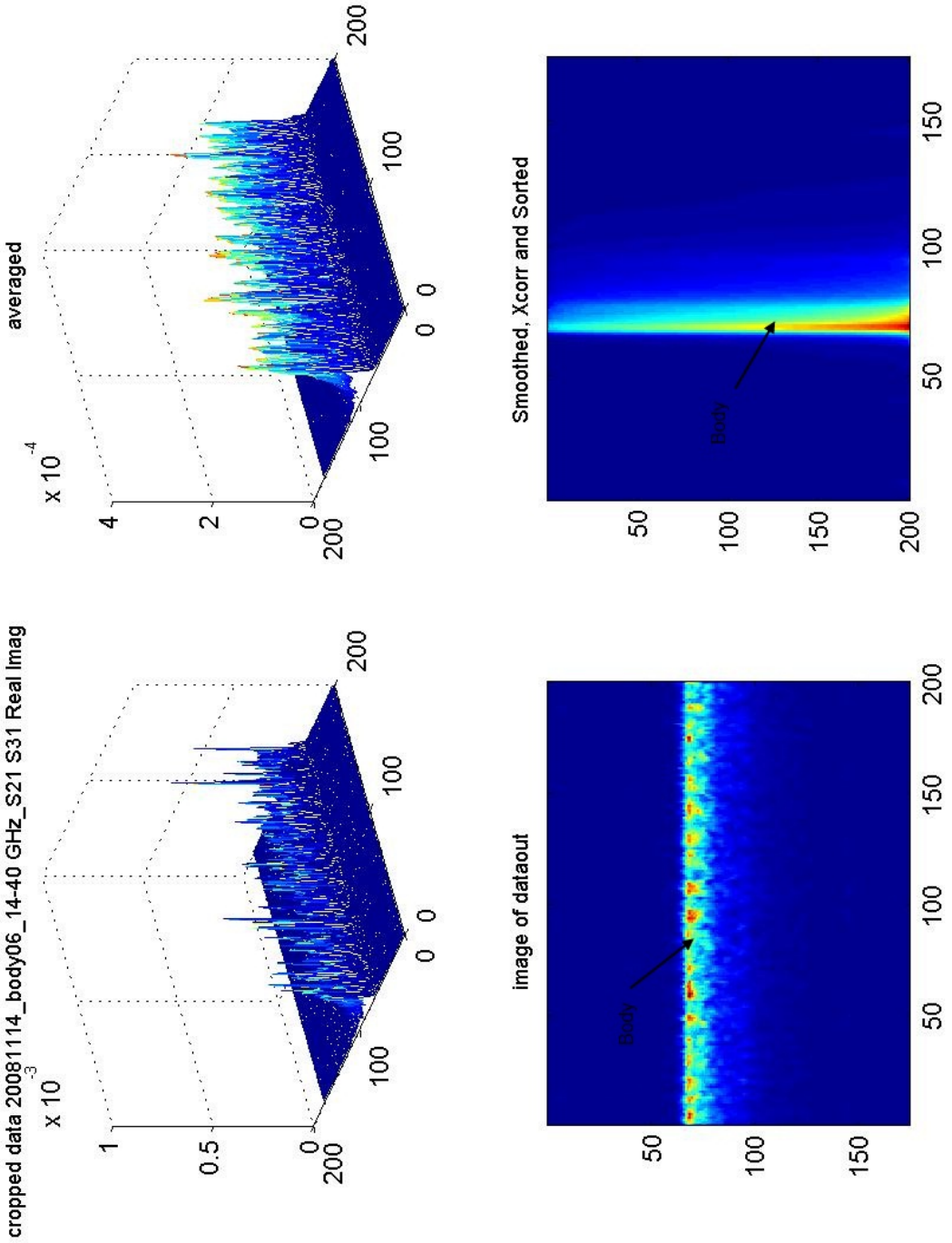

Figure 6.3: Body only, data set 6

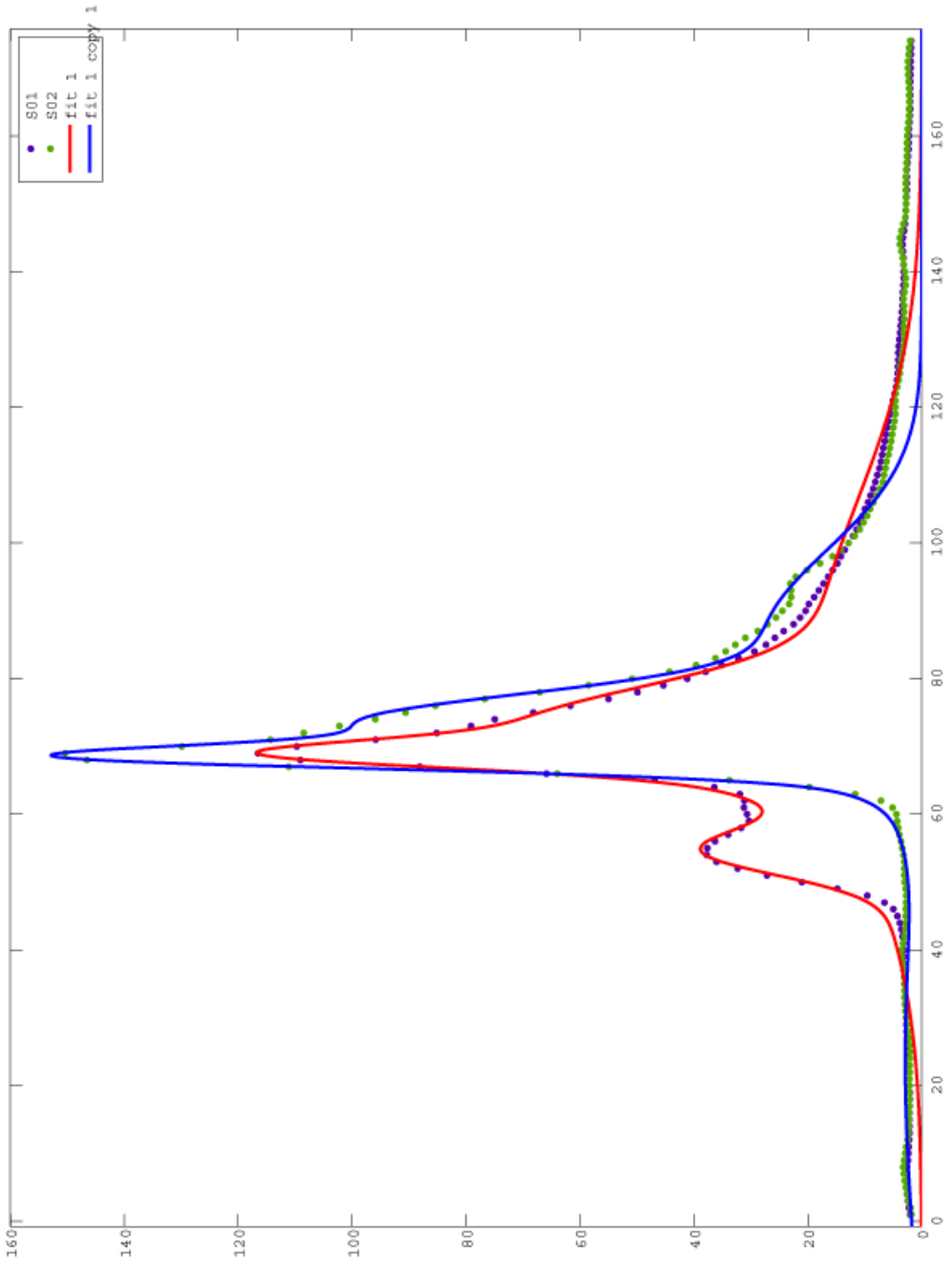

Figure 6.4: Gaussian curves fitted to data set 6

6.2.4 VNA data collection

The VNA was used as a swept frequency source to collect frequency data points and 200 sweeps. The resultant complex data are read in by Matlab, the Inverse Fast Fourier Transform is used to transform from frequency to time domain and the data are transformed from frequency to optical depth space; the absolute value of the IFFT of the frequency data are plotted against optical depth. The data was then time gated to remove the unwanted points and then passed to the Matlab script to correlate and sort it. Matlab is used to apply an averaging filter, then cross-correlation and re-ordering the data by maximum correlation coefficient. Taking the mean across all the sweeps and then fitting the sum of four Gaussian curves to the data are done using the Matlab function 'cftool'. The parameters of the Gaussian are taken from the fitting function in Matlab as amplitude, position and width, so a 3 column by 4 row array is produced. This array is then sorted by increasing position, so that the parameters are in order. The data are then input to a neural network and trained. The training data are formatted into a 3 by 4 array; 3 columns: amplitude, position and width and 4 rows, for each Gaussian fitted to the data. The targets therefore, have to be 1 1 1 and 0 0 0, because the targets have to equal the number of columns of the data.

To auto-gate the data, the average (mean) is found in the direction of the sweeps, so that one column can be plotted. The maximum value is found and then points -150 and +149 are found, these are used to crop the array. The conversion from optical depth to array index is not needed.

To simplify the data and make the training of the neural network more reliable, the data was simplified to a pattern of body and wax peak (a double peak) or body only (a single peak). This data was taken using the 30cm lens to focus the beam on to the target.

Fitting Gaussian curves to the data doesn't always identify all of the peaks, some of the fits miss the peaks in the data and therefore the neural network doesn't have sufficient data to train on as shown in figure 9.9.

Training the neural network on the Gaussian parameters of curve amplitude, curve

position and curve width and specifying targets of 1,1,1 for threat data and 0,0,0 for non-threat data produced the correct training data from three targets i.e. 1 for a threat or 0 for a non-threat. Presenting the network with previously unseen data produced the correct outputs in 88% of cases.

Re-training the neural network on strong and weak data sets produced good results when the training set was alternate threat and non-threat. 8 test sets of threat, then non-threat were tried. The results were good, 94% of the test set were correctly classified as threat or non-threat. Further results are presented in chapter 9 and the code is shown in sections 12.10 and 12.11.

Simulated explosives have been detected when held against the body and can be distinguished from the body without explosives. After training with representative data a neural network has been used to classify each data set as either threat or non-threat. This method works well provided that the Gaussian curves fit well to the data. Poorly fitting curves lead to mis-classified results, so this method could be unreliable unless a method of checking the fit of the curves was included.

Chapter 7

Gaussian Optics

7.1 Gaussian Optics

7.1.1 Lens Materials

Choosing a material for a millimetre wave lens involves selecting a dielectric material with a low loss and a suitable refractive index. PTFE (Polytetrafluoroethylene also known as the brand name Teflon) is the microwave lens material typically chosen for its very low loss at microwave frequencies. Other considerations are cost, density and ease of manufacture of lens shape. PTFE has a low loss and suitable refractive index, but it is expensive compared with PE (Polyethylene) and has a higher density so is heavier for a given lens diameter. Therefore, PE was chosen as the lens material, as the lenses are designed to go into a portable system, so weight is a design consideration. PE is also easier to manufacture lenses from as it does not deform when machined, unlike PTFE.

Lamb (Lamb, 1996) gives the refractive index, n, dielectric constant, ϵ, and loss tangent, $tan\ \delta$ for PTFE and PE as shown in table 7.1, at 94GHz and 300K.

Material	n	ϵ	$tan\ \delta$
PTFE(Teflon)	1.4370	2.065	0.00021
PE	1.5185	2.3058	0.00037

Table 7.1: Refractive index, n, dielectric constant, ϵ, and loss tangent, $tan\ \delta$ for PTFE and PE at 94GHz and 300K.

7.1.2 Theory of Gaussian Beams

The Rayleigh criterion is given by equation 7.1 and is the limit to angular resolution as a result of Fraunhofer diffraction (far field); contrasting this with the equivalent expression for a Gaussian beam, given by equation 7.2

Angular resolution, θ, is given by

$$\theta = 1.22\frac{\lambda}{D} \tag{7.1}$$

where λ is wavelength and D is aperture diameter.

$$2\frac{\lambda}{(\pi\omega_0)} \equiv 1.273..\frac{\lambda}{D} \tag{7.2}$$

The linear diameter of the spot, r is given by

$$r = 2.44\frac{f\lambda}{D} \tag{7.3}$$

where f is the focal length of the lens, λ is wavelength and D is the lens diameter and the units are the same as the wavelength.

Diffraction theory says that a light beam will spread as it propagates, therefore it is impossible to have a perfectly parallel beam.

Gaussian optics gives:

The Gaussian focussed spot size, ω_F, is given by

$$\omega_F = \frac{\lambda f M^2}{\pi\omega_L} \tag{7.4}$$

where λ is wavelength, f is focal length of the lens, $M^2 = 1$ for a Gaussian beam and ω_L is the lens radius (Melles-Griot, 2009).

A Gaussian TE_{00} (the lowest transverse Electromagnetic mode) laser beam made

perfectly flat will quickly acquire curvature and begin spreading, as given by

$$R(z) = z[1 + (\frac{\pi\omega_0^2}{\lambda z})^2] \tag{7.5}$$

$$\omega(z) = \omega_0[1 + (\frac{\lambda z}{\pi\omega_0^2})^2]^{1/2} \tag{7.6}$$

where z is the distance propagated from the plane where the wavefront is flat, λ is the wavelength of light, ω_0 is the radius of the $1/e^2$ irradience contour at the plane where the wavefront is flat, $\omega(z)$ is the radius of the $1/e^2$ contour after the wave has propagated a distance z, and $R(z)$ is the wavefront radius of curvature after propagating a distance z (Melles-Griot, 2009).

Therefore, a Gaussian beam can be focused to a beam waist at some distance from a lens or the cassegrain antenna and then will begin diverging as given by the above equations.

7.2 Lens Designs

7.2.1 Lenses for a 15 to 20cm spot size at 7 metres

Focal length (m)	Frequency GHz	lens diameter (m)	Spot size (cm)
5	94	0.15	13
6	94	0.15	15.6
7	94	0.15	18.2

Table 7.2: A table of calculated focal length, frequency of operation, lens diameter and spot size for a polyethylene lens.

$$\theta = \frac{1.22\lambda f}{D} \tag{7.7}$$

where θ is the spot size in metres, λ is the wavelength in metres, f is focal length of the lens in metres and D is the diameter of the lens in metres.

If f=7m, λ = 0.0032m and D=0.18m, then the spots size will be 15cm.

Cornbleet (1976) defines a hyperbolic lens surface as

$$r = \frac{f(\nu - 1)}{\nu cos\theta - 1} \tag{7.8}$$

where r is the radius of curvature, ν is refractive index, f is focal length of the lens and θ is the angle of the incident rays to the lens axis.

In polar coordinates, if R is radius of curvature, ν is refractive index and f is focal length of the lens, then

$$R = (\nu - 1)f \tag{7.9}$$

Providing that $\theta << 1$ and $\nu = 1.5$ for polyethylene and $f = 0.3$ (lens to horn distance), so $R = 0.15$ metres.

Therefore, this gives a lens with 150mm radius of curvature, 300mm focal length and 180mm diameter for a spot size of 15cm at 7 metres, as shown by table 7.2.

7.2.2 COMSOL modelling of lens

A model was drawn in Comsol using the perfectly matched layer boundary conditions and a lens model with radius of curvature, R = 0.15 m, focal length 0.3m and n=1.5.

The lens is to be incorporated into a prototype detector system. The image plane will be adjustable (the position of the lens relative to the horn). The radius of curvature was calculated from the Cartesian form of the hyperbolic lens equation (Cornbleet, 1976). The horn feed was specified to have the dimensions of a w-band waveguide (75 to 110 GHz).

The lens diameter is a trade off between the diffraction limited spot size at 7m for a 18cm lens; which is 15cm and the size of lens which will fit the prototype detector. The lens was reduced to 17cm so it will fit the allocated box. The area modelled by Comsol was 0.4 by 1.1 metres. This is limited by the number of mesh points required for a given frequency (75GHz) and the amount of computer memory available to the software. The mesh size was 0.0015m ($1.5/4\lambda$). With the lens 24cm from the horn, the model produces a roughly parallel beam. With the lens 30cm from the horn, the

model produces a parallel beam, as shown in figure 4.2.

There was a requirement to put a camera through the lens to help with aiming the millimetre wave beam towards a target. To model the effect this would have on the beam pattern of the lens, a COMSOL (2009) model was drawn. A 30mm square was put in front of the lens, with its boundary conditions set to perfect electric conductor, this gives the effect of a metallic box. Comparing the beam pattern before and after shows that there is only a small reduction in amplitude and a slight increase in side lobes, of about 12%. This showed that it would be possible to put a camera through the lens without disrupting the beam pattern noticeably.

A lens of 18cm diameter was incorporated into a prototype detector system and has been used to detect the presence or absence of guns and explosives simulants at a distance of a few metres.

7.2.3 Modelling of 220GHz Lens

There was a requirement to make the detection system more compact, so to reduce the lens size, higher frequency is needed or the operating range will be reduced; as shown by equation 7.7. It is not an advantage to go to terahertz frequencies because the atmospheric attenuation increases. For an operating frequency of 220GHz the wavelength is 1.36mm. The refractive index of polyethylene is n=1.5, so for a focal length of 300mm, this gives a radius of curvature of 150mm. For a lens diameter of 100mm, the diffraction limit gives a 120mm spot size at 7 metres.

Chapter 8

Cassegrain Imager

8.1 Introduction

A cassegrain antenna was tested as a possible solution to increasing the stand-off range of a detection or imaging system. A cassegrain reflecting antenna was proposed instead of a lens because reflecting elements have low loss compared to lenses which have reflective losses associated with the beam passing through the material, the antenna itself can be made mechanically steerable and the mount arrangement can be simpler than with a lens. The cassegrain antenna is optically equivalent to a lens of the same size.

In Geometric Optics, the beam of a cassegrain antenna is normally assumed to be parallel, with the focal point at infinity. The system requirements were to focus at distances up to 10 metres, which would require refocussing of the antenna, giving diffraction limited spot sizes up to 120mm. Figure 8.1 shows the diameter of the smallest spot size for distances of 10cm to 25 metres. The secondary mirror of the cassegrain antenna is the focussing element of the system and the distance between the primary mirror and the secondary mirror gives the systems focal length, so this would need to be adjusted. Figure 8.3 shows a ray trace diagram of a cassegrain antenna.

The mechanics of the existing system did not allow for easy adjustment, so after preliminary tests of the beam pattern and focal point of the system it was decided to design a new focussing mechanism. This allows for easier focussing of the beam by adjusting the distance between the primary and secondary mirrors.

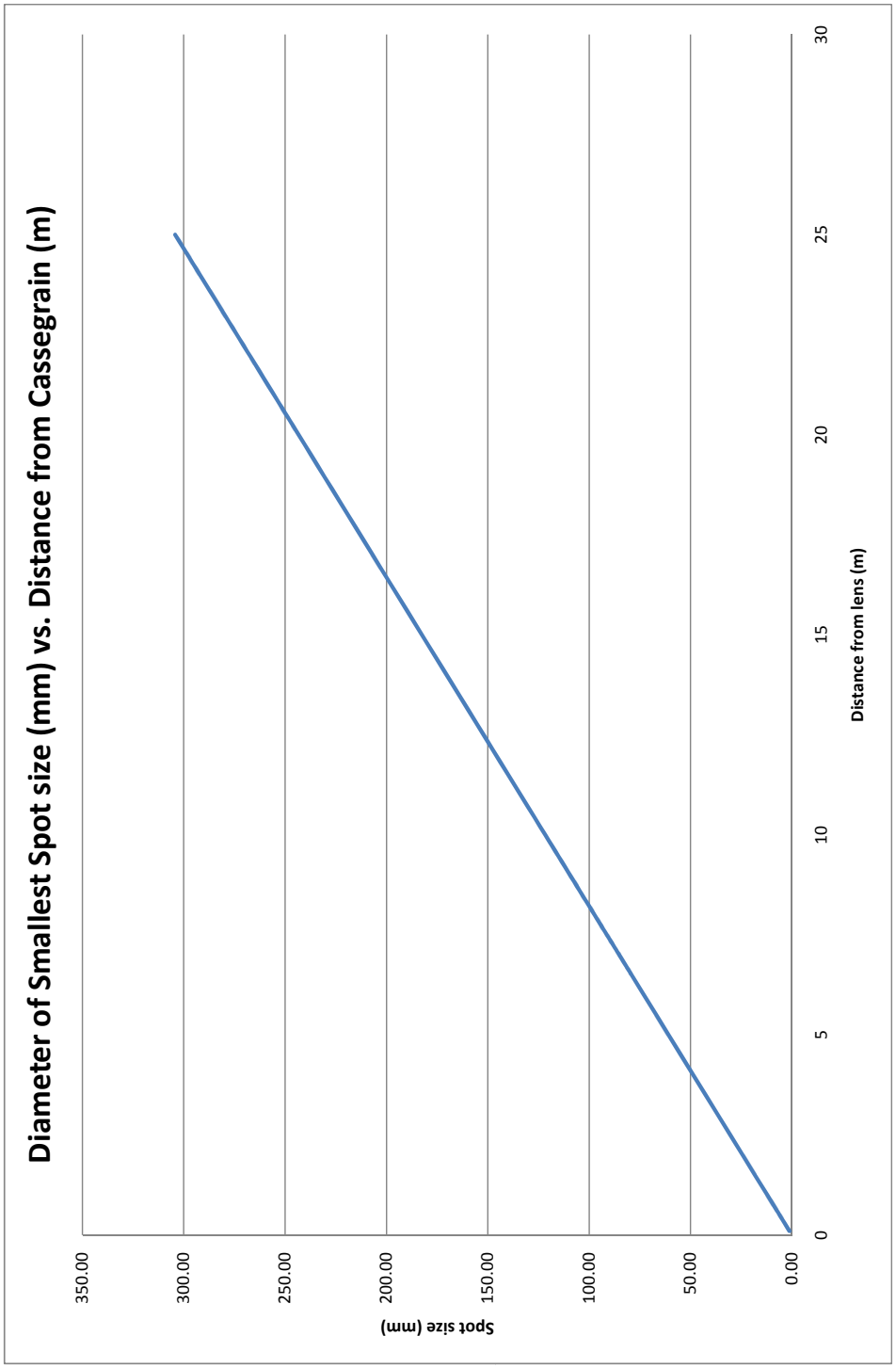

Figure 8.1: This figure shows the diameter of the smallest spot size of the Cassegrain for distances of 10cm to 25 metres from the dish at 3mm wavelength.

8.1.1 Increasing stand-off distance

To increase the stand-off range of a detection system, a cassegrain antenna is used because the Cassegrain has the major advantage that it is folded as there are two reflectors, this reduces system length by a factor of 2. A cassegrain antenna allows for easy focussing of the beam at various distances by adjusting the position of the secondary mirror, this could easily be motorised, if required.

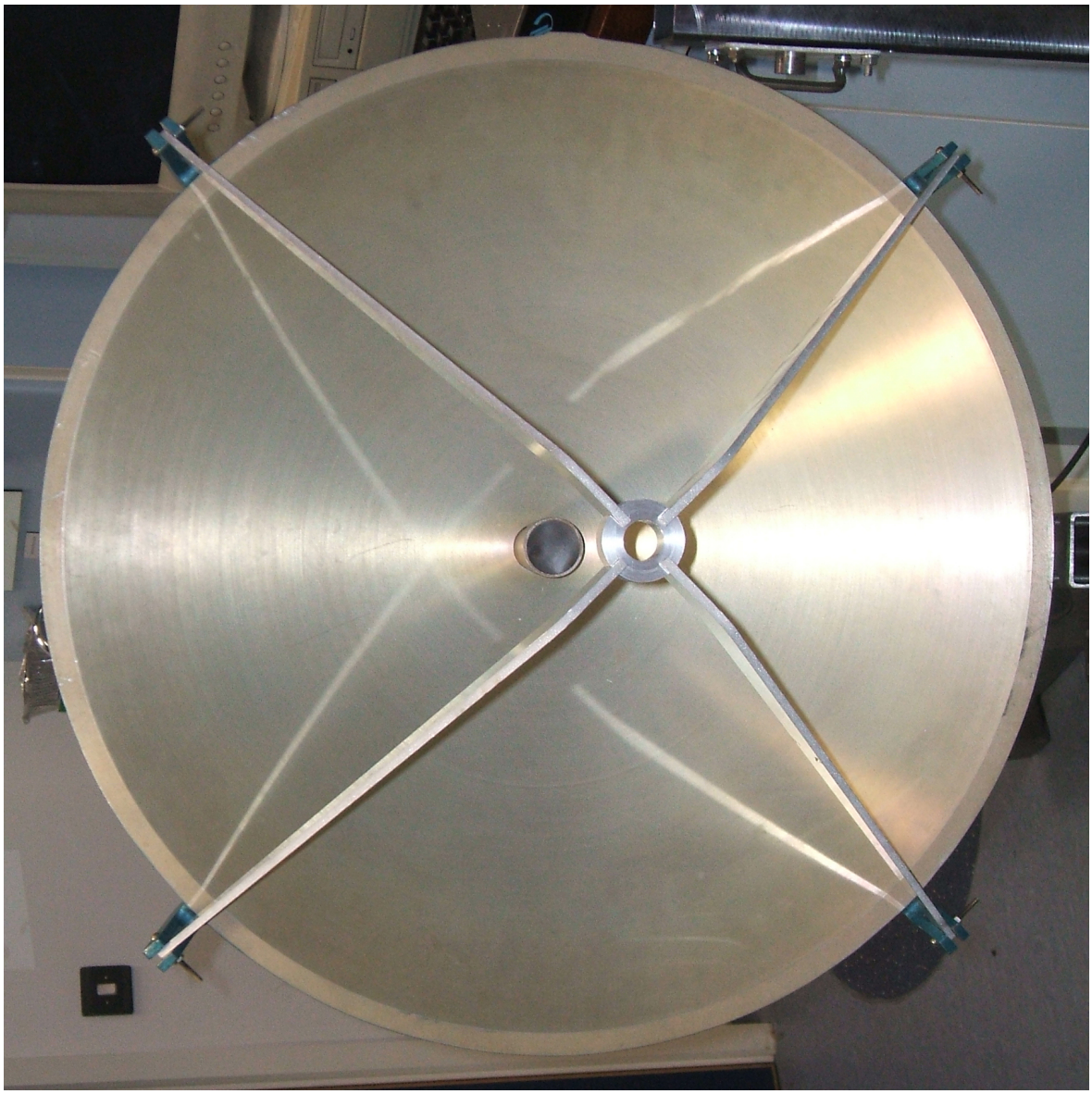

Figure 8.2: This figure shows the cassegrain with the new mount for the secondary mirror.

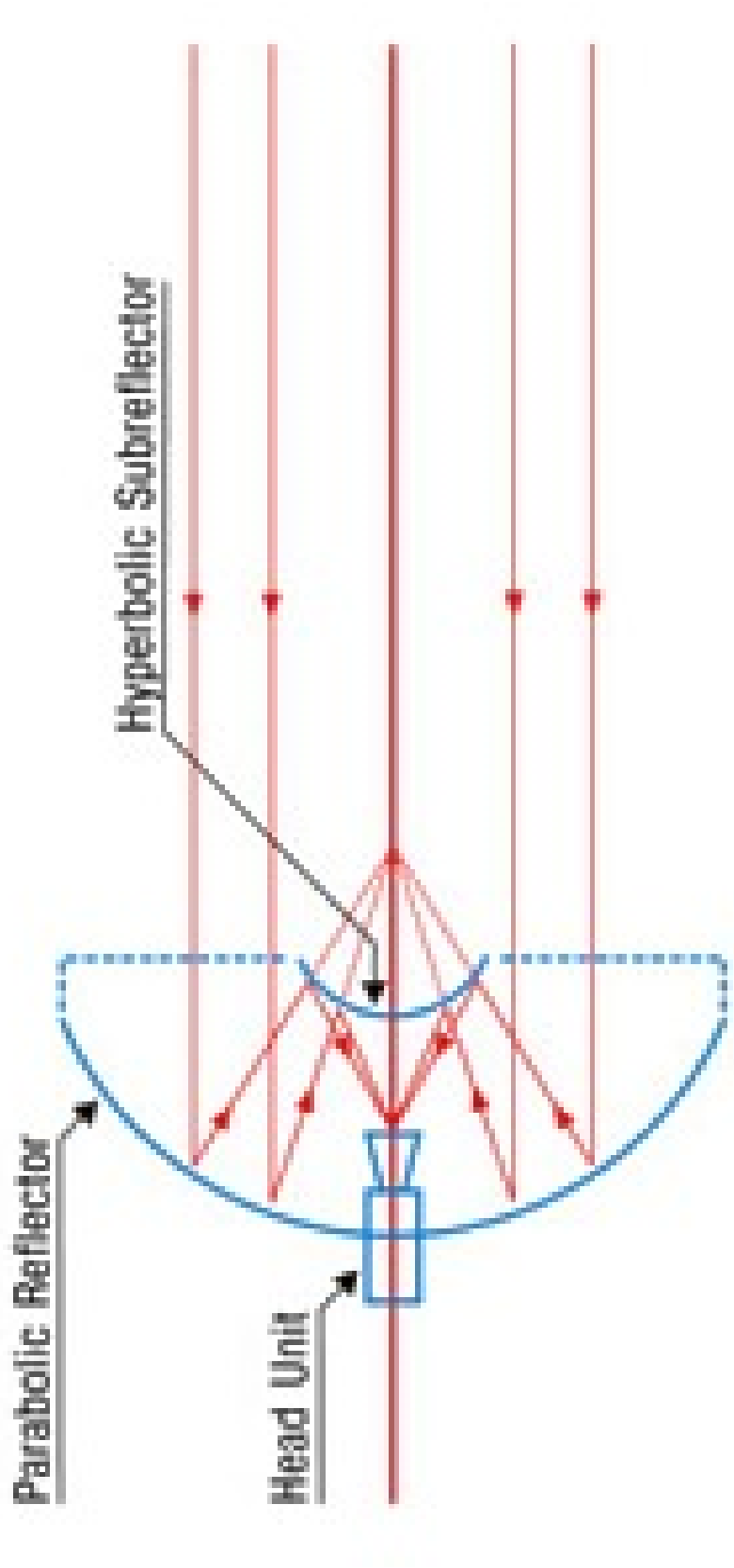

Figure 8.3: This figure shows a ray trace diagram of a cassegrain reflecting antenna (Elva, 2003).

8.2 Passive Imaging System

The imaging system consists of a MMIC receiver, mounted on wave guide at the focal point of the cassegrain antenna which is behind the dish. The output of this receiver is then connected to a DC amplifier which allows for the DC offset to be compensated for and the DC level to be amplified. The circuit board for the amplifier also includes a regulated power supply for the MMIC receiver as shown in figure 8.5. The printed circuit board was designed using Proteus (Labcenter-Electronics, 2010) design software and then manufactured by Manchester Metropolitan University. The schematic is shown in figure 8.4.

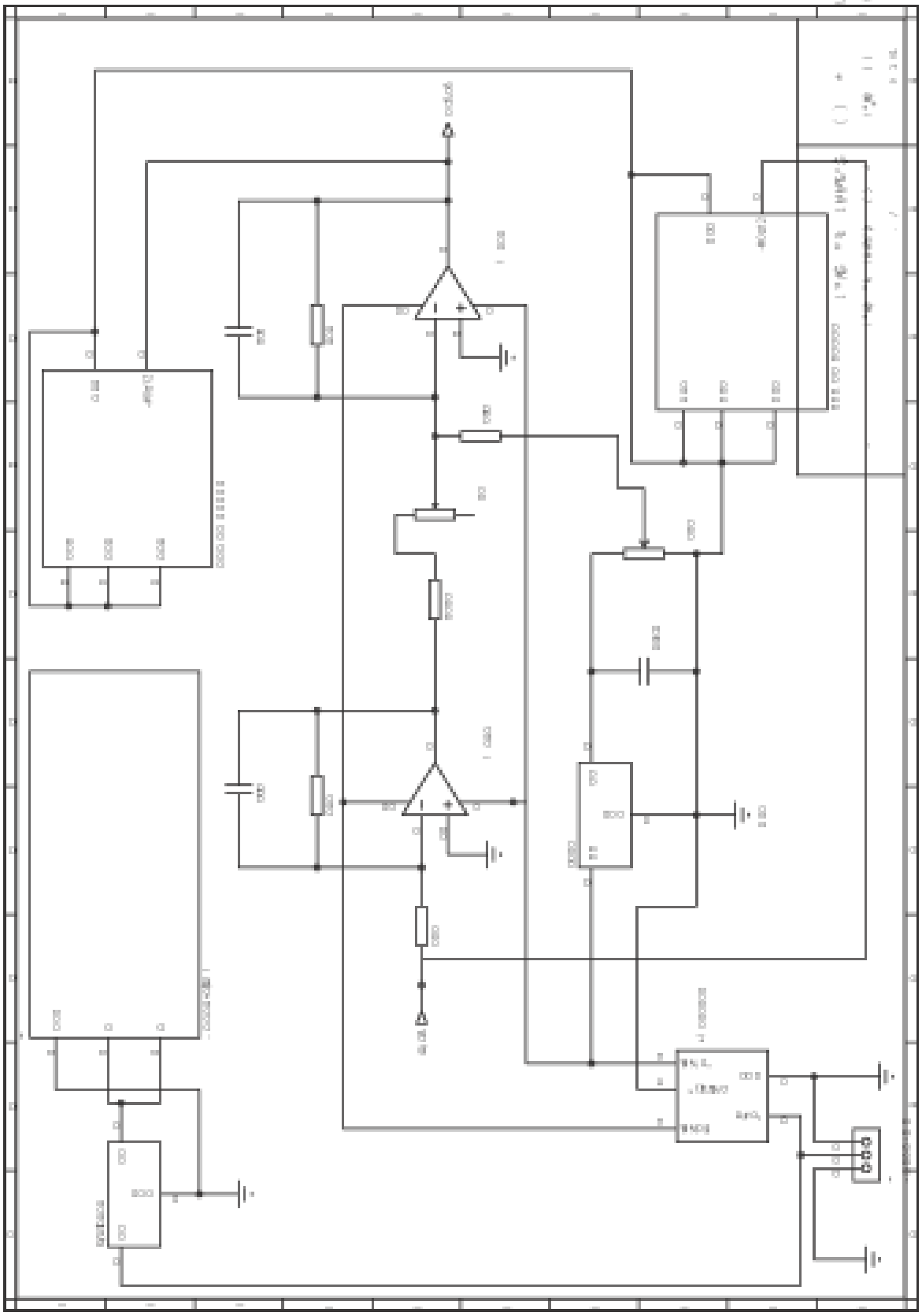

Figure 8.4: This figure shows the schematic layout of the amplifier circuit.

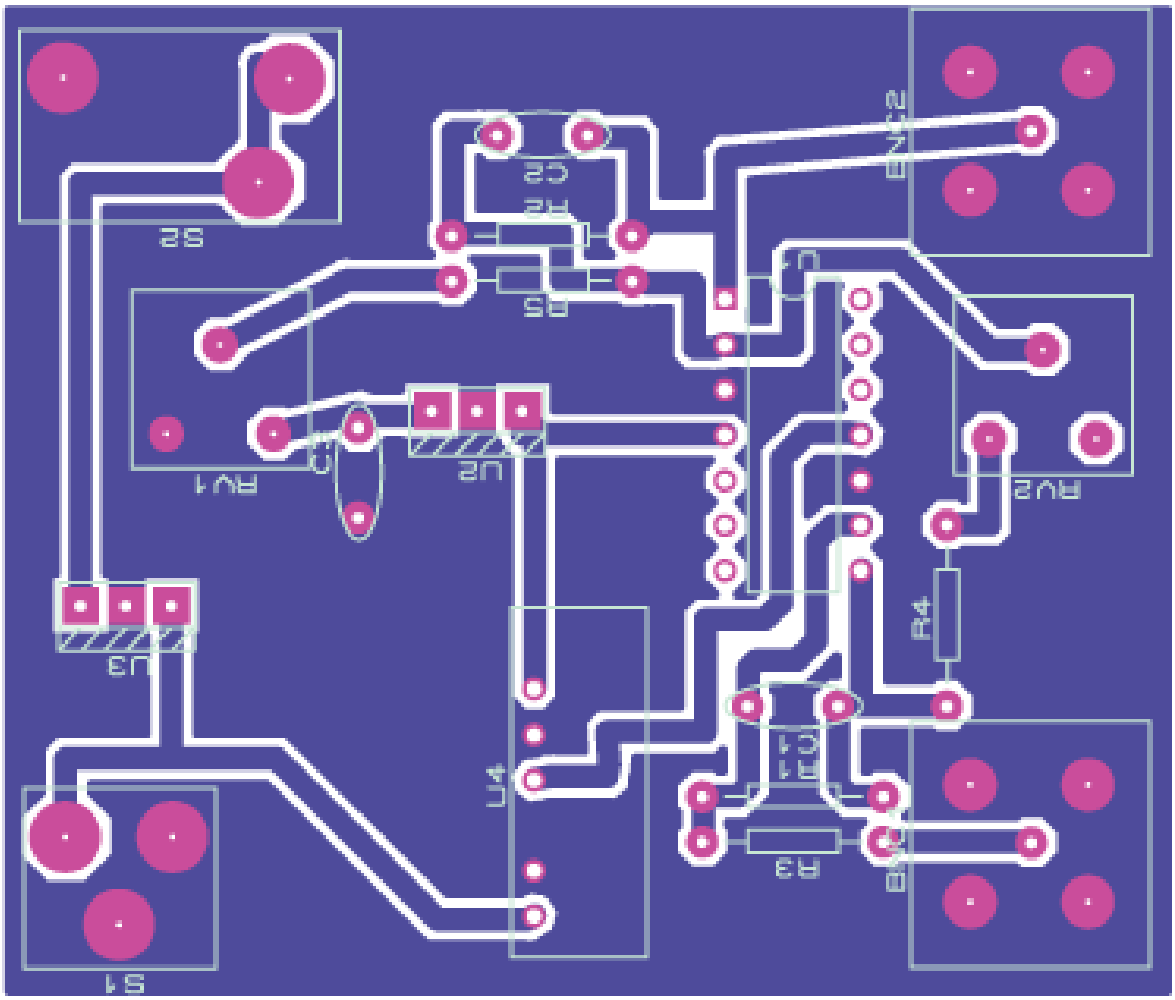

Figure 8.5: This figure shows the circuit board layout of the amplifier circuit.

8.3 Mechanical Assembly

The mechanical assembly and drive system for pointing the antenna were designed and built by another member of the research group (Leonard, 2010). This also incorporates a PIC controller for the drive system. The PIC controller accepts three numbers in a decimal format, for the axis to move, either 1 or 2; the speed to move at, 0 to 255; and the position to move to 0 to 255. There are limits however to stop the antenna running into the mount, so in practice this is 20 to 220. A Matlab (Math-Works, 2009) script was written to raster scan the antenna in a 21 by 21 point grid and take data at each point. This is the amplified voltage output from the MMIC receiver. The data are taken using a National Instruments card (National-Instruments, 2010) and takes 1000 points each time the antenna pauses, this produces an array of 1000 by 441 points and to convert this to an image in Matlab, the data are averaged to produce an array of 1 by 441 and then rearranged to an array of 21 by 21 pixels.

As the mechanical parts for the secondary mirror were being manufactured, initial tests using the dish and the waveguide were done by scanning 21 by 21 points. Figures 8.6, 8.7 and 8.8 show passive imaging results for an incandescent light bulb placed 30cm from the antenna; a rectangular sheet of copper covered circuit board using 500 points per pixel and again using 1000 points per pixel. The objects can be seen clearly in each case as bright spots on the image.

The "spider" mount for the secondary mirror was designed and built by (Leonard, 2010). To align the mount for the secondary mirror with the focal point of the cassegrain a centre ring was made to hold a laser pointer and this was then used to align the mount with the waveguide in the centre of the dish. By removing the receiver from the end of the waveguide the optics can be aligned by keeping the laser spot in the centre of the Mylar window on the waveguide and the laser spot through the end of the waveguide. The secondary mirror mount was glued together and the alignment checked. After the glue had dried, the antenna was centred in its mount, so that the middle of the range is when the antenna points forwards and the waveguide is horizontal, this was so that the centre of the image comes from the centre of the raster

scan.

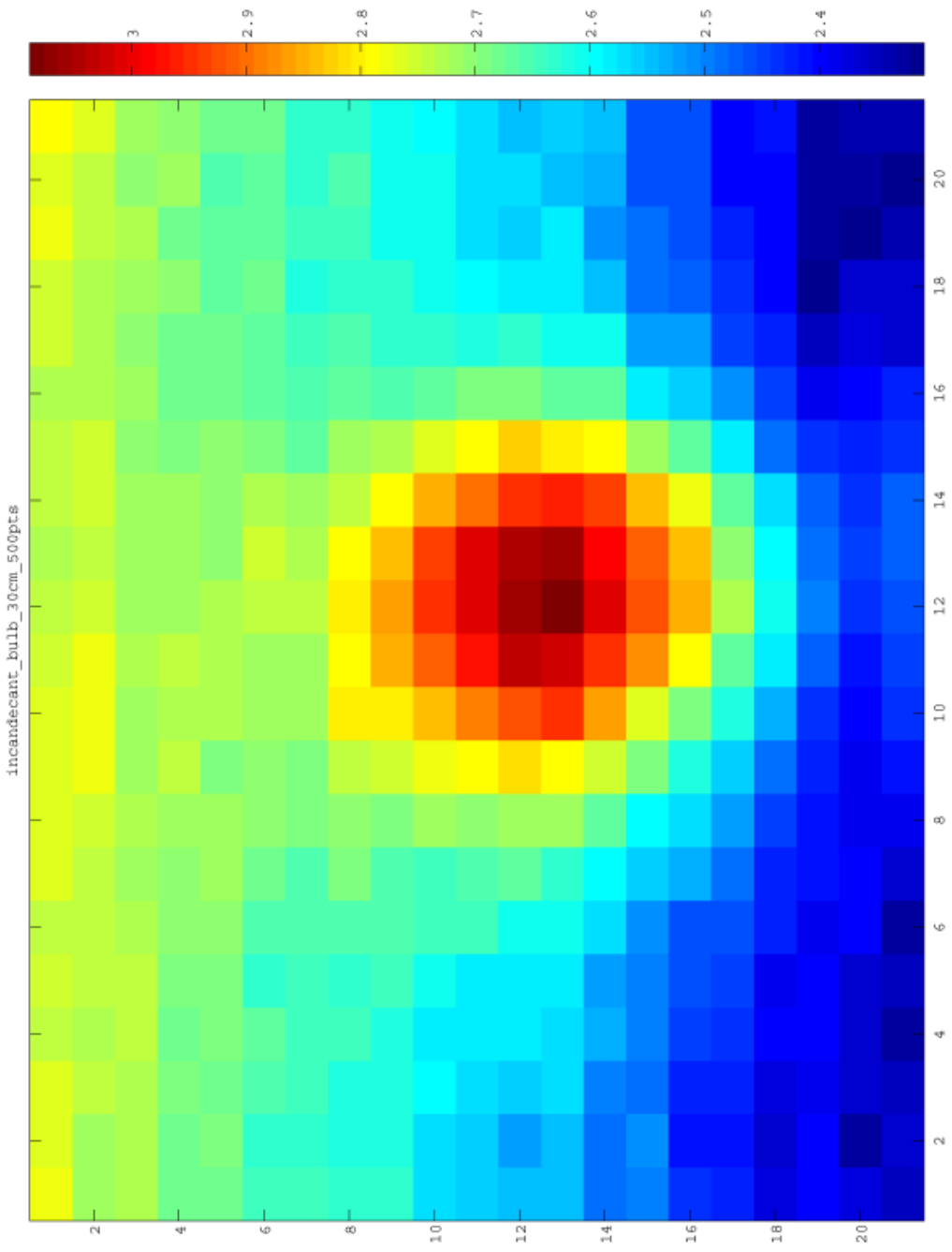

Figure 8.6: An incandescent light bulb at 30cm from the cassegrain antenna, collecting 500 points at each pixel.

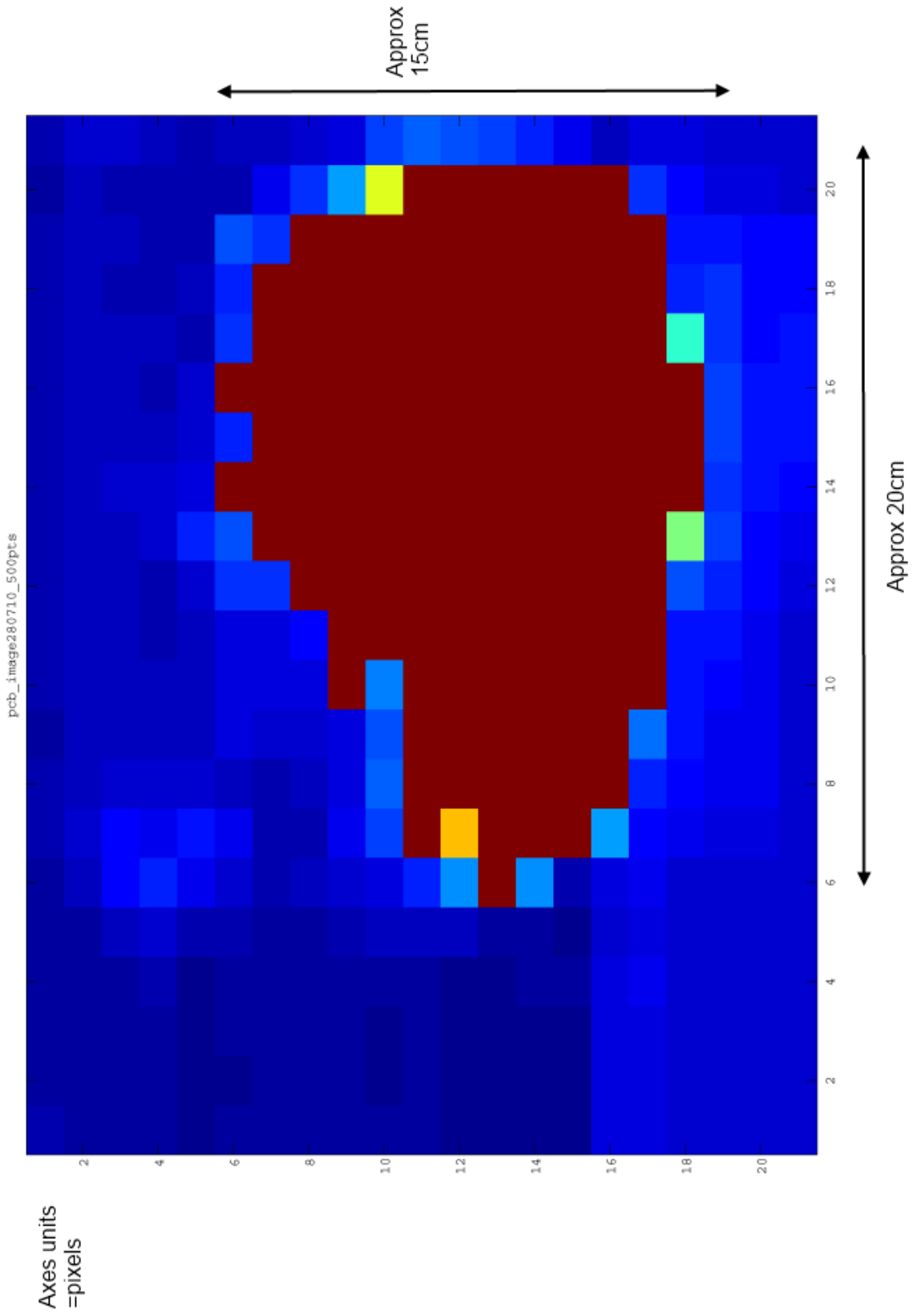

Figure 8.7: Heat image of a piece of copper circuit board, collecting 500 points at each pixel.

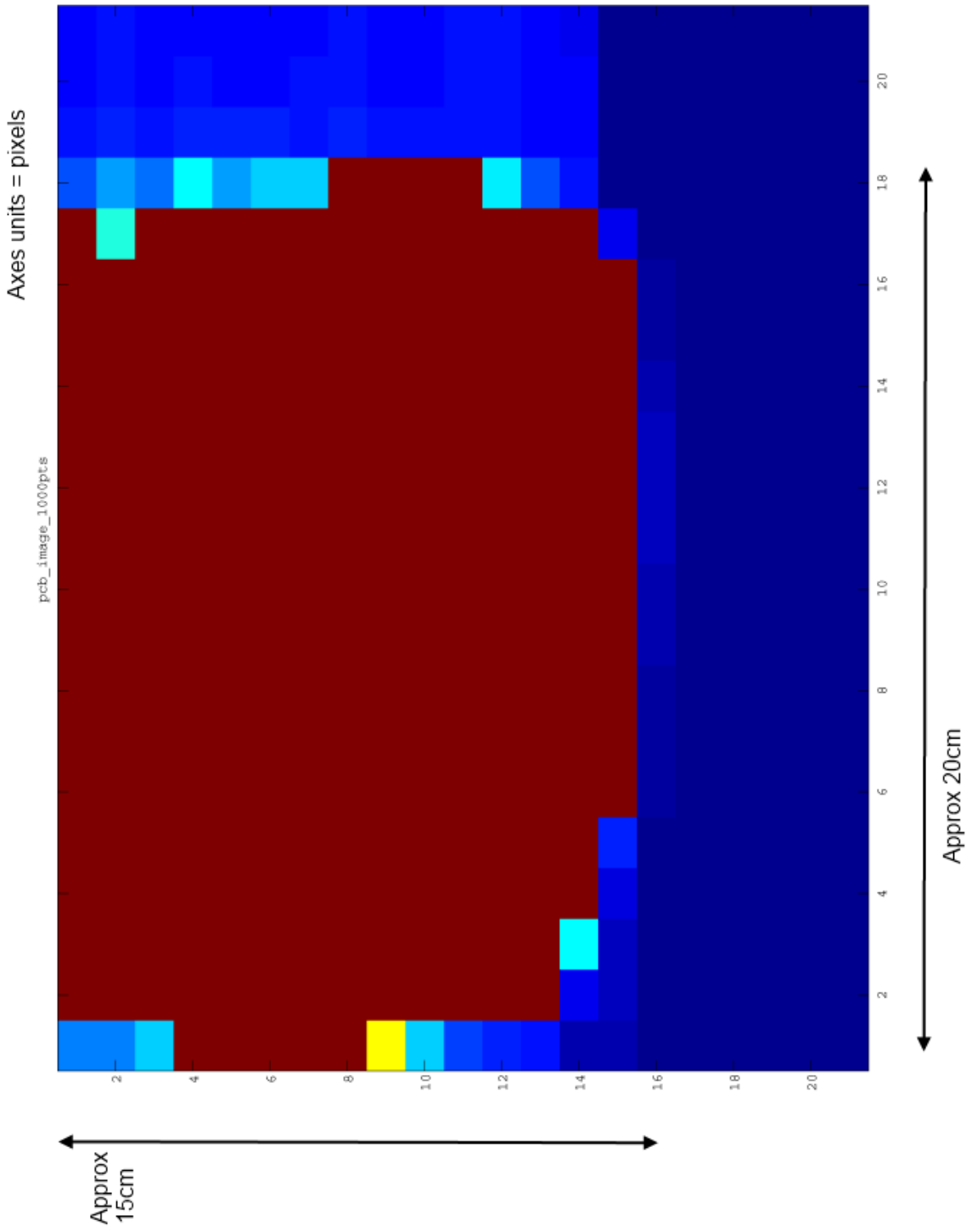

Figure 8.8: Intensity image of a piece of copper circuit board, collecting 1000 points at each pixel.

The cassegrain system can be aligned by mounting the laser pointer such that it is aligned with the beam axis of the antenna, it is then easy to see where the antenna is pointing and align it with its target. A passive image of a person sat in a chair was tried with increments of 10cm, giving 441 pixels and then again with increments of 5, giving 1764 pixels. This is shown in figures 8.9 and 8.10. The outline of a person can clearly be seen. The acquisition time for the high resolution image was one hour.

In the image of a person, the background goes from blue (low) to red (high) values of intensity. This seems to be a characteristic of the MMIC receiver drifting in amplitude with time. The drift seems to be linear. To test this, absorbing foam was placed over the feed to the antenna and an image taken. This should produce an image with just the noise from the receiver. The drift can be compensated for by subtracting the absorber data from the actual data from a scene.

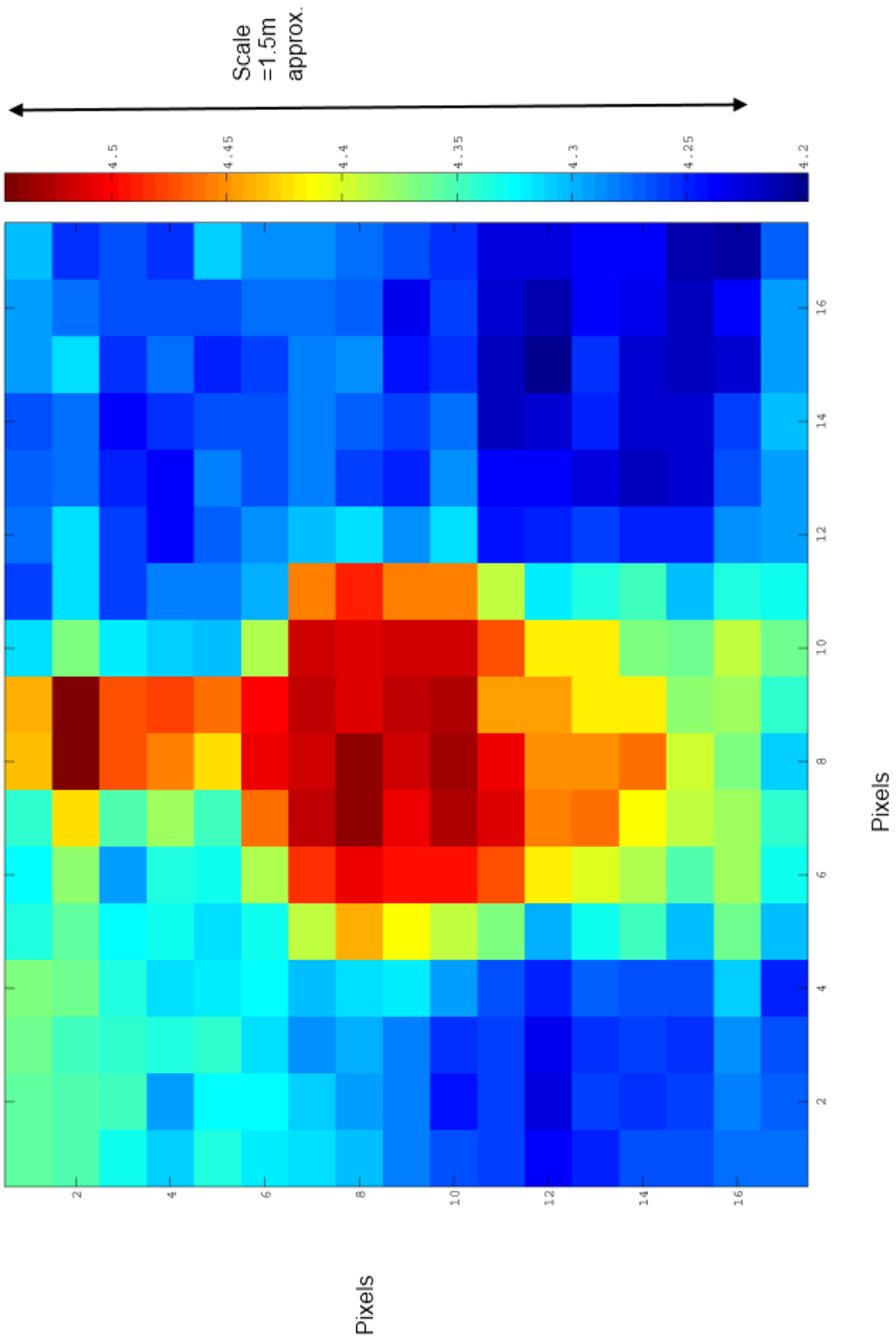

Figure 8.9: A low resolution image of a person sat in a chair.

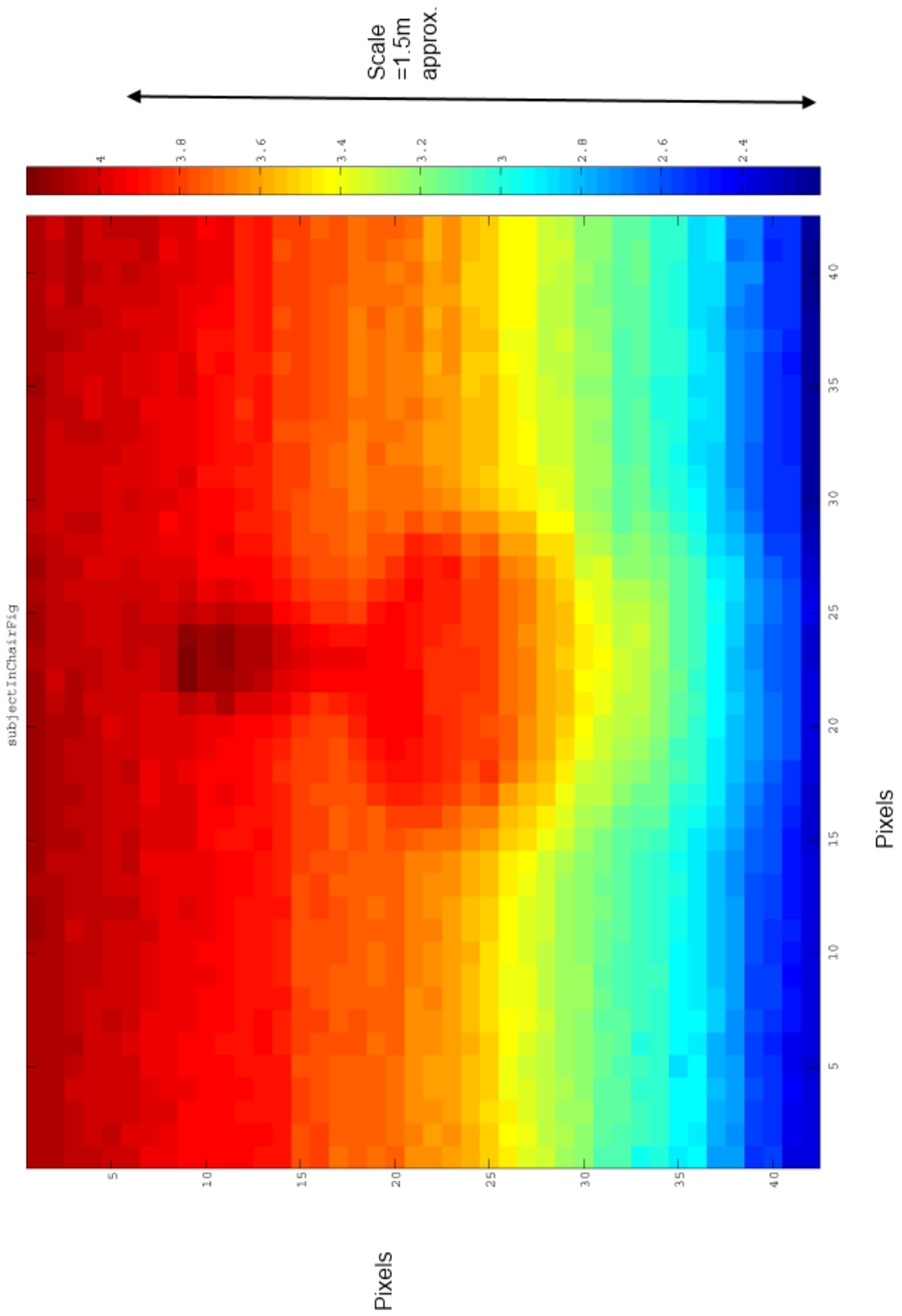

Figure 8.10: A higher resolution image of a person sat in a chair. The image shows a drift in the receiver which is shown in the figure by the change in colour from blue to red. This is due to the instability of the receiver with time.

The image shows the noise drifts in the same way, so it can be assumed that the amplitude of the receiver is drifting linearly with time.

8.4 Active Imaging

An active image was tried with a 441 pixel active scan and a bright pixel can be seen where the stainless steel bottle was, then this was repeated with a 1764 pixel active scan which shows a few more bright pixels for the bottle where stronger reflections occur. This is shown in figure 8.11.

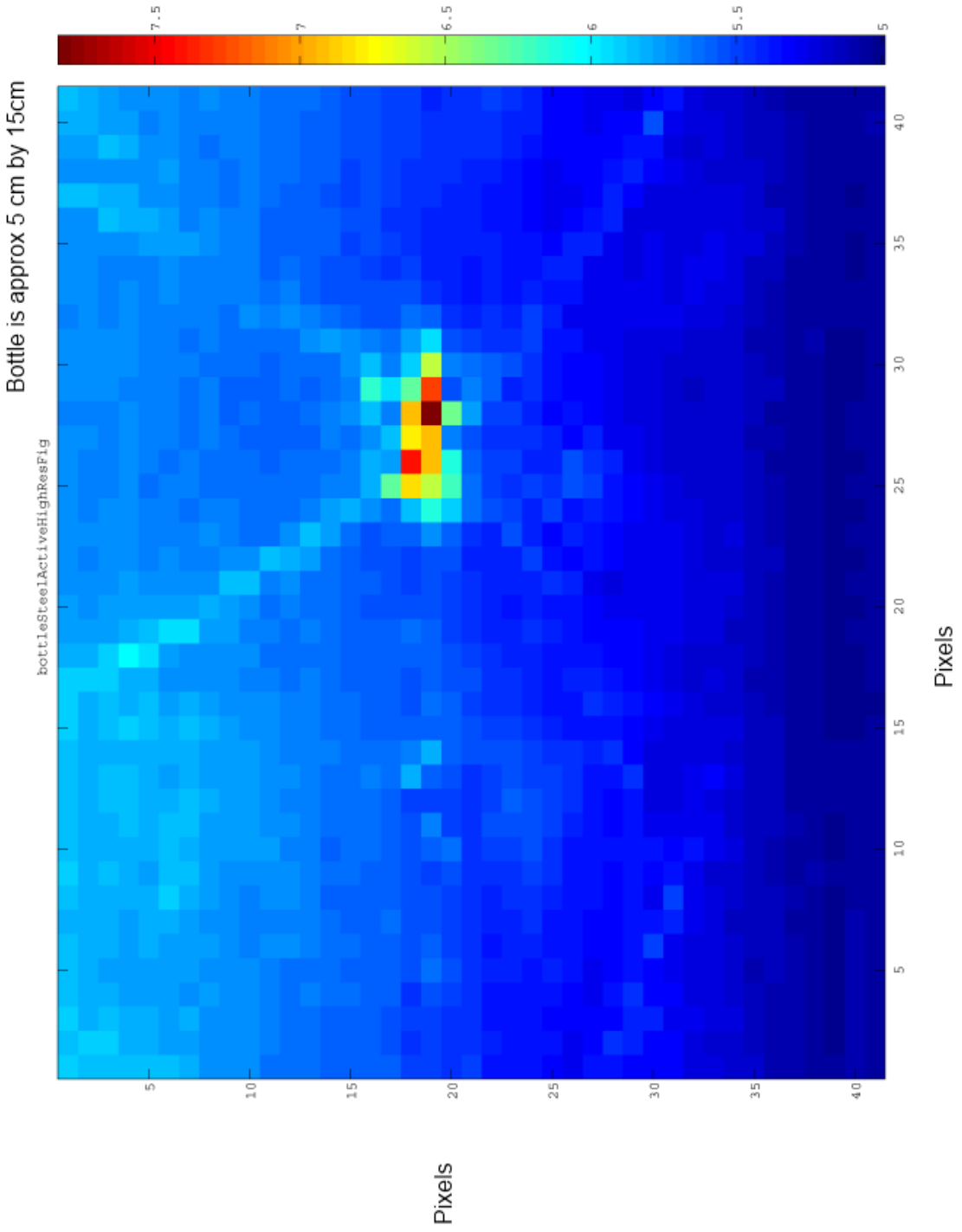

Figure 8.11: An active image of a stainless steel bottle a few metres away from the antenna.

The secondary mirror was set 13cm from the waveguide at the centre of the dish, this puts the focal point of the cassegrain at infinity, as described in section 2.3.

The water barrel and candle were placed on a table a distance of three metres from the cassegrain and a 1764 pixel active scan was done, then the candle was removed and an active scan repeated. The results are shown in figures 8.12 and 8.13 respectively. The figure with the candle shows a few more bright reflections than the water barrel only. The transmitter is placed three metres to the side of the cassegrain, so that the transmitter, receiver and object under test form a triangle.

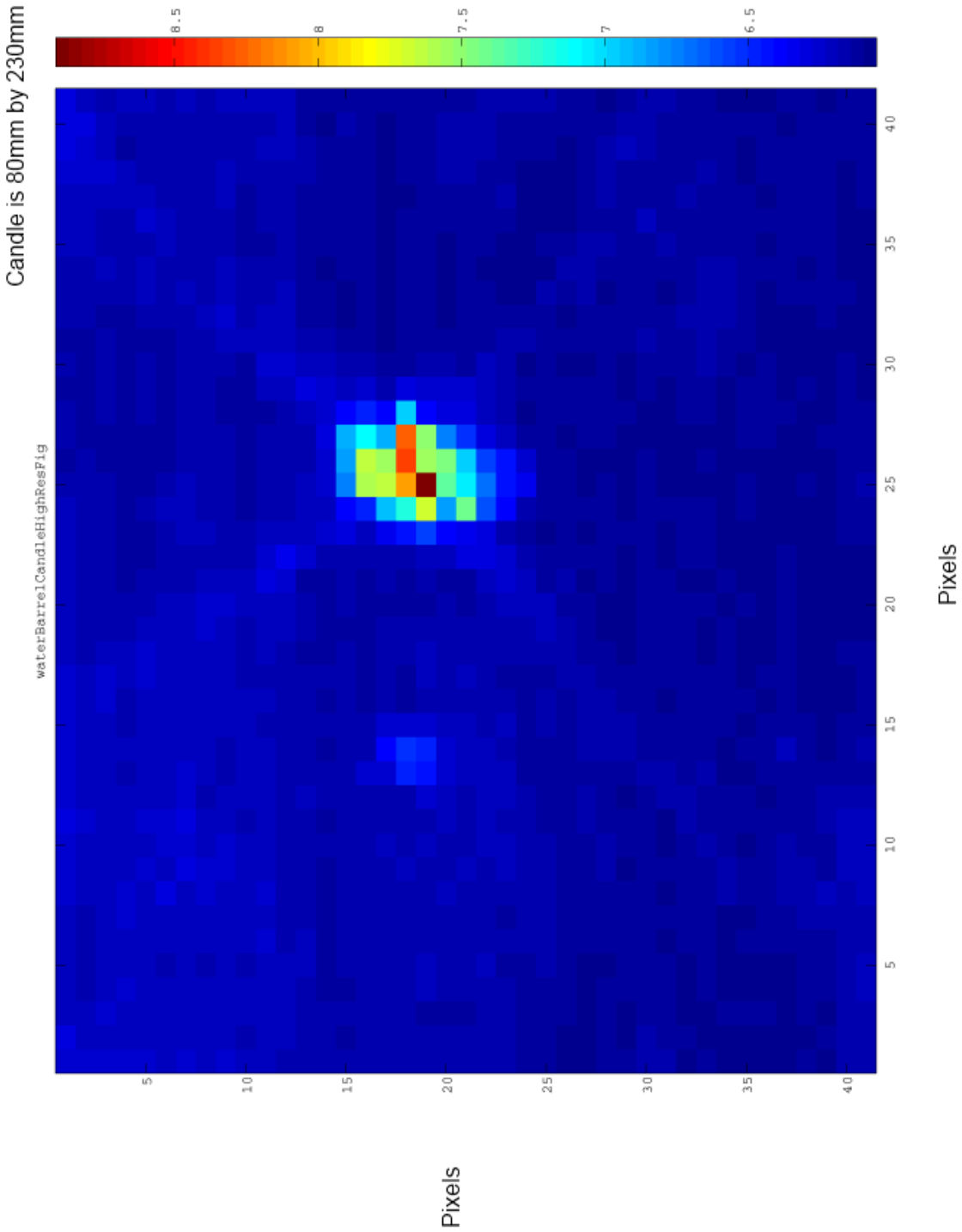

Figure 8.12: A High resolution image of the candle placed in front of a ‘water barrel’.

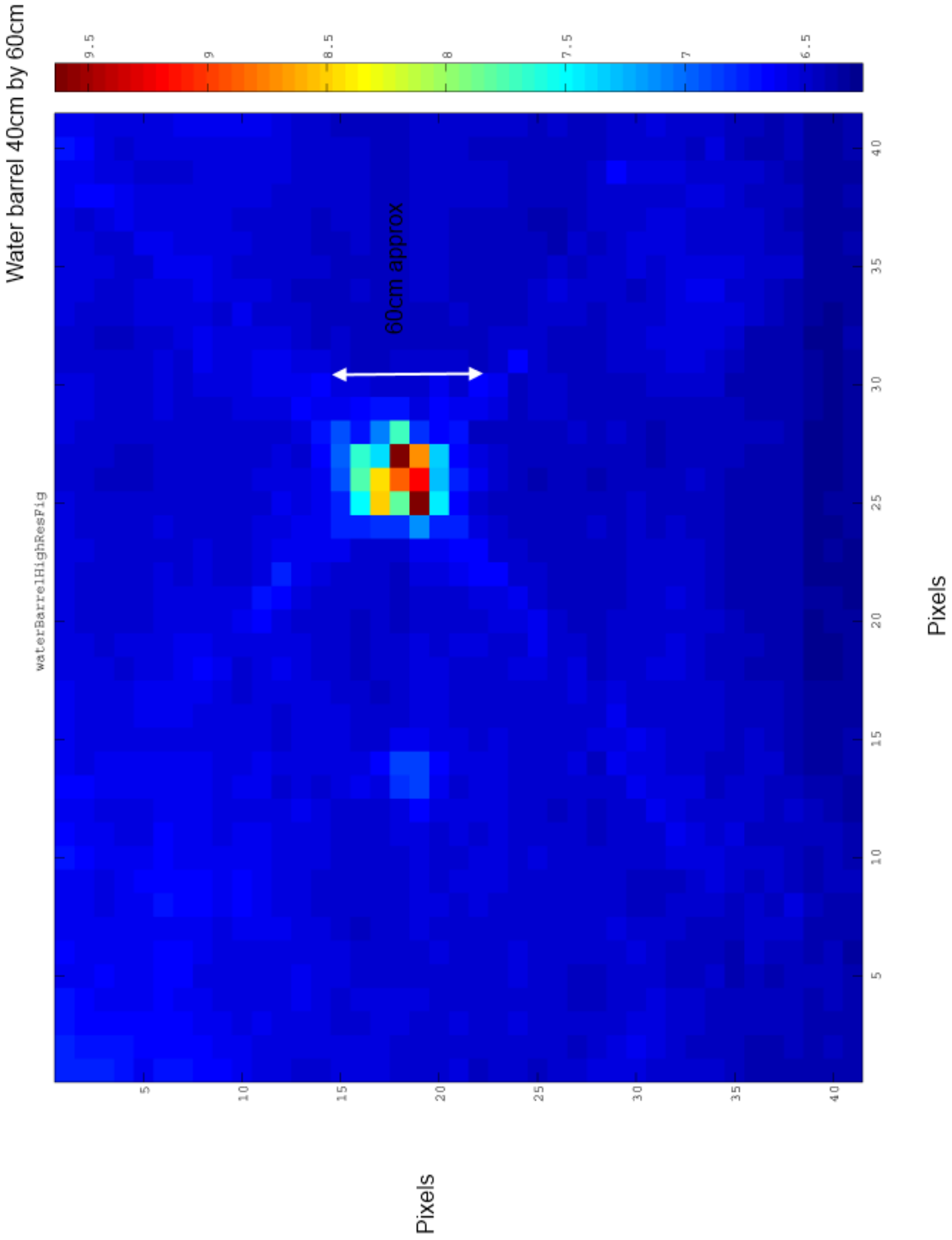

Figure 8.13: This figure shows the ‘water barrel’ on its own.

These images are showing X-shaped diffraction spikes, optical telescopes with secondary mirrors show diffraction spikes according to the number of 'legs' the 'spider' or secondary mirror bracket has, particularly on bright point sources. If there are 3 legs then there are 6 spikes, one up and one down for each leg. If there are 4 legs then there are 8 spikes, but only 4 spikes are seen because the spikes overlap.

The spikes are present for the candle with the water barrel and the water barrel only and also for the steel bottle with no water backing. To try to show that the spikes were due to diffraction effects one of the legs of the 4 way spider was covered in microwave absorbing foam and the scan repeated, no effect was visible.

This problem was probably due to a lack of dynamic range in the DC amplifier, the small signals are scaled up and the larger signals are truncated; this was solved by changing the gain of the amplifier. The DC amplifier after the MMIC went into saturation (when the output is viewed on an oscilloscope), was therefore no longer giving valid data.

The values of the variable resistors needed changing to allow for a greater offset in gain and DC level. Before this was tried, a thin piece of absorber was placed over the transmitter to act as an attenuator and the sweep was repeated, this was to show that the power level at the receiver was the problem, because the absorber acts as an attenuator and the power level reaching the receiver is reduced.

The diffraction spikes are probably visible due to the dynamic range of the DC amplifier being limited, so the larger responses are cut off, so when the images are scaled the diffraction spikes show up out of the noise. Changing the value of resistor R5 in the circuit shown in figure 8.4 changed the amplification of the circuit. The value of R5 was reduced to 3.9k ohms from 4.7k ohms.

The active scans are carried out using a swept frequency source that is not synchronised with the detector. To synchronise the scans with the frequency source, a six times multiplier is driven with a sweep generator which is swept from 12.5 to 18.33 GHz, producing an output frequency range of 75 to 110 GHz. The cassegrain is swept in a raster scan pattern and stops at each point, Matlab then triggers the sweep oscil-

lator to sweep the frequency for each pixel of the scan. The MMIC receiver is placed at the focus of the cassegrain and is used as a detector. The voltage output of the detector is read by a analogue to digital converter (ADC) into Matlab. The output power of the multiplier is limited by a 10dB attenuator between the output and the waveguide horn.

The MMIC receiver being used was found to have a poor gain versus frequency response so has been replaced by one with a flatter gain versus frequency response. A poor gain versus frequency response was a problem because if the amplitude versus frequency response of the receiver is flat, then the IFFT of the reflected signal measures the target, if the receiver response is not flat then the target response is distorted.

The multiplier has been put on the end of the feed of the cassegrain and the receiver is placed at the side of the cassegrain, with a variable attenuator on the input followed by a waveguide horn, at a height just below the cassegrain's dish. The DC amplifier was taken out of the system because the receiver has a high enough output for the ADC. A variable attenuator was put between the horn and the input to the receiver to stop the receiver saturating, as shown by the waveform on the oscilloscope appearing flat topped. The system block diagram is shown in figure 8.16.

The output power of the sweep oscillator was initially set to 0dBm for a wax target at 2 metres and then increased to 4dBm for a wax target at 4 metres. The antenna and the target were aligned using the laser collimator turned outwards, the antenna is set to the centre of a sweep for alignment. Then the secondary mirror was adjusted for maximum amplitude on the oscilloscope. Matlab software is then used to raster scan the cassegrain across the scene. The reflected frequency response is shown in figure 8.14 for a point where the candle wax was in the beam of the antenna. The figure shows a peak at an optical depth of around 120mm, this is the depth of the paraffin wax candle times its refractive index, n, of 1.5.

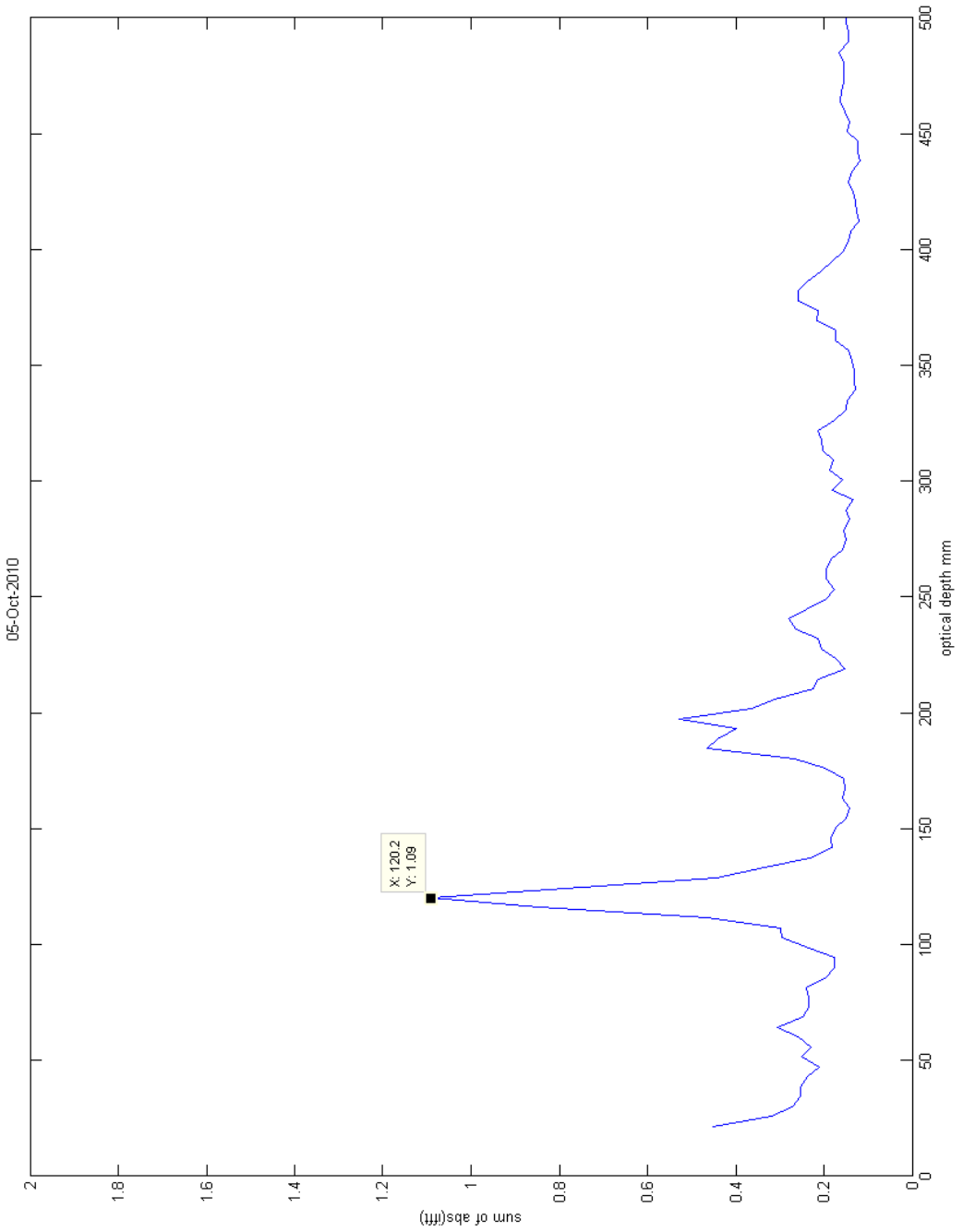

Figure 8.14: This figure shows a peak at an optical depth of 120mm which is consistent with the optical depth of the candle, i.e. actual depth times refractive index.

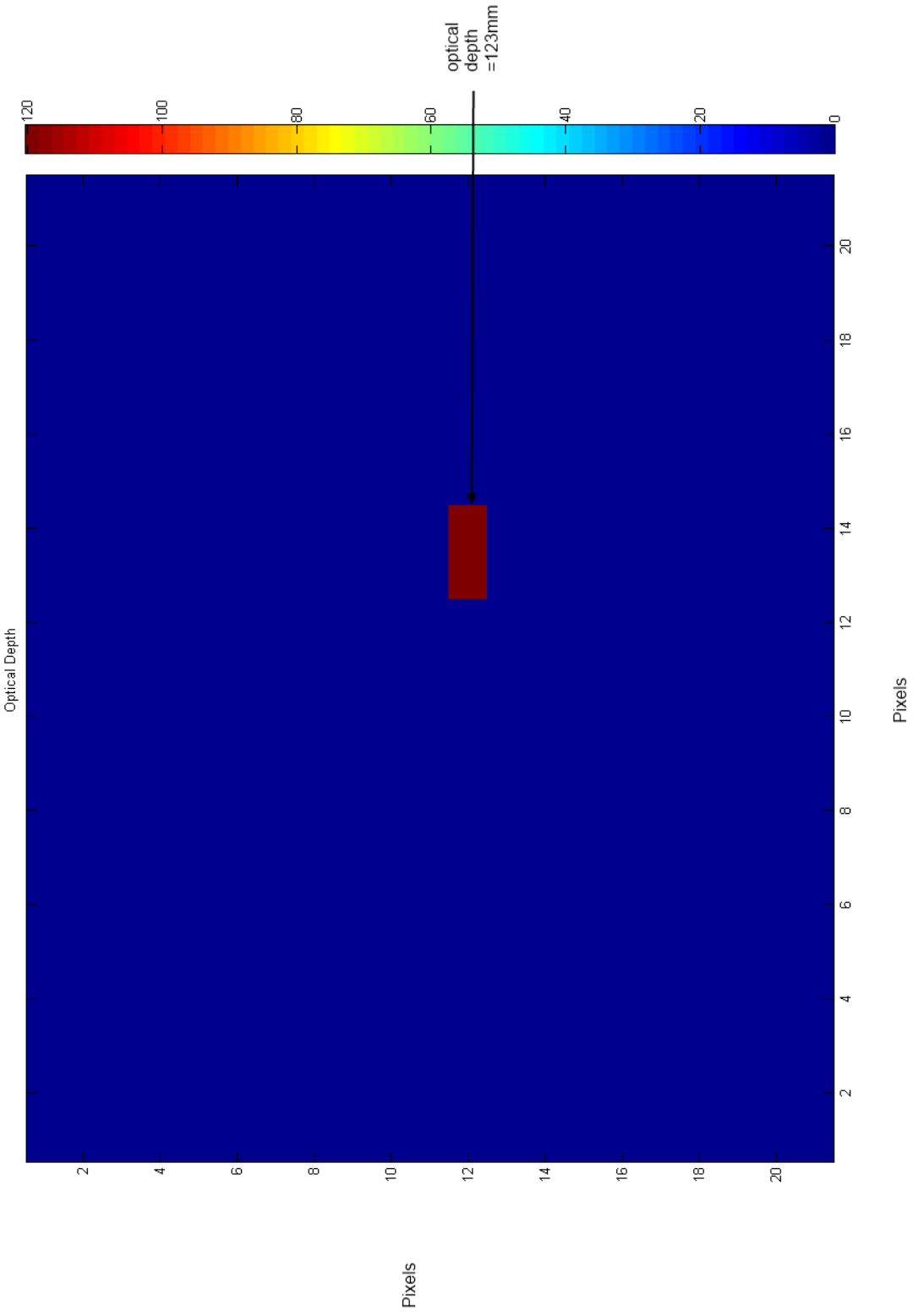

Figure 8.15: This figure shows where the optical depth peak amplitude measured at each pixel over a scene were over a threshold of 20% of the full range.

To process the data, it is read into Matlab and the IFFT is carried out, then the number of data points is converted to optical depth for the x-axis. Then the data are thresholded, if it is over the threshold then the point in the optical depth array is read and then plotted in a raster scan. If it is not over the threshold, then that value in the 2D plot is set to zero. The threshold for figure 8.15's data is 20% of the maximum for that data set. This produces a optical depth plot of the scene. The threshold is set so that only points on the raster scan where the object is in the beam are shown. The background is under the threshold level so is not shown. This de-clutters the image.

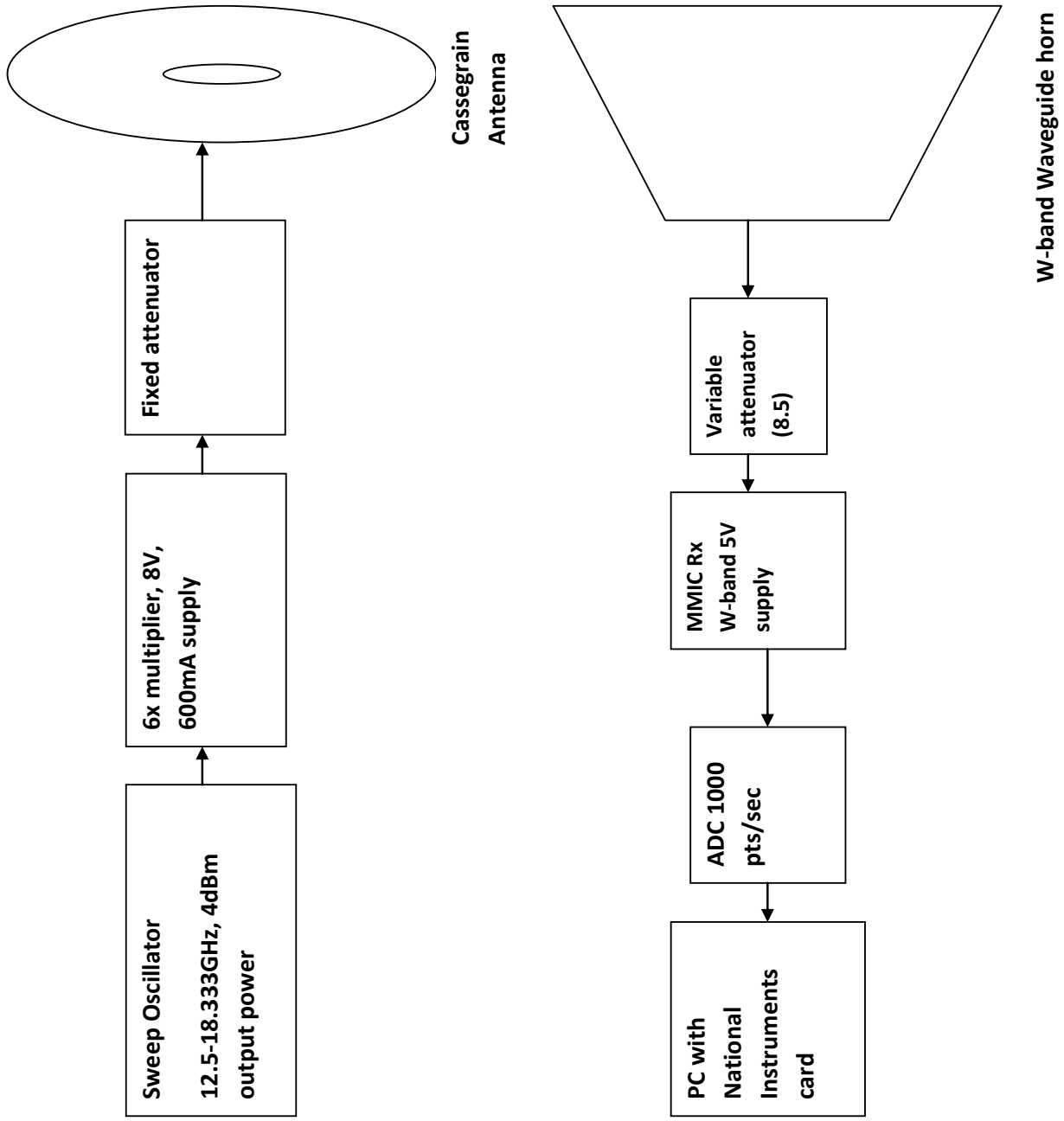

Figure 8.16: This figure shows the system block diagram of the cassegrain transmitter and receiver system.

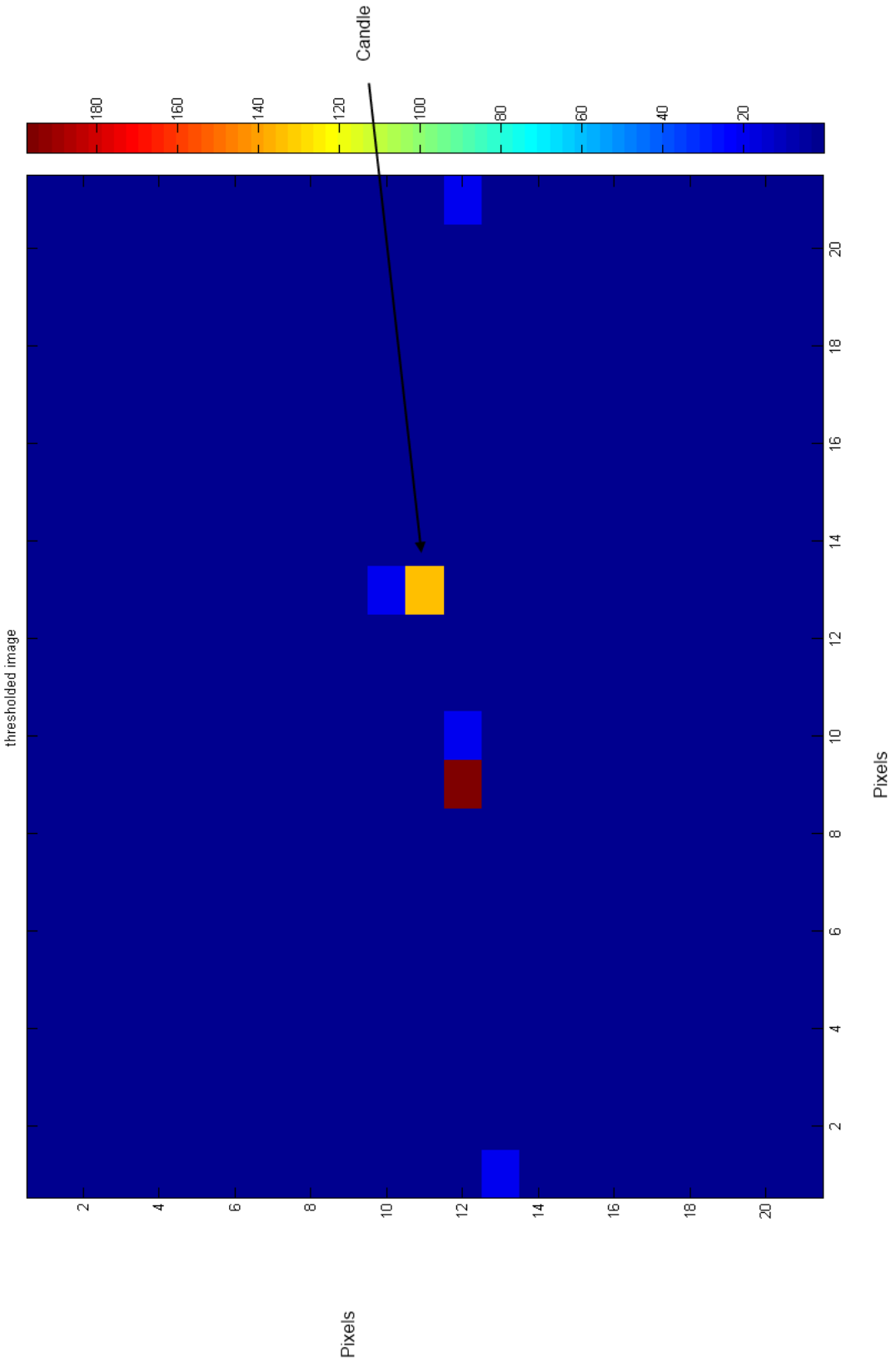

Figure 8.17: The candle in front of the water barrel at 4m. This data are thresholded and then only depths over the threshold are plotted.

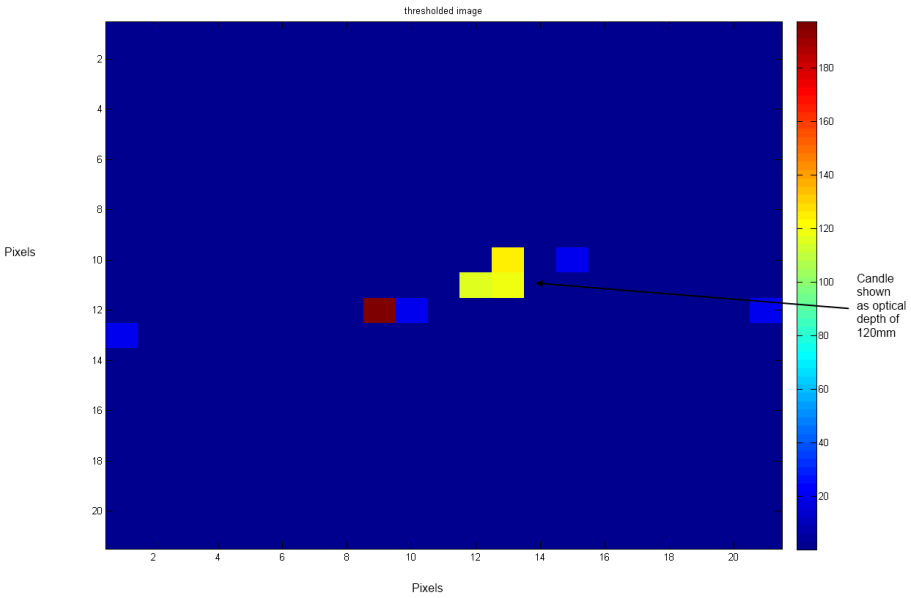

(a) The candle in front of the water barrel at 4m. This data are thresholded and then only depths over the threshold are plotted. Repeated.

(b) A photo of the same scene.

Figure 8.18: Cassegrain data of candle in front of water barrel, with photograph of scene underneath.

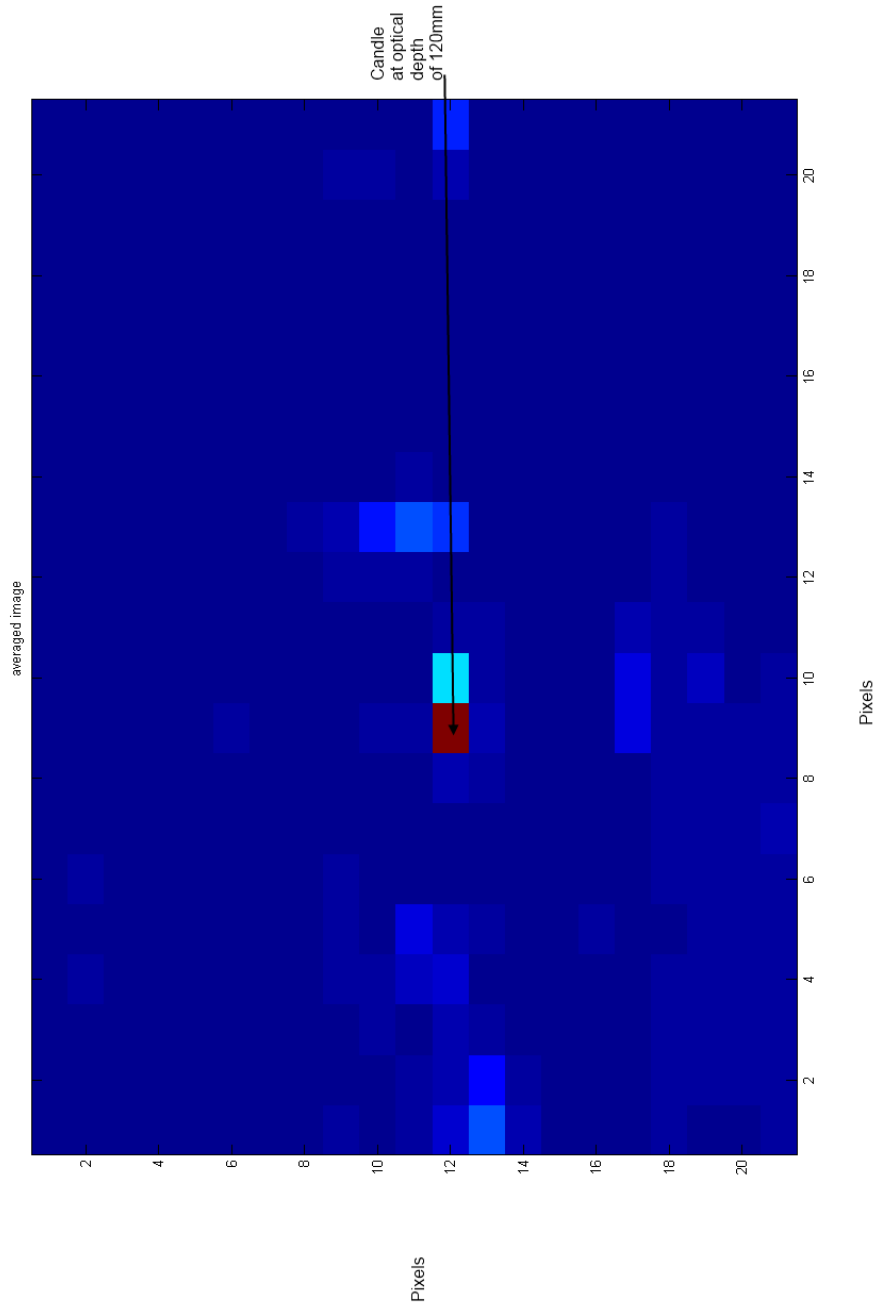

Figure 8.19: The candle in front of the water barrel at 4m, image 1.

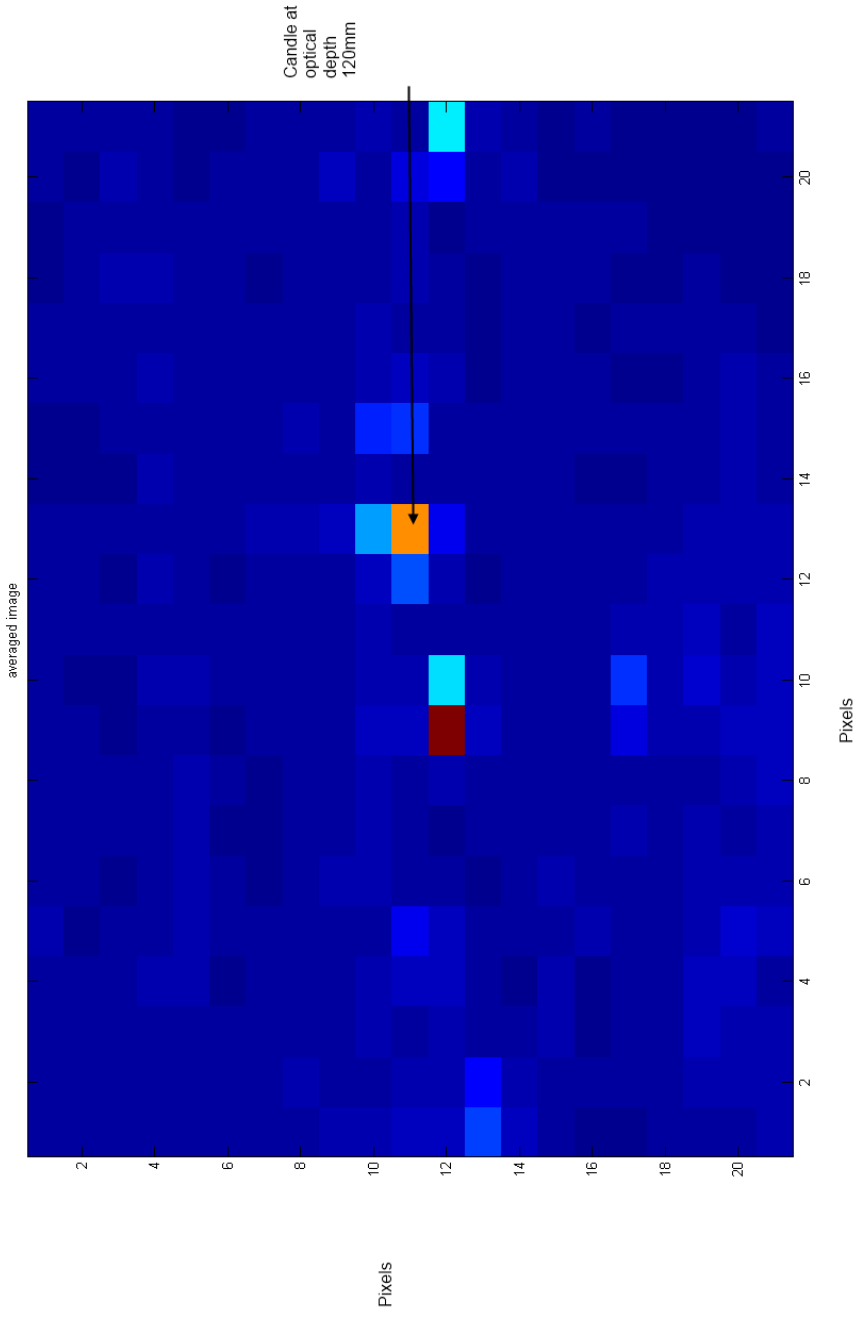

Figure 8.20: The candle in front of the water barrel at 4m, image 2.

Using the same method, the candle in front of the water barrel was tried; figure 8.17 shows the results. The candle is detected as a depth in front of the barrel, it is the pixel at a depth of 120mm. Figure 8.18 shows the same scene, repeated, this time the candle is clearly shown.

Different methods of producing an image were tried, thresholding the amplitude of the IFFT and then reading off the value of the optical depth and plotting this as an image as shown in figures 8.17 and 8.18. Another method takes the mean of the Fourier transform spectrum and plots this a pixel at a time to form an image of received power, as shown in figures 8.19 and 8.20.

To show if the system had made a detection or not, the data from the thresholded results were overlaid on an image of the scene which has been reduced to the same number of pixels in the raster scan. In this way the images can be aligned. Figures 8.21 and 8.22 show the thresholded results, the low resolution image of the scene and figure 8.23 shows the combined images. The combined images show the ability to detect objects in front of the background, e.g. a weapon hidden on the body.

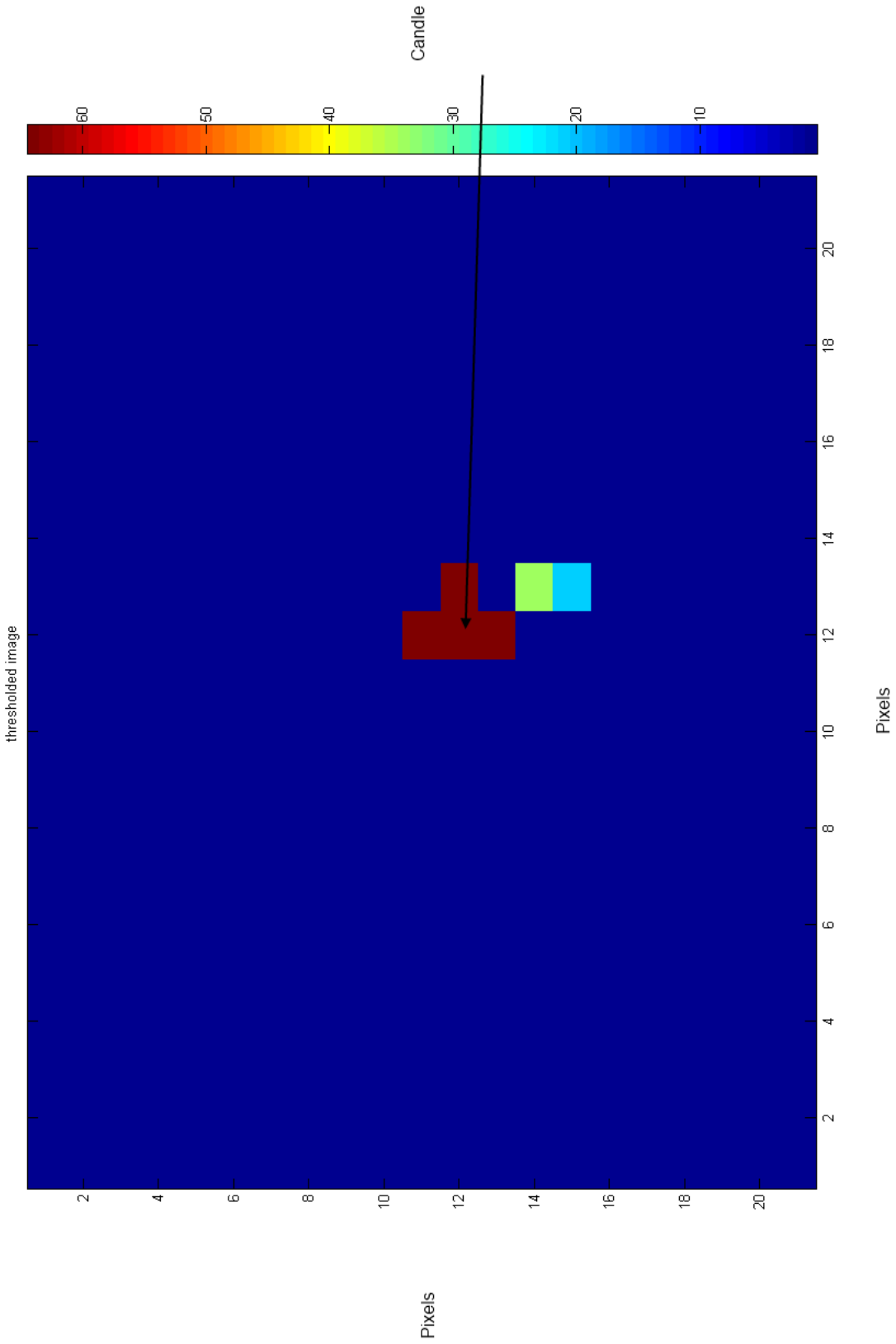

Figure 8.21: This figure shows the thresholded image of the candle on a chair. Points above the threshold are plotted. Points below the threshold are set to zero.

Figure 8.22: This figure shows an image which has been reduced in pixel count to the same number of pixels as the raster scan of the cassegrain imager. It shows a low resolution image of the candle.

Figure 8.23: This figure shows the data overlayed as dots onto the visible image.

8.5 Measuring Cassegrain Beam Pattern

8.5.1 Beam pattern measurements

The diffraction limited step size of the cassegrain antenna is given by

$$\theta = 1.22\lambda/D \tag{8.1}$$

where λ is the wavelength, D is the diameter of the lens and θ is the smallest step size in radians. If λ=3mm, D=640mm, θ=0.0057 radians. The smallest step size might be limited by the mechanical step size of the antenna. The antenna sweep was measured as 1.8 metres using a laser pointer at a distance of 3.5 metres from a wall. From trigonometry, this gives a sweep angle of 29 degrees. For 21 pixels across a sweep, the resolution per pixel is then 1.4 degrees (0.024 radians).

8.5.2 Antenna Measurements

To measure the beam pattern of the antenna the receiver was moved in front of the antenna where the object under test would be. The receiver was placed 3 metres from the transmitter and then the antenna was swept across the field of view. The output power was varied from 0, 2 and 5 dBm and the scan was repeated.

The subreflector was set at 13cm from the feed of the primary dish and a laser pointer was used to align the receiver with the transmitter at the correct height. The average power at each point was plotted as an image. These images show the wideband beam pattern of the antenna for each power level. The spot size given by these results is de-focused. The position of the secondary reflector needs to be varied to find the position that gives minimum spot size for a given distance.

The spot size for a given power level, 5dBm, with the receiver at 3 metres, was measured. To stop the power level saturating the receiver, two variable attenuators were put on the input of the receiver. The absolute power level is not known. The subreflector was moved from 12, 13 and 15cm and the beam pattern was measured

using a raster scan of 21 by 21 points using a step size of two. The figures 8.24, 8.25 and 8.26 show the results for each of these. The horn was removed from the receiver to reduce the gain.

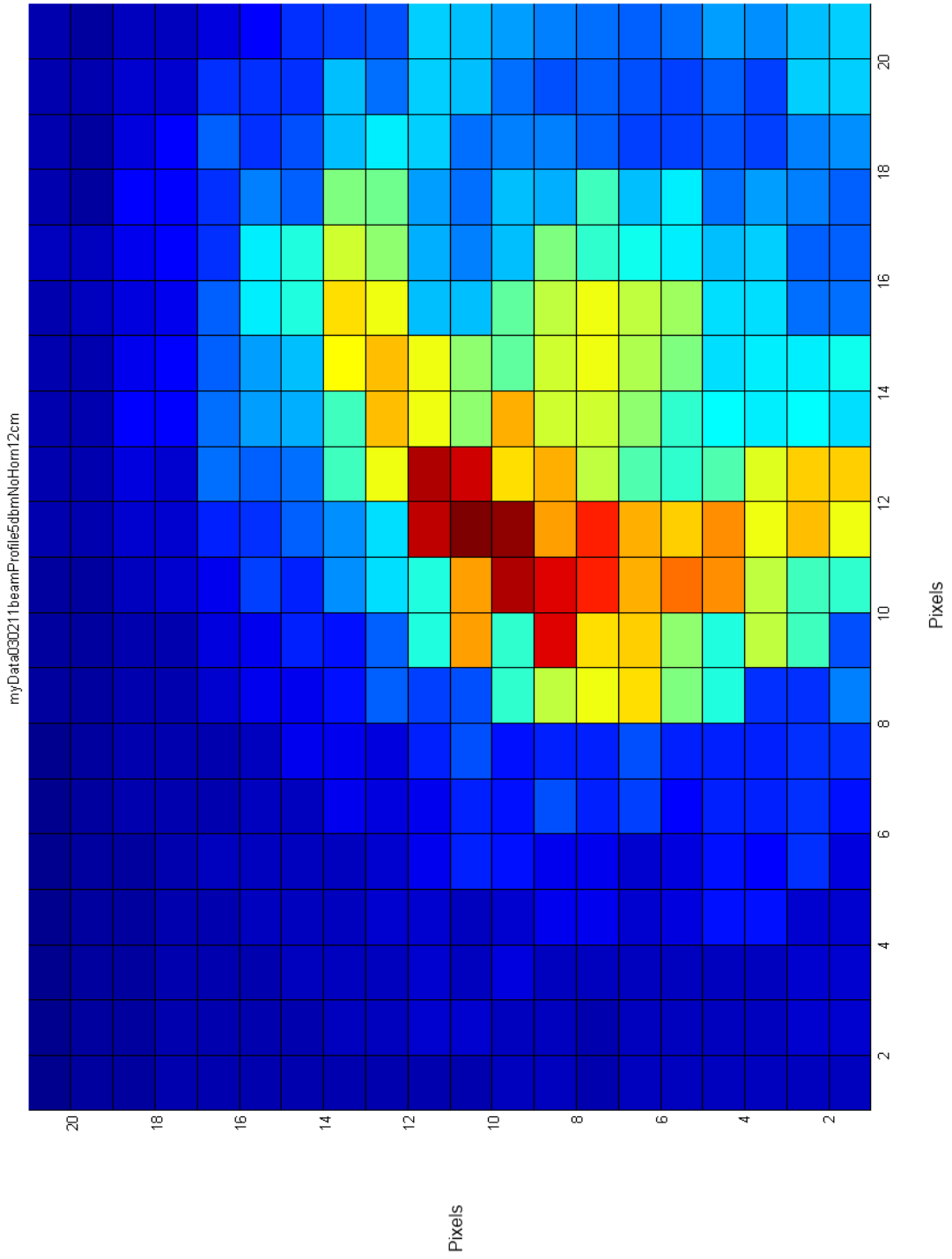

Figure 8.24: This figure shows the beam profile with the subreflector set to 12cm, this is the point where the beam is de-focussed.

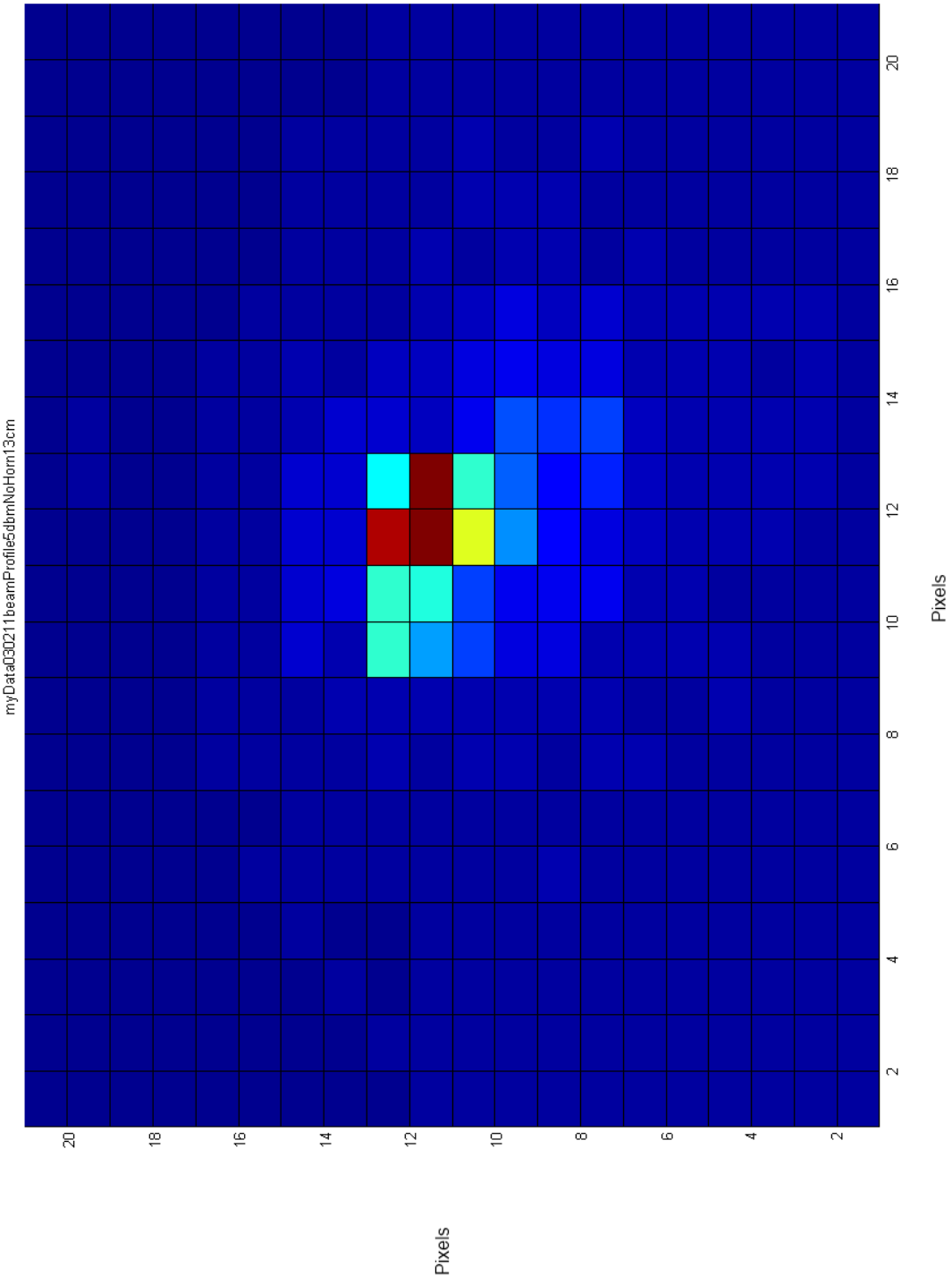

Figure 8.25: This figure shows the beam profile with the subreflector set to 13cm, this is the point where the beam is assumed to be parallel.

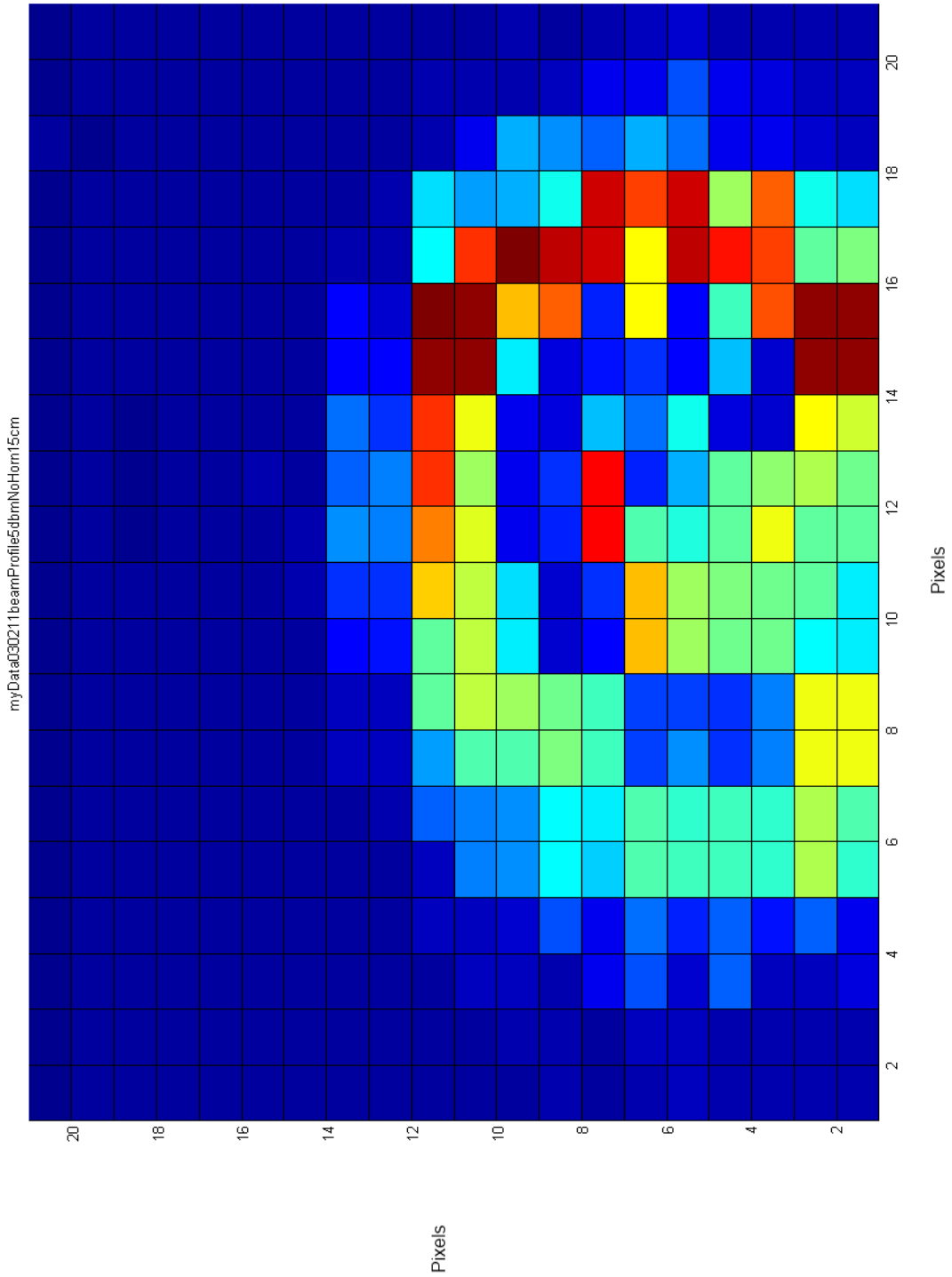

Figure 8.26: This figure shows the beam profile with the subreflector set to 15cm, this means that the beam will be brought to a focus closer to the transmitter.

8.6 Data processing with average, xcorr, sort algorithm

The technique used was an active imaging technique (A spatial map is formed so this might be called an image; The image is a optical depth contrast image), which raster scans a millimetre wave beam across a target. The beam is formed by a cassegrain antenna which has been modified to focus at various distances. The system measures the optical depth at each point of the scan. This depth is then plotted on a grid to form a scene. If a depth was detected in front of the body then this was considered a detection of a potential weapon.

8.6.1 Scanning Antenna

A commercial cassegrain millimetre wave antenna was modified so that the position of the secondary reflector could be moved to focus the beam at various distances (Leonard, 2010). The antenna was mounted so that it could be driven in two axes and raster scanned across a scene. The transmitter was placed at the focus of the dish and consisted of a six times multiplier and a sweep oscillator (Agilent, 2011) swept from 12.5 GHZ to 18.3GHz, giving an output of 75 to 110 GHz. A MMIC receiver was placed to one side of the cassegrain with a 20 dB gain horn. The signal was processed using Matlab (Math-Works, 2009).

The cassegrain is swept in a raster scan pattern and stops at each point, Matlab then triggers the sweep oscillator to sweep the frequency for each pixel of the scan. The voltage output of the detector is read by a analogue to digital converter (ADC) into Matlab. The transmitter power of the multiplier is limited by a 10dB attenuator between the output and the waveguide horn. The system block diagram is shown in figure 8.16.

Due to the difficulties of using real explosives a substitute with similar dielectric properties was required. Several authors (Hu et al., 2006),(Yamamoto et al., 2004) and (Shen et al., 2005) quote the refractive index for plastic explosives as between 1.5 and 1.6. Therefore, paraffin wax was chosen as a target as it has a refractive index of 1.5 (Lamb, 1996) and is easy to reshape and is inert at room temperature.

8.6.2 Results

The output power of the sweep oscillator was initially set to 0dBm for a wax target at 2 metres and then increased to 4dBm for a wax target at 4 metres. The antenna and the target were aligned using a laser pointer, the antenna was set to the centre of a sweep for alignment. Then the secondary mirror was adjusted for maximum received signal. Matlab software was then used to raster scan the cassegrain across the scene. The reflected frequency response is shown in figure 8.14 for a point where the paraffin wax was in the beam of the antenna. The figure shows a peak at an optical depth of 120mm, this is the depth of the paraffin wax times its refractive index, n, of 1.5 (Lamb, 1996).

To process the data, it was read into Matlab and the inverse Fourier transform was carried out, then the number of data points were converted to optical depth for the x-axis. Then the data was thresholded, if it was over the threshold then the point in the optical depth array was read and then plotted in the raster scan. If it was not over the threshold, then that value in the 2D plot was set to zero.

Using the same method, the wax in front of the water barrel was tried, figure 8.18 shows the results. The wax was detected as a depth in front of the barrel, it is the pixel at a depth of 120mm.

To show if the system had made a detection or not, the data from the thresholded results were overlaid on an image of the scene which has been reduced to the same number of pixels in the raster scan. In this way the images can be aligned.

Figure 8.23 shows the combined images. The combined images can be used to detect objects in front of the background, e.g. a weapon hidden on the body.

8.6.3 Signal processing algorithm applied to cassegrain results

A signal processing algorithm was previously developed by the author (Andrews et al., 2009) which averages, sorts by cross-correlation coefficients and then sorts the data by amplitude to remove weak sweeps from the data set. This algorithm has the effect of aligning the data and cancelling out the effects from a moving target. This has been applied to data obtained with a stationary antenna and highlights the presence of a dielectric in front of the body. To process the data from the cassegrain, the data was first Inverse Fast Fourier Transformed and then put through the algorithm. Figure 8.27 shows the wax in front of the water barrel, clearly visible as a peak at the optical depth of the wax. Figure 8.28 shows how a metal scourer does not have much, if any, depth when placed against the body, being metallic it reflects strongly.

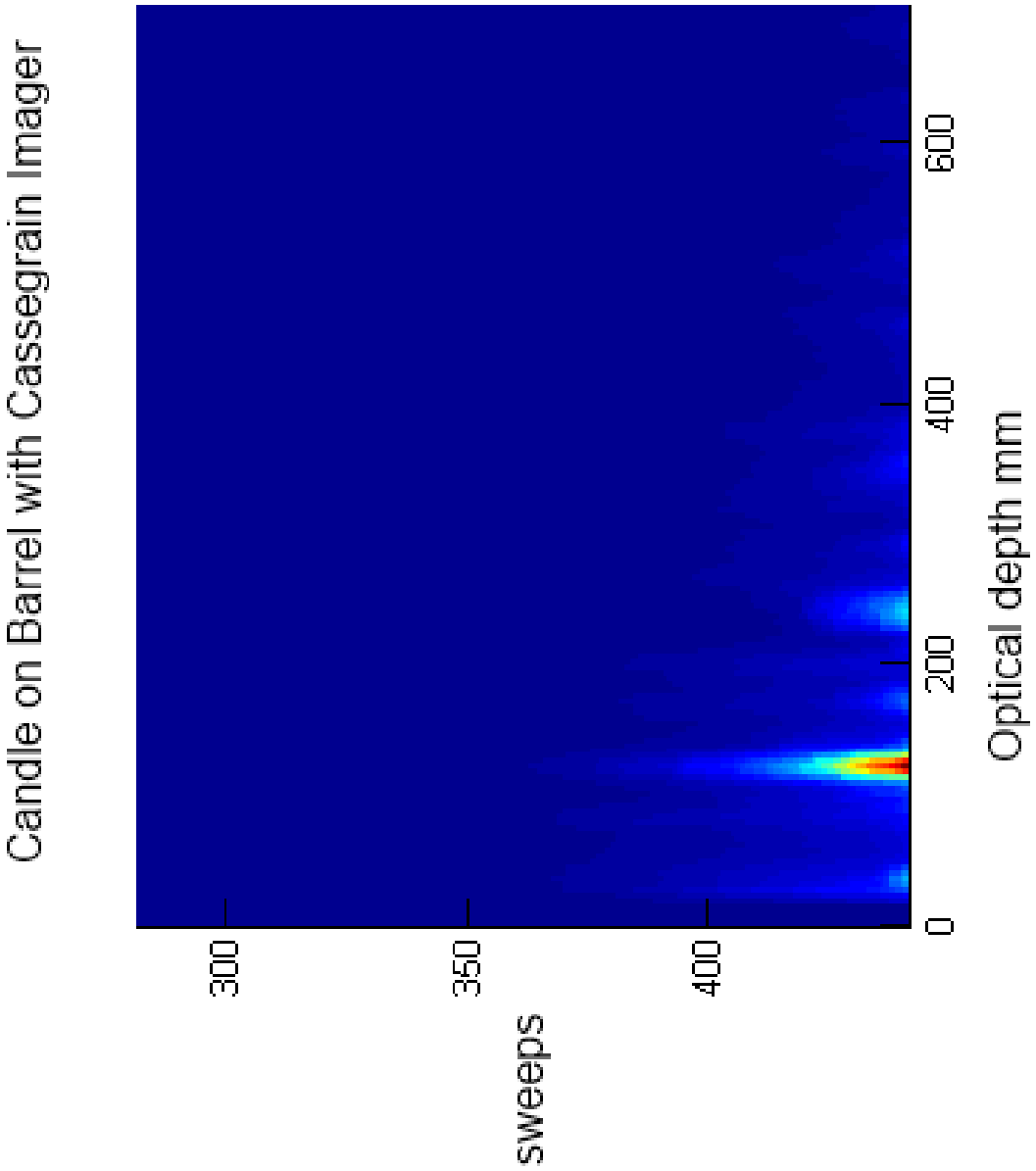

Figure 8.27: Cassegrain data taken with direct detection of the wax in front of a water barrel.

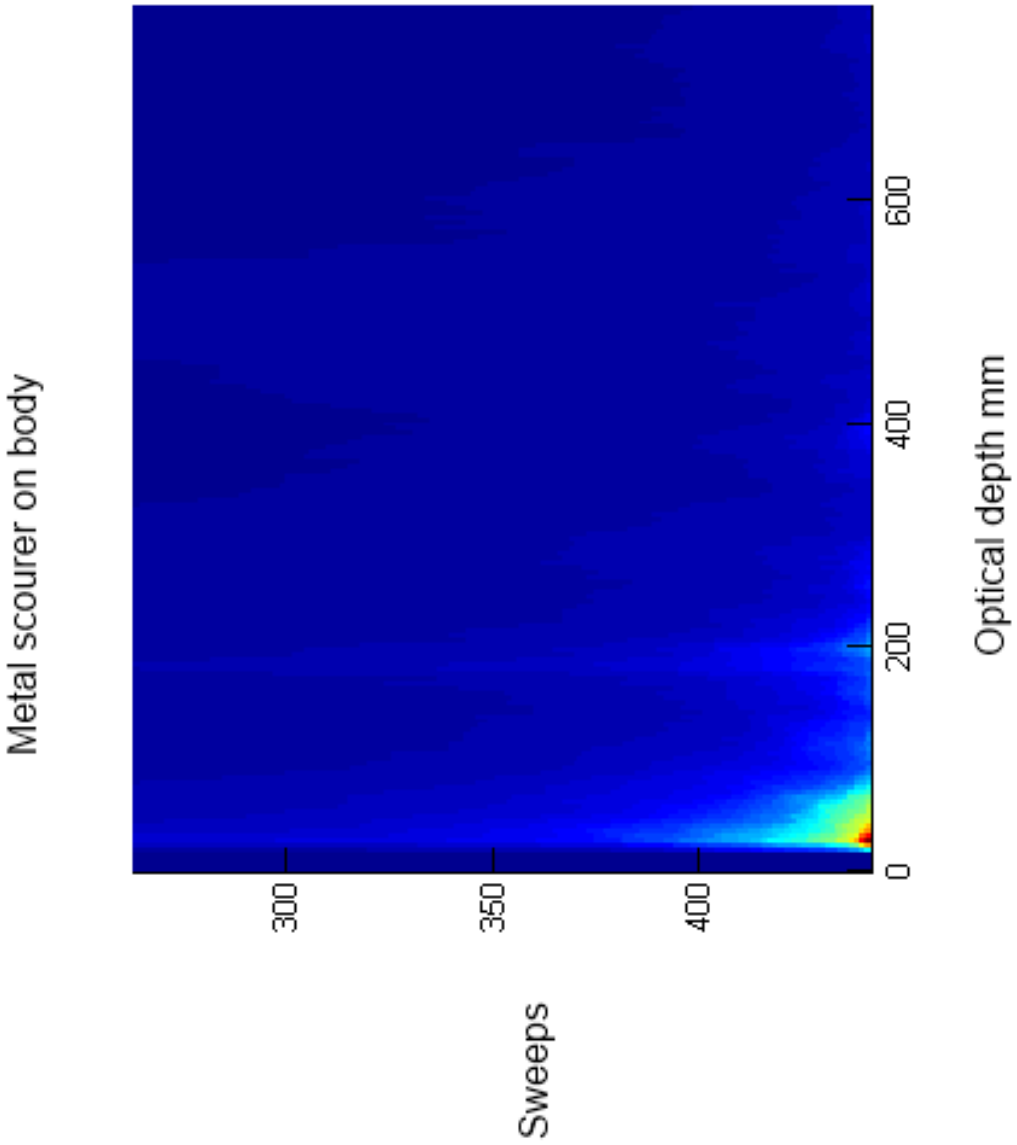

Figure 8.28: Cassegrain data taken with direct detection of a metal scourer in front of the body.

8.6.4 Conclusions

Passive imaging using a MMIC receiver and the cassegrain antenna produced some images where a person could be seen. The contrast in these images is poor as they were done indoors. Further work should included trying this outside so that the sky can be used as a cold reference.

Using the modified cassegrain antenna and a swept frequency source, the data can be processed to either form an image of the scene or be processed using the signal processing algorithm developed earlier to produce a plot showing the optical depth of objects in front of the body. The wax block (candle) was detected at 4 metres using an active swept-frequency approach.

Placing the wax block in front of the water barrel was also tried to simulate a human target, the wax block was detected in front of the simulated body. It was found that over laying the optical depth data onto an optical image of the scene helped a human operator to see if a detection had been made.

The technique was tested with human targets carrying simulated explosives but further work will be needed to make the imaging system real-time. The data was processed using the algorithm developed previously and the results clearly show when the target is carrying explosives in front of the body.

Further work includes using more objects on body and using the data after processing to train an artificial neural network to classify targets as a threat or non-threat rather than a human operator classifying the results. The range should also be extended up to 10 metres and included as training data to the neural network classifying algorithm.

Chapter 9

Results and Discussion

9.1 Data Collection

Time domain data from the VNA was collected for 200 sweeps of 14 to 40GHz. 200 sweeps are used because this is the number of sweeps which can be collected in a reasonable time, produce a manageable data file and to get a reasonable variability in the data set. The band of 14 to 40 GHz is used because it is the maximum bandwidth of the waveguide. The sweep is limited by the wavelengths that will propagate along a given wave guide. Figure 9.1 shows the maximum sweep range after IFFT'ing the data.

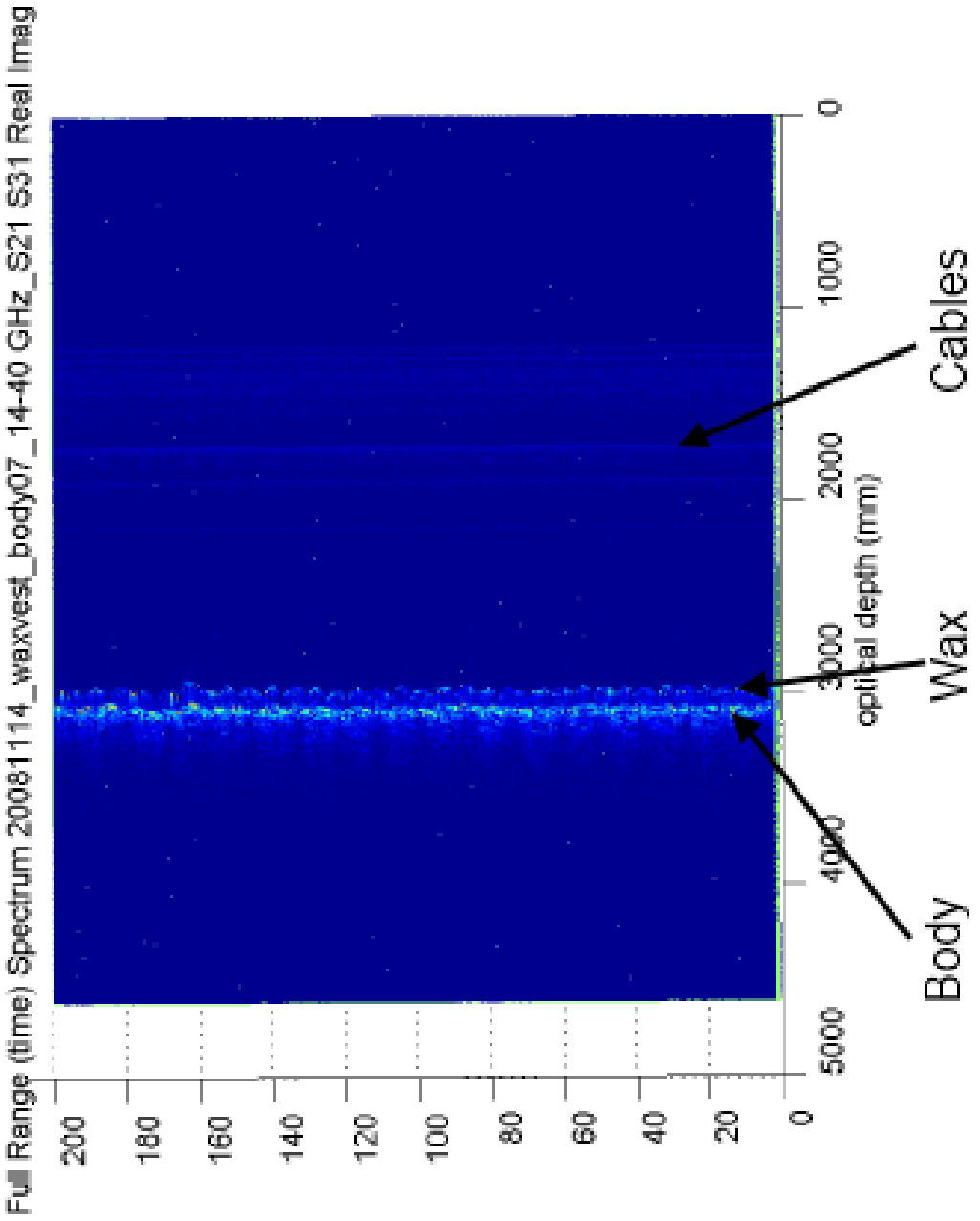

Figure 9.1: This shows all of the data after inverse Fourier transform of the raw data data.

This data was then gated to leave the region containing the body and simulated explosives data. The data forms a 3-D array in Matlab, as shown by figure 9.2.

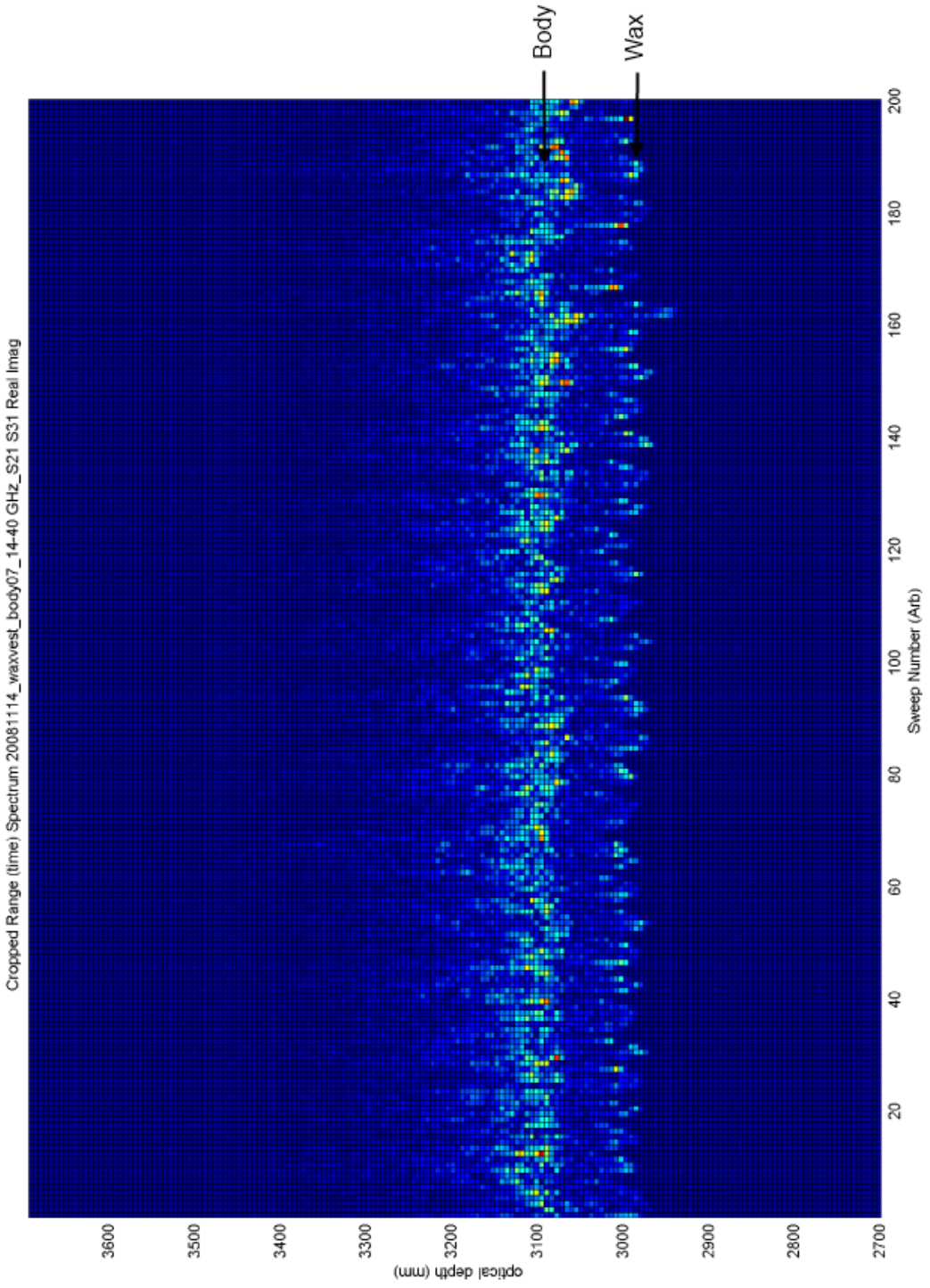

Figure 9.2: This figure shows the data after cropping to the region of interest.

Table 9.1: A table of training data extracted from the Gaussian fit, there is a set of data like this for each training data set.

Amplitude	Position	Width
71.5	5.3	30.1
5.9	36.0	97.1
40.5	86.9	18.3
84.3	102.0	16.8

9.1.1 Network Training using Gaussian Parameters

Using the Matlab image processing toolbox, a 3 by 3 averaging filter is then applied to remove any spurious points, as shown in the top right of figure 9.3. The data are then aligned by correlation coefficient, so that similar sweeps are aligned on more than one feature, as shown in figure 9.3 at the bottom left. The data are then sorted by amplitude and plotted as an image. The data still consists of a 3-D array, as shown in figure 9.3 bottom right. This should be compared with figure 9.4, taken without the wax. The extra peak around 3000, due to the wax is clearly seen.

This 3-D array is then averaged to obtain a single curve, over 200 sweeps as shown in figure 9.5, this is to reduce the amount of data presented to the neural network. The sum of four Gaussian functions is then fitted to this data for curves containing explosives in front of the body and those not. The Gaussian parameters are peak amplitude, peak position and peak width. There are 4 sets of data, one for each curve, which produces a 4 by 3 array in Matlab as shown in table 9.1. This array is then sorted by position of the curve. This data are then used to train an artificial neural network, with 2 sets of 'threat' and 'non-threat' data. The targets for the network are 1 1 1 and 0 0 0, one each for amplitude, position and width. Two data sets of either threat or non-threat are used to produce a data set to train the neural network on quickly, to test if this is a viable solution, then the training data can be expanded later.

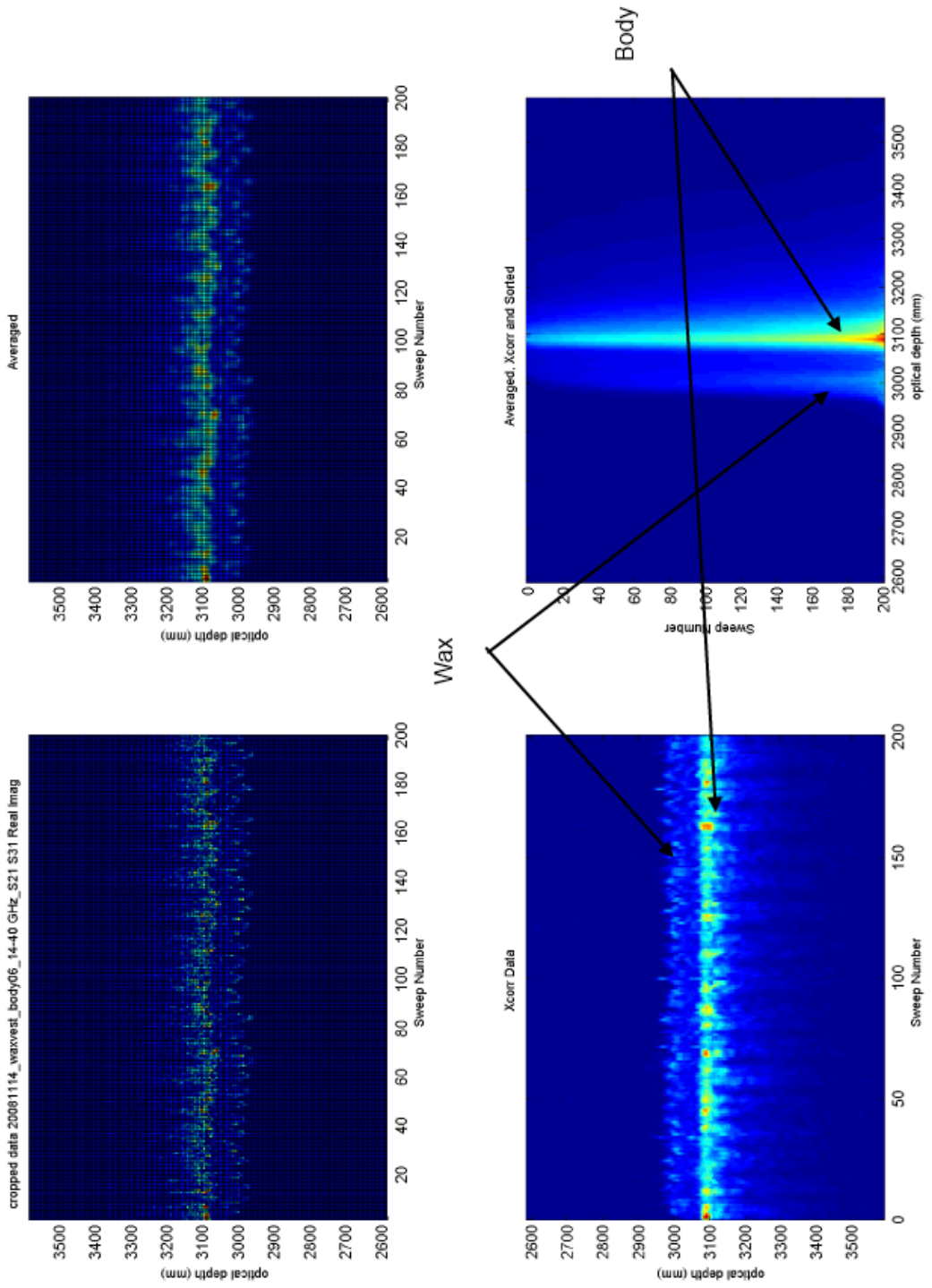

Figure 9.3: Wax in front of body, data set 6. Top left shows the data after ifft. Top right shows data after averaging filter applied. Bottom left shows data after cross-correlation and alignment is carried out and bottom right shows the data after being sorted by amplitude and plotted as an image.

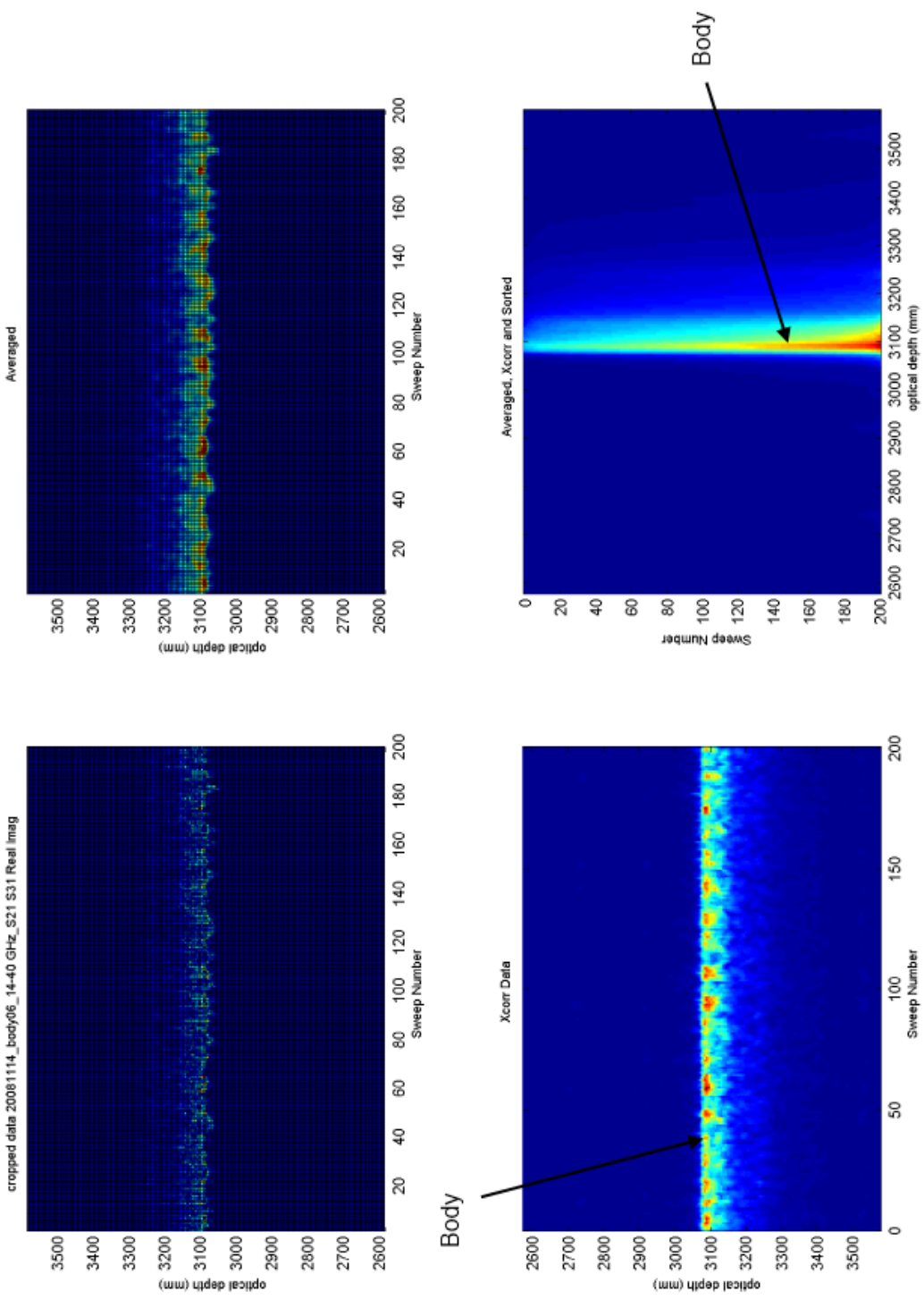

Figure 9.4: As figure 9.3, but without wax in front of body, data set 6

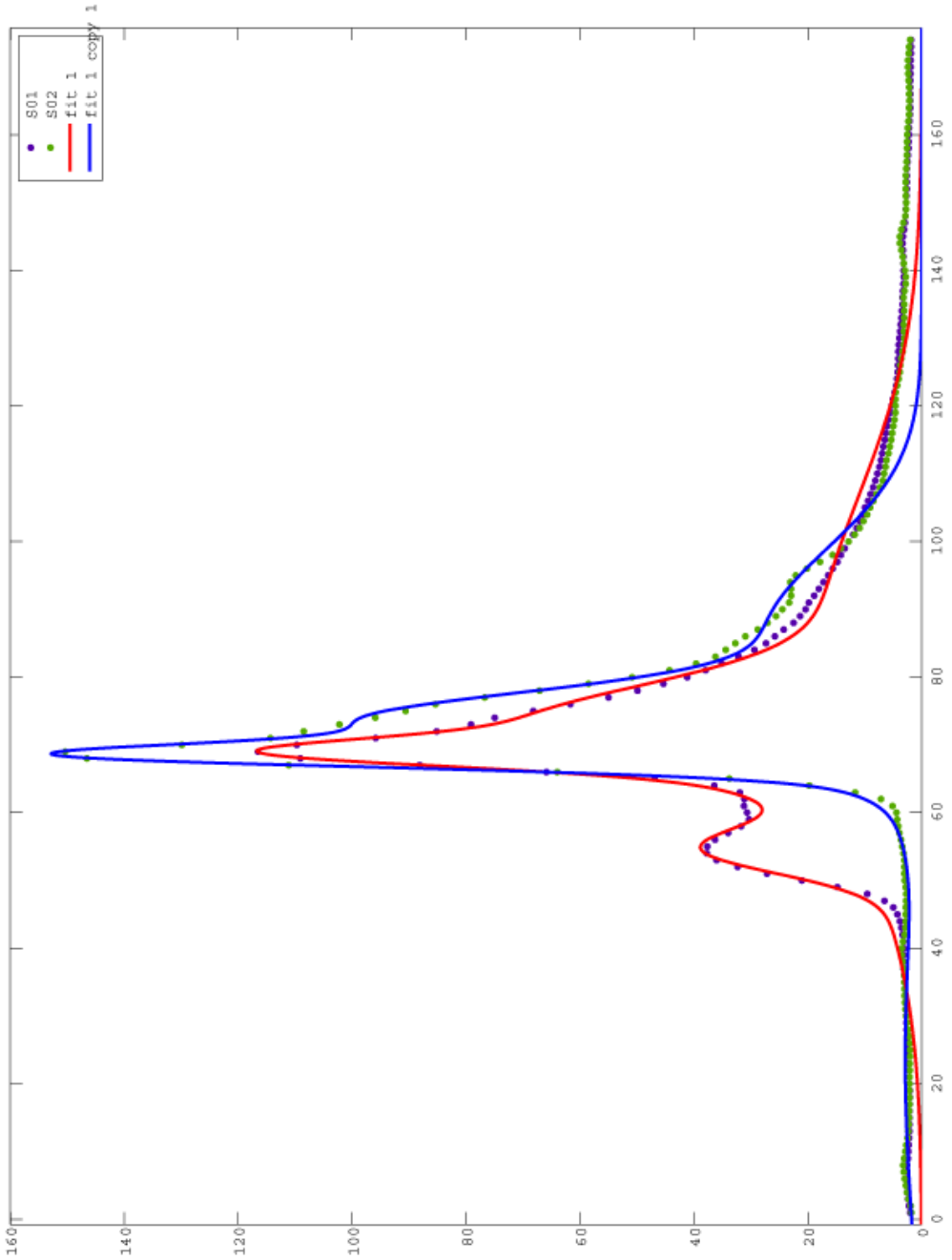

Figure 9.5: This figure shows the averaged data after fitting the Gaussian curves to it, this pattern is presented to the ANN for training, it reduces the number of inputs required by the network. The curves show the data averaged over 200 sweeps and then fitted with Gaussian curves.

Each new set of data are processed in the same way and then presented to the network, the network produces an output in the range 0 to 1, for each of the training parameters, amplitude, position and width, so a typical output would be 0.9959, 0.4628, 0.2456. A Matlab GUI was used to provide an indicator either red or green, threat or non-threat, based on the average of the three outputs. So greater than 0.5 gives red and less than 0.5 gives green. This could be improved by giving a sliding scale of threat out of ten, i.e. 0 to 1 in 0.1 increments. A further condition needs to be added of 'unclassified', for results in the region of 0.5, because a result of 0.5 is no better than a guess. The bounds of confidence of threat or non-threat need to be established.

9.1.2 Averaging and Cross-correlation

The filter 'imfilter' from the Matlab image processing toolbox was used as a pre-processing step to the neural network because using correlation alone was failing to train the network. Training on data above a given threshold was tried, but this made redundant too much data to train the network on. Averaging, aligning by correlation coefficient and then sorting by amplitude produced good results by training on one set of data and testing on a further two data sets of 200 sweeps. This was then increased to 4 training sets and 16 test sets.

To show that all the steps are necessary, removing the averaging step from the pre-processing of the data results was tried. The neural network incorrectly identified non-threat data sets as threats. The data are more spread out and spurious points could be causing the mis-classification, so the averaging step was left in the programme.

Figure 9.3 shows the wax in front of the body, the wax peak can be seen to the left of the main body response. Figure 9.4 shows the body only response, the signal is clean and shows a sharp cut-off in front of the body response. The data in figure 9.3 shows a weaker 'wax response' than the data shown in figure 9.6, this is due to the wax being present in fewer sweeps due to movement of the target. Table 9.6 shows the training data for a neural network which was trained on 2 sets of alternate 'wax on body' and 'body only' data. It is in very close agreement with the targets as would be expected from the training data.

Table 9.7 shows the results from testing the neural network trained in table 9.6, the 16 sets of data are correctly classified in 15 out of 16 cases. The body alone results are 0.12 or better (closer to the target of zero), except body03. Body03 has been incorrectly classified as a threat (closer to 1 than 0) this could be due to under training the network i.e. more training sets are required. The body with wax in front results are all 0.75 or better (closer to the target of 1) for the 8 'threat' data sets.

Figures 9.5 and 9.8 show the averaged data after fitting the Gaussian curves to it. This is the pattern that is presented to the neural network for training and testing. The data are simplified and the number of inputs to the network are reduced.

The fit of the Gaussian curves to the data for training the neural network isn't always a good fit from the Matlab Curve fitting toolbox, so programmatically fitting the Gaussian curves to the data was tried. Training on data processed in this way gave results where the body plus the simulated explosive were classified correctly as threats but the body alone was incorrectly classified in most cases as a threat, this method wasn't satisfactory.

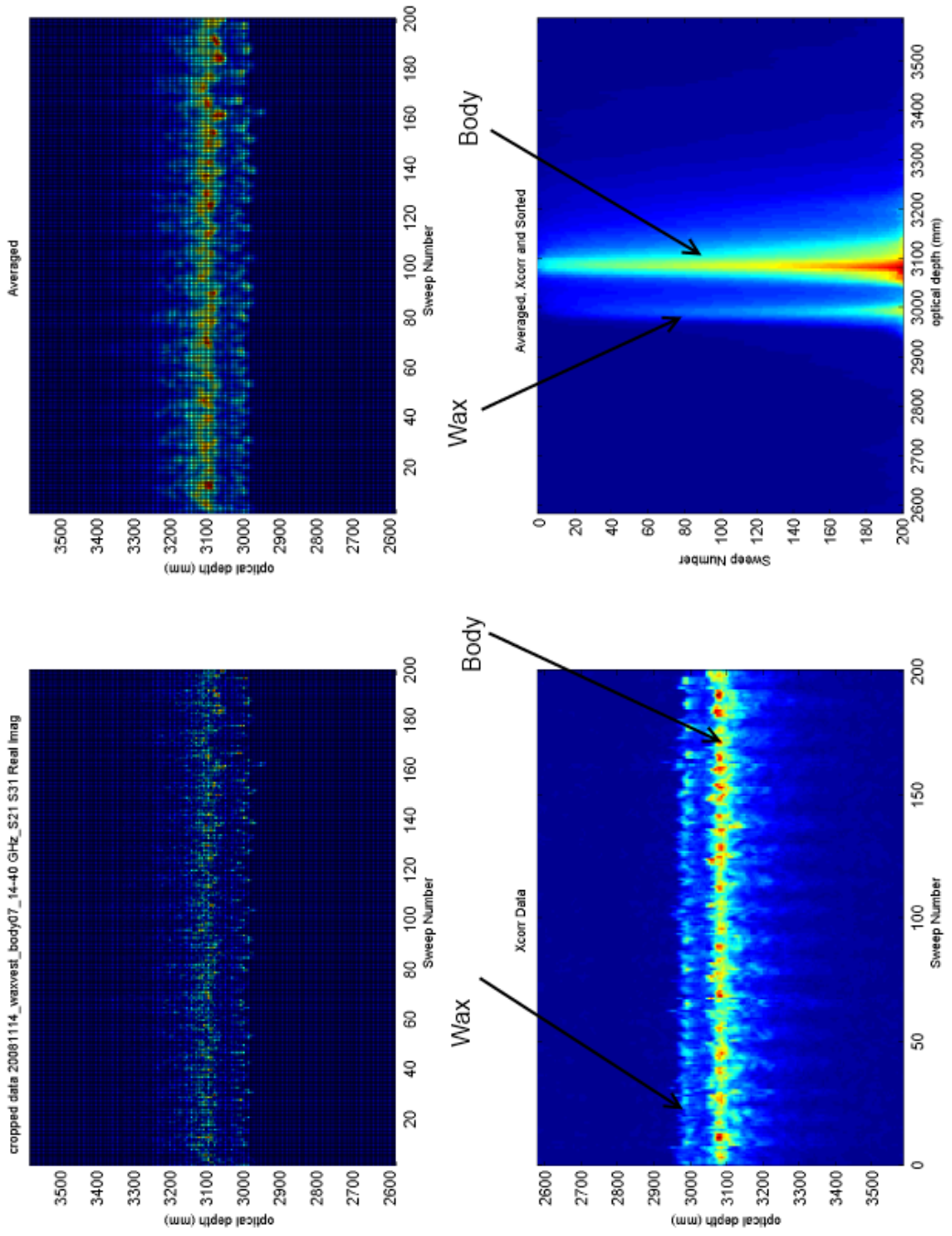

Figure 9.6: Wax in front of body, data set 7

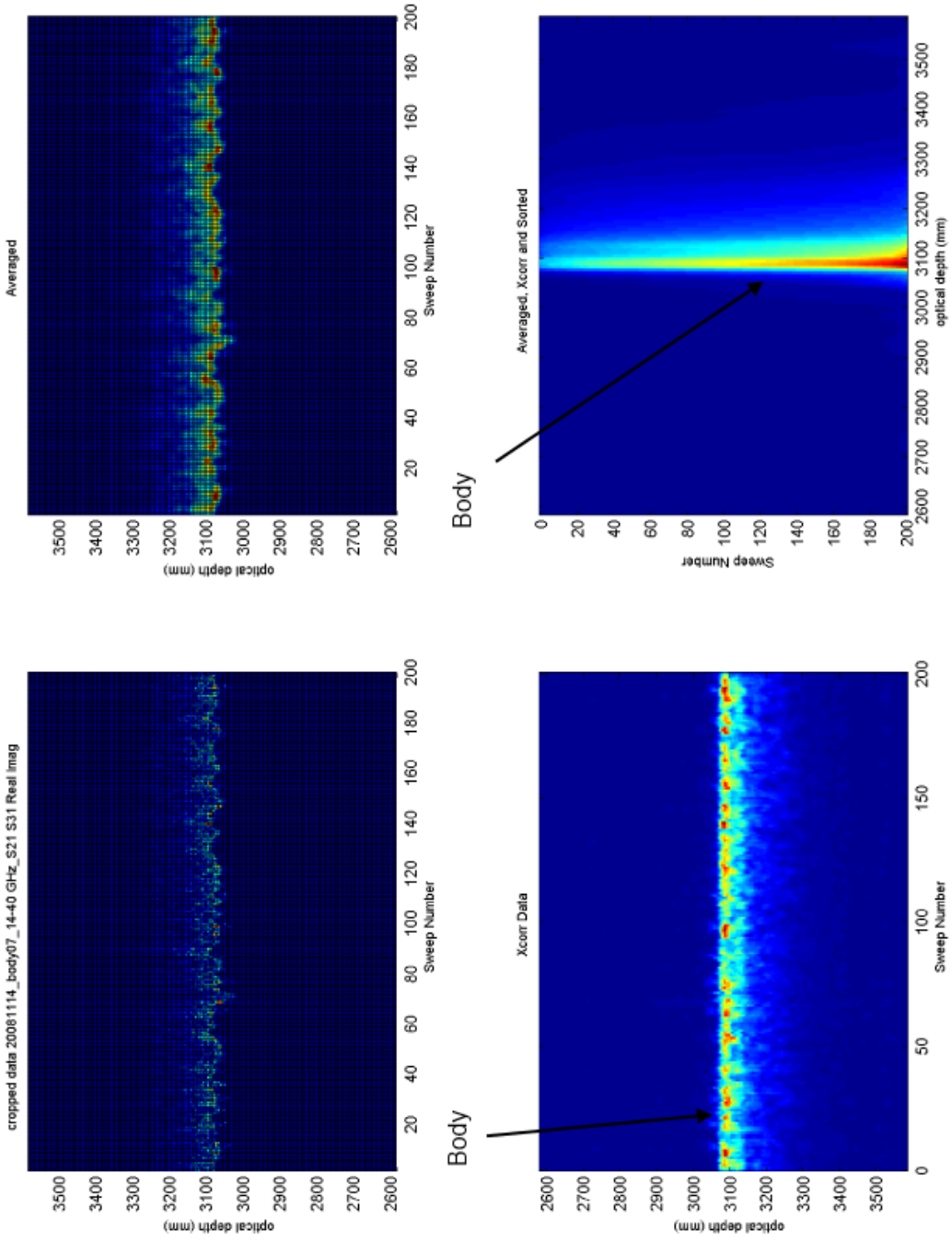

Figure 9.7: Body only, data set 7

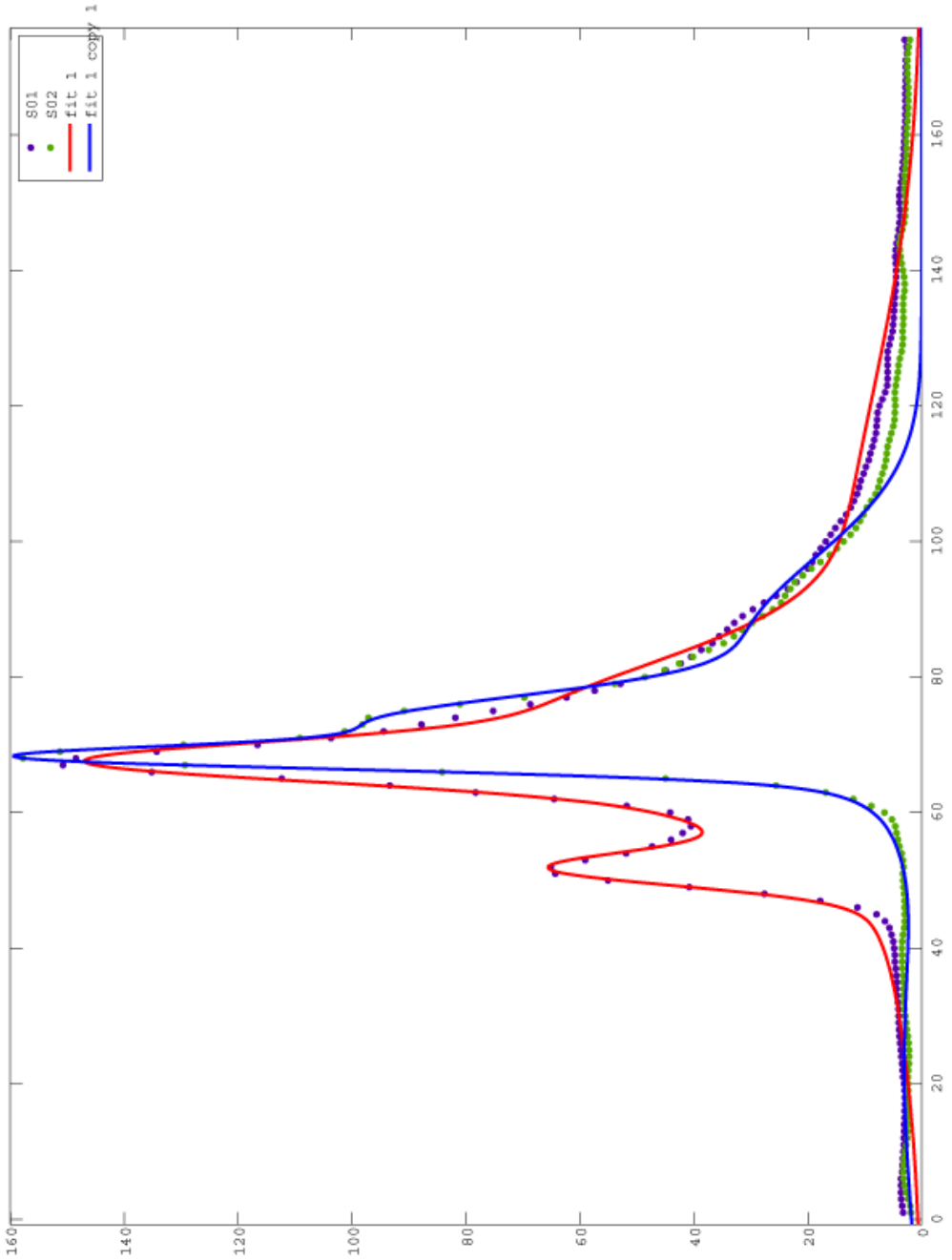

Figure 9.8: This figure shows the averaged data after fitting Gaussian curves to it. The figure shows a peak in front of the body response (red line); this indicates the presence of a 'suicide vest'. The blue line shows the body only response, i.e. no 'suicide vest' present.

9.1.3 Genetic Algorithm Curve Fitting

A genetic algorithm (G.A.) was tried to fit the same four Gaussian curves to the data. This was slower than the curve fitting toolbox, but it improved the fit to the data. The genetic algorithm generates 12 parameters and minimises the error between the data and the fitted function until some criteria is met, e.g. number of iterations. The neural network is then trained on these parameters. The G. A. fitted the Gaussian curves to the training data well, but when the neural network was tested the function missed the response from the simulated explosive in three out of 16 tests and was incorrectly classifying the body response in four out of 16 cases, as shown in figure 9.9.

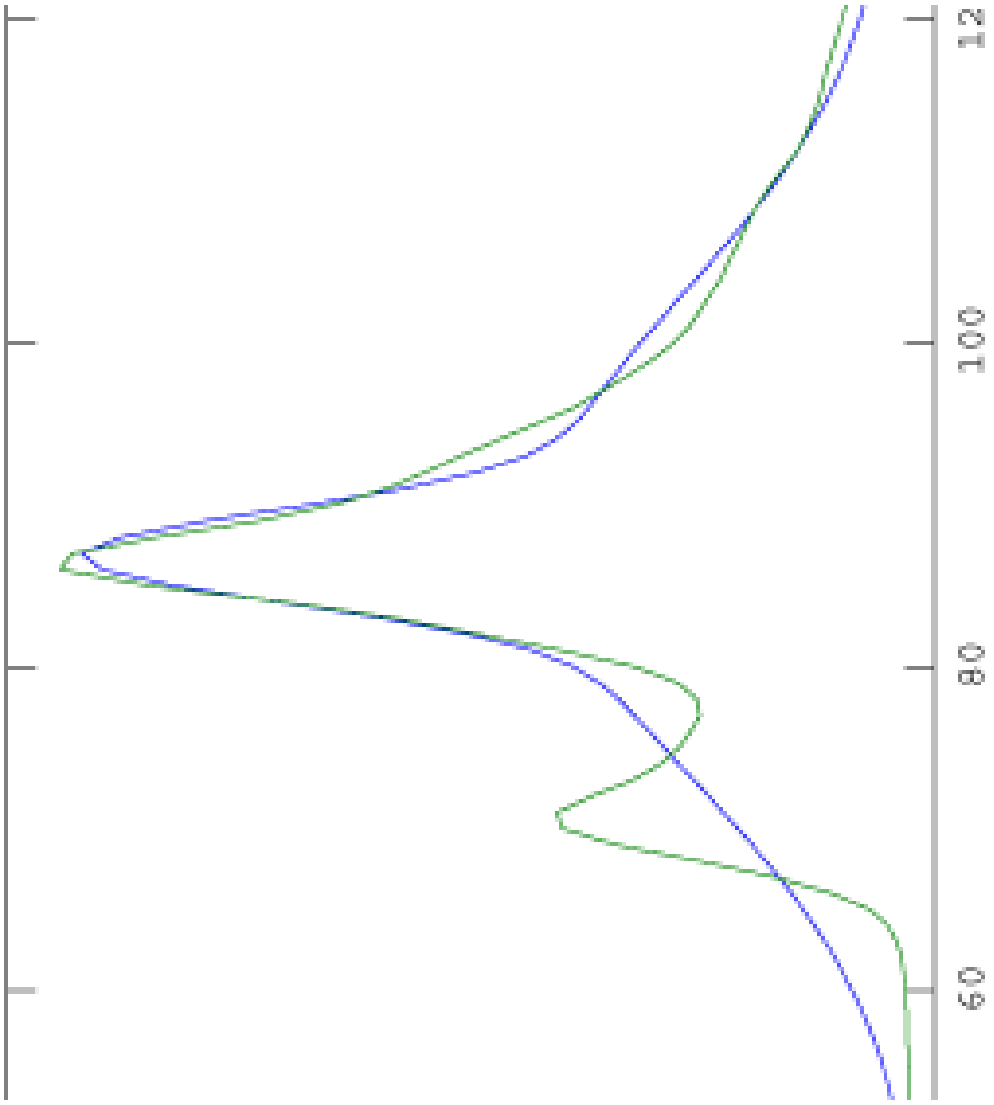

Figure 9.9: The genetic algorithm was missing the data when fitting curves.

The data which is averaged for training the neural network is taken from 200 sweeps which are averaged with a 2 by 2 averaging mask and then aligned by cross-correlation and then sorted. This leaves two peaks for the explosives data. To increase the true positive rate of the neural network, cropping the 100 weakest responses from the data was tried. This was to leave the sweeps where the target was most likely to be in the beam of the transmitter. This works well and has been left in as a pre-processing step, as shown in figure 9.10.

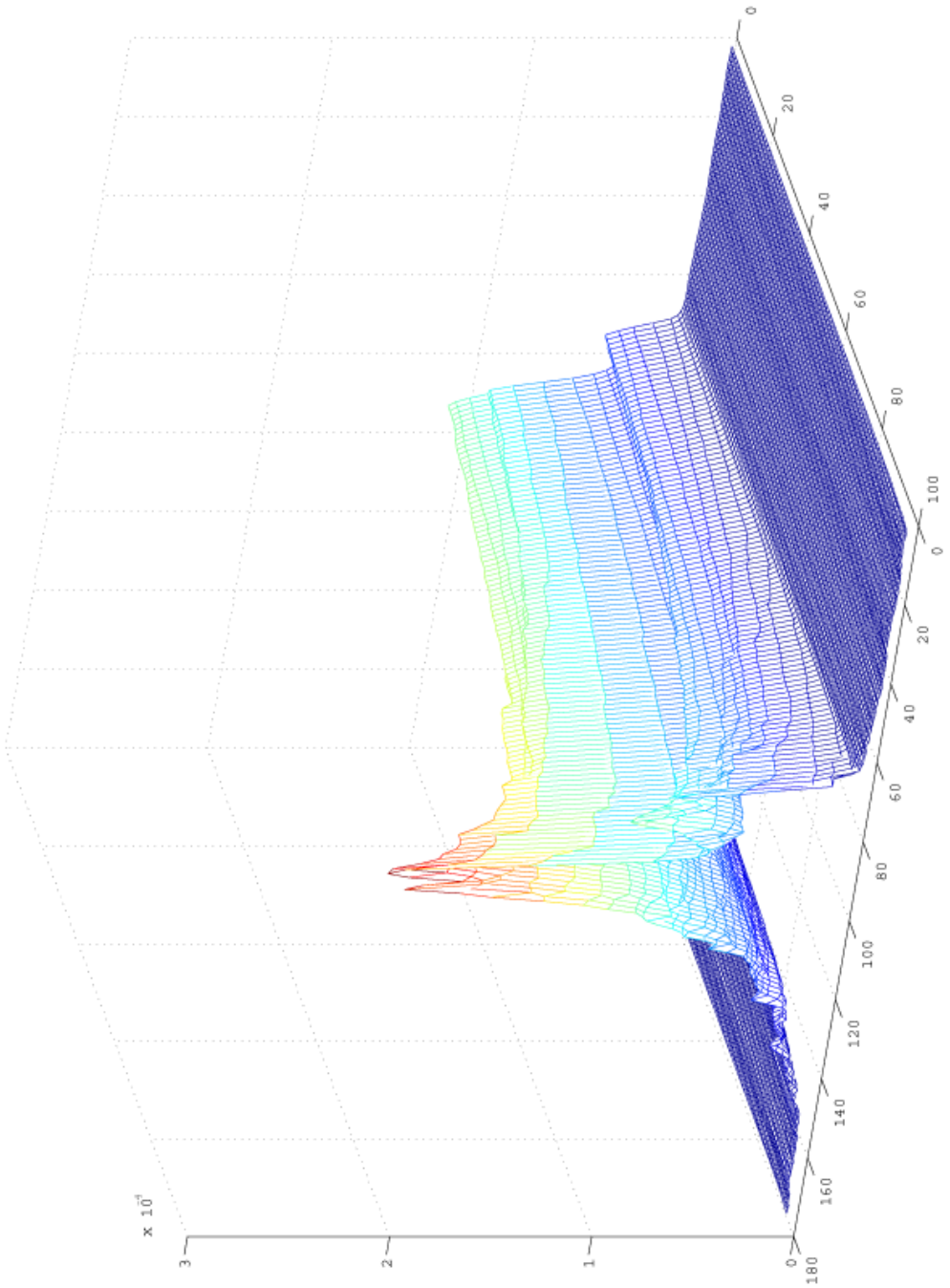

Figure 9.10: This data has been sorted by amplitude.

Training the neural network from the G.A. fitted data gave six out of ten correct classifications; whereas training the neural network with the curve fitting toolbox data gave eight out of ten correct classifications. To test if the neural network was being over trained, the number of training iterations or epochs was reduced to 1000 from 5000. The neural network failed to meet its goal of 0.01 in 1000 iterations. Three of the ten test data sets were correctly classified. Varying the number of hidden layer neurons didn't improve the success rate.

Further data was collected using the VNA as transmitter and receiver; using the 300 mm diameter lens to focus the beam onto the target. It is important to ensure that the beam is focused on the target, that it does not overspill the target at the edges and is not pointing out into the lab. The data was collected by measuring the gain between two horns connected to the VNA. This data was then IFFT and presented to the algorithm for processing and then the GA was used to fit curves to this data. This data was then used to train the neural network; it was found that the neural network failed to train because the data was too complex for it to classify. To reduce the complexity of the data being presented to the neural network, the data was reduced to 'wax peak' as shown in figure 9.11 or 'no wax peak' as shown in figure 9.12 and then using the G.A. to fit a curve to this data, the neural network was trained. Presenting unseen data to the neural network resulted in incorrect classifications of threat or not a threat with this processing method.

To achieve this needed the body responses aligning to each other, each data set was aligned to the same channel number by its maximum value. This data was then cropped to leave a narrow sub-section of the original averaged data. The parameters from the G.A. were then used to train the neural network. The neural network incorrectly classifies the data as threat and non-threat, it appears to be over trained; an over trained network is trying to fit to noisy data.

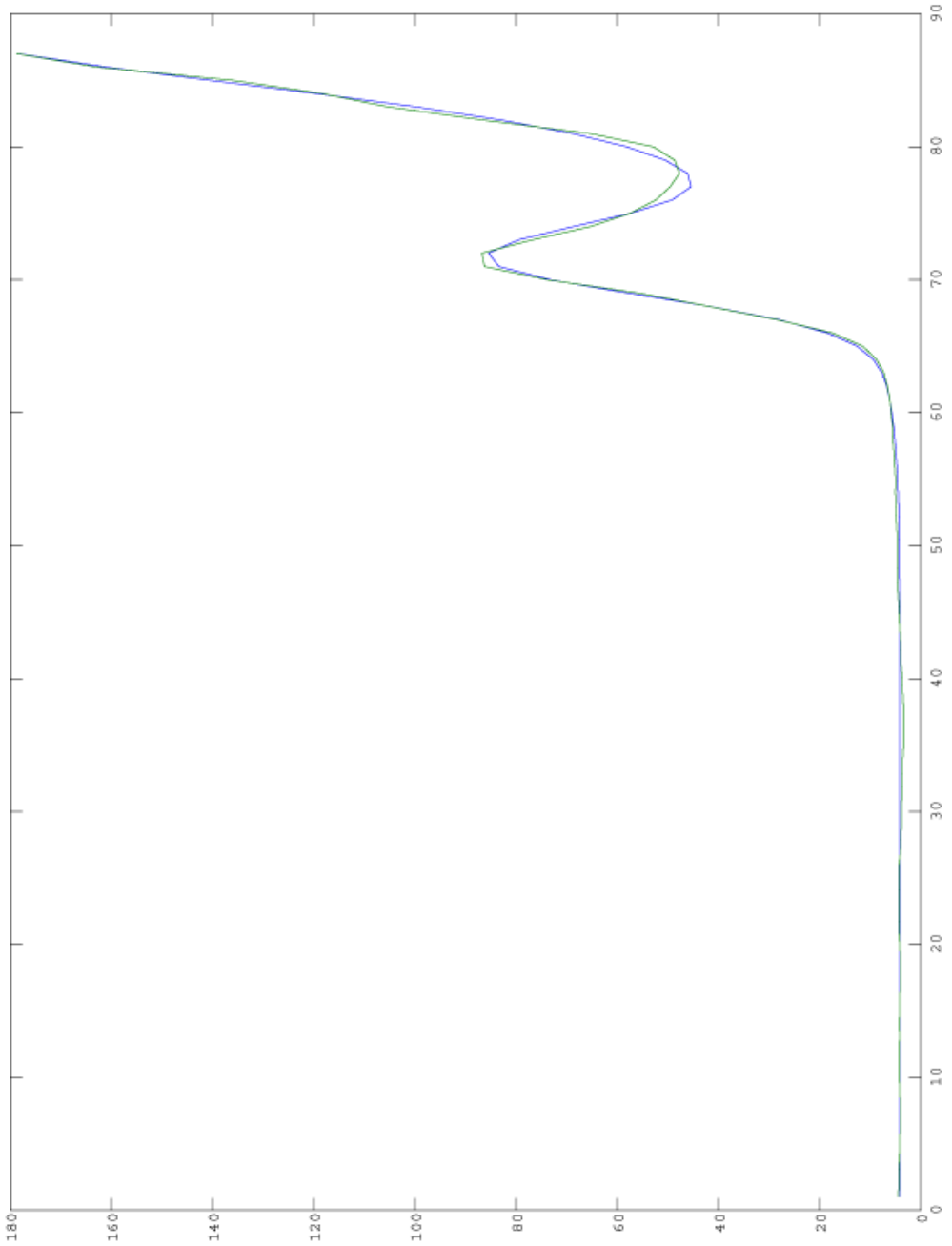

Figure 9.11: This figure shows the data with the 'suicide vest' present cropped at its maximum value, through the body response, leaving the peak from the simulated explosives visible in front of the body.

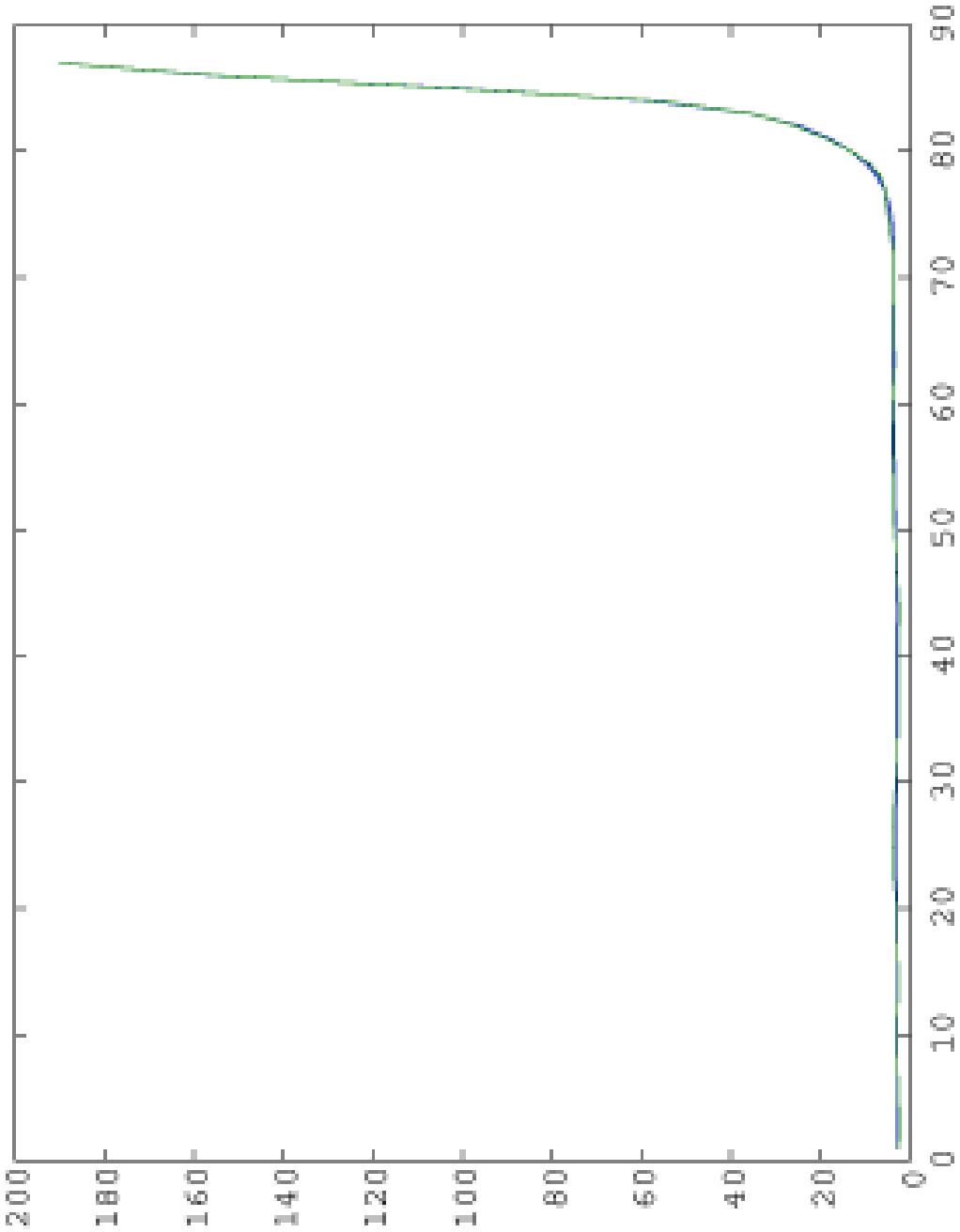

Figure 9.12: This figure shows the data with the body alone, cropped at its maximum value, through the body response, with nothing visible in front of the body, i.e. no 'suicide vest' present.

Table 9.2: Training data of six data sets for shuffle, xcorr and sorted data.

Object under test	target 1	target 2	target 3
training data			
wax+body06	0.9787	0.8556	0.9555
body06	0.0371	0.0966	0.0445
wax+body07	0.8772	0.8715	0.9859
body07	0.0368	0.0966	0.0521
wax+body08	0.8786	0.8695	0.9857
body08	0.2313	0.1081	0.0405

9.1.4 Simplifying the Data

To simplify the training of the network and to speed up the classification of each test data set; the data are averaged, correlated and sorted and then averaged across sweeps. Then the data sets are aligned by the maximum value; usually the body response, and all the data points to the left (on the x-axis) of the maximum value were taken to train the network on. This is a version of the processing algorithm without any curve fitting routine. A training data set comprising of threat co-polarisation, threat cross-polarisation, non-threat co-polarisation and non-threat crossed polarisation was correctly classified as threat data but fails on the non-threat data. This was then expanded to take six training data sets instead of four and the network was trained.

The neural network with six training sets as shown in table 9.2 was tested on 14 data sets and correctly classifies 13 out of 14 of the data sets as shown in table 9.3, but doesn't always get all three of the targets correct.

The 300 mm lens is needed to focus the beam onto the target, the 100 mm lens does not produce a sufficiently narrow beam. Some data sets were showing a double body response, this could be caused by a target stepping forward during the data collection. To align these responses, cross-correlation was added in both the x and y directions. This aligns all of the body responses and all of the wax responses with themselves. This produces correct classification with four training data sets and two test data sets.

Table 9.3: Test data of 16 data sets, alternate threat and non-threat, suicide vest present then absent.

Testing results	Target 1	Target 2	Target 3
wax+body09	0.0174	0.8147	0.0832
body09	0.0397	0.0306	0.0399
wax+body10	0.8575	0.8715	0.9859
body10	0.0370	0.0920	0.0416
wax+body01	0.0668	0.6897	0.0415
body01	0.0376	0.0961	0.0504
wax+body02	0.6452	0.0970	0.0541
body02	0.2091	0.0965	0.0391
wax+body03	0.5045	0.8706	0.0564
body03	0.0370	0.0966	0.1708
wax+body04	0.9792	0.8469	0.1739
body04	0.4430	0.0534	0.8292
wax+body05	0.0918	0.6403	0.0388
body05	0.0317	0.0967	0.0400

Table 9.4: Artificial neural network training data.

training results	score out of 17	target	% certainty
wax+body01	8	1	47
body01	10	0	59
wax+body02	12	1	71
body02	11	0	64

9.1.5 Varying the number of data points in the training data

The data are processed by correlating the data in the x and y directions and then taking the 100 strongest responses from 200 sweeps. The average of the sweeps is then taken and the training data are aligned by their maximum values (body responses). There are four training data sets. The data are then cropped to ignore the body response. This data are then cropped again to ignore data below 10% of the maximum value, so the wax response is removed from the background. The neural network is trained on 20 data points for each training set. The number of points will vary depending on the threshold. The network has four sets of targets which have the same number of elements as the individual data sets e.g. 20 ones or 20 zeros. Processing the test data in the same way and plotting a histogram of the results provides a graphical indication of the classification result as shown in figures 9.13 and 9.14.

Table 9.5: Artificial neural network testing data.

training results	score out of 17	target	% certainty
wax+body03	7	1	41
body03	8	0	47
wax+body04	11	1	65
body04	9	0	53
wax+body05	10	1	59
body05	8	0	47
wax+body06	9	1	53
body06	9	0	53
wax+body07	10	1	59
body08	10	0	59

The network was trained on four data sets as shown in table 9.4 and tested on 12 data sets, as shown in table 9.5. Eight of the 12 test sets were classified correctly; the histograms showed clearly if the data was threat or non-threat, i.e. mostly ones or mostly zeros, as shown in figures 9.13 and 9.14. These figures give a clear indication of the neural networks classification of either 'suicide vest' present or no threat present.

Further development of the software is to expand it to use co-polarisation and crossed-polarisation for training and testing the neural network. This will provide more information on which to base a threat decision.

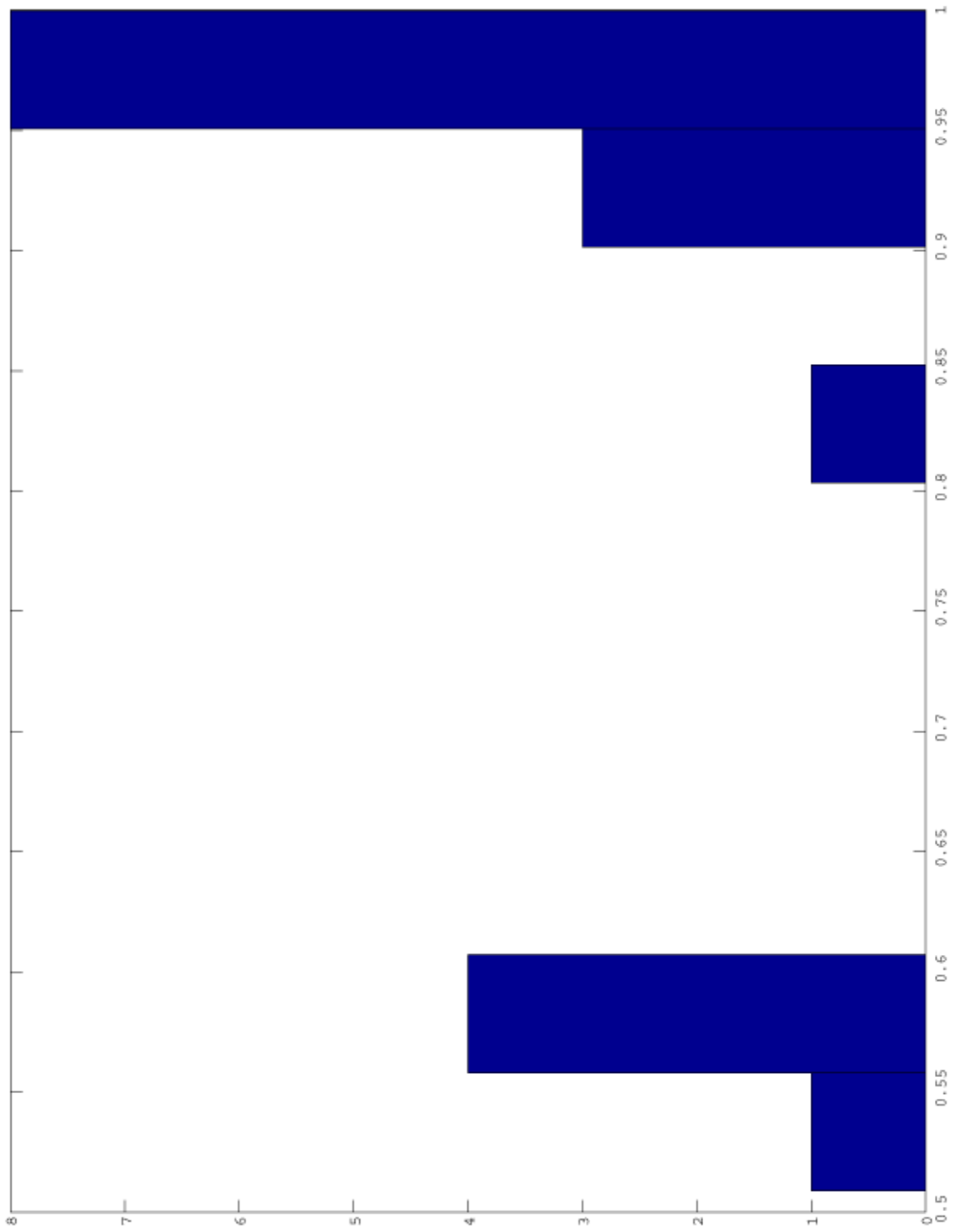

Figure 9.13: A histogram of the neural network classification ‘threat’ result.

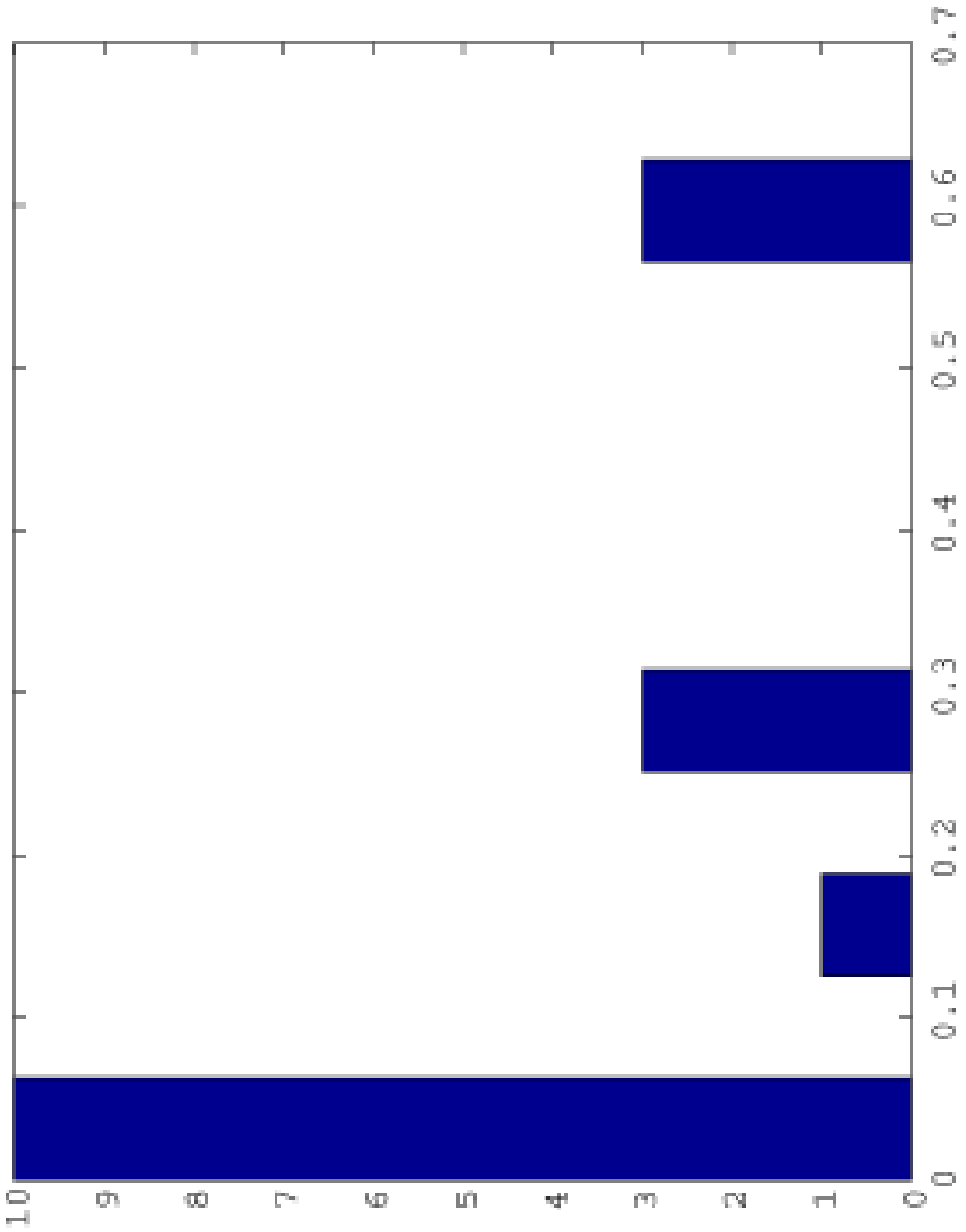

Figure 9.14: A histogram of the neural network classification ‘non-threat’ result.

Table 9.6: A table of training results for a neural network

Training data	Target 1	Target 2	Target 3
wax-body01	0.9885	0.8655	0.9225
body01	0.0629	0.1429	0.0777
wax-body07	0.9986	0.9826	0.7981
body07	0.0552	0.1229	0.0752

Table 9.7: A table of test results for a trained neural network, trained on 2 sets of alternate threat, non-threat data, the training results are shown in table 9.6. There are 16 test data sets for the ANN trained in table 9.6, the test results show it is well trained as only one of the data sets is incorrectly classified.

Test data	Target 1	Target 2	Target 3
wax-body02	0.9985	0.9794	0.7481
body02	0.0754	0.1190	0.0714
wax-body03	0.9983	0.9885	0.7949
body03	0.9932	0.9715	0.6181
wax-body04	0.9987	0.9873	0.8054
body04	0.0575	0.1109	0.1213
wax-body05	0.9985	0.9848	0.8034
body05	0.0563	0.1121	0.1166
wax-body06	0.9987	0.9863	0.8047
body06	0.0563	0.1103	0.1133
wax-body08	0.9605	0.9869	0.7481
body08	0.0579	0.1108	0.1143
wax-body09	0.9901	0.9728	0.7470
body09	0.0879	0.1081	0.1106
wax-body10	0.9986	0.9837	0.8026
body10	0.0661	0.1121	0.1138

Chapter 10

Conclusions and Future Work

10.1 Conclusions

Simulated explosives have been detected when held against the body by using a microwave active radar system in the form of a vector network analyser, and can be distinguished from the body only; demonstrating that millimetre wave radar is a feasible technique for on body explosives detection.

A deployable system that uses dielectric lenses has been designed; it can be used to focus a microwave beam onto a target at a standoff distance, the lens was designed using the theory of Gaussian optics.

A neural network has been used to classify each data set as either threat or non-threat. Table 9.7 shows that 94% of the classifications by the fully developed network were correct. This could be improved for a deployable system with further training sets.

Extensive signal processing algorithms in Matlab have been used to collect data from a VNA and to train a neural network. This network can be saved and then tested in real-time. The current system uses 200 sweeps which take a few minutes to collect, this system needs modifying to use less sweeps in the averaging and classification step; shortening the sweep time would also be a great advantage. The real-time system needs testing with multiple repetitions and different subjects and also with a variety

of non-threat objects such as mobile phones and keys.

Dielectric lenses were designed, manufactured and tested as part of a prototype system. A cassegrain antenna and receiver system was assembled and tested; incorporating the lenses or cassegrain antenna into a deployable system is left for further work.

Commercial MMIC wide band amplifiers and mixers were used as a receiver system, developing this into a portable system is left for further work.

10.2 Future Work

The range to the target needs to be extended and added to the neural network training set as an input for training, so that the target can be selected by range as well as amplitude and the network can be trained on a weak response and recognise that a weak response is further away than a stronger response. The thresholds used in the Matlab user interface need to be decided on; where the threshold for threat, not sure and non-threat are. The number of training sets to the network needs to be increased by recording more VNA data. The neural network also needs training and testing on a range of non-threat objects such as mobile phones, music players, keys and wallets etc. The time-gating of the data needs also to reflect the known range instead of just the maximum amplitude of the data, so that the correct target is always selected. Using different people as targets would be an advantage because this ensures that the network can classify more than one body type with and without threat objects. The VNA operates from 10MHz to 40GHz, and this is convenient for initial measurements, but increasing the frequency by using a portable super-heterodyne system will mean an increase of operating frequency to 75 to 110GHz and so smaller optics and microwave components which results in a more portable system.

The microwave beam needs scanning over the target and a mechanical means of moving the lens and feed horn needs to be devised; the transmitter and receiver need to follow each other in parallel so that at least two different points on a target can

be checked or the entire system needs to be portable and maneuverable enough to be manually scanned across a target.

The detection system needs to be a deployable device, which can be used by security personnel in a way which will not draw attention to them, so the system needs to be light weight and portable. It also needs to be easy to operate.

The VNA provides relatively slow data acquisition, moving to a 75 to 110 GHz, but super-heterodyne system will give high speed data acquisition.

Once the detection system is functioning reliably then the next stage is field testing. This is when the user interface and ease of operation will be tested and refined.

The standoff distance can be increased by using a larger lens or going to a higher frequency, as discussed above.

Multiple detectors could be useful in two ways; the system currently uses one polarisation only, the co-polarisation. If another receiver were added then the crossed-polarisation can also be used. This is useful for detecting metallic objects and explosives containing shrapnel. Explosives containing no metallic fragments produce a very small response in the crossed polarisation to the transmitter, so this isn't used to detect explosives only.

Chapter 11

Summary

The basic function of a radar is to detect a target and determine its range, in concealed explosives detection classification of target (threat or non-threat) is sort, i.e. determining if the target is a threat or not. The operation of the radar system is to transmit a continuous wave signal and receive the reflection from the target. The reflected radar waveform contains information encoded into the frequency domain by amplitude modulation resulting from interference effects from the depth of any explosive (dielectric) present. The range to the target can also be found from data in the time domain. The motivation for this project was to detect concealed explosives from their radar signature and distinguish them from other objects normally carried by people, these other objects are known as pocket clutter (Hausner & West, 2007). The detector needed to operate at a standoff distance so that targets could be checked for explosives without their knowledge. A standoff distance in this case is around ten metres.

The Inverse Fast Fourier Transform can be used to convert from frequency to time domain, using the time domain has the advantage of being able to extract the time of flight or distance to the target.

Time-domain data from radar reflections has been collected from subjects carrying simulated explosives vests and those not. This data has been pre-processed and presented to a feed forward back propagation neural network which was trained and then tested on new previously unseen data. The data are sorted and aligned to a reference

distance (the body) in order to significantly improve the results. Aligning the data removes the effect of the persons movement.

A signal processing algorithm has been developed and used to take real-time data from the Vector Network Analyser (VNA) and to train the neural network with it. A VNA is a continuous wave (CW) transmitter which can be swept in frequency and simultaneously used as a receiver on a different port. It can be used to send data to an external computer for further processing.

The trained network can be saved and recalled for testing, so that the network does not have to be trained before each test (Math-Works, 2009). Matlab is used because it has built in routines that allow neural networks to be created quickly and data to be easily formatted as training data for the neural network.

A practical system including focusing optics has been designed and manufactured for frequencies centred on an atmospheric window around 94GHz to focus a millimetre wave beam at a stand-off distance up to 7 metres. This design forms the basis of a prototype detector system that could be deployed in the field. The lenses and other components were modelled using COMSOL (2009) and a ray-tracing software package (Lambda-Research, 2005). COMSOL (2009) is a finite element analysis software package which allows you to draw your model, specify the physics involved and then solve and post-process the results.

Future work for this project will include improving the sweep time so that real-time data can be collected and the development of a prototype deployable system which can be field tested.

The objective of designing a transmitting and receiving system for significant stand off distances and to be able to detect the presence of a potential threat is well under way. It will be developed further into a deployable system.

Bibliography

Agilent. 2011, Agilent, Internet, http://www.agilent.com, accessed June 2011

Agurto, A., Li, Y., Tian, G., Bowring, N., & Lockwood, S. 2007, in Networking, Sensing and Control, 2007 IEEE International Conference on, IEEE, 443–448

Alabaster, C. M. 2004, PhD thesis, Cranfield University, https://dspace.lib.cranfield.ac.uk/bitstream/1826/251/2/AlabasterPhD.pdf

Andrews, D. A., Rezgui, N. D., Smith, S. E., et al. 2008, in Millimetre Wave and Terahertz Sensors and Technology, ed. K. A. Krapels & N. A. Salmon, Vol. 7117 (SPIE), 71170J

Andrews, D. A., Smith, S., Rezgui, N., et al. 2009, in Passive Millimeter-Wave Imaging Technology XII, ed. R. Appleby & D. A. Wikner, Vol. 7309 (SPIE), 73090H, orlando, FL, USA

Appleby, R. 2004, Royal Society of London Transactions Series A,, 362, 379

Appleby, R. & Anderton, R. 2007, Proceedings of the IEEE, 95, 1683

Appleby, R., Anderton, R., Price, S., et al. 2003, Proceedings of SPIE, 5077, 1

Appleby, R. & Wallace, H. 2007, IEEE Transactions on Antennas and Propagation, 55, 2944

Bowring, N., Baker, J., & Alder, J. 2007, Networking, Sensing and Control, 2007 IEEE International Conference on, 437

Bowring, N. J., Baker, J. G., Rezgui, N. D., Southgate, M., & Alder, J. F. 2007, in Presented at the Society of Photo-Optical Instrumentation Engineers (SPIE) Conference, Vol. 6540, Optics and Photonics in Global Homeland Security III. Edited by Saito, Theodore T.; Lehrfeld, Daniel; DeWeert, Michael J.. Proceedings of the SPIE, Volume 6540, pp. 65401M (2007).

Brooker, G. 2005, in 1st International Conference on Sensing Technology, 152–157

Brown, S. F. 2008, Scientific American, 84

Burke, B. & Graham-Smith, F. 2010, An introduction to radio astronomy (Cambridge University Press)

Chen, H., Lee, S., Rao, R., Slamani, M., & Varshney, P. 2005, Signal Processing Magazine, IEEE, 22, 52

COMSOL. 2009, COMSOL Software, `http://www.comsol.com`

Cooper, K., Dengler, R., Llombart, N., et al. 2008, Microwave Theory and Techniques, IEEE Transactions on, 56, 2771

Cornbleet, R. 1976, Microwave Optics (Publisher)

Costianes, P. 2005, Applied Imagery and Pattern Recognition Workshop, 2005. Proceedings. 34th, 2

Currie, N., Demma, F., Ferris Jr, D., et al. 1995, Proceedings of SPIE, 2567, 124

Currie, N. C. & Brown, C. E. 1987, Principles and Applications of Millimeter-wave Radar (Artech House), p277

Dallinger, A., Schelkshorn, S., & Detlefsen, J. 2005, GeMiC

Derham, T., Kamoda, H., Iwasaki, T., & Kuki, T. 2007, Microwave Conference, 2007. KJMW 2007. Korea-Japan, 181

Dickinson, J., Goyette, T., Gatesman, A., et al. 2006, Proceedings of SPIE, 6212, 62120Q

Dill, S., Peichl, M., & Suess, H. 2007, in Proceedings of SPIE, Vol. 6548, 65480L

Dill, S., Peichl, M., & Suess, H. 2007, in Society of Photo-Optical Instrumentation Engineers (SPIE) Conference Series, Vol. 6548, Society of Photo-Optical Instrumentation Engineers (SPIE) Conference Series

Doyle, R., Lyons, B., Lettington, A., et al. 2004, in Proc. SPIE, Vol. 5619, 90–97

Doyle, R. & McNaboe, J. 2006, NATO Security through Science Series, NATO Security through Science Series (Springer), iSBN 978-1-4020-5157-9

Elva. 2003, A Cassegrain Reflector, Internet, `http://www.elva-1.com/products/microwave/dual_reflect.html`, accessed April 2011

Essen, H., Wahlen, A., Sommer, R., et al. 2007, Electronics Letters, 43, 1114

Fackler ML, M. J. 1988, Am J Forensic Med Pathol, 9(3), 218, pMID: 3177350

Federici, J., Schulkin, B., Huang, F., et al. 2005, Semicond. Sci. Technol, 20, S266

Fernandes, C. 1999, Antennas and Propagation Magazine, IEEE, 41, 141

GeorgiaStateUniversity. 2011, Blackbody curve at 300K, Internet, `http://hyperphysics.phy-astr.gsu.edu/hbase/bbrc.html#c4`

Gibson, P. 2000, Introductory Remote Sensing, Principles and Concepts, 1st edn. (Routledge)

Goldsmith, P., Hsieh, C., Huguenin, G., Kapitzky, J., & Moore, E. 1993, Microwave Theory and Techniques, IEEE Transactions on, 41, 1664

Goldsmith, P. & Moore, E. 1984, Microwave Journal, July 1984, 153

Grafulla-Gonzalez, B., Haworth, C., Harvey, A., et al. 2005, LECTURE NOTES IN COMPUTER SCIENCE, 3687, 48

Grossman, E., Luukanen, A., & Miller, A. 2004, Proceedings of SPIE, 5411, 68

Hannan, P. 2002, Antennas and Propagation, IRE Transactions on, 9, 140

Harmer, S., Bowring, N., Andrews, D., et al. 2012, IEEE Microwave Magazine, 13, 160

Hausner, J. & West, N. 2007, Microwave Symposium, 2007. IEEE/MTT-S International, 765

Haworth, C., De Saint-Pern, Y., Petillot, Y., Trucco, E., & Edinburgh, U. 2005, Imaging for Crime Detection and Prevention, 2005. ICDP 2005. The IEE International Symposium on, 1

Hecht, E. 2002, Optics (Addison Wesley)

Herman, I. P. 2007, Physics of the Human Body (Springer), iSBN 978-3-540-29603-4

Howald, R., Clark, G., Hubert, J., & Ammar, D. 2007, Technologies for Homeland Security, 2007 IEEE Conference on, 234

Hu, Y., Huang, P., Guo, L., Wang, X., & Zhang, C. 2006, Physics Letters A, 359, 728

Ibrahim, A., Liu, K., Novak, D., & Waterhouse, R. 2007, Acoustics, Speech and Signal Processing, 2007. ICASSP 2007. IEEE International Conference on, 2

ICNIRP. 1998, Health Physics, 74, 494

Jefferies, D. 2012, S-parameters, website, `http://personal.ee.surrey.ac.uk/Personal/D.Jefferies/sparam.html`

Jenkins & White. 1982, Fundamentals of Optics (Whiley)

Jones, B. 1998, Medical Imaging, IEEE Transactions on, 17, 1019

Kemp, M., Baker, C., & Gregory, I. 2006, Stand-Off Detection of Suicide Bombers and Mobile Subjects, 151

Kraus. 1988, Antennas (McGraw-Hill)

Kraus. 1999, Electromagnetics with Applications (McGraw-Hill)

Labcenter-Electronics. 2010, Proteus PCB design software, Software, http://www.labcenter.com

Lamb, J. 1996, International Journal of Infrared and Millimeter Waves, 17, 1997

Lambda-Research. 2005, OSLO EDU, Internet, http://www.lambdares.com/education/oslo_edu/, accessed May 2011

Leonard, D. 2010, Cassegrain mechanical and controller design, Mechanical design and build, manchester Metropolitan University

Lesurf, J. 1990, Millimetre-wave Optics, Devices and Systems (Taylor and Francis)

Levanon, N. 2004, Radar Signals (Wiley), copyright 2004 John Wiley and Sons from www.knovel.com

Macfarlane, D., Lesurf, J., & Robertson, D. 2002, in Proceedings of SPIE, Vol. 4719, 350

Martin, C., Lovberg, J., Dean, W., & Ibrahim, E. 2007, in Proceedings of SPIE, Vol. 6548, 654806

Math-Works. 2009, Matlab Software, http://www.mathworks.co.uk

McMillan, R., Currie, N., Ferris, D.D., J., & Wicks, M. 1998, in Microwave and Millimeter Wave Technology Proceedings, 1998. ICMMT '98. 1998 International Conference on, 1 –4

Mead, K. 2002, Testimony to the Committee on Appropriations, Subcommittee on Transportation, US House of Representatives

Melles-Griot. 2009, Gaussian Beam Optics, Internet, http://www.cvimellesgriot.com/products/Documents/TechnicalGuide/Gaussian-Beam-Optics.pdf

Millitech. 2009, GOLA, website, http://www.millitech.com/AntennaQuasioptical.htm

National-Instruments. 2010, http://www.ni.com/, Internet site

of St-Andrews, U. 2011, What are MM Waves?, Internet, http://www.st-andrews.ac.uk/~mmwave/mmwave/what2.html, accessed September 2011

P-N Designs, I. 2011, Homodyne receivers, Internet, http://www.microwaves101.com/encyclopedia/receivers_homodyne.cfm

Pepper, D. W. 1992, The Finite Element Method (Taylor and Francis)

Peratta, C., Peratta, A., Hand, J., et al. 2010, Medical Physics, 37, 5561

Qiang, L. & Conners, R. W. 2006, IEEE TRANSACTIONS ON SYSTEMS, MAN, AND CYBERNETICS PART C: APPLICATIONS AND REVIEWS, vol.36, 750

Ramo, S. & Whinnery, J. R. 1994, Fields and Waves in Communication Electronics, 3rd edn. (John Wiley and Sons, New York)

Read, F. H. 1980, Electromagnetic Radiation (Wiley)

Rezgui, N., Andrews, D., Bowring, N., Harmer, S., & Southgate, M. 2008, in Society of Photo-Optical Instrumentation Engineers (SPIE) Conference Series, Vol. 6948, Society of Photo-Optical Instrumentation Engineers (SPIE) Conference Series

RFcafe. 2012, Loss tangent, website, http://rfcafe.com

Robinson, L. A., Weir, W. B., & Young, L. 1972, An RF time-domain reflectometer not in real time, GMTT International Microwave Symposium Digest Vol. 72, No. 1, 30

Rosker, M., Wallace, J., & Bruce, H. 2007, Microwave Symposium, 2007. IEEE/MTT-S International, 773

Shen, Y., Lo, T., Taday, P., et al. 2005, Applied Physics Letters, 86, 241116

Silva, E. 2001, High Frequency and Microwave Engineering (Butterworth-Heinemann)

Silver. 1949, Microwave Antenna Theory and Design (McGraw-Hill)

Sinyukov, A., Zorych, I., Michalopoulou, Z., et al. 2008, Comptes rendus-Physique

Skolnik, M. I. 1990, Radar Handbook, 2nd edn. (McGraw-Hill), online version available at: http://www.knovel.com/web/portal/browse/display?_EXT_KNOVEL_DISPLAY_bookid=701&VerticalID=0

Tamyis, N. M. 2005, Proc. of the 28th URSI General Assembly, http://www.ursi.org/Proceedings/ProcGA05/pdf/KP.45(0805).pdf

Timms, G., Bunton, J., Brothers, M., & Archer, J. 2007, Wireless Broadband and Ultra Wideband Communications, 2007. AusWireless 2007. The 2nd International Conference on, 32

Volkov, L., Voronko, A., & Berendakova, N. 2008, Infrared, Millimeter and Terahertz Waves, 2008. IRMMW-THz 2008. 33rd International Conference on, 1

Wang, Z. & Dou, W. 2006, Journal of Electromagnetic Waves and Applications, 20, 1643

Watabe, K., Shimizu, K., Yoneyama, M., & Mizuno, K. 2003, Microwave Theory and Techniques, IEEE Transactions on, 51, 1512

WikiCommons. 2011, Rectangular Function, Internet, http://en.wikipedia.org/wiki/

Wikimedia-Commons. 2010, EM Spectrum Properties, Internet, http://commons.wikimedia.org/wiki/File:EM_Spectrum_Properties_edit.svg, accessed September 2011

Yamamoto, K., Yamaguchi, M., Miyamaru, F., et al. 2004, JAPANESE JOURNAL OF APPLIED PHYSICS PART 2 LETTERS, 43, 414

Yeom, S., Lee, D., Son, J., et al. 2011, Optics Express, 19, 2530

Zhang, L., Hao, Y., Parini, C., & Mary, Q. 2007, Antennas and Propagation, 2007. EuCAP 2007. The Second European Conference on, 1

Chapter 12

Appendices

12.1 SPIE paper 2008 (Andrews et al., 2008)

Detection of concealed explosives at stand-off distances using wide band swept millimetre waves

David A. Andrews, Nacer D. Rezgui, Sarah E. Smith, Nicholas Bowring*, Matthew Southgate, John G. Baker.
Dept. of Engineering, Manchester Metropolitan University, Chester St., Manchester M1 5GD, UK.

ABSTRACT

Millimetre waves in the range 20 to 110 GHz have been used to detect the presence and thickness of dielectric materials, such as explosives, by measuring the frequency response of the return signal. Interference between the reflected signals from the front and back surfaces of the dielectric provides a characteristic frequency variation in the return signal, which may be processed to yield its optical depth [Bowring et al, Meas. Sci. Technol. 19, 024004 (2008)]. The depth resolution depends on the sweep bandwidth, which is typically 10 to 30 GHz. By using super-heterodyne detection the range of the object can also be determined, which enables a signal from a target, such as a suicide bomber to be extracted from background clutter. Using millimetre wave optics only a small area of the target is illuminated at a time, thus reducing interference from different parts of a human target. Results are presented for simulated explosive materials with water or human backing at stand-off distances. A method of data analysis that involves pattern recognition enables effective differentiation of target types.

Keywords: FMCWR, Millimetre waves, Explosives, Drugs, Standoff detection.

*n.bowring@mmu.ac.uk phone +44 161 247 6271; fax +44 161 247 1633; www.mmu.ac.uk

1. INTRODUCTION

The increasing incidence of terrorist activity and in particular so called “suicide bombers” has heightened the need amongst security services for instrumentation to detect weapons and explosive devices at standoff distances. Unlike the case of handguns and “fragmentation” devices where the weapon contains a significant amount of metal giving a clear radar signature, some plastic explosive devices consist mainly of dielectric material and different identification techniques need to be employed. A promising technique to detect dielectric layers by wide band frequency scanned radar has been reported previously by us [1, 2]. This has been further developed and this work will be described in this paper.

After a review of currently available techniques for remotely detecting dielectric material such as explosives, drugs or contraband concealed on the person and the desired features of an operational device, the principles of our method are described. An outline of several practical systems using frequency scanned millimeter waves is given and representative results presented. Methods of data analysis including use of artificial neural networks (ANN) are described and assessed.

2. CURRENT TECHNIQUES

The detailed requirements of a detection system depends on the specific operational circumstances under which it is being deployed, however a number of desirable representative features may be identified when surveying the literature:

(a) The ability to work at a distance from the subject,
(b) A fast response time, comparable with video refresh rates for example,
(c) The use of a frequency band that penetrates normal clothing,
(d) Ability to work outside in an uncontrolled environment.

Millimetre Wave and Terahertz Sensors and Technology, edited by Keith A. Krapels, Neil A. Salmon,
Proc. of SPIE Vol. 7117, 71170J · © 2008 SPIE
CCC code: 0277-786X/08/$18 · doi: 10.1117/12.800382

2.1 Passive microwave imaging

Passive imaging relies on picking up the microwave emission from the subject using a sensitive wideband receiver or detector array. This radiation has two components: the natural thermal radiation from the subject, which depends on the temperature and emissivity of the surface and reflected radiation from the sky or internal lighting, which varies with surface reflectivity. By scanning the direction of the collected beam an image of the subject can be built up and displayed to the operator. A concealed dielectric slab attached to the body may become visible due to its different temperature, emissivity or reflectivity compared to the surrounding clear body area. Published work [3-5] shows that under optimum conditions explosive materials can be detected by this method, though the articles state that it can have some operational difficulties:

(a) The signal contrast from dielectrics can be quite low,
(b) The image refresh time for good signal to noise is rather slow,
(c) Operational performance is sensitive to environment, in particular under outside conditions,
(d) The instrument requires experienced interpretation by the operator to discern threat features,
(e) Possible privacy issues in viewing images of subject.

2.2 Active microwave imaging

With active imaging the subject is illuminated by a usually coherent microwave source and the return signal detected [6-8]. Coherent detection has a number of advantages by giving high signal to noise and fast image update speeds. Beam steering to generate the image can be achieved electronically by synthetic aperture techniques as well as by mechanical means. In addition, through measurement of the phase of the return signal, the range may also be determined. Through using more than one receiver and appropriate signal processing it is also possible to build up a 3D or holographic image of the subject [7-8]. A concealed dielectric slab attached to the body may visible due to its different reflectivity or being apparently forward of the surrounding body surface. Under optimum conditions explosive materials can be detected by this method, but it can have possible difficulties:

(a) The signal contrast from dielectrics can still be quite low,
(b) It still requires experienced interpretation by the operator to discern threat features,
(c) A single frequency scan can lead to fringing effects which complicate interpretation of the image,
(d) Possible privacy issues in viewing images of subject,
(e) Possible safety and legal issues in exposing subjects to microwaves without prior agreement.

2.3 THz spectroscopy and imaging

The development of sources and detectors operating in the Terahertz region (0.2 to 2 THz) has led to some further enhancements in imaging technology [9-12]. The shorter wavelength gives improved spatial resolution at stand-off distances leading to more compact systems. An additional feature available, which becomes possible when a higher frequency range is used, is the ability to determine the chemical composition of the target object through its reflection spectrum. Absorption at characteristic spectral lines causes the return signal from explosives to vary with frequency in a different manner to that of the surrounding body surface. This can be used to overlay the image displayed to the operator to indicate areas showing a suspicious chemical signature. However a major obstacle to the employment of higher frequencies is the increased absorption of common clothing materials, which seriously attenuates the return signal [13]. The technology is also less advanced and more costly than at lower frequencies.

It is apparent that though microwave imaging can form a basis of an explosives detection system, alternative methods to alert the operator to the presence of suspicious material would however be of considerable value. Such a method is described in the next section.

3. PRINCIPLE OF OPERATION

The technique uses active scanned mm waves. Consider as in Fig. 1, a plane wave $\exp\{-2\pi f(t-z/c)\}$ with amplitude E_T and frequency f incident in the z direction on a parallel slab of dielectric material of thickness d, refractive index n and distance L from the transmitter. The return wave E_R consists of reflections R and R' from the front and back faces of the dielectric slab. If the backing material can be approximated as a semi-infinite layer of refractive index n' and multiple reflections are neglected, then

$$E_R = E_T \{R + R' \exp(4j\pi fnd/c)\} \exp(4j\pi fL/c) \quad (1)$$

where $R = \frac{(n-1)}{(n+1)}$, $R' = \frac{(n'-n)}{(n'+n)}$ and c is the velocity of light. The relative phase shift between the reflections from the front and back faces gives rise to frequency-dependent interference between the two signals. If the return signal is measured by a square law detector, such as a diode, then

$$|E_R|^2 = |E_T|^2 \{|R|^2 + |R'|^2 + 2|R||R'|\cos(4\pi fnd/c)\} \quad (2)$$

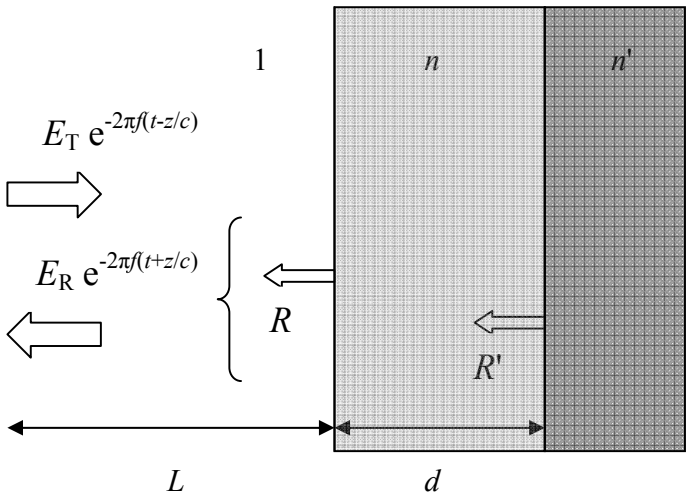

Fig. 1. Incident plane waves from the left reflect off the front and back faces of the dielectric block of thickness d and refractive index n backed by material of refractive index n' and combine at a detector situated near the source.

This shows explicitly the sinusoidal dependence on frequency. The period of the oscillation is proportional to the optical depth of the material nd. By Fourier transformation of the recorded signal the position of the peaks gives the optical depth of the sample [1-2]. For the application of explosives detection, a significant peak within a band of optical depth 10-50 mm may be used as an indicator of the presence of a suspicious object.

The above analysis may be generalized to include loss in materials by using a complex refractive index and more complicated geometries [1-2]. It may also be noted that equation (1) implicitly contains the range L of the object. In fact the return signal may be separated into two factors: a modulation envelope dependent on optical depth nd and a carrier wave factor dependent only on L. By measuring the phase of the return signal by using a super-heterodyne or homodyne receiver, both factors can be extracted. By digital filtering, the returns from a specific band of ranges may be selected for analysis. Fourier transforming the envelope of the filtered signal leads to the optical depth spectrum for the target area only and rejects background objects present at a different range.

The minimum optical depth which may be measured by this technique, depends on the frequency range Δf swept over by the microwave source as $c/\Delta f$. So wideband sources and detection systems are required with a typical sweep of ~20 GHz. However the absolute frequency is not determined by this requirement, so for example 20-40 GHz and 80-100 GHz would be equally suitable from this respect.

A major consideration when using this technique with a human body as backing, is the complex return signal found from reflections from different parts of the torso. Signals from the arms appear with a different time delay than those from the chest and lead to interference effects very similar to the explosives signature. It should be emphasized that this is not an imaging technique, so the signal on the detector is a sum from all the targets within the field of view of the receiver. To address this problem two approaches have been successfully tried and are described here.

3.1 Spatial selection

An alternative approach is to restrict the angular aperture of the detector so that it only receives signals from one part of the body at a time. By increasing the frequency and using quasi-optical techniques it is feasible to achieve a small enough spot size at stand-off distances. However, it is important to provide ways to ensure alignment of the mm wave beam on the correct part of the target. The precise methods of target tracking such as sensor fusion, are well known and therefore outside the scope of this work.

3.2 Range selection

By using the range information, from for example a vector network analyzer (VNA), it is possible to differentiate between signals from different parts of the body. In particular, the earliest response is often from the torso at the position of a "suicide vest". Noting that taking the complex inverse Fourier transform (iFFT) of equation (1) leads to peaks separated in time by $2nd/c$.

$$\overline{E}_R(t) = E_T\{Rf(t-2L/c) + R'f(t-2L/c-2nd/c)\} \tag{3}$$

By aligning the time resolved signals with respect to the leading edge of the body response, the presence of a small additional response proportional to R ahead of the main reflection R' gives an indication of the presence of the dielectric layer.

4. RESULTS

4.1 Direct detection

The measurements were taken using the experimental arrangement described previously [10]. Briefly, the output of an Agilent E8257D microwave signal generator drives a Millitech AMC-10 times six active frequency multiplier. An Elva ZBD-10 mmw diode detector is used to measure the received power and can be preceded a Millitech LNA-10 20dB low noise microwave amplifier. The signal generation system can provide a stepped or continuous frequency sweep in 100ms from 75 to 110 GHz with an output ~0.1mW. The transmitter horn was placed close to the focus of a 300mm diameter, 400mm focal length polyethylene lens both mounted on a steerable rack, which also includes the detector assembly. A high gain horn is used to collect the signal from the target area and the detected signal is amplified using a current amplifier and digitised synchronously with the sweep using a National Instruments NI6132 data acquisition card.

Rectangular targets of approximately 25-30mm thickness were made of candle wax, which closely resembles the dielectric properties of some plastic explosives and could be evaluated alone, mounted on a water barrel target or strapped to the torso of a human target. The typical results are shown in Fig. 2 and 3. The sinusoidal variation in the frequency scan due to the wax slab is also clearly seen when backed by a water barrel or human body. Clear signals are also seen in the Fourier transformed data corresponding to an optical depth around 40mm for the wax targets.

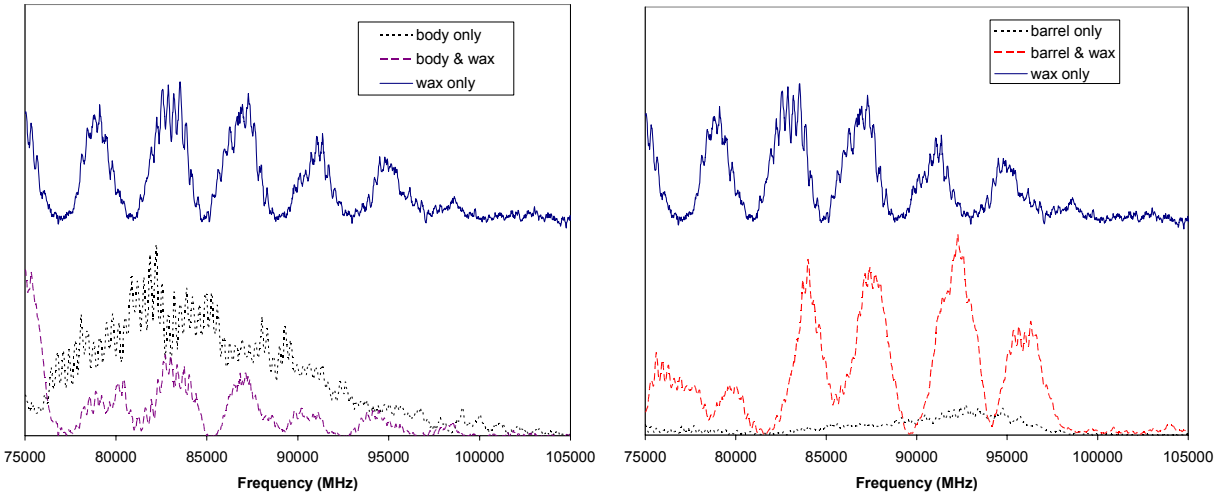

Fig. 2. Measured frequency spectrum of signals from a wax block attached to (a) human body and (b) a water barrel. For clarity, the "wax alone" signal has been displaced vertically in this and the following figures.

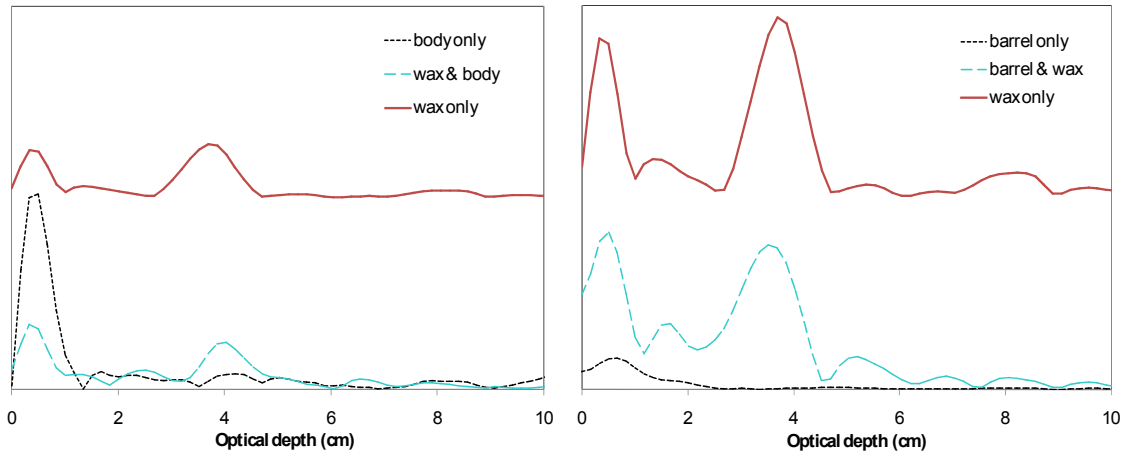

Fig. 3. Fourier transformed signals as for Fig. 2 with a wax block attached to (a) human body and (b) a water barrel.

4.2 VNA

An Agilent E8363B/N4420B VNA is used to provide both the source and detection facilities for a sweep range of 14 to 40 GHz. This instrument includes a swept source and calibrated super-het detection system. The output power of 2mW is several orders of magnitude below the recommended safe exposure limits [13] at the target range. The measurement ports are connected directly to K-band square horns by low loss coaxial cables. The transmitted polarization is horizontal and the receiver horns can be aligned either horizontal (Co-pol) or vertical (X-pol). In this instance only Co-pol measurements are used. The transmitter horn also utilizes a 100mm diameter lens to deliver a loosely focused beam to the target area.

The return signal is measured at typically 801 points across the swept frequency range in 200ms and downloaded to the PC. The number of points required is determined by the need to provide an unambiguous range determination up to the maximum distance of the target. The VNA also provides a real time display of the calculated equivalent time domain signal by an internal chirp transform algorithm.

Fig. 4 shows some measured VNA responses for the same wax target, alone and backed by a plastic barrel filled with water or a human body torso. Time resolved reflections are seen from the front and back surfaces of the wax slab, the later being in contact with the front surface of the backing object. The clearly resolved peaks are separated as expected, by the characteristic optical depth of the dielectric, around 40mm. This suggests that time domain signals can provide a promising method of identifying the presence of explosives.

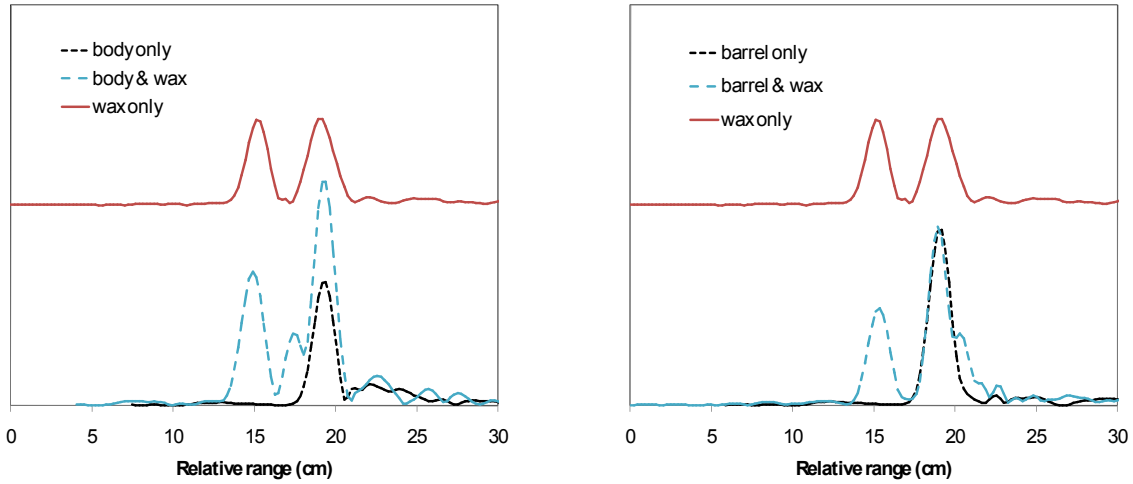

Fig. 4. Time domain signals measured with a VNA of a wax slab attached (a) body and (b) a water barrel showing the reflections from the front and back surfaces of the dielectric.

However under practical conditions the visibility of the early pulse is reduced and in addition the backing signal from the body is more complex. Fig. 5 shows a compilation of superposed traces obtained with 200 successive sweeps obtained from a human body target with and without a wax block attached to the body. When a human target backing is used, the wax slab and body typically rotate together in the beam through ±10º. It will be seen that even with quite modest variations in body position, the measured response considerably changes.

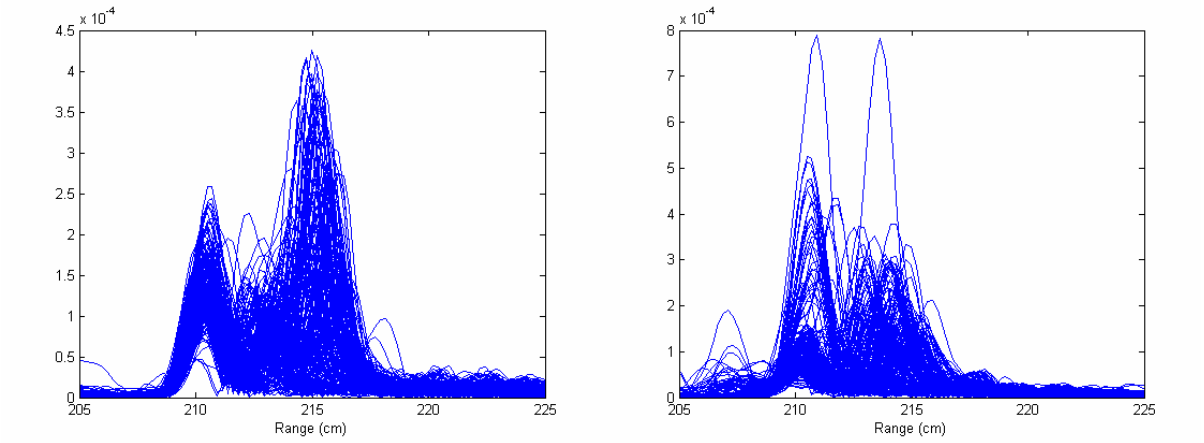

Fig. 5. Superposed time domain signals from 200 successive measurements of (a) body alone and (b) with a wax block strapped to the torso.

Since the range of the target is continually changing, a method for aligning the signals in time is required. The displayed traces in Fig. 5 have been aligned with respect to the time at which the signal first reaches a fixed fraction *f* of its maximum height. The choice of *f* depends on the type of signal expected, but should be selected to trigger off the leading edge of body response, but not off the earlier dielectric response. A value of 25% has been used here.

From inspection of Fig. 5, it is apparent that most of the wax signals show a small increasing signal just before the main body signal due to the reflections from the wax slab, which is not present when the body alone is present. To reliably detect the presence of this signal requires more sophisticated data analysis and this is discussed in the next section.

5. DATA ANALYSIS

To be able to use this technique to detect explosives with good efficiency requires a data analysis system, which can select the characteristic "explosives" signature, but ignore the variability in signal from the "body" part of the target. One method of processing, which is able to do this without prior knowledge of this signature, is an artificial neural network (ANN). Basically it is a non-linear filter to which the measured signals are supplied as inputs. The outputs of the network are the probabilities that a threat is present or not present. To set up the network a training set of measured signals is provided containing examples of both threat and non-threat scenarios and the network is optimized such that it gives the correct outputs for these examples. A similar trial set of measured signals is then presented to the network and the success of the network estimated from the number of correctly assigned outputs with a probability of above 50%. Details of the neural network approach used here, is discussed in more depth in [14].

It is important to process the data before putting it into the network to make best use of its input range and to reduce unnecessary variability of the data, which is not contributing to the desired result. In this case the data is Fourier transformed as shown above and in the case of the VNA results also aligned in time. Scaling of the data is also important, either globally or individually on each scan so that only the shape is used.

Table 1 shows the results from a typical training session with the two VNA data sets shown in Fig. 5. Each data set contains 200 independent signals and those used for training are marked by an asterisk. It is apparent that good discrimination is found when the other data sets are tested.

Table 1. ANN scores for VNA data files tested on a trained network. A full signal range of 65cm or a selected portion can be used for training and testing. Note, since the network outputs must either be "threat" or "no threat", the scores add up to 200, which is the total number of scans.

Data set	205-270 cm		205-225 cm only		205-215 cm only	
	threat	no threat	threat	no threat	threat	no threat
Body only 1	40	160	23	177	11	189
Body only 2	49	151	38	162	10	190
Body only 3*	0	200	0	200	7	193
Body with wax 1	154	46	140	60	113	87
Body with wax 2	162	38	156	44	193	7
Body with wax 3*	200	0	200	0	182	18

In Table 1, the effect is also shown of truncating the signals used for training and testing. This effectively cuts out more of the later signals from the human target and concentrates on the early response from the dielectric. It is apparent that this process on the whole improves the performance.

As another example, a multiple set of examples similar to those in Fig. 2 were taken using direct detection in the 75-110GHz. Either the direct frequency domain or the Fourier transformed version as shown in Fig. 3 can be used as input. Better discrimination is achieved using the transformed version. In this case, only 40 samples were used and the measurements were done at different target ranges. Each range was trained separately.

Table 2. ANN scores for direct detection 75-110GHz data files tested on a trained network. Note, since the outputs must either be "threat" or "no threat", the scores add up to 40 the total number of scans.

Data set	Range (m)	Optical depth spectrum		Frequency spectrum	
		threat	no threat	threat	no threat
Body only 1*	2	0	40	0	40
Body only 2		13	27	13	27
Body only 3		14	26	9	31
Body with wax 1*		40	0	40	0
Body with wax 2		27	13	33	7
Body with wax 3		27	13	25	15
Body only 1*	3	0	40	0	40
Body only 2		14	26	11	29
Body only 3		9	31	9	31
Body with wax 1*		40	0	40	0
Body with wax 2		18	22	33	7
Body with wax 3		40	0	36	4
Body only 1*	5	0	40	0	40
Body only 2		11	29	10	30
Body only 3		13	27	9	31
Body with wax 1*		40	0	39	1
Body with wax 2		18	22	24	16
Body with wax 3		18	22	23	17

The results are less successful than for the VNA measurements, but some discrimination is seen at least up to 3m range. It might be noted that some though reduced discrimination is still seen using the original frequency spectra rather than the Fourier transformed or depth spectra. This is probably due to an overall increase in reflected power from the dielectric surface.

Though discrimination scores are not approaching 100%, the confidence may be greatly improved by combining the results from repeated measurements. It should be emphasized that though these examples were taken at a repetition rate of 2-5 per second, which was limited by the data acquisition software used. Acquisition rates of 20-100 per second are readily achievable without significant loss of signal to noise. This would enable multiple signals to be analyzed and the results polled within a response time of less than a second.

6. CONCLUSIONS

A technique is presented here which enables dielectric material, such as explosives worn on the body to be identified at standoff distances. The results presented here show that a technique based on the interference of reflected millimetre waves from the front and back faces of a dielectric block, can be used to detect its presence remotely by using a wideband swept source. This method may be implemented using a direct detection of the target signal and Fourier transformation of its frequency spectrum and can be achieved at frequencies over 75GHz where microwave optics may be used to produce a small spot size, thus simplifying the response from human targets. An alternative approach in which the phase of the return signal is also measured, allows the range distribution to be calculated, analysis of which also shows up the presence the dielectric layer. An analysis procedure using ANN shows good results in identifying the presence of dielectric material worn on the body.

REFERENCES

[1] Bowring, N. J., Baker, J. G., Rezgui, N. D. and Alder, J. F. , "A sensor for the detection and measurement of thin dielectric layers using reflection of frequency scanned millimetric waves", Meas. Sci. Technol. 19, 024004 (2008).

[2] Bowring, N. J., Baker, J. G., Rezgui, N. D., Southgate, M. and Alder, J. F. , "Active millimeter wave detection of concealed layers of dielectric material," Proc. SPIE 6540, 65401M (2008).

[3] Appleby, R., Anderton, R. N., Price, S., Salmon, N. A., Sinclair, G. N., Coward, P. R., Barnes, A. R., Munday, P. D., Moore, M., Lettington, A. H. and Robertson, D. A. , "Mechanically scanned real time passive millimeter wave imaging at 94GHz," Proc. SPIE 5077, 1-6 (2003).

[4] Appleby, R. , "Passive millimeter-wave imaging and how it differs from terahertz imaging," Phil. Trans. R. Soc. Lond. A 362, 379-394 (2004).

[5] Sheen, D. M., McMakin, D. L., Collins, H. D., Hall, T. E. and Severtsen, R. H. , "Concealed explosive detection on personnel using a wideband holographic millimeter-wave imaging system," Proc. SPIE 2755, 503-513 (1996).

[6] Martin, C. A., Lovberg, J. A., Dean, W. H. and Ibrahim, E., "High resolution passive millimeter-wave security screening using few amplifiers," Proc. SPIE 6548, 654806 (2007).

[7] Sheen, D. M., McMakin, D. L. and Hall, T. E. , "Cylindrical millimeter-wave imaging technique and applications," Proc. SPIE 6211, 62110A (2006).

[8] Corredoura, P., Baharav, Z., Taber, B. and Lee, G., "Miillimeter-wave imaging system for personnel screening: scanning 10^7 points a second and using no moving parts," Proc. SPIE 6211, 62110B (2006).

[9] Sinyukov, A., Zorych, I., Michalopoulou, Z-H., Gary, D., Barat, R. and Federici, J. F., "Detection of explosives by terahertz synthetic aperture imaging – focusing and spectral classification," C. R. Physique 9, 248-261 (2008).

[10] Kemp, M. C., Taday, P. F., Cole, B. E., Cluff, J. E., Fitzgerald, A. J. and Tribe, W. R. , "Security applications of terahertz technology," Proc. SPIE 5070, 44-52 (2003).

[11] Dobroiu, A., Otani, C. and Kawase, K. , "Terahertz-wave sources and imaging applications", Meas. Sci. Technol. 17, R161-R174 (2006).

[12] Dickinson, J. C., Goyette, T. M., Gatesman, A. J., Joseph, C. S., Root, Z. G., Giles, R. H., Waldman, J. and Nixon, W. E. , "Terahertz imaging of subjects with concealed weapons, " Proc. SPIE 6212, 62120Q (2006).

[13] International Commission on Non-Ionizing Radiation Protection, "Guidelines for limiting exposure to time-varying electric, magnetic, and electromagnetic fields (up to 300 GHz)," Health Physics 74, 494-522 (1998).

[14] Bowring, N. J., Andrews, D. A., Rezgui, N. D., Southgate, M., Smith, S. E., Harmer, S. W. and Atiah, A. , "A multifaceted active swept millimeter-wave approach to the standoff detection on concealed weapons," Proc. SPIE 7117, 711706 (2008).

12.2 SPIE paper 2009 (Andrews et al., 2009)

A swept millimeter-wave technique for the detection of concealed weapons and thin layers of dielectric material with and without fragmentation.

David A. Andrews, Sarah Smith, Nacer Rezgui, Nicholas Bowring*, Matthew Southgate, Stuart Harmer.
Dept. of Engineering, Manchester Metropolitan University, Chester St., Manchester M1 5GD, UK.

ABSTRACT

Active millimetre wave systems, operating at frequencies up to 110 GHz have been used to detect the presence of both concealed dielectric and metallic objects at standoff distances. Co- and cross-polarized superheterodyne or direct detectors are used to differentiate between metallic and purely dielectric objects. The technique determines the thickness of a dielectric target and detects the presence of concealed handguns or fragmentation by utilising the pattern of the responses from both the co- and cross-polarized detectors. The returned signals are processed and analysed by an artificial neural network, which classifies the responses according to their correspondence to previous training data.

1. INTRODUCTION

The threats faced by authorities round the world include the effective detection of many types of concealed weapons, ranging from handguns through to devices worn by suicide bombers. An effective method of detecting these types of threats in a deployable manner is the subject of this paper and in particular the need for a portable non-imaging system is required, for example for use in random checks in an urban environment.

The threat from terrorists has changed recently. A potential terrorist could be carrying, for example, concealed guns on the body or in a bag, or a suicide vest with or without fragmentation. In this paper, we investigate a general solution to these threats.

The use of passive imaging technology in the mm-wave or sub-THz wavebands where the thermal emission of the body or illumination by the cold sky is used to form images [1] is the subject of much current research. These techniques are becoming more effective and are being adopted in many indoor environments, particularly airports, and some outdoor applications where portability is less of an issue. The use of imaging is less effective outdoors due to the illumination effects described in [1].

Where guns or knives are concerned, one approach that seems to offer long term promise in terms of a generally aspect independent technique, where the position of the gun is less important, is based on extracting the Late Time Response (LTR) of these reasonably large objects in response to a short or chirped pulse. This technique is well described in the literature [2,3,4]. However the approach of collecting and analysing the transient response of the target presents problems when that target has a small conducting surface from which surface currents can radiate and the illuminating pulse power is limited, as shown by the work of Novak and Gashinova[5,6], who use Vector Network Analysers in Time Domain Reflectometry mode in an attempt to determine the pulsed response of handguns in the band 26-40 GHz using, particularly, the LTR. The effectiveness of any target identification system is based on the aspect invariance of the information gathered and the ability to then determine the presence or not of a target item. This aspect independence is only present in the late time transients in the form of exponentially decaying sinusoidal EM fields in the time domain radiated from the objects surface, although the amplitude of these late time responses are extremely small. The parameters extracted are the complex resonant frequencies that make up these decaying oscillations, these have the desired aspect invariance. These effects however are strongest when the wavelength of the illuminating radiation

Passive Millimeter-Wave Imaging Technology XII, edited by Roger Appleby, David A. Wikner, Proc. of SPIE
Vol. 7309, 73090H · © 2009 SPIE · CCC code: 0277-786X/09/$18 · doi: 10.1117/12.818875

approaches the size of the object [7] making its potential for deployable systems limited by the physical size of the antennas required, although this does not preclude its deployment in fixed situations.

In this paper we present techniques based on UWB radar and Early Time Responses (ETR), which detect the presence of concealed guns or explosive materials at standoff distances. For explosives we have made improvements on a previously presented method [8,9] based on multiple reflections from the front and back surfaces of the dielectric material. For guns and fragmentation devices the polarisation rotation of the return signal is utilised to distinguish metal objects from the background signal reflected from the human body.

We have used a neural network to learn typical range dependent responses from the weapons after some degree of pre-processing and alignment of the returned signals and the neural network is trained on representative sets of data from backgrounds, i.e. the body alone, and the body plus the gun in various orientations. Some techniques to optimise the performance of these networks are described.

2. DETECTION OF THIN DIELECTRIC LAYERS WITHOUT FRAGMENTATION

The technique outlined here relies on the use of a wide band swept millimetre waves, in conjunction with a co-polarised superheterodyne detector. Consider as in Fig. 1, a plane wave $\exp\{-2\pi f(t-z/c)\}$ with amplitude E_T and frequency f incident in the z direction on a parallel slab of dielectric material of thickness d, refractive index n and distance L from the transmitter. The return wave E_R consists of reflections R and R' from the front and back faces of the dielectric slab. If the backing material can be approximated as a semi-infinite layer of refractive index n' and multiple reflections are neglected, then

$$E_R = E_T \{R + R' \exp(4j\pi fnd/c)\} \exp(4j\pi fL/c) \tag{1}$$

where $R = \frac{(n-1)}{(n+1)}$, $R' = \frac{(n'-n)}{(n'+n)}$ and c is the velocity of light. The relative phase shift between the reflections from the front and back faces gives rise to frequency-dependent interference between the two signals. If the return signal is measured by a square law detector, such as a diode, then the return signal can written as:

$$|E_R|^2 = |E_T|^2 \{|R|^2 + |R'|^2 + 2|R||R'|\cos(4\pi fnd/c)\} \tag{2}$$

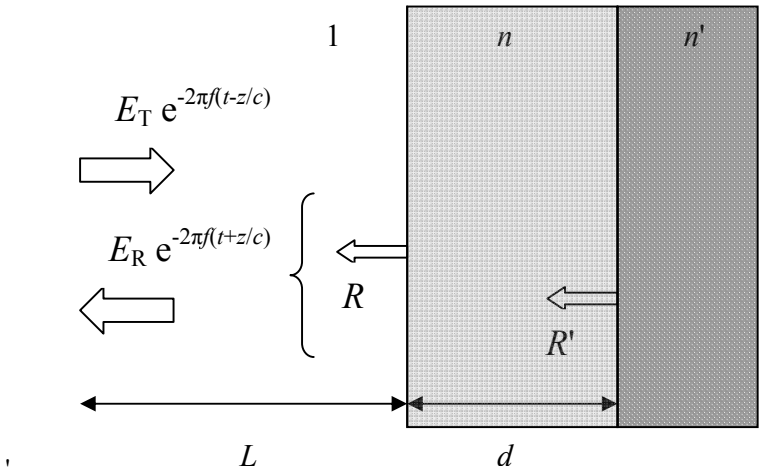

Fig. 1. Incident plane waves from the left reflect off the front and back faces of the dielectric block of thickness d and refractive index n backed by material of refractive index n' and combine at a detector situated near the source.

This shows explicitly the sinusoidal dependence on frequency. The period of the oscillation is proportional to the optical depth of the material *nd*. By Fourier transformation of the recorded signal the position of the peaks gives the optical depth of the sample [8,9]. For the application of explosives detection, a significant peak within a band of optical depth 10-50 mm may be used as an indicator of the presence of a suspicious object. The signal processing steps described in this section below make use of the relative invariance in the depth of this layer to identify suicide type devices.

It may also be noted that equation (1) implicitly contains the range L of the object. By measuring the phase of the return signal by using a super-heterodyne or homodyne receiver, both the range and the thickness of the dielectric layer may be determined, which enables background objects present at a different range to be rejected.

The minimum optical depth which may be measured by this technique, depends on the frequency range Δf swept over by the microwave source as $c/\Delta f$. So wideband sources and detection systems are required with a typical sweep of ~20 GHz. However the absolute frequency is not determined by this requirement, so for example 20-40 GHz and 80-100 GHz would be equally suitable from this respect.

A major consideration, when using this technique with a human body as backing, is the complex return signal found from reflections from different parts of the torso. Signals from the arms appear with a different time delay than those from the chest and lead to interference effects very similar to the explosives signature. It should be emphasized that this is not an imaging technique, so the signal on the detector is a sum from all the targets within the field of view of the receiver. To address this problem two approaches have been successfully tried and are described here.

2.1 Spatial selection

An approach is to restrict the angular aperture of the detector so that it only receives signals from one part of the body at a time. By increasing the frequency and using quasi-optical techniques it is feasible to achieve a small enough spot size at stand-off distances. However, it is important to provide ways to ensure alignment of the mm-wave beam on the correct part of the target. The precise methods of target tracking such as sensor fusion, are well known and therefore outside the scope of this work.

2.2 Range selection

By utilizing the range information, from a super-heterodyne type receiver or a vector network analyzer (VNA), it is possible to differentiate between signals from different parts of the body. In particular, the earliest response is often from the torso at the position of a "suicide vest". Noting that taking the complex inverse Fourier transform (iFFT) of equation (1) leads to peaks separated in time by 2*nd/c*.

$$\overline{E}_R(t) = E_T\{Rf(t-2L/c) + R'f(t-2L/c-2nd/c)\} \tag{3}$$

It is the aim of the technique outlined below to optimally align the time resolved signals with respect to the leading edge of the body response, such that the presence of a small additional response proportional to R ahead of the main reflection R' gives an indication of the presence of the dielectric layer.

For the data presented in this section, 200 wide band sweeps in the range 14 to 40 GHz were acquired from the *co-polarised* detector, while the target was actively illuminated at the same swept wavelength. This is to build up a representative data sample of a target moving around in the beam. The complex data set was transformed into the time domain using the Inverse Fourier Transform (IFFT), producing a plot of amplitude against optical depth against sweeps. The data is then range gated to eliminate responses other than those from the target. Small variations in the data are reduced using a 3 by 3 averaging filter applied to the two dimensional data set.

A crucial step in the data analysis is then to re-order according to optical depth, with the aims of grouping together similar responses and hence removing the time dependent behaviour of the target, which tends to be chaotic. The data is reordered by maximum cross-correlation coefficient, both to move similar data sets together, and to align the time

dependent responses according to maximum similarity. Since the predominant return is from the body, this has the practical effect of aligning the responses with respect to the front surface of the torso, in a manner derived from that presented in [9]. The data is then sorted by amplitude in the direction of the sweeps.

Figure 2 shows the results of these signal processing steps on two data sets, the first of the body alone and the second from the body wearing a concealed suicide vest. Figure 2 (left) shows the unprocessed optical depth response, over 200 sweeps, of a person moving around in a beam. Figure 2 (right) shows the result of applying the smoothing, correlation and sorting steps outlined above. It is evident from figure 2 that there is no dielectric layer, whereas on figure 3, the response from the front of the dielectric layer, of approximately 2 cm in depth, strapped to the torso can be clearly seen before and after processing.

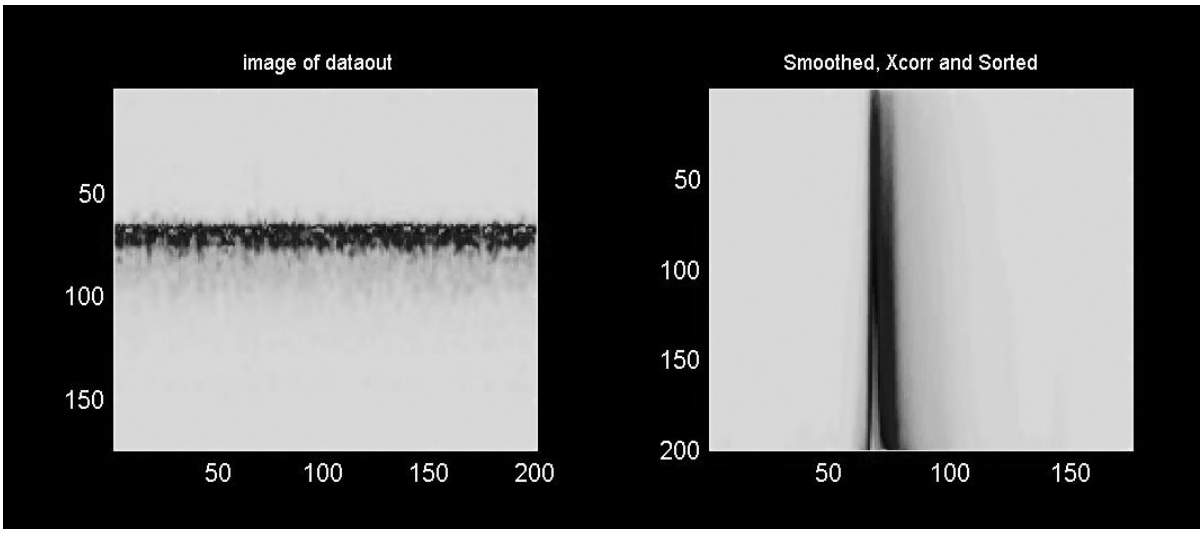

Fig.2. A 2D representation of the time domain signals from 200 successive measurements of the body alone, pre and post processing with cross-correlation and subsequent sorting.

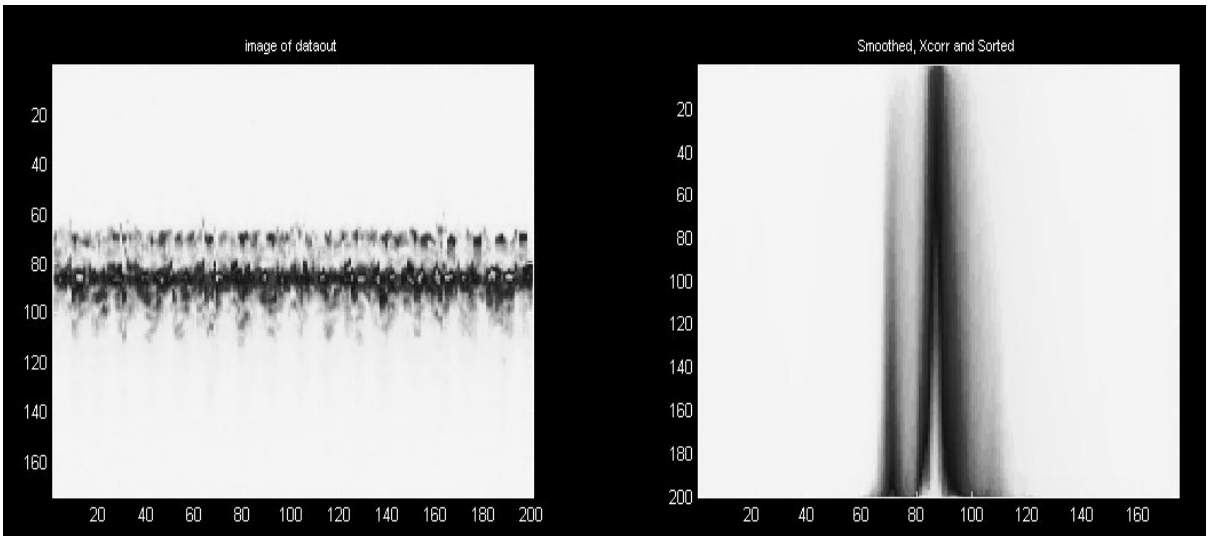

Figure 3. A 2D representation of the time domain signals from 200 successive measurements of a body with a wax block strapped to the torso, pre and post processing. The addition reflection caused by a layer of dielectric can clearly be seen.

The data is normalised to 256 data points to present the subsequent Gaussian fitting routine with consistent inputs. This is repeated for four data sets, alternating threat and non-threat. The mean is calculated across a proportion of the sweeps (e.g. the strongest 25%). The final two steps involve:

Step 1 – Fitting the average of the strongest responses with up to four Gaussian peaks. Four peaks have been chosen as this empirically gives a reasonable fit to the responses. The amplitude, position, and width are determined using a non-linear optimisation process to find the lowest chi-squared value.

Step 2. The 12 parameters extracted from the fitting process are sorted according to amplitude. A back propagation neural network classifier is then trained on typical responses from targets with and without concealed dielectric layers.

Figure 4 below shows typical responses from an averaged, correlated and sorted data set. The left hand figure is that of a body alone, whereas the right hand figure demonstrates the response from a dielectric layer set in front of the body.

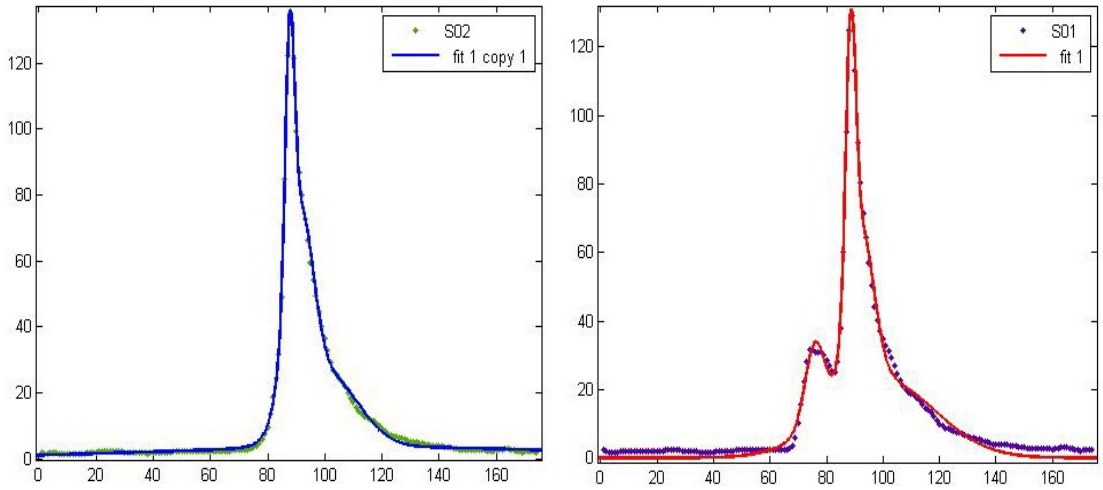

Fig. 4. Averaged responses from a body alone (left) and a body with a concealed dielectric layer (right). The result of fitting four Gaussian peaks is presented using the solid line.

The results presented in the following table are representative outputs from the neural network. A pre-trained network is presented with eight sets of 'threat' data and eight sets of eight sets of 'non-threat' data. A standard back propagation network with 24 inputs, XYY hidden nodes and a single linear output node was used. Non-linear tansig neurons were used for the hidden and input nodes, whereas a linear output neuron was used in order to give an indication of the closeness of the match with a previous training profile. An output of 1 indicates a probable threat. A suicide type vest consisting of 2 cm thick dielectric slabs of irregular shape was used for the trial.

Table 1. The results of a trial of twenty data acquisition runs from a human target alone, or the same target wearing a concealed vest containing 2 cm thick slabs of dielectric.

Data	**Result**	**Correct?**
Wax + body 1	0.8629	Y
Body 1	0.6324	N
Wax + body 2	0.6900	Y
Body 2	0.1114	Y

Wax + body 3	0.8649	Y
Body 3	0.1081	Y
Wax + body 4	0.8664	Y
Body 4	0.1186	Y
Wax + body 5	0.8910	Y
Body 5	0.2163	Y
Wax + body 8	0.9450	Y
Body 8	0.1055	Y
Wax + body 9	0.9153	Y
Body 9	0.1064	Y
Wax + body 10	0.8334	Y
Body 10	0.1058	Y

3. DETECTION OF GUNS AND FRAGMENTATION DEVICES

The experimental system is as used previously [9,10], consisting of an Agilent E8363B/N4420B VNA with horn transmitter and detector, but with an additional receiver horn orientated cross-polar to the transmitter. Numerical simulations and practical measurements show that the received signal from complex metal objects such as guns exhibits a much greater cross-polar component than from smooth reflectors such as the human body [10].

Figure 5 shows a representative set of signals obtained with a human body target carrying a gun, wearing a wax block and neither. The signals as a function of range have been aligned to the channel where the co-polar signal first reaches 50% of the maximum signal, i.e. at the surface of the body. Only the 30 channels in front of the body are retained and in the case of the cross-polar also the 20 after, giving a total of 80 channels for input to the network. Inspection of Figure 5 shows that a stronger signal (darker colour) is obtained in the cross-polar when the weapon is present. A strong signal is also obtained in the co-polar when the wax is in front of the body surface.

Unlike the analysis in the previous section each sample is fed directly to the network without averaging and a decision is made on each one. The network has three mutually exclusive outputs, corresponding to “no threat”, “explosives threat” or “gun threat”. The network has one hidden layer of m nodes and is optimised by back-correction. In Table 2 the results of training sets of 150 samples are given. The scores are given for a network trained on the first two sets of data. In this case only examples with a gun threat are used. This is extended in Table 3 where examples including an “explosives threat” (wax block) are also included. In both cases reasonable distinction between the threat types is achieved, however to try to improve this performance various modifications to the network were investigated.

For this example, 1100 training samples were used and the network tested on a similar 1156 samples. The Error Rate is defined as the fraction of samples wrongly categorised by the trained network. Normally the networks are trained for sufficient number of epochs such that the error rate no longer decreases (typically 100).

Table 2 Results of network training on sets of 150 samples taken from the data set to distinguish between gun threat and no threat (*indicates training sets) and the effect of applying a 90% “confidence” filter or “context” input.

	All results		90% confidence filter		Using 3 sample “context” input	
	Gun	No threat	Gun	No threat	Gun	No threat

Body 1 *	5	145	5	144	0	150
Body & gun 1 *	148	2	144	2	150	0
Body 2	39	111	33	109	30	120
Body & gun 2	112	38	107	38	140	10
Body 3	47	103	45	100	37	112
Body & gun 3	122	28	121	26	139	11
Body 4	40	110	38	108	12	138
Body & gun 4	126	24	124	18	143	7

Table 3 Results for training to identify gun and explosive threats simultaneously and the effect of "context" by inputting 3 samples simultaneously.

	Each sample input separately			Using 3 sample "context" input		
	Gun	No threat	Explosives	Gun	No threat	Explosives
Body 1 *	2	148	0	0	150	0
Body & gun 1 *	145	3	2	150	0	0
Body & Expl. 1 *	6	2	142	0	0	150
Body 2	55	78	17	55	88	7
Body & gun 2	121	18	11	135	5	10
Body & Expl. 2	26	38	86	20	22	108
Body 3	55	76	19	74	69	7
Body & gun 3	122	24	4	123	19	8
Body & Expl. 3	38	27	85	33	13	104
Body 4	16	94	40	30	88	32
Body & gun 4	122	21	7	135	10	15
Body & Expl. 4	31	20	99	6	15	129

In Figure 6 the error rate is shown as a function of nodes *m* on the hidden layer. Increasing the number nodes improves the ability of the network to reproduce the training set and the error rate falls. However when the network is tested on a new unseen set of data, the error rate is almost independent of m for values above 3. This indicates that the network is responding to only a small number of features within the data.

Grouping the data input into a fewer number of separate channels (i.e. binning the data) has some advantage in optimising network performance. The effect of reducing to 10 channels by grouping and averaging 8 adjacent channels is also shown on the left of Figure 6. Note that though the ability of the network to reproduce the training set is less effective, the performance on the unseen set is significantly improved. This suggests that filtering the data input decreases the complexity of the network and improves its performance if only a few features are required to make a decision.

Another option is to input information as to the change of samples in time or sample "context". Instead of inputting the samples singly, a composite sample consisting three successive samples is presented in one go. The error rate is now calculated for the composite samples. The results shown on the right in Figure 6 show a marked improvement on the test samples (see also Tables 2 and 3). However, if instead of composite samples, the average of three successive samples is used, then very similar results are also obtained. This suggests that the major effect is the reduction of variability in the sample set by averaging. Even though the system noise of the detection system is not significant, the variable reflections from the target are behaving as random noise and can be reduced by averaging whilst preserving some of the features relevant to making the threat decision.

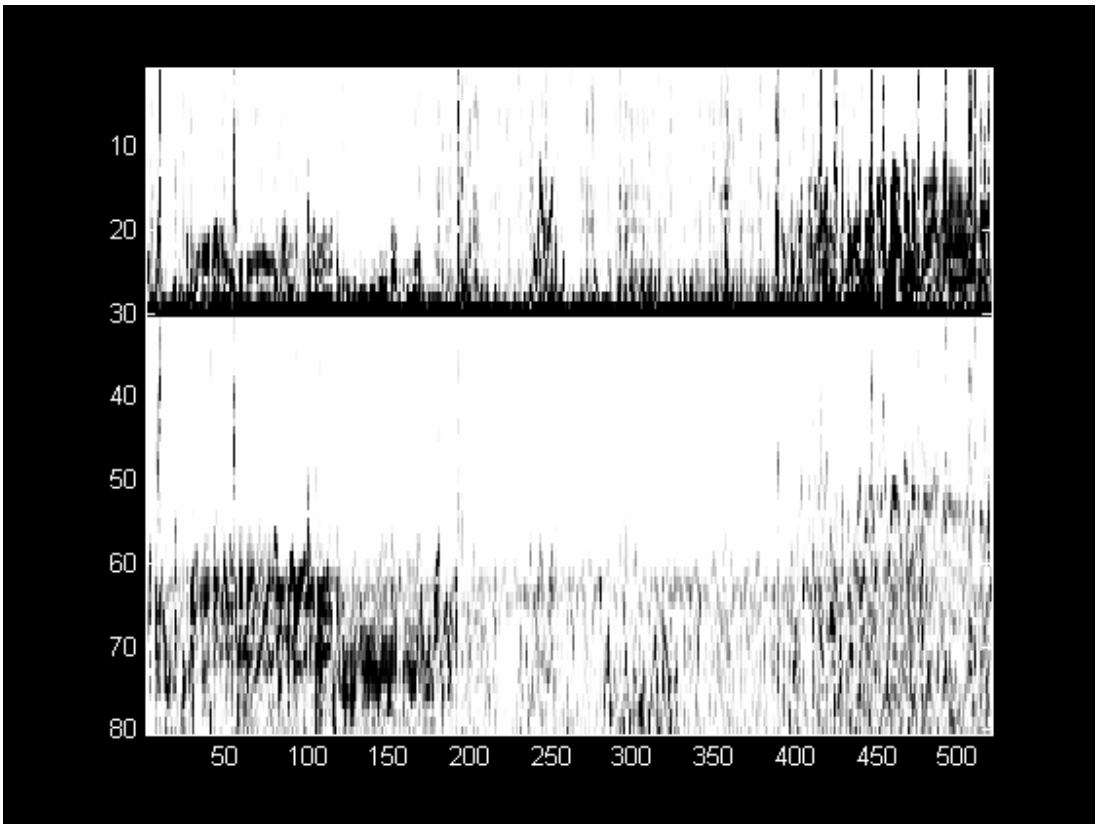

Fig. 5. Greyscale representation of 520 return signals from a human target at 2m range; signals 1-110 are carrying a gun and 400-520 wearing a 20mm layer of explosive stimulant (wax). Range channels 1-30 are from the Co-polar horn and 31-80 from the Cross-polar horn.

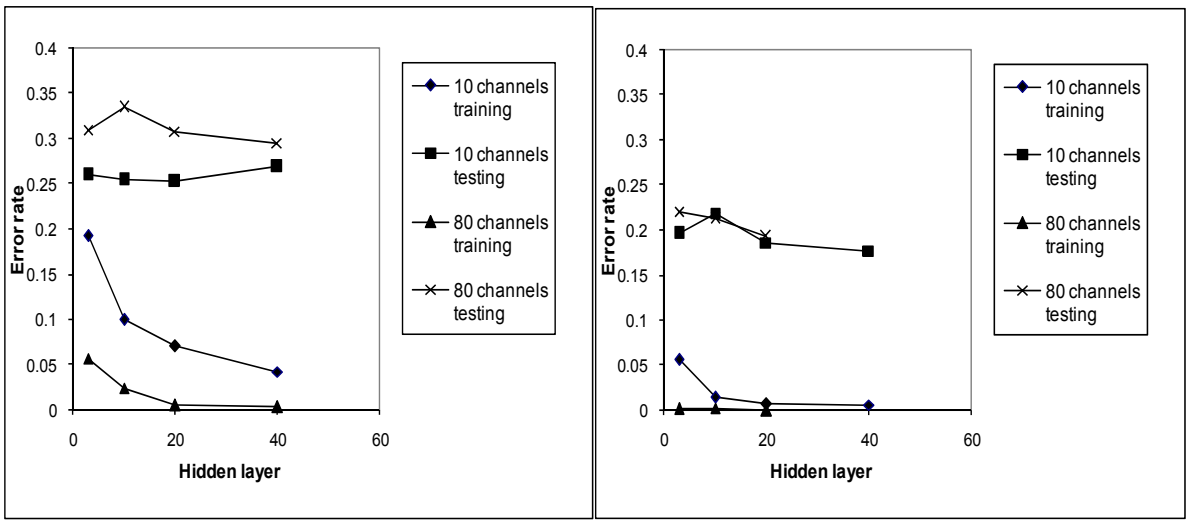

Fig. 6. The error rate is shown as a function of number of hidden layer nodes m for training and testing data segments treated as 10 or 80 channel input. On the right is the behaviour when three samples are added at the same time showing the effect of "context" or averaging.

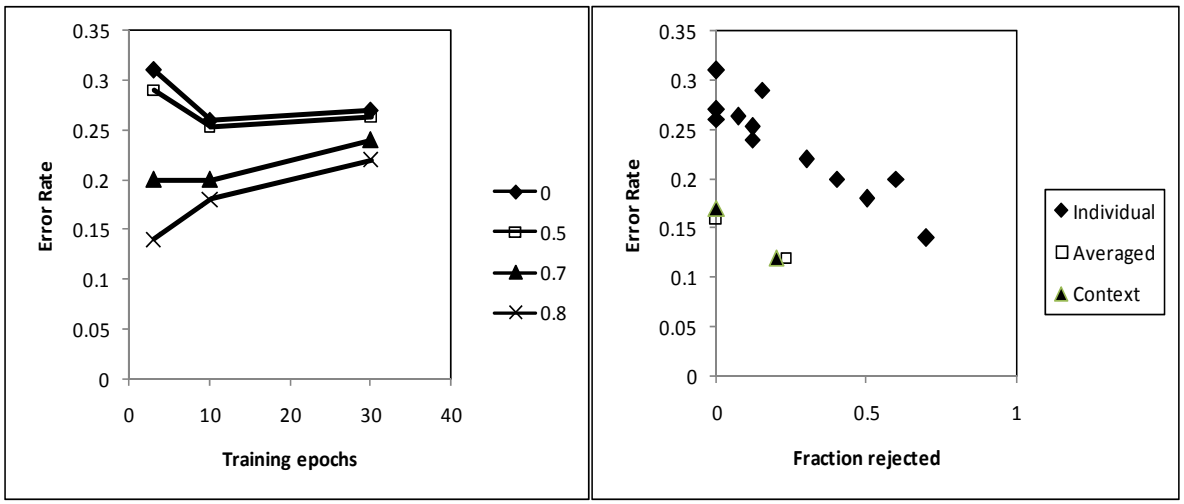

Fig. 7. Reduction of error rate when network outputs with a confidence less than the value shown are rejected. On the left the variation in error rate with training epochs is shown for different confidence levels and on the right as a function of the fraction rejected. Results are presented for single presentation of samples, composite samples for "context" and averages of three successive samples.

A number of other network features have been also been explored including different neurons ("tansig" or "logsig") and training conditions, but another technique which has proved useful, is to estimate the confidence in the network decision. The analogue output of the network is between 0 and 1 and gives an indication of the "confidence" of the network in the decision made. If only decisions with a confidence greater than a certain threshold level are retained then a reduction in error rate is achievable, but at the expense of throughput. This is illustrated in Figure 7. It might be noted that this improvement is most noticeable when the network is lightly trained, i.e. fewer training epochs. More extensive training tends to lead to a distribution of outputs more polarised towards the extreme values of 0 and 1.

In summary, we have shown that the performance of a simple neural network can be improved by a combination of data selection and output filtering to reduce the error rate n this example from over 30% to under 15%. In practice, multiple decisions from successive samples would be polled and an alarm signalled after the number of threat decisions reaches a threshold level. With modern data acquisition and processing the collection and testing of 100 samples could be completed within a fraction of a second, enabling significant polling of signals before an alarm is passed on to the user.

4. CONCLUSIONS AND FUTURE WORK

The results of a simple laboratory system using UWB radar have demonstrated the ability to detect concealed handguns and explosive materials worn on a human target. The use of a range of signal processing techniques, including cross correlation, non-linear least squares fitting and the subsequent application of artificial neural networks has been shown to be effective at categorising targets in terms of type of threat and various techniques for enhancing performance have been presented.

The results presented were taken using a commercial VNA system working from 14–40 GHz, which limited the standoff range used (2m). This can be significantly increased by going to higher frequencies, for example 75–110GHz, where quasi-optical techniques can be used.

REFERENCES

[1] Appleby, R., "Passive millimeter-wave imaging and how it differs from terahertz imaging," Phil. Trans. R. Soc. Lond. A 362, 379-394 (2004).

[2] Baum, C.E., Rothwell, E.J., Chen, K.-M. and Nyquist, D.P. ,"The singularity expansion method and its application to target identification", Proceedings of the IEEE, 79, 1481-1492 (1991).

[3] Richards, M.A.,"SEM representation of the early and late time fields scattered from wire targets" Antennas and Propagation, IEEE Trans.Ant. Propagation, 42, 564–566 (1994).

[4] Lui, H.-S., and Shuley, N. V. Z., "Radar target identification using a 'banded' E-pulse technique", IEEE Trans. Antennas Propag., 54, 3874-3881(2006).

[5] Novak D., Waterhouse R. and Farnham A., "A Millimeter-wave weapons detection system", Proceedings of the Applied Imagery and Pattern Recognition Workshop, 34, no. 19-21, Oct. 2005

[6] Gashinova, M., Cherniakov, M. and Vasalos A., "UWB signature analysis for detection of body-worn weapons", Radar. CIE '06. International Conference on Radar, Oct. 2006: 1-4 Location: Shanghai, China. (2006).

[7] Harmer S., Bowring N., Andrews D., Atiah A., "Ultra Wide Band Aspect Independent Detection of on Body Concealed Weapons using The Out of Plane Polarised Late Time Response", 5th ESA Workshop on Millimetre Wave Technology and Applications & 31st ESA Antenna Workshop, Noordwijk, May 2009

[8] Bowring, N. J., Baker, J. G., Rezgui, N. D. and Alder, J. F. , "A sensor for the detection and measurement of thin dielectric layers using reflection of frequency scanned millimetric waves", Meas. Sci. Technol. 19, 024004 (2008).

[9] Andrews, D. A., Rezgui, N. D., Smith, S. E., Bowring, N., Southgate, M. and Baker, J. G., "Detection of concealed explosives at stand-off distances using wide band swept millimeter waves", Proc. SPIE, Vol. 7117, 7117-19 (2008)

[10] Bowring, N. J., Andrews, D. A., Rezgui, N. D., Southgate, M., Smith, S. E., Harmer, S. W. and Atiah, A. , "A multifaceted active swept millimeter-wave approach to the standoff detection on concealed weapons," Proc. SPIE 7117, 711706 (2008).

12.3 Research Seminar Presentation

Research Seminar Presentation to Department of Engineering and Technology, MMU, March 2009.

Concealed Weapons Detection

Sarah Smith

Abstract

- Standoff detection of concealed explosives.
- Measure the optical depth of the explosive.
- Data analysis using neural networks.
- Results from simulated explosives.
- Summary

Passive Imaging vs. Active Detection

- There is a requirement for a detection system which will detect explosives on a person out in the street or other open area.
- Passive systems work at close range and suffer from problems with contrast due to the sky temperature.
- Privacy issues with imaging people.

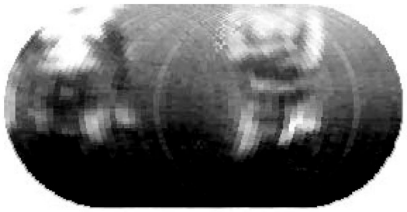

R. Appleby. Passive millimetre-wave imaging and how it differs from terahertz imaging. *Royal Society of London Transactions Series A,, 362(1815):379* 393, 2004.

Concealed Weapons Detection

- Millimetre wavelengths can be used to detect explosives hidden under clothing.
- Data from a Vector Network Analyser (VNA) can be used to train a neural network which will then classify the subject under test as a threat or not a threat.
- A VNA is both a transmitter and receiver of microwave or millimetre wave radiation
- We use paraffin wax as a simulant, as it has similar dielectric properties to explosives.

How do we ‘deliver’ millimetre wave radiation to the target?
Answer: Millimetre wave lenses

- This slide shows a pair of millimetre wave lenses designed to focus a beam at a standoff distance of 10 metres.
- The lenses are 30cm diameter and form a focal spot of 13cm at 10 metres operating at 94GHz.

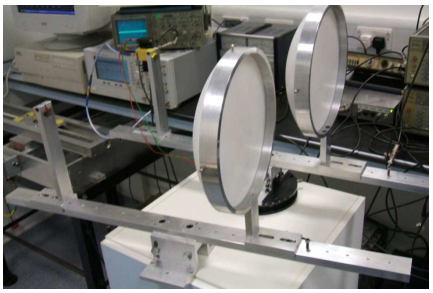

Millimetre wave optics vs. light

- Millimetre waves are approaching the wavelength of light so can be thought of as behaving in a similar way. This Quasi-optical region is described by Gaussian Optics.

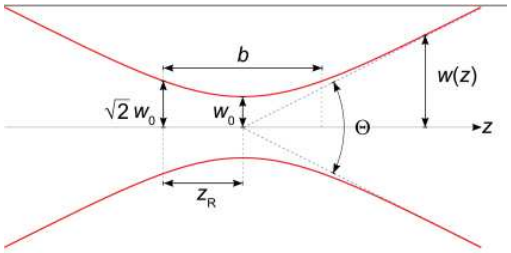

- http://en.wikipedia.org/wiki/Gaussian_beam

COMSOL model of lens

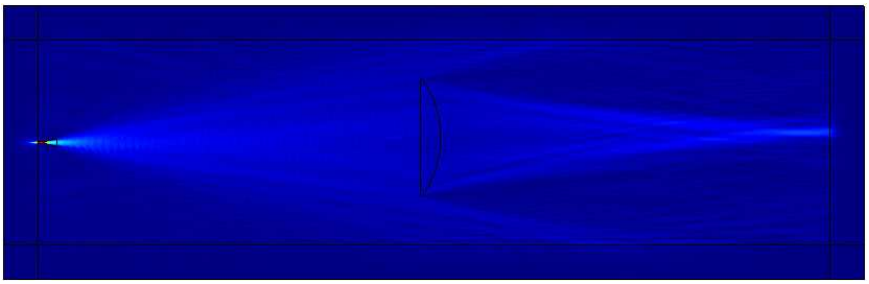

Optical depth

- Optical depth is a property of materials which is their thickness multiplied by their refractive index.
- When wax is held in front of the body, two peaks are obtained from the Fourier transformed reflections. The first one is from the wax and the second from the body.

Data Analysis

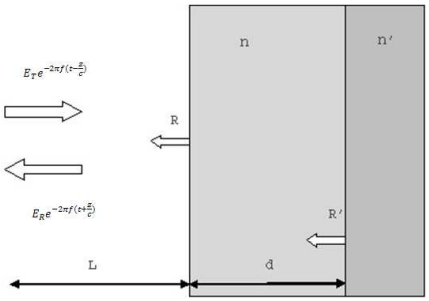

- The reflections have a sinusoidal dependence on frequency, the optical depth of the material, nd is proportional to the period of oscillation.
- This sinusoid is Fourier transformed to show optical depth.

D. A. Andrews, N. D. Rezgui, S. E. Smith, N. Bowring, M. Southgate,
and J. G. Baker. Detection of concealed explosives at stand-off distances using wide band
swept millimetre waves. Volume 7117, page 71170J. SPIE, 2008.

Direct Detection Data

- Fourier transforming the received signal gives the optical depth of the explosives (or other dielectric) under test.
- Optical depth = depth x refractive index material
- FFT peak at optical depth 127mm, refractive index of wax = 1.51*, gives a depth of 84mm. Width of wax block 80mm.

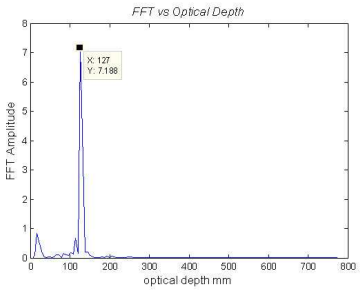

*MISCELLANEOUS DATA ON MATERIALS FOR MILLIMETRE AND SUBMILLIMETRE OPTICS
James W. Lamb

Methods

- Frequency is swept from 14 to 40 GHz.
- The VNA (vector network analyser) is used to transmit a signal which reflects from the front surface of the wax and passes through the wax and reflects from the back surface.

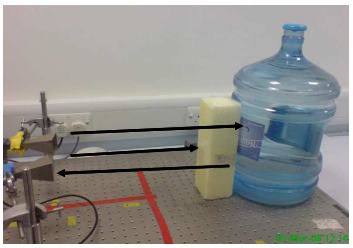

•These reflections add together and are received by the other port of the VNA.

Wax block from VNA data

A dielectric layer shows up as an additional reflection of generally constant position in front of the body.

Reflections from front surface of explosives simulant

Reflections from body/water barrel

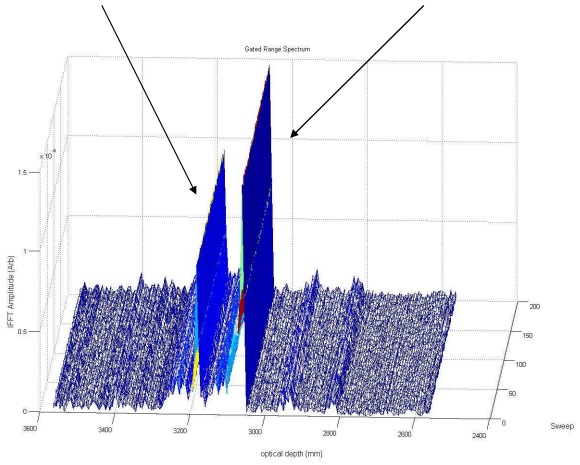

Multiple sweeps

Data from an on-body target

Fourier transformed data vs. Optical depth vs. Sweep number

Explosive layer not apparent in unprocessed data

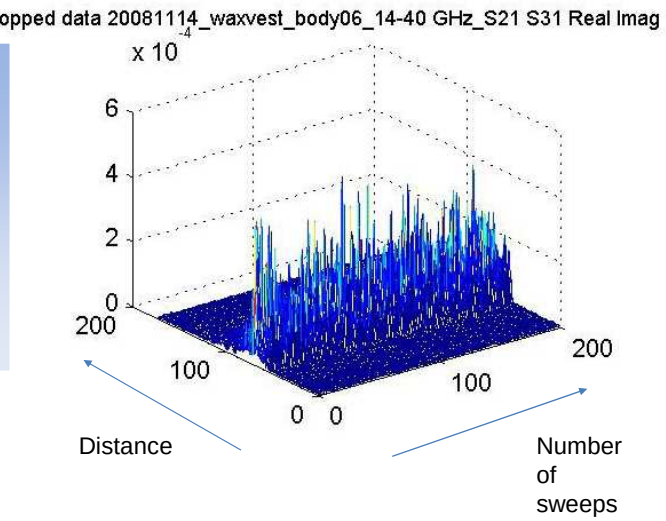

Processing steps

- Align the responses by using the strongest reflections, or by correlation of different data sets
- Smooth irregularities caused by movement and ‘glint’
- Sort according to strength of response

Person wearing concealed dielectric layer

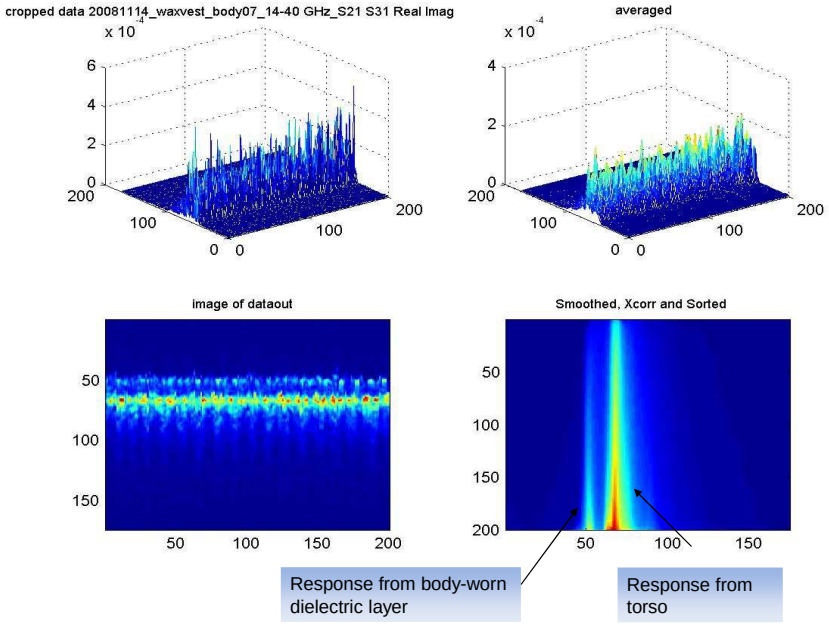

No concealed dielectric layer

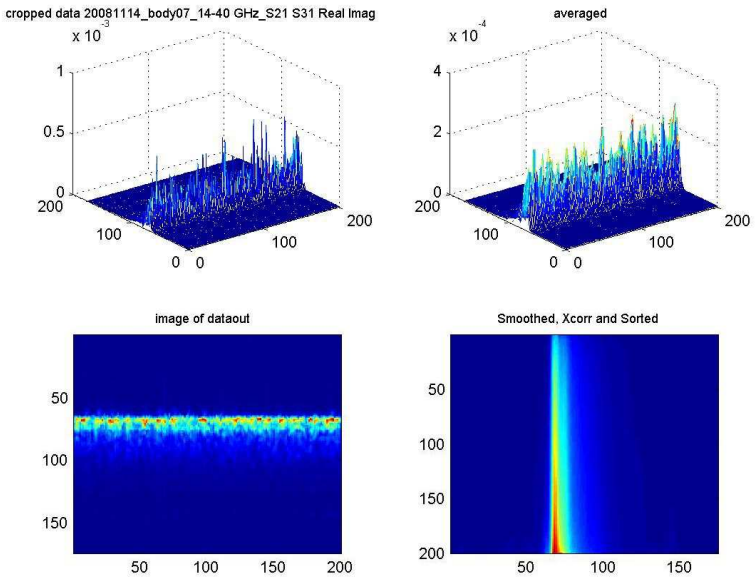

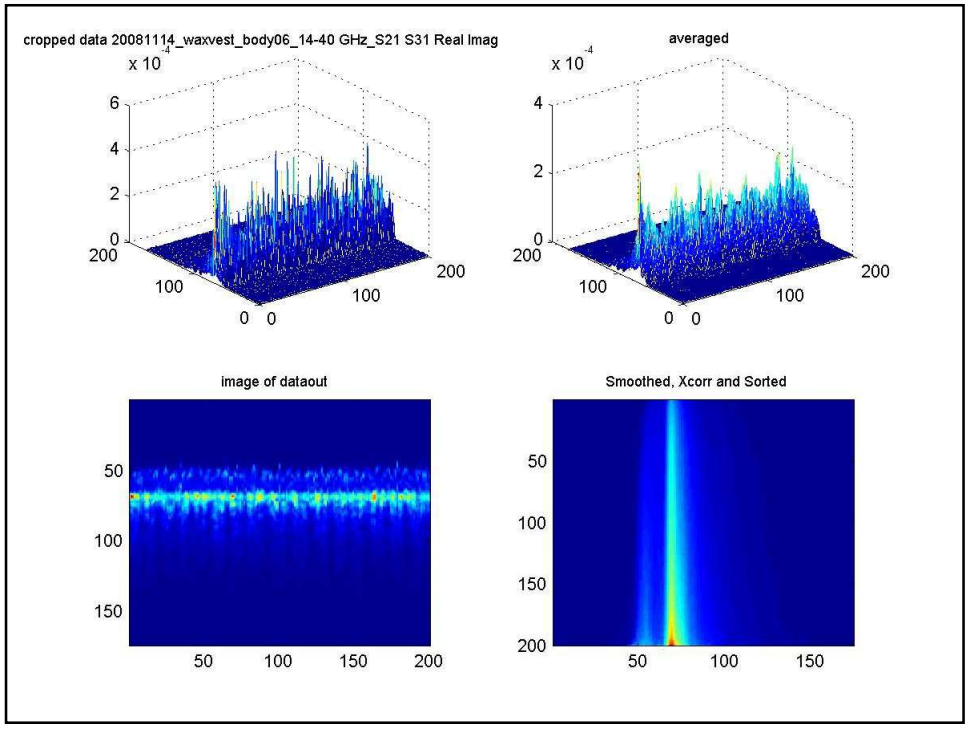
cropped data 20081114_waxvest_body06_14-40 GHz_S21 S31 Real Imag
x 10^-4
6
4
2
0
200
100
0
0
100
200
averaged
x 10^-4
4
2
0
200
100
0
0
100
200
image of dataout
50
100
150
50
100
150
200
Smoothed, Xcorr and Sorted
50
100
150
200
50
100
150

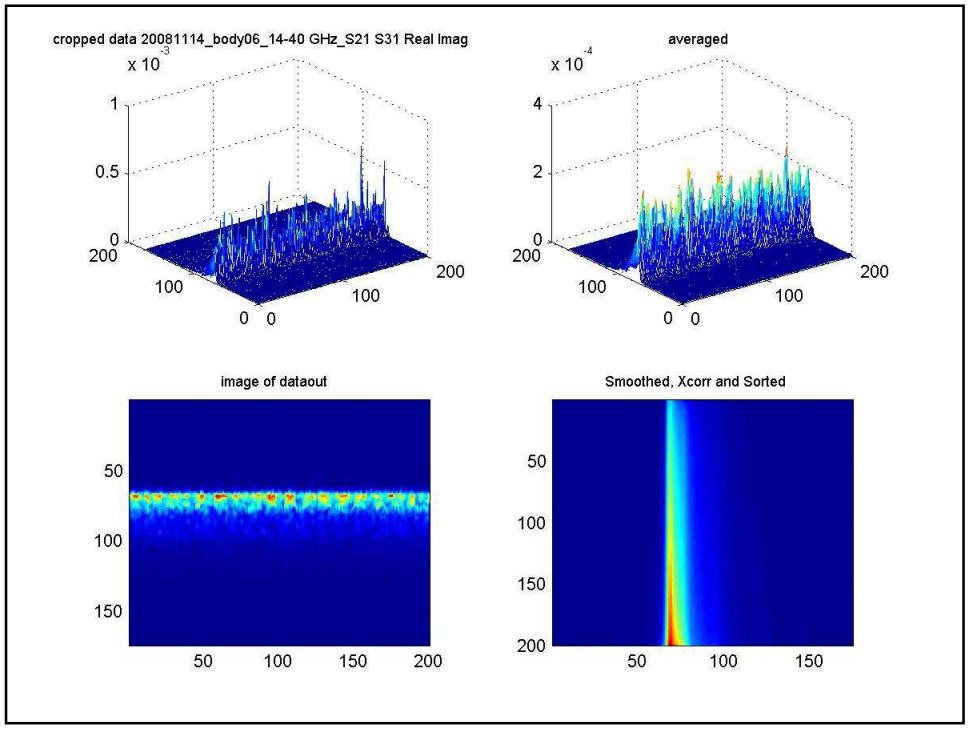
cropped data 20081114_body06_14-40 GHz_S21 S31 Real Imag
x 10^-3
1
0.5
0
200
100
0
0
100
200
averaged
x 10^-4
4
2
0
200
100
0
0
100
200
image of dataout
50
100
150
50
100
150
200
Smoothed, Xcorr and Sorted
50
100
150
200
50
100
150

Simulated explosive (wax) + body – training data

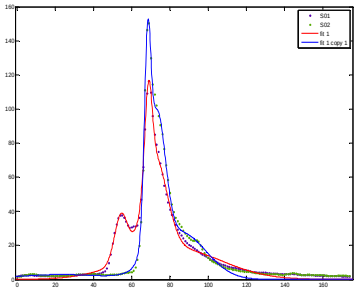

- Gaussian curves are then fitted to the data using Matlab's curve fitting toolbox. The red curve shows wax + body and the blue curve shows the body only.

Data	Result	Correct?
Wax + body 1	0.8629	Y
Body 1	0.6324	N
Wax + body 2	0.6900	Y
Body 2	0.1114	Y
Wax + body 3	0.8649	Y
Body 3	0.1081	Y
Wax + body 4	0.8664	Y
Body 4	0.1186	Y
Wax + body 5	0.8910	Y
Body 5	0.2163	Y
Wax + body 8	0.9450	Y
Body 8	0.1055	Y
Wax + body 9	0.9153	Y
Body 9	0.1064	Y
Wax + body 10	0.8334	Y
Body 10	0.1058	Y

- The neural network is tested by presenting it with new data formatted in the same way as the training data.

Summary

- Millimetre wavelengths can be used to detect explosives hidden under clothing at a standoff distance.
- This data is collected with a VNA.
- A neural network is used to classify it as a threat or not a threat.
- The data is correlated and sorted so that it is clear when there is a threat present and when there is not.

12.4 Poster

Poster displayed in Department of Engineering and Technology, MMU, June 2008.

Detecting Concealed Handguns

S. E. Smith, M. Southgate, N. Rezgui, D. Andrews, N. Bowring

Detecting concealed handguns is at the forefront of research due to increasing concerns about gun crime and terrorism. Traditional ways of detecting guns, such as metal detectors create choke points in crowded public areas. Airports, railway stations and police on the street need new ways to detect guns from a safe standoff distance. Our research aims to detect handguns hidden under clothing using millimetre wavelength radiation. This is a safe technique to use unlike X-ray scanners which are only suitable for baggage. Privacy issues are avoided by using a non-imaging approach.

Experiment The technique uses swept millimetre wave CW signals with a 26GHz bandwidth. Two microwave horns are used, one for transmit and one for receive, as shown in figure 1. The reflected signal from the target contains interference fringes as the radiation reflects from the surface of the gun and the body of the person carrying it.

Figure 1—Starter pistol under test with water backing to simulate a person carrying it.

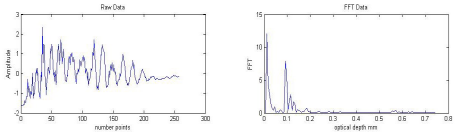

Figure 2—The raw data and its Fourier transform vs. Optical depth

These fringes contain dimension information about the gun. The raw data is Fourier transformed and plotted against optical depth as shown in figure 2. The optical depth is related to the dimensions of the weapon under test. The Fourier transformed scans are plotted against scan number to build up a picture of the presence of a threat object while the person is moving. This can be used to identify the presence of a gun or other benign object, such as a mobile phone. [1]

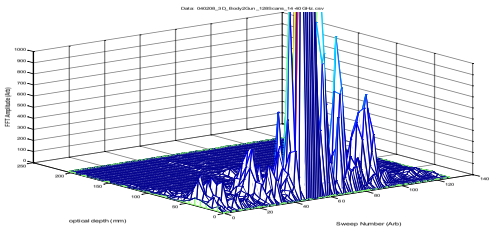

Figure 3—Person carrying starter pistol.

Results Figure 3 shows the signature of a starter pistol carried by a person and figure 4 shows the signature of the person only. The person in the figures is moving slowly while 128 scans of the frequency range are measured. A strong reflection is obtained from the gun as in figure 3 and a weak reflection for the body only as in figure 4.

Neural Networks can be used to recognise these patterns and to classify them as threat or non-threat objects. The scans are given to a feed-forward back propagation network, one at a time and it is trained on the data to give an output of zero or one. When tested the network gives good results on threat and non-threat objects.

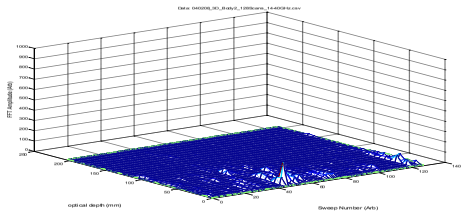

Figure 4—Person only.

Conclusion It can be shown that using swept millimetre wavelengths a starter pistol can be detected under clothing at a standoff distance. Neural Networks can be used to classify the resulting reflections as threat or non-threat objects, after post-processing using Fourier transforms. Further work includes increasing this distance to ten metres and automating the detection of threat and non-threat objects.

References [1] Standoff Detection of Concealed Handguns. N. Rezgui, D. Andrews, N. Bowring, S. Harmer, M. Southgate. Proc. SPIE 2008. Passive Millimeter-Wave Imaging Technology XI. Edited by Appleby, Roger; Wikner, David A. Proceedings of the SPIE, Volume 6948, pp. 69480L-69480L-9 (2008).

12.5 IEEE Microwave Magazine 2012 (Harmer et al., 2012)

Acknowledgment

The author thanks Dr. Kate Remley, Editor of *IEEE Microwave Magazine*, and the reviewers for their insightful suggestions that improved this article.

References

[1] S. Goldman, "Phase noise leakage through a mixer," *MSN CT*, pp. 80–96, Nov. 1987.

[2] J. Vey, M. M. Driscoll, E. P. EerNisse, R. T. Filler, R. M. Garvey, W. J. Riley, R. C. Smythe, and B. D. Weglein, "The effects of acceleration on precision frequency sources," U.S. Army Lab. Command Electron. Technol. Dev. Lab., Fort Monmouth, NJ, *Res. Dev. Tech. Rep. SLCET-TR-91-3* (Rev. 1).

[3] G. R. Kurzenknabe, "Phase noise under vibration in crystal oscillators," in *Measurement Product Dig.*, May/June 1989, pp. 33–35.

Correction

Due to a production error, four references were left out of the Application Note by Samuel J. Caprio [1] in the last issue. The following are the correct references that should have appeared on the list, with added information that should have appeared in the citation of the reference in text (e.g., equation number, etc.). We apologize for this error and any confusion it may have caused.

[12] W. Bishop, "Interferometer accuracy and DOA cell size tradeoffs," private communication, Apr. 19, 1978.

[13] D. C. Schleher, *Electronic Warfare in the Information Age*. Boston: Artech House, 1999, pp. 380–381, (6.10) and (6.6.12).

[14] R. L. Goodwin, "Ambiguity-resistant three- and four- channel interferometers," Tactical Electronic Warfare Division, Naval Res. Lab., Washington, DC, p. 23, Table 3-1.

[15] S. J. Caprio, "Effects of single-tone spurious signals in ESM receivers," *Microwave J.*, vol. 53, no. 10, pp. 64–70, Oct. 2010, (8) and Figure 1.

[16] R. L. Goodwin, "Ambiguity-resistant three- and four- channel interferometers," Tactical Electronic Warfare Division, Naval Res. Lab., Washington, DC, pp. 4–5, Figs. 1 and 2.

Reference

[1] S. J. Caprio, "Specifying upper bounds on phase noise in phase-locked oscillators in electronic warfare systems—Part I [Application Notes]," *IEEE Microwave Mag.*, vol. 11, no. 7, pp. 96–112, 2011.

Digital Object Identifier 10.1109/MMM.2011.2178290
Date of publication: 13 January 2012

A Review of Nonimaging Stand-Off Concealed Threat Detection with Millimeter-Wave Radar

■ **Stuart William Harmer, Nicholas Bowring, David Andrews, Nacer Ddine Rezgui, Matthew Southgate, and Sarah Smith**

There is now, more than ever before, a need for technologies that enable the screening of people from a distance. A wide variety of weapons can be easily concealed under clothing and carried into crowded public sites to target national infrastructure, spread fear, and inflict mass murder and casualties. The most feared and devastating terrorist weapon is the suicide bomb or person borne improvised explosive device (PBIED). Such devices are relatively simple to conceal on the body, and successful detection is required at considerable distance or stand-off range before the bomber reaches the target area.

Current electromagnetic screening technologies, such as metal detectors, explosive trace detection, and x-ray backscatter are very restricted in the coverage, stand-off capability, flexibility, and efficacy they afford. Perhaps the most widely known of these technologies is millimeter-wave or submillimeter-wave imaging [1]–[7], where millimeter-wave images are interpreted by a trained human operator or by computer algorithm to ascertain the presence or absence of concealed threats. Millimeter-wave imaging is certainly the most commonly employed technique for stand-off detection of concealed threats.

A prerequisite of a screening system based on imaging is the ability to form an image in which there exists a contrast between concealed items and the human body. This condition requires that the portion of the

Stuart William Harmer (swharmer@googlemail.com), Nicholas Bowring, David Andrews, Nacer Ddine Rezgui, Matthew Southgate, and Sarah Smith are with The School of Electrical and Electronic Engineering at Manchester Metropolitan University, Manchester, U.K.

Digital Object Identifier 10.1109/MMM.2011.2174125
Date of publication: 13 January 2012

 1527-3342/12/$31.00©2012 IEEE

electromagnetic spectrum utilized for image formation is not significantly attenuated by standard clothing and textiles and also that the objects to be resolved have physical properties, temperature, emissivity, reflectance, etc., which are different from that of the human body to provide contrast in the formed image. Also important is that the image formed has sufficient spatial detail so that the shape of the object can be recognized sufficiently well for the identification of concealed objects to be made, for example, to enable the user to discriminate between a benign object, such as a mobile phone handset, and a handgun. The only portion of the electromagnetic spectrum where these conditions are readily met is in the millimeter-wave and submillimeter-wave region. In this region, imaging systems with sufficiently high spatial resolution can be realized using the comparably small antenna sizes needed for a practical and deployable system.

The science of millimeter-wave imaging is based on spatially mapping the distribution of radiometric contrast in a scene. For passive imaging, this contrast is a function of the temperature and emissivity distribution of the scene and the reflectance distribution within the scene [8]. In an outdoor environment, the apparent temperature of the sky is very different from the human body temperature and, therefore, climactic conditions contribute significantly to the quality of the image formed. Active millimeter-wave imaging uses artificially generated radiation to illuminate the scene. Here the formed image is dominated by the scene's reflectance distribution, which is sensitive to the orientation of reflecting surfaces and their diffusivity and specular reflections. This gives rise to areas of high brightness, known as "glinting," which can plague the active methods [9]. Recently, there has been interest in combining passive and active millimeter-wave imaging techniques to improve imaging capability [10] and in making use of the different polarizing effect of concealed items from that of the human body to enhance discrimination [11]–[13].

Millimeter-wave imaging has limitations, some of which are best described by quasi-optical analysis, in that the imagery and the figures of merit of that imagery can be described in a similar way to those used to characterize the performance of an optical or infrared image capture system. There are two main limitations to the image quality obtainable from millimeter-wave imaging systems: spatial resolution and radiometric sensitivity. Spatial resolution characterizes the smallest features of the scene that can be resolved in the image. For a given frequency band of operation (millimeter-wave radiation is the band occupied from 30 GHz to 300 GHz) and camera aperture size, the smallest feature in the object resolvable in the image will scale linearly with range. At long ranges, the image resolution will be much poorer than for the same target closer in. Spatial resolution of several millimeters is typically attainable at a range of

Current electromagnetic screening technologies, such as metal detectors, explosive trace detection, and x-ray backscatter are very restricted in the coverage, stand-off capability, flexibility, and efficacy they afford.

3 m with a good, passive millimeter imaging system. Spatial resolution is limited by the frequency band that the millimeter-wave camera operates over, where higher frequency bands give finer resolution and the aperture size of the optical components of the imaging system are reduced. The aperture size of the receiver elements that comprise the sensitive area for signal detection is also important for determining the spatial resolution of the camera, however, a reduction in size of these indefinitely does not improve resolution beyond the diffraction limit set by the system's aperture. Sensitivity is determined by receiver noise, the receiver collection area, and the dwell time of the camera. Optical aperture and the receiver aperture are typically matched to give the largest receiver aperture possible while keeping the system diffraction limited by the optical aperture of the system. This is done to maximize sensitivity of the receiver while not degrading spatial resolution. Integration or dwell time is limited by the need for real-time video frame rate capture, however, the intensity of natural emission from the human body in the millimeter region is very low compared with that in the infrared spectrum (about two orders of magnitude fewer photons emitted per unit area per unit time). Accordingly, dwell times need to be longer for low-noise millimeter-wave imagery than is required for thermal imagery, although this disadvantage is offset by the fact that millimeter-wave receivers have better thermal noise performance than their infrared counterparts. Typical noise levels in a state-of-the-art passive millimeter-wave imaging system are approximately equivalent to a 0.4 K temperature differential, limiting contrast to this level. Existing millimeter-wave imaging systems periodically sample different solid angles of the total field of view, building up the entire scene by scanning and overlapping these smaller angled samples. This can be done with a single receiving channel by scanning the directional pattern of receiving antenna, modified by the addition of refractive or reflective quasi-optical elements across the two dimensions of the scene or by using multiple receiver channels and scanning spatially, thus building up multiple image pixels at every scanning position. Scanning millimeter-wave cameras have low frame rates and strict requirements are imposed by the mechanical scanning of the beam steering optics. The operation of scanning can be made redundant if a sufficient number of receiver channels are used such that the

The operation of scanning can be made redundant if a sufficient number of receiver channels are used such that the required field of view can be met solely by the total viewing angle obtained.

required field of view can be met solely by the total viewing angle obtained. This approach is identical in concept to the focal plane arrays that are used to capture images in the optical and infrared bands of the electromagnetic spectrum. The disadvantages of such systems include the difficulty of positioning a large number of receiver channels in the focal plane of the antenna, problems arising in constructing arrays with spatially overlapping beams, and the very high total cost of the systems, which is dominated by the increased number of receiver channels required to achieve the required field of view. Millimeter-wave imaging is a very well understood, highly developed and mature technology and improvements in performance will now come at a high cost, both financially and in development time.

Millimeter-Wave Radar

A promising alternative method of concealed threat detection is to avoid image formation altogether and the restrictions that an imaging approach imposes, the greatest of which are those of limited spatial resolution and scene contrast, making interpretation and identification of concealed objects by millimeter-wave imaging difficult and often unreliable. But the essential ability of millimeter-wave radiation to penetrate clothing and gather information on concealed objects must be retained. A millimeter-wave radar system has the ability to probe objects concealed under clothing with identification of those objects being carried out by analysis of the scattered radar return [14]–[22]. This has distinct advantages over imagery.

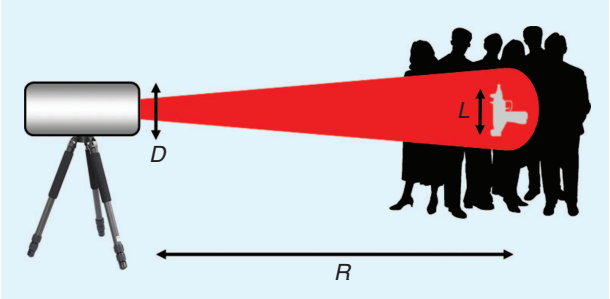

Figure 1. *An illustration of a millimeter-wave radar system in use to individually screen people in a crowd scenario. The beam can be aimed at an individual at standoff ranges; guidance of the beam is achieved by colocation of video imagery provided by a camera mounted on the system.*

- Interpretation of millimeter-wave imagery is difficult and does not lend itself well to autonomous decision making, whereas interpretation of scattered radar returns can, for certain types of objects, be far quicker, more reliable, and discriminatory.
- Spatial resolution requirements for a radar system are far more relaxed, since imagery is not being sought. Consequently, stand-off ranges can be extended considerably beyond those achievable with an imaging technique.
- Speed of operation of a radar system is higher than for a millimeter-wave imaging system, with capture rates well in excess of 50 frames per second possible.
- Radar systems are mechanically simpler than scanned millimeter-wave imaging cameras since the scene does not need to be scanned using rapidly moving mirrors, as the radar is a point and detect system.
- The radar system can be integrated with conventional video or infrared imagery to show the position of the millimeter-wave beam in real time.
- Size and weight saving of a millimeter-wave radar system over an imaging system are considerable as a result of the reduced number of components, optics, mechanical drives, and power requirements.
- The cost of a radar system is significantly lower since fewer expensive millimeter-wave components are required and expensive optical components are not required.

Highly directional antennas may be made at millimeter-wave frequencies so that quasi-optical beams of millimeter radiation may be used to probe the target at large stand-off ranges, where the beam width or spot size may be sufficiently localized to cover an area commensurate with, or smaller than, a typical human torso (see Figures 1 and 2). Smaller beam sizes are required to detect smaller objects reliably, and therefore there is always a trade-off between aperture size, stand-off range, frequency, and minimum resolvable target size. The relationship between these competing parameters can be effectively summarized by the expression: $L \leq Rc/Dv$, where L is the largest linear dimension of the concealed object to be detected, R is the range to the target, c is the speed of light in vacuum, D is the diameter of the antenna aperture, and v the frequency of the millimeter-wave radiation. A beam that is considerably smaller than the largest linear dimension of a concealed object will fail to characterize the whole object fully since the radar return will not originate from the entire object. Conversely a beam that is considerably wider than the largest linear dimension of a concealed object will not localize the object sufficiently, and the radar return will contain the signatures of other nearby items (see Figure 3).

Over the last few years, there have been several nonimaging millimeter and microwave radar-based products released and patents filed that describe these systems, which claim to be able to detect various threat items concealed on the human body. Currently, there are a handful of companies that are offering radar-based concealed threat detection devices. Ariel University Research and Development Company Ltd have developed a small, hand-held device [23]–[24]. This system sends out a train of millimeter-wave pulses using a modulated Gunn oscillator and measures characteristics of the scattered radar return. An autonomous threat decision is made based on comparing these measurements to a library of previously measured threat situations. Safe Zone Systems [25]–[26] have filed a number of patents for a microwave-based radar system for concealed threat detection, and sell such a system for the detection of concealed threats. The Safe Zone Systems apparatus illuminates the target with a microwave pulse and uses the natural resonances of the object to enable an autonomous threat-or-no-threat decision to be made. The Science, Engineering, and Technology (SET) Corporation has developed the CounterBomber system [27]–[28], which is currently deployed by U.S. forces in Iraq and Afghanistan and is probably the most advanced of the current commercially available technologies. This system has recently attracted very significant funding, with a US$ 50 million contract being awarded from the U.S. Army to detect suicide bombers at long range (~100 m). CounterBomber uses heterodyne millimeter-wave receivers to obtain polarimetric

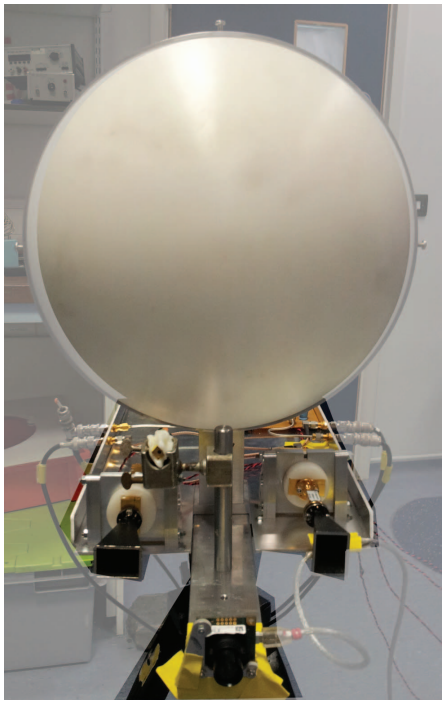

Figure 2. *Photograph of an early prototype of a radar-based concealed threat detection system developed at Manchester Metropolitan University; signal processing and autonomous threat detection is carried out in real time on a remote PC.*

A promising alternative method of concealed threat detection is to avoid image formation altogether and the restrictions that an imaging approach imposes.

radar information of the illuminated target. The system automatically tracks the radar beam onto the person to be screened by using video imagery from a colocated video camera, and delivers an autonomous threat decision to the user.

The authors of this article, based in the School of Electrical and Electronic Engineering at Manchester Metropolitan University, have developed a W-band (75–110 GHz) millimeter wave, polarimetric radar system and have recently been granted a U.K. patent for this invention [29]. The authors' system shares some common features with earlier work in the area [23]–[28], but also has features which make it distinct from other millimeter-wave radar devices. Direct comparison of the performance of the authors' system with similar systems has not been made although it is clear that the CounterBomber system is commercially at a more advanced stage and has almost certainly undergone more rigorous field trials. The equipment has been developed for the detection of threat objects, particularly PBIED, concealed under clothing upon the human body at stand-off ranges of up to 25 m; a system that operates at longer range is planned. In operation, the system implements swept frequency continuous wave radar with low-cost components to deliver a compact, ultrawide bandwidth (UWB), high resolution (around ~ 10 mm) radar system capable of detecting, discriminating, and identifying a wide

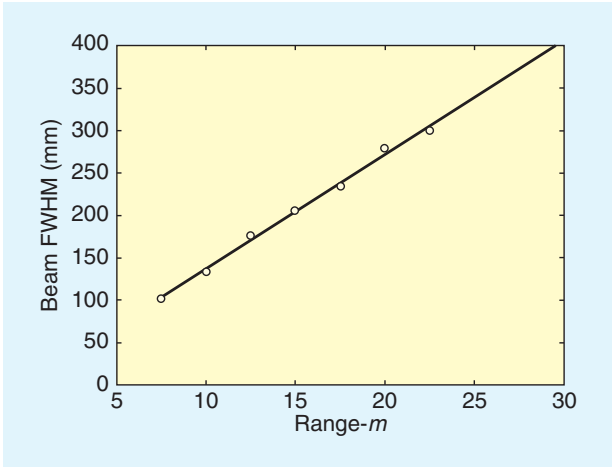

Figure 3. *Measured FWHM (3 dB points) of the Manchester Metropolitan University concealed threat radar system's beam at 94 GHz for various ranges are shown by circular marker points; the theoretical beam width is represented by the continuous line.*

spectrum of concealed threat items. Although not required for PBIED fragmentation device detection, where a simple co- and cross-polarized radar return amplitude ratio is all that is required, threat detection can be rendered autonomously by application of a neural network to the scattered polarimetric, time domain radar return. Such a system may be taught to alarm or reject certain classes of objects, allowing both highly specific and broad spectrum threat detection [16]–[20]. The overall cost of the system described here is kept low by use of direct detection receivers, which are considerably less expensive than implementing a heterodyne receiver operating over the same wide frequency band. The millimeter-wave radar system described is by no means a foolproof method of detecting and identifying objects concealed on the human body, and false positive and false negative detection events are certainly observed using this system. False alarms are generally more prevalent when attempting to detect smaller objects, and objects that present a shape that is easily mimicked by benign objects, e.g., a metal cased fountain pen and a small knife. Larger objects and those that have a unique shape, e.g., a large handgun, are easier to detect and classify [16]. Object orientation on the body also contributes to the ease or difficulty of detection and identification of concealed objects. For example, a handgun presented side on is more easily detected than the same weapon in a frontal aspect. Such effects mean that detection and identification is best carried out while the person being screened is walking and presenting an ever-changing body aspect with respect to the millimeter radar system.

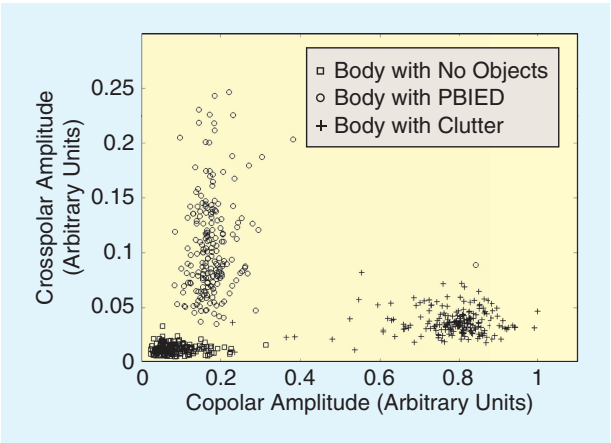

Figure 4. *Measured radar amplitude returns from the Manchester Metropolitan University concealed threat radar system showing polarimetric discrimination of a person with (circle symbols) and without a PBIED (diamond symbols) and with concealed nonthreat items (plus symbols) at a range of 25 m. Multiple scans are taken and the amplitude of the radar return in both copolarized and cross-polarized channels are plotted, in this case there is very obvious clustering such that the case where a PBIED is present is clearly differentiable.*

There are two key radar principles that we make use of for threat detection: polarization changes induced by the concealed object, and the axial structure profile information of the concealed object. Polarimetric information is realized by transmitting millimeter radiation with electric field aligned horizontally (across the body), to minimize the radar cross section of an upright human body, and measuring the scattered field both horizontally and vertically (along the body) using two receiver channels (see Figure 4). Reorientation of a fraction of the incident horizontally polarized millimeter-waves into the vertical polarization state is predominantly due to multiple reflections in the case of fragmentation within a PBIED, whereas for single solid items, which do not give rise to multiple reflections, the reorientation is due to stronger reflection of electric field components in certain directions than in others, and is thus a function of the object's shape and symmetry.

Axial structure profile is measured by transmission of UWB millimeter-wave radar waveforms to spatially resolve scattering surfaces that are sufficiently separated. The achievable axial resolution is

$$\Delta R \geq \frac{c}{2BW},$$

where BW is the bandwidth scanned. By scanning over the entire W-band (~ 35 GHz), features separated by only ~ 10 mm are resolvable, allowing the presence of objects in front of the body, usually under layers of clothing, to be ascertained (see Figure 5). This high-range resolution is a key factor, which helps distinguish the Manchester Metropolitan University system from similar systems disclosed in patents [24], [26], [28]–[29].

The radar front-end is based on monolithic microwave integrated circuit (MMIC) direct-detection receivers connected to orthogonally orientated, horizontal and vertical gain horns and a voltage controlled oscillator (VCO) and multiplier to provide the swept frequency output. The transmitter is a gain-horn located at approximately the focal length of a 300 mm diameter polyethylene lens (see Figure 6). A reasonable estimate of the upper usable beam width of 350 mm, commensurate with the typical width of the human body, sets the maximum effective range of the system to ~ 25 m (see Figure 3). Range-to-target information is provided by a conventional radar range-finding technology.

Both copolarized and cross-polarized radar return signals are transformed from the frequency domain to the time domain and scaled according to the range at which the target is measured to be. This accounts for the wide variation in signal strengths that the system encounters over the variable stand-off operating range at which screening can take place, currently from a few meters out to 25 m. The scaled temporal data is then fed to a neural network classifier which has a priori

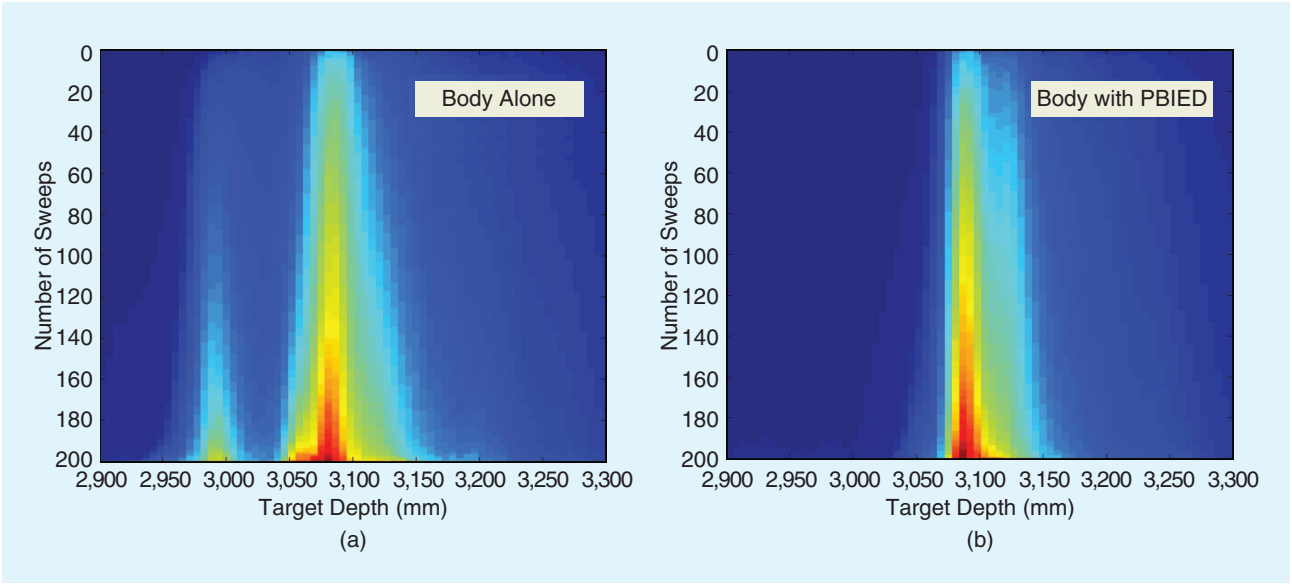

Figure 5. *Axial depth profiles for a person at an indicated range of ~ 3 m. The plots show the strength of return (red being highest and blue zero) at different ranges (horizontal axis) as a function of increasing numbers of frequency scans of target (vertical axis). (a) is for a body with no explosive device while (b) is for a body with a PBIED without any fragmentation; the device clearly shows up as a area of significant radar return immediately in front of the body response.*

trained networks for items of interest; these training sets can include a broad spectrum of threat objects or can instead focus on very specific items. Detection and discrimination of PBIED containing shrapnel components (see Figures 7 and 8) is particularly effective, with the system being able to differentiate successfully between a person carrying such a device and a person without an explosive device but carrying the usual accoutrements of modern living such as a mobile phone, iPod, car keys, wallet, etc, at ranges up to 25 m (see Figure 4).

Fragmentation components of a simulated PBIED present such a good target because the small fragments whose size is around one centimeter to provide a strong cross-polarized return from a large body area, which is not reproduced by any other commonly carried benign objects. The exact type of fragmentation used, including nails, nuts and bolts, and ball bearings, did not greatly affect performance. Other, smaller, threat items, such as handguns, can be detected and differentiated with some success, but at lesser standoff ranges, where the beam size is smaller and more suited to the detection of these items. By taking multiple scans, a more robust detection of the threat level can be made. The effect of multiple scans on the discrimination of PBIED by both polarimetric and axial profile determination is shown in Figures 4 and 5. In walking tests, where the subject walks towards the radar system as readings are taken, the range-scaled polarimetric data clearly allows differentiation between a person carrying a simulated

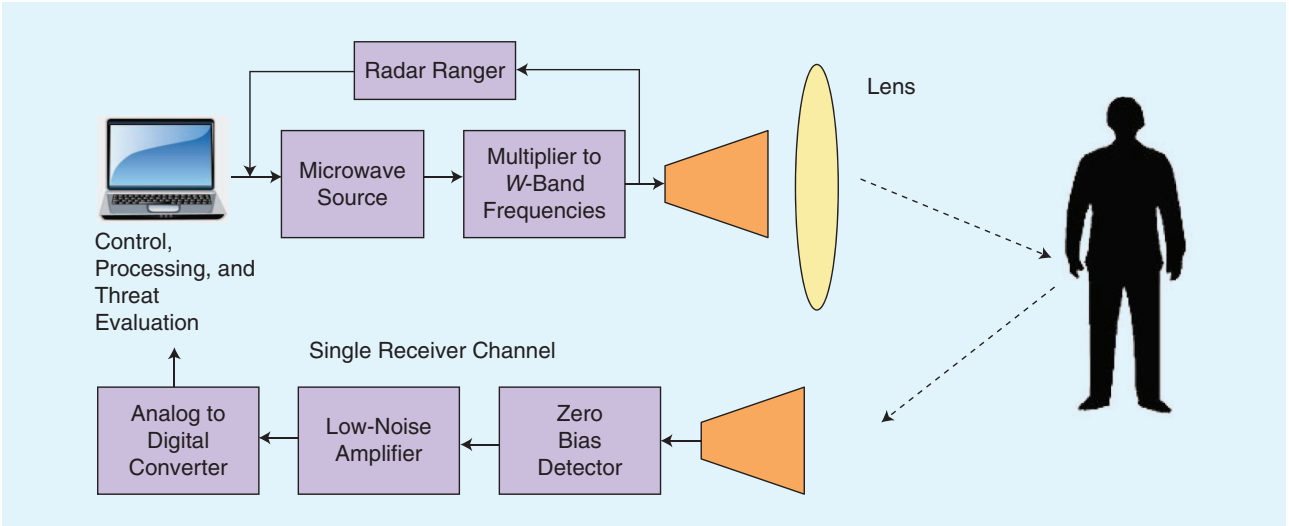

Figure 6. *Schematic of Manchester Metropolitan University concealed threat detection radar system showing major system blocks.*

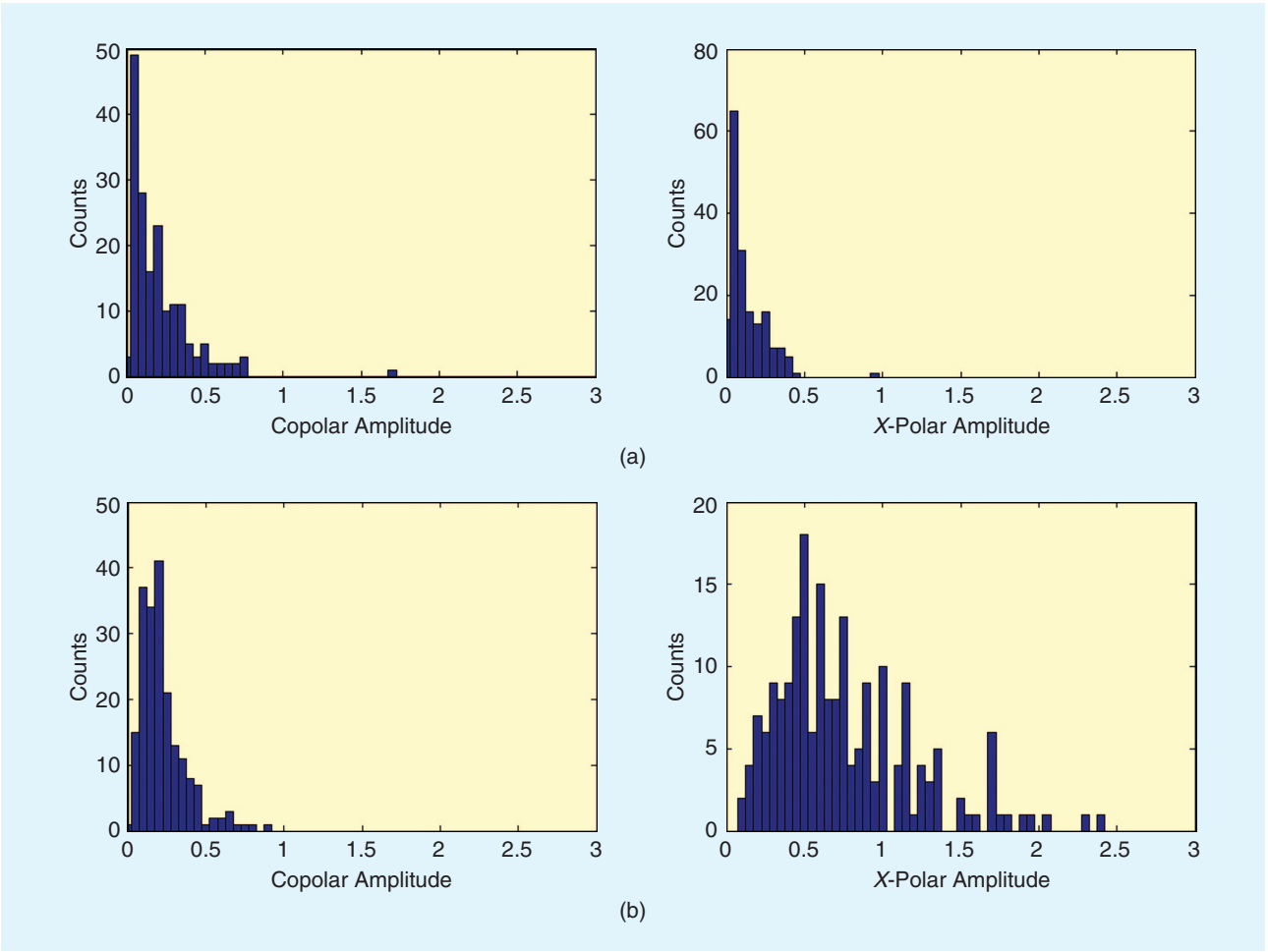

Figure 7. *Amplitude histograms of radar return in copolarized and cross-polarized (X-polar) channels for (a) a person without a PBIED and (b) with PBIED. The data was taken for a person walking toward the radar system, each data point has been range scaled (to remove effects of range on amplitude), and normalized with reference to a test target.*

PBIED, as shown in Figure 9, and a person without such a device as in Figure 7.

Although millimeter-wave imaging is a useful technology for security screening of people, the technique currently has limitations which prevent the effective

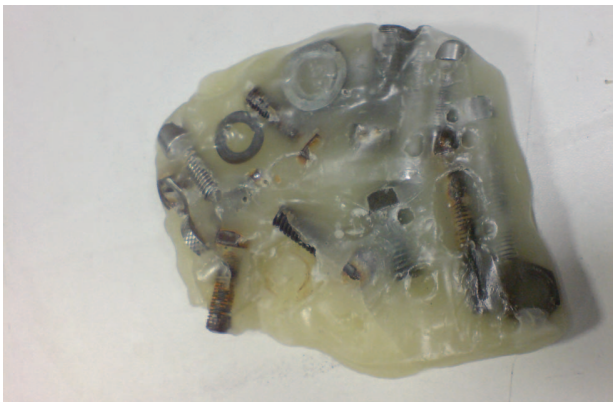

Figure 8. *A representative example of a piece of a simulated PBIED used in system testing at Manchester Metropolitan University; shrapnel is embedded in wax to mimic a suicide vest. Other samples were made using nails and ball-bearings embedded in wax and results were similar.*

Figure 9. *Simulated PBIED suicide vest used in system testing at Manchester Metropolitan University.*

detection of threat items, and in particular PBIED, at useful standoff ranges (> 20 m). UWB millimeter-wave radar systems can detect the presence or absence of certain concealed threat objects at ranges in excess of 20 m by reliance on information carried in the scattered radar return from the person. Consequently, millimeter radar offers a viable alternative, and a potentially complementary screening method to conventional millimeter-wave imaging, and will undoubtedly find increasing use in concealed threat detection.

References

[1] R. Appleby and R. N. Anderton, "Millimeter-wave and submillimeter-wave imaging for security surveillance," *Proc. IEEE*, vol. 95, no. 2, pp. 1683–1690, Aug. 2007.

[2] S. Oka, H. Togo, N. Kukutsu, and T. Nagatsuma, "Latest trends in millimeter-wave imaging technology," *Progress Electromagn. Res. Lett.*, vol. 1, pp. 197–204, 2008.

[3] M. C. Kemp, A. Glauser, and C. Baker, "Recent developments in people screening using terahertz technology—Seeing the world through terahertz eyes," in *Proc. SPIE*, 2006, vol. 6212, pp. 27–34.

[4] R. Appleby and H. B. Wallace, "Standoff detection of weapons and contraband in the 100 GHz to 1 THz region," *IEEE Trans. Antennas Propagat.*, vol. 55, no. 11, pp. 2944–2956, Nov. 2007.

[5] J. F. Federici, B. Schulkin, F. Huang, G. Dale, R. Barat, F. Oliveira, and D. Zimdars, "THz imaging and sensing for security applications—Explosives, weapons and drugs," *Semiconduct. Sci. Technol.*, vol. 20, no. 7, pp. S266–S280, July 2005.

[6] D. Sheen, D. McMakin, and T. E. Hall, "Three-dimensional millimeter-wave imaging for concealed weapon detection," *IEEE Trans. Microwave Theory Tech.*, vol. 49, no. 9, pp. 1581–1592, 2001.

[7] L. V. Volkov, A. I. Voronko, N. L. Volkova, and A. R. Karapetyan, "Active MMW imaging technique for contraband detection," in *Proc. 33rd European Microwave Conf.*, 2003, pp. 531–534.

[8] S. E. Clark, J. A. Lovberg, C. A. Martin, and V. Kolinko, "Passive millimeter-wave imaging for airborne and security applications," in *Proc. SPIE*, 2003, vol. 5077, pp. 16–21.

[9] P. F. Goldsmith, C. T. Hsieh, G. R. Huguenin, J. Kapitzky, and E. L. Moore, "Focal plane imaging systems for millimetre wavelengths," *IEEE Trans. Microwave Theory Tech.*, vol. 41, no. 10, pp. 1664–1675, Oct. 1993.

[10] R. Zouaoui, R. Czarny, F. Diaz, A. Khy, and T. Lamarque, "Multisensor millimeter-wave system for hidden objects detection by collaborative screening," in *Proc. SPIE*, 2011, vol. 8022.

[11] D. M. Sheen, T. E. Hall, R. H. Severtsen, D. L. McMakin, B. K. Hatchell, and P. L. J. Valdez, "Standoff concealed weapon detection using a 350-GHz radar imaging system," in *Proc. SPIE*, 2010, vol. 7670 , pp. 117–126.

[12] D. M. Sheen, D. L. McMakin, W. M. Lechelt, and J. W. Griffin, "Circularly polarized millimeter-wave imaging for personnel screening," in *Proc. SPIE*, 2005, vol. 5789.

[13] D. M. Sheen, D. L. McMakin, T. E. Hall, and R. H. Severtsen, "Active millimeter-wave standoff and portal imaging techniques for personnel screening," in *Proc. IEEE Conf. Technologies for Homeland Security*, 2009, pp. 440–447.

[14] A. S. Ibrahim, K.J. R. Liu, D. Novak, and R. B. Waterhouse, "A subspace signal processing technique for concealed weapons detection," in *Proc. IEEE ICASSP*, 2007, pp. 401–404.

[15] J. Hausner and N. West, "Radar based concealed threat detector," in *Proc. IEEE MTT-S Int. Microwave Symp.*, 2007, pp. 765–768.

[16] N. Rezgui, D. Andrews, N. Bowring, S. Harmer, and M. Southgate, "Standoff detection of concealed handguns," in *Proc. SPIE.*, 2008, vol. 6948.

[17] D. A. Andrews, S. E. Smith, N. Rezgui, N. J. Bowring, M. Southgate, and S. W. Harmer, "A swept millimetre-wave technique for the detection of concealed weapons and thin layers of dielectric material with or without fragmentation," in *Proc. SPIE*, 2009, vol. 7309.

[18] D. A. Andrews, N. Rezgui, S. E. Smith, N. J. Bowring, M. Southgate, and J. G. Baker, "Detection of concealed explosives at standoff distances using wide band swept millimetre waves," in *Proc. SPIE.*, 2008, vol. 7117.

[19] D. A. Andrews, N. J. Bowring, N. D. Rezgui, M. Southgate, E. Guest, S. W. Harmer, and A. Atiah, "A multifaceted active swept millimetre-wave approach to the detection of concealed weapons," in *Proc. SPI*, 2008, vol. 7117.

[20] N. J. Bowring, J. G. Baker, N. Rezgui, M. Southgate, and J. F. Alder, "Active millimetre wave detection of concealed layers of dielectric material," in *Proc. SPIE*, 2007, vol. 6540.

[21] L. Yong, Y. T. Gui, N. J. Bowring, and N. Rezgui, "A microwave measurement system for metallic object detection using swept frequency radar," in *Proc. SPIE*, 2008, vol. 7117.

[22] A. Agurto, Y. Li, G. Y. Tian, N. Bowring, and S. Lockwood, "A review of concealed weapon detection and research on perspective," in *Proc. IEEE ICNSC*, 2007, pp. 443–448.

[23] [Online]. Available: http://arielrnd.com/

[24] B. Kapilevich and A. Lipeles, "Hand-held device and method for detecting concealed weapons and hidden objects," *International Application 148327*, June 18, 2007.

[25] [Online]. Available: http://www.detectanddefeat.com/

[26] J. Hausner and J. M. West, "Object detection method and apparatus," *U.S. Patent 0 052 576*, Mar. 8, 2007.

[27] [Online]. Available: http://www.setcorp.com/

[28] R. J. Douglass, J. D. Gorman, and T. J. Burns, "System and method for standoff detection of human carried explosives," U.S. Patent 7 800 527, Oct. 11, 2005.

[29] N. Bowring, D. Andrews, N. D. Rezgui, and S. Harmer, "Remote detection and measurement of objects," U.K. Patent 2 458 764, Mar. 18, 2009.

12.6 Matlab code ms_3d_dataplot.m

```
%FFT and scale for optical depth
[filename, pathname] = uigetfile('*.*', 'Pick a data file');
if isequal(filename,0) | isequal(pathname,0)
    disp('User pressed cancel')
else
    disp(['User selected ', fullfile(pathname, filename)])
end
%import raw data and format values into array called data.
data = csvread(filename, 1, 0);

%number of points
sweepPoints=length(data);
nrOfSweeps=size(data);
nrOfSweeps=nrOfSweeps(2:2);

%the MATLAB DFT can only handle even numbers of points so
%are there an even number of points?
if(rem(sweepPoints,2)==1) % odd number
    sweepPoints=sweepPoints-1; % so remove the last point
    data=data(1:sweepPoints,1:nrOfSweeps);
end


%start and stop frequencies GHz
startFreqStr = input('Enter the start freq GHz: ','s');
startFreq=str2double(startFreqStr);

stopFreqStr = input('Enter the stop freq GHz: ','s');
stopFreq=str2double(stopFreqStr);

%sweepFreqencies = frequencies spaced depending on the number of points
   in the array
```

```
sweepFreqencies = linspace(startFreq,stopFreq,sweepPoints);
sweepFreqencies=sweepFreqencies';

sweepData = data(1:sweepPoints, 1:nrOfSweeps);



count = 1;
while (count <= nrOfSweeps)
    y = data(1:sweepPoints, count:count);
 %remove zero offset
% back = input('Remove background Y/N: ','s');
% if(back=='y' || back=='Y')
p = polyfit(sweepFreqencies,y,1);
%plot( p)
p1 = polyval(p,sweepFreqencies);
p2= y - p1;



%BURG
% poles1 = input('Enter number of poles for Burg: ','s');
% poles=str2double(poles1);
% poles=80;
% Pxx = pburg(p2,poles,points);



% figure(3)
y=fft(p2,sweepPoints);
Pyy=y.*conj(y)/sweepPoints;

%speed of light
c=3e8;

%range
bandwidth = stopFreq - startFreq;
```

```
%1/range
inv_bandwidth=1/bandwidth;

%half number points
half_points=sweepPoints/2;

%max x-scale value
max_val=half_points*inv_bandwidth;

%write x values into an array
array=linspace(max_val,-max_val,sweepPoints);
array=array';

%convert to optical depth in mm
%frequency must be in GHz
depth=array.*((c*1000)/(2*1e9));

%just need half_points
depth2=depth(1:half_points,1);
Pyy2=Pyy(1:half_points,1);
depth2=flipud(depth2);

%put fft'd data into array
fftdata(1:half_points,count:count)=Pyy2;
optDepth(1:half_points,count:count)=depth2;

count = count + 1;
end


rangingData = optDepth(1:length(optDepth));

%get the maximum desired range for the plot
rangeStr = input('Enter the maximum range to plot [Max Range]: ','s');
% if nothing entered so set to max range
```

```
if(isempty(rangeStr))
    distance = length(fftdata);

% else find the element that is just grater than the requested distance
else
    range = str2double(rangeStr);
    distance = 1;
    while(rangingData(distance) < range)
        distance = distance+1;
    end
end
1;

xscale = linspace(1,nrOfSweeps,nrOfSweeps);
yscale = optDepth(1:distance, 1:nrOfSweeps);
plotdata = fftdata(1:distance, 1:nrOfSweeps);
h = figure(), meshz(xscale, yscale, plotdata);



%figure; meshz (fftdata); figure(gcf)
 ylabel('optical depth (mm)','FontSize',12)
 xlabel('Sweep Number (Arb)','FontSize',12)
 zlabel('FFT Amplitude (Arb)','FontSize',12)
 %title(filename,'FontSize',12)
 title(['Data: ',(filename)],'FontSize',10,'Interpreter','none')
```

12.7 Matlab code sum_scans_only.m

```
%adds up all the values along an optical
%depth and then divides by the number of scans.
depth=depth2;
%sum scans
S=sum(fftdata');
```

```
S=S/256;
depth=optDepth(1:961,1:1);
figure,plot(depth,S)
title('Averaged over scans','FontSize',10,'Interpreter','none')
xlim ([0 250]);
```

12.8 Matlab code nn_fft_stationary_data.m

```
%clear workspace and close figures
clear, close all

%Get 3D plot
ms_3d_dataplot

%Get average over all scans
%adds up all the values along an optical
%depth and then divides by the number of scans.
depth=depth2;
%sum scans
S=sum(fftdata');
S=S/256;
% depth=optDepth(1:961,1:1);
% figure,plot(depth,S)
% title('Averaged over scans','FontSize',10,'Interpreter','none')
% xlim ([0 250]);

%normalise data between 0 and 255
Max=max(S);
Min=min(S);
range=Max-Min;
S=((S./range)*256);

%Get 3D plot
ms_3d_dataplot
```

```
%Get average over all scans
%adds up all the values along an optical
%depth and then divides by the number of scans.
depth=depth2;
%sum scans
S1=sum(fftdata');
S1=S1/256;
depth=optDepth(1:961,1:1);
figure,plot(depth,S1)
title('Averaged over scans','FontSize',10,'Interpreter','none')
xlim ([0 250]);

%normalise data between 0 and 255
Max=max(S1);
Min=min(S1);
range=Max-Min;
S1=((S1./range)*256);

I=S;
J=S1;

in=15;
inp=in*in;

%check labels all match when you copy and paste!
I = imresize(I,[in in],'bicubic');
J = imresize(J,[in in],'bicubic');

I = reshape(I,inp,1);
I=double(I);

J = reshape(J,inp,1);
J=double(J);
```

```
%inputs
count=1;
while(count<=inp)
    input(count:count,1:2)=[0 255];
    count=count+1;
end

% newff[input range in layer 1; input range in layer 2 etc],[number
   neurons 1st layer, number neurons 2nd layer],{'transfer func 1st layer
   ','ouput layer transfer func'},'training function');
%NET.trainParam.mem_reduc =2;
net=newff(input, [20 1],{'tansig','tansig'},'trainlm', 'learngd', 'mse');
% 100 inputs, 20 hidden and 1 output neuron
%use tansig for both layers, learning functions set to defaults for
%feed-forward, back prop network.
%
%input data
% X=[I,J,K,L];
X=[I,J];
%targets
t=[1 0];
% t=[1 0 1 0];
% set goal
net.trainParam.goal= 0.01;
% train network
[net,tr]=train(net,X,t);
%simulate network
candle1=sim(net,I)
water0=sim(net,J)
%
%%%%%%%%%%test with new data%%%%%%%%%%%%%%%%%%%%%%%%%%%%%
nn_fft_test_data
```

12.9 Matlab code nn_fft_test_data.m

```
%test network with similar data
%
%Get 3D plot
ms_3d_dataplot_test

%Get average over all scans
%adds up all the values along an optical
%depth and then divides by the number of scans.
depth=depth2;
%sum scans
T=sum(fftdata');
T=T/256;
depth=optDepth(1:961,1:1);
% figure,plot(depth,T)
% title('Averaged over scans','FontSize',10,'Interpreter','none')
% xlim ([0 250]);

%normalise data between 0 and 255
Max=max(T);
Min=min(T);
range=Max-Min;
T=((T./range)*256);

T = imresize(T,[in in],'bicubic');

T = reshape(T,inp,1);
T=double(T);
test=sim(net,T)
```

12.10 Matlab code detector_gui3.m

```
function varargout = detector_gui3(varargin)
% DETECTOR_GUI3 M-file for detector_gui3.fig
```

```
%      DETECTOR_GUI3, by itself, creates a new DETECTOR_GUI3 or raises
   the existing
%      singleton*.
%
%      H = DETECTOR_GUI3 returns the handle to a new DETECTOR_GUI3 or the
    handle to
%      the existing singleton*.
%
%      DETECTOR_GUI3('CALLBACK',hObject,eventData,handles,...) calls the
   local
%      function named CALLBACK in DETECTOR_GUI3.M with the given input
   arguments.
%
%      DETECTOR_GUI3('Property','Value',...) creates a new DETECTOR_GUI3
   or raises the
%      existing singleton*.  Starting from the left, property value pairs
    are
%      applied to the GUI before detector_gui3_OpeningFcn gets called.
   An
%      unrecognized property name or invalid value makes property
   application
%      stop.  All inputs are passed to detector_gui3_OpeningFcn via
   varargin.
%
%      *See GUI Options on GUIDE's Tools menu.  Choose "GUI allows only
   one
%      instance to run (singleton)".
%
% See also: GUIDE, GUIDATA, GUIHANDLES

% Edit the above text to modify the response to help detector_gui3

% Last Modified by GUIDE v2.5 16-Jan-2009 11:36:40

% Begin initialization code - DO NOT EDIT
```

```
gui_Singleton = 0;
gui_State = struct('gui_Name',       mfilename, ...
                   'gui_Singleton',  gui_Singleton, ...
                   'gui_OpeningFcn', @detector_gui3_OpeningFcn, ...
                   'gui_OutputFcn',  @detector_gui3_OutputFcn, ...
                   'gui_LayoutFcn',  [] , ...
                   'gui_Callback',   []);
if nargin && ischar(varargin{1})
    gui_State.gui_Callback = str2func(varargin{1});
end

if nargout
    [varargout{1:nargout}] = gui_mainfcn(gui_State, varargin{:});
else
    gui_mainfcn(gui_State, varargin{:});
end
% End initialization code - DO NOT EDIT


% --- Executes just before detector_gui3 is made visible.
function detector_gui3_OpeningFcn(hObject, eventdata, handles, varargin)
% This function has no output args, see OutputFcn.
% hObject    handle to figure
% eventdata  reserved - to be defined in a future version of MATLAB
% handles    structure with handles and user data (see GUIDATA)
% varargin   command line arguments to detector_gui3 (see VARARGIN)

% Choose default command line output for detector_gui3
handles.output = hObject;

% Update handles structure
guidata(hObject, handles);

% UIWAIT makes detector_gui3 wait for user response (see UIRESUME)
% uiwait(handles.figure1);
```

```
% --- Outputs from this function are returned to the command line.
function varargout = detector_gui3_OutputFcn(hObject, eventdata, handles)
% varargout  cell array for returning output args (see VARARGOUT);
% hObject    handle to figure
% eventdata  reserved - to be defined in a future version of MATLAB
% handles    structure with handles and user data (see GUIDATA)

% Get default command line output from handles structure
varargout{1} = handles.output;



% --- Executes on button press in pushbutton1.
function pushbutton1_Callback(hObject, eventdata, handles)
% hObject    handle to pushbutton1 (see GCBO)
% eventdata  reserved - to be defined in a future version of MATLAB
% handles    structure with handles and user data (see GUIDATA)
load nnet_peak_find_workspace
[test_threat1,test_nonthreat1] = nnet_peak_find_test(net)
test_col2=mean(test_threat1)

if(test_col2 > 0.5)
set(handles.text1,'Backgroundcolor','red');
end
if (test_col2 < 0.5)
set(handles.text1,'Backgroundcolor','green');
end
```

12.11 Matlab code nnet_peak_find.m

```
%threshold, xcorr and sort
shuffle_xcorr3
S=sort_xcorr';
```

```
M=max(max(S));
S=S./M;
S=S.*256;
filename

%Get 3D plot
shuffle_xcorr3
S1=sort_xcorr';
M1=max(max(S1));
S1=S1./M1;
S1=S1.*256;
filename

%threshold, xcorr and sort
shuffle_xcorr3
S2=sort_xcorr';
% length1=length(S2);
% t1=ones(length1);
% t1=t1(1:length1,1:1);
M2=max(max(S2));
S2=S2./M2;
S2=S2.*256;
filename

%Get 3D plot
shuffle_xcorr3
S3=sort_xcorr';
% length2=length(S3);
% t2=zeros(length2);
% t2=t2(1:length2,1:1);
M3=max(max(S3));
S3=S3./M3;
S3=S3.*256;
filename
%
```

```
%gaussian_fitting_test.m
S=S';
S01=mean(S);
S1=S1';
S02=mean(S1);
length1=length(S01);
x01=linspace(0,length1,length1);
% [coeffvals1,coeffvals2] = gaussian4fit_lower0_mk2(S01,S02);
[coeffvals1,coeffvals2] = gaussian4fit_lower0_mk3(S01,S02);

%gaussian_fitting_test2.m
S2=S2';
S03=mean(S2);
S3=S3';
S04=mean(S3);
% [coeffvals3,coeffvals4] = gaussian4fit_lower0_mk2(S03,S04);
[coeffvals3,coeffvals4] = gaussian4fit_lower0_mk3(S03,S04);
%
%sort coeffecients by position ascending order only
sort_coeff_position
B1=double(B1);
B2=double(B2);
B3=double(B3);
B4=double(B4);
%

inp= 4;  %number of inputs
count=1;
while(count<=inp)
    myInput(count:count,1:2)=[0 255];
    count=count+1;
end
net=newff(myInput, [30 1],{'logsig','logsig'},'trainlm', 'learngdm', 'mse');
% P
% P1
```

```
%check that 3 peaks have been found, if not pad array
% CheckArray=[3 4]
% EqualityCheck = isequal(CheckArray, arrayCheck)
% if(EqualityCheck == 0)
%     P = padarray(P,[2 0],'post') %assumes just one peak found, what happens if there are 2
% end
% EqualityCheck2 = isequal(CheckArray, arrayCheck2)
% if(EqualityCheck2 == 0)
%     P1 = padarray(P1,[2 0],'post')
% end
%
% %limit the size of the array to 3x3
% P=P(:,2:4)
% P1=P1(:,2:4)

X=[B1 B2 B3 B4];
t1=[1 1 1];
t0=[0 0 0];
t=[t1 t0 t1 t0]
% t=t';
net.trainParam.goal= 0.01;
net.trainParam.epochs = 500;
[net,tr]=train(net,X,t);

% training_threat1=sim(net,coeffvals1)
% training_nonthreat1=sim(net,coeffvals2)
% training_threat2=sim(net,coeffvals3)
% training_nonthreat2=sim(net,coeffvals4)
training_threat1=sim(net,B1)
training_nonthreat1=sim(net,B2)
training_threat2=sim(net,B3)
training_nonthreat2=sim(net,B4)
```